THE JOURNAL
OF
CHEMICAL PHYSICS

VOLUME 20, NUMBER 6 JUNE, 1952

Radial Distribution Functions and the Equation of State of Fluids Composed of Molecules Interacting According to the Lennard-Jones Potential*

JOHN G. KIRKWOOD,† VICTOR A. LEWINSON,‡ AND BERNI J. ALDER§
Gates and Crellin Laboratories of Chemistry, California Institute of Technology and the Sterling Chemistry Laboratory, Yale University
(Received March 6, 1952)

The integral equation for the radial distribution function of a fluid composed of spherical molecules interacting according to a modified Lennard-Jones potential has been integrated in the Kirkwood approximation and in the Born-Green approximation over a wide range of temperature and density. The distribution functions so obtained have been used to calculate the equation of state and the thermodynamic functions of the fluid. The calculated thermodynamic functions are compared with the experimental values for liquid argon.

I

IN the statistical mechanical theory of the liquid state,[1-4] the equation of state and the thermodynamic functions of the fluid are related to the potential of intermolecular force $V(R)$ and the radial distribution function $g(R)$ in the following manner:

$$\begin{aligned}
&\frac{pv}{NkT}=1-\frac{2\pi N}{3vkT}\int_0^\infty R^3\frac{dV}{dR}g(R)dR,\\
&\frac{E}{NkT}=\tfrac{3}{2}+\frac{2\pi N}{vkT}\int_0^\infty R^2V(R)g(R)dR,\\
&\mu=NkT\ln p+\mu^E+\mu^*(T),\\
&\mu^*(T)=\lim_{p\to 0}[\mu-NkT\ln p],\\
&\frac{\mu^E}{NkT}=\frac{4\pi N}{vkT}\int_0^1\int_0^\infty R^2V(R)g(R,\xi)dRd\xi-\ln\frac{pv}{NkT},
\end{aligned}\tag{1}$$

where p is the pressure, v the molar volume, E the molar internal energy, μ the chemical potential, N the Avogadro number, k Boltzmann's constant, and T is the thermodynamic temperature. In the expression for the chemical potential, it is necessary to employ the radial distribution function $g(R, \xi)$ for a pair of molecules, one of which, i, is partially coupled to those of the rest of the fluid, corresponding to a total potential of intermolecular force

$$V_N(\xi)=V_{N-1}+\xi\sum_{\substack{k=1\\ \neq i}}^{N}V(R_{ik}).\tag{2}$$

Systems of integro-differential equations for the average densities in the configuration space of sub-sets of n molecules have been developed in equivalent forms by Kirkwood,[1] Born and Green,[2] Mayer,[3] and Yvon.[4] When the systems of integral equations are closed by the superposition approximation[1] in the space of molecular triplets, the following integral equation for the radial distribution function is obtained:

$$\begin{aligned}
&\ln g(R,\xi)=-\beta\xi V(R)+\frac{\pi N}{vR}\int_0^\infty\{K(R-r,\xi),\\
&\qquad -K(R+r,\xi)\}r[g(r)-1]dr,\\
&K(t,\xi)=-2\beta\int_0^\xi\int_{|t|}^\infty sV(s)g(s,\xi)dsd\xi;\quad K,\\
&K(t,\xi)=\beta\xi\int_{|t|}^\infty(s^2-t^2)\frac{dV}{ds}g(s,\xi)ds;\quad BGY,
\end{aligned}\tag{3}$$

* This work was carried out with support from the ONR under Contract N6 onr-244 with the California Institute of Technology and Contract NOnr-410 (00) with Yale University.
† Present address: Sterling Chemistry Laboratory, Yale University, New Haven, Connecticut.
‡ Present address: Mellon Institute, Pittsburgh, Pennsylvania.
§ Present address: Department of Chemistry, University of California, Berkeley, California.
[1] J. G. Kirkwood, J. Chem. Phys. **3**, 300 (1935).
[2] M. Born and H. S. Green, Proc. Roy. Soc. (London) **A188**, 10 (1946).
[3] J. E. Mayer, J. Chem. Phys. **15**, 187 (1947).
[4] J. Yvon, Actualites Scientifiques et Industrielles (Hermann et Cie, Paris, 1935), p. 203.

where the first form of the kernel $K(t, \xi)$ corresponds to the Kirkwood formulation and the second to that of Born and Green and Yvon.

Equation (3) has been solved numerically for a fluid consisting of rigid spherical molecules with no attractive forces by Kirkwood, Maun, and Alder.[5] In the present article we present numerical solutions of Eq. (3) for a fluid composed of spherical molecules interacting with a modified Lennard-Jones potential, to be described in detail below, together with the equation of state and the thermodynamic functions based upon this potential and the radial distribution functions $g(R)$ so obtained. The rigid sphere solutions of Kirkwood, Maun, and Alder serve as the starting point in an iterative procedure leading to solutions for molecules interacting with the modified Lennard-Jones potential.

It is convenient to express the potential V and Eq. (3) in dimensionless or reduced form. We shall use a two-parameter potential,

$$V(R)=\epsilon\gamma(x), \quad x=R/a, \tag{4}$$

where ϵ and a are, respectively, an energy and a length characteristic of the molecules. With the definitions

$$\lambda_0=(4\pi Na^3/v) \tag{5}$$

$$g(-x)=g(x) \tag{6}$$

$$\gamma(-x)=\gamma(x), \tag{7}$$

we can write the integral equation (3) as follows:

$$\ln g(x, \xi)=-\beta\epsilon\xi\gamma(x) + \frac{\lambda_0}{4x}\int_{-\infty}^{\infty} K(x-s, \xi)s[g(s)-1]ds, \tag{8}$$

$$K^{(K)}(t, \xi)=-2\beta\epsilon\int_{|t|}^{\infty} ds\int_0^{\xi} d\xi\cdot s\gamma(s)g(s, \xi), \tag{9}$$

$$K^{(B)}(t, \xi)=\beta\epsilon\xi\int_{|t|}^{\infty} ds\cdot(s^2-t^2)g(s, \xi)\left[\frac{d\gamma(s)}{ds}\right]. \tag{10}$$

The superscripts (K) and (B) will be used to refer to the Kirkwood and the Born-Green-Yvon formulations, respectively,

When we choose a form for the potential $\gamma(x)$ and solve (8) we will obtain a radial distribution function and thermodynamic functions which will be useful, by appropriate choice of ϵ and a, for all fluids possessing this potential of intermolecular force. The Lennard-Jones[6,7] potential

$$\gamma_L(x)=(4/x^{12})-(4/x^6) \tag{11}$$

is widely applicable to nonpolar fluids; here a is the finite value of R for which $V(R)$ vanishes. At liquid densities, however, neither iterative procedures nor the method of Fourier transforms accomplished the solution of (8) with the potential $\gamma_L(x)$. We shall now describe a modified potential and a series expansion of $\ln g(x)$ in inverse powers of temperature which bring (8) into soluble form.

The modified potential $\gamma_m(x)$ combines the rigid spherical core with the Lennard-Jones potential, as follows:

$$\gamma_m=\gamma_0+\gamma_1;$$

$$e^{-\beta\epsilon\xi\gamma_0(x)}=0,\ 0\leqslant x<1,\ \xi>0;\ e^{-\beta\epsilon\xi\gamma_0(x)}=1,\ x\geqslant 1 \text{ or } \xi=0$$

$$\gamma_1(x)=0,\ 0\leqslant x<1;\ \gamma_1(x)=\gamma_L(x),\ x\geqslant 1. \tag{12}$$

We confine our attention to the fully-coupled potential ($\xi=1$), writing

$$g(x, 1)=g(x); \tag{13}$$

we define[8]

$$\ln g(x)=-\beta\epsilon\gamma_0(x)+[\psi(x)/x];$$

and we expand $\psi(x)$, $g(x)$, and $K(t)$ in power series:‖

$$\psi(x)=\psi_0(x)+\beta\epsilon\psi_1(x)+(\beta\epsilon)^2\psi_2(x)+\cdots, \tag{14}$$

$$g(x)=g_0(x)\left[1+\beta\epsilon\frac{\psi_1(x)}{x} + (\beta\epsilon)^2\left\{\frac{\psi_1^2(x)}{2x^2}+\frac{\psi_2(x)}{x}\right\}+\cdots\right], \tag{15}$$

$$K(t)=k_0K_0(t)+\beta\epsilon K_1(t)+(\beta\epsilon)^2K_2(t)+\cdots. \tag{16}$$

Here,

$$g_0(x)=\exp\{-\beta\epsilon\gamma_0(x)+[\psi_0(x)/x]\}, \tag{17}$$

$$k_0^{(K)}=\langle g_0\rangle=\int_{|t|}^{1} se^{\psi(s)/s}ds \Big/ \int_{|t|}^{1} sds, \tag{18}$$

$$k_0^{(B)}=g(1)=g_0(1)[1+\beta\epsilon\psi_1(1) + (\beta\epsilon)^2\{\tfrac{1}{2}\psi_1^2(1)+\psi_2(1)\}+\cdots], \tag{19}$$

$$K_0^{(K)}(t)=K_0^{(B)}(t)=(t^2-1) \text{ if } t^2<1;\ =0 \text{ if } t^2\geqslant 1, \tag{20}$$

$$K_1^{(K)}(t)=-2\int_{|t|}^{\infty} g_0(s)s\gamma_1(s)ds, \tag{21}$$

$$K_1^{(B)}(t)=\int_{|t|}^{\infty}(s^2-t^2)g_0(s)\left[\frac{d\gamma_1(s)}{ds}\right]ds, \tag{22}$$

$$K_2^{(B)}(t)=\int_{|t|}^{\infty}(s^2-t^2)g_0(s)\frac{\psi_1(s)}{s}[d\gamma_1(s)/ds]ds. \tag{23}$$

When we substitute the expansions (14)–(16) into the integral equation (8) and collect and equate to zero the coefficients of powers of $(\beta\epsilon)$, we obtain the

[5] Kirkwood, Maun, and Alder, J. Chem. Phys. **18**, 1040 (1950).
[6] J. E. Lennard-Jones, Physica **4**, 941 (1937).
[7] J. Corner, Trans. Faraday Soc. **44**, 914 (1948).

[8] Kirkwood, Maun, and Alder, J. Chem. Phys. **18**, 1040 (1950). In Eq. (12) ff of that paper, the quantities γ, g, ψ, and ϕ must receive the subscript zero to conform to the present notation.

‖ See Appendix I for details in the expansion of the kernel.

following set of integral equations:

$$\psi_0(x)=\frac{\lambda}{4}\int_{-\infty}^{\infty}K_0(x-s)s[g_0(s)-1]ds; \tag{24}$$

$$\psi_r(x)=m_r(x)+\frac{\lambda}{4}\int_{-\infty}^{\infty}K_0(x-s)g_0(s)\psi_r(s)ds; \quad r=1, 2, 3, \cdots. \tag{25}$$

Equation (24) is exactly the hard-sphere equation previously solved,[8] and the relation of λ to λ_0 is unchanged, *viz.*:

$$\lambda_0=[g_0(\lambda^{(K)}; x=1)]^{-\frac{1}{2}}\int_0^{\lambda^{(K)}}[g_0(\lambda', x=1)]^{-\frac{1}{2}}d\lambda' =[\langle g_0\rangle]^{-1}\lambda^{(K)}, \tag{26}$$

$$\lambda_0=[g_0(\lambda^{(B)}; x=1)]^{-1}\cdot\lambda^{(B)}. \tag{27}$$

The complexity of $m_r(x)$ increases rapidly with r. For example:

$$m_1{}^{(K)}(x)=-x\gamma_1(x)+\frac{\lambda_0}{4}\int_{-\infty}^{\infty}K_1(x-s)s[g_0(s)-1]ds, \tag{28}$$

$$m_1{}^{(B)}(x)=-x\gamma_1(x)+\psi_1(1)\psi_0(x) +\frac{\lambda_0}{4}\int_{-\infty}^{\infty}K_1(x-s)s[g_0(s)-1]ds, \tag{29}$$

$$m_2{}^{(B)}(x)=\psi_2(1)\psi_0(x)+\tfrac{1}{2}\psi_1{}^2(1)\psi_0(x) +\frac{\lambda_0}{4}\int_{-\infty}^{\infty}K_2(x-s)s[g_0(s)-1]ds +\frac{\lambda_0}{4}\int_{-\infty}^{\infty}K_1(x-s)g_0(s)\psi_1(s)ds +\frac{\lambda}{4}\int_{-\infty}^{\infty}K_0(x-s)g_0(s)\left[\frac{\psi_1{}^2(s)}{2s}\right]ds +\frac{\lambda\psi_1(1)}{4}\int_{-\infty}^{\infty}K_0(x-s)g_0(s)\psi_1(s)ds. \tag{30}$$

Since $m_1(x)$ contains the large term $-\gamma_1(x)$, ψ_1 should express the principal effect of adding the potential γ_1 to the rigid sphere core γ_0 in (12).

II. SOLUTIONS OF THE EQUATIONS

Because of the simple kernel $K_0(x-s)$, (24) and (25) can be solved numerically by a modified iterative process. It is based upon a theorem which has been given only in the following approximate form. Suppose we have an nth trial solution of (24) or (25), $\psi_r{}^{(n,\,\mathrm{IN})}(x)$, which differs by $\omega^{(n)}(x)$ from the true solution:

$$\psi_r{}^{(n,\,\mathrm{IN})}(x)=\psi_r(x)+\omega^{(n)}(x). \tag{31}$$

If we insert this $\psi_r{}^{(n,\,\mathrm{IN})}(x)$ into the right-hand side of (24) or (25) so as to obtain its iterate, $\psi_r{}^{(n,\,\mathrm{OUT})}(x)$, and if, in the convolution of $\omega^{(n)}(x)$, we approximate the kernel $K_0(t)$ by a Dirac δ-function,

$$K_0(t)\doteq-(4/3)\delta(t), \tag{32}$$

we obtain

$$\psi_r{}^{(n,\,\mathrm{OUT})}(x)\doteq\psi_r(x)-\tfrac{1}{3}\lambda g_0(x)\omega^{(n)}(x). \tag{33}$$

Since $g_0(x)$ is always positive and not greatly different from unity, it will be seen that the true solution, on the average, lies between the input and the output.¶ We may form an $(n+1)$th input as a linear combination of

$$\psi_r{}^{(n,\,\mathrm{IN})} \text{ and } \psi_r{}^{(n,\,\mathrm{OUT})};$$

$$\psi_r{}^{(n+1,\,\mathrm{IN})}(x)=\alpha^{(n)}\psi_r{}^{(n,\,\mathrm{OUT})}(x) +(1-\alpha^{(n)})\psi_r{}^{(n,\,\mathrm{IN})}(x). \tag{34}$$

From (31) and (33),

$$\alpha^{(n)}\doteq(3/\lambda+3). \tag{35}$$

With the assistance of Professor Stanley P. Frankel, it was possible to set up IBM equipment,** including the 604 Electronic Calculator to perform the entire iteration cycle of (25). The principal mathematical transformation required is a double partial integration of

$$\int_{-\infty}^{\infty}K_0(x-s)g_0(s)\psi_r(s)ds,$$

so as to convert a time-consuming and expensive convolution into much simpler multiple integrations. The functions $m_1{}^{(B)}$, $m_1{}^{(K)}$, and $m_2{}^{(B)}$ were calculated by hand on desk calculators, except for the convolutions involving $K_1(x-s)$, which were performed by the IBM equipment in a straightforward way, and the terms $\psi_r(1)\psi_0(x)$ in $m_r{}^{(B)}$. The machines then multiplied an input $\psi_r{}^{(n,\,\mathrm{IN})}(s)$ by $g_0(s)$, integrated repeatedly as required for the convolution with $K_0(x-s)$, formed $\psi_r{}^{(n,\,\mathrm{IN})}(1)\psi_0(x)$ (if needed), and printed out both $\psi_r{}^{(n,\,\mathrm{OUT})}$ and $\psi_r{}^{(n+1,\,\mathrm{IN})}$, using a prearranged value of α. Each cycle required about half an hour of machine time. The original input $\psi_r{}^{(0,\,\mathrm{IN})}$ was obtained by a few cycles of hand-iteration and guesswork from a rough estimate based on a fraction ($\leqslant\frac{1}{2}$) of $m_r(x)$ and, if available, on $\psi_r(x)$ for neighboring values of λ. For the first machine cycles, where $\psi_r{}^{(n,\,\mathrm{OUT})}-\psi_r{}^{(n,\,\mathrm{IN})}$ may be large, it was important to use small values of $\alpha^{(n)}(\sim0.1)$ to prevent divergence. As $\psi_r{}^{(n,\,\mathrm{IN})}$ becomes a better solution of (25) with increasing n, $\alpha^{(n)}$ may be increased for faster convergence.

Tables I and II (excluding columns *I*, *II*, *III*, and *IV*, which will be discussed later) present the results

¶ We have glossed over three points here: (a) In the treatment of Eq. (24), the exponential $e^{\omega/x}$ must be expanded, keeping only the linear term. (b) (32) is rather rough, especially for $1\leqslant x<2$, where the step function behavior of $g_0(x)$ at $x=1$ is involved. (c) The term $\omega^{(n)}(1)\psi_0(x)$ in $m_r(x)$ has been neglected.

** For details, see the Ph.D. dissertation of B. J. Alder, California Institute of Technology, 1951.

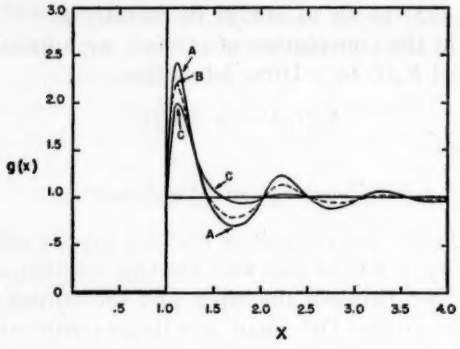

FIG. 1. Theoretical radial distribution function $g_2(x)$ *versus* reduced distance x. Fixed temperature ($\beta\epsilon=0.8$, $T^*=1.25$), increasing density (A, $\lambda=5$, $v^*=3.46$; B, $\lambda=20$, $v^*=1.48$; C, $\lambda=27.4$, $v^*=1.22$).

of these calculations. Tables of ψ_0 to two decimal places have been published previously;[8] they have since been sufficiently refined by hand calculations to justify giving a third figure. The last row of Table I shows the maximum difference between each ψ-function and its iterate [i.e., $\psi_r^{(\mathrm{OUT})}(x)-\psi_r^{(\mathrm{IN})}(x)$], which is a measure of how close the function is to a correct solution of (24) or (25). From these ψ-functions, one can compute the radial distribution function and the thermodynamic properties of a fluid over a considerable range of density (roughly $\frac{1}{3}$ to 3 times the density at the critical point) and of temperature (from high temperatures down to about $\frac{2}{3}$ of the critical temperature).

Figures 1 and 2 exhibit the influence of temperature and of density on $g(x)$, the radial distribution function. It will be seen that increasing density (increasing λ) at constant temperature (Fig. 1), and decreasing temperature (increasing $\beta\epsilon$) at constant density (Fig. 2) both tend to pack the molecules into a more orderly array [higher peaks in $g(x)$]. Also, as x, the distance between two molecules, becomes large, there is no longer any correlation between their positions, and so $g(x)$ tends to unity. All these facts are qualitatively in agreement with experiment. A quantitative comparison for argon is presented in Fig. 3, using the experimental data of

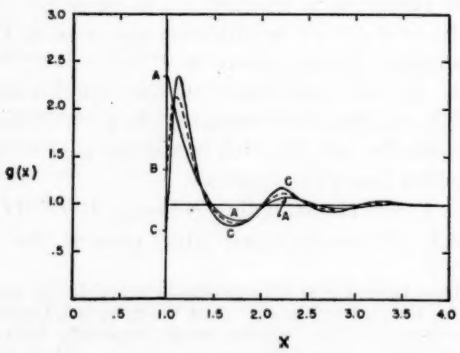

FIG. 2. Theoretical radial distribution function $g_2(x)$ *versus* reduced distance x. Fixed density ($\lambda=20$), decreasing temperature (A, $\beta\epsilon=0$, $T^*=\infty$; B, $\beta\epsilon=0.6$, $T^*=1.67$; C, $\beta\epsilon=1.2$, $T^*=0.83$).

Eisenstein and Gingrich;[9,10] here the unit of length a has been chosen so that the experimental and calculated first peaks of $g(x)$ occur at the same value of x. The differences are no larger than the experimental uncertainties.

The theoretical radial distribution function used here, which is correct to terms in $\psi_2(x)$, will be called $g_2(x)$:

$$g_2(x)=\exp\{-\beta\epsilon\gamma_0(x)+[\psi_0(x)+\beta\epsilon\psi_1(x)+(\beta\epsilon)^2\psi_2(x)]/x\}. \quad (36)$$

This includes terms with higher powers of $(\beta\epsilon)$ than $(\beta\epsilon)^2$; in fact, all terms in (15) containing only ψ_0, ψ_1, and ψ_2 are included. If ψ_2, ψ_4, $\cdots$ are small, $g_2(x)$ is a better approximation to $g(x)$ than if terms in (15) only up to $(\beta\epsilon)^2$ were retained. Since $\psi_2(x)$ is gratifyingly small compared to $\psi_1(x)$, one might hope that the series (14) might be cut off after $\psi_2(x)$. Evidence will be presented later, however, which indicated that higher terms are small but not entirely negligible.

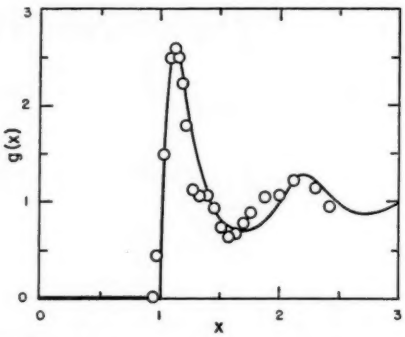

FIG. 3. Radial distribution function $g(x)$. Solid line, theoretical $g_2(x)$($\lambda=27.4$, $\beta\epsilon=1.2$, or $v^*=1.22$, $T^*=0.83$). Points, experimental for argon (see reference 9) (91.8°K, $p=1.8$ atmos).

In columns *I*, *II*, *III*, and *IV* of Tables I and III, some "exact" ψ-functions are tabulated—"exact" in the sense that they were calculated without the use of the temperature expansion (14). They were obtained by hand calculation, using an iterative process which was successful only for small λ or small $\beta\epsilon$. The kernel $K(l)$ [Eq. (10)] was computed from a first approximation $\exp[-\beta\epsilon\gamma_m(x)]$ for *I* and *II*; $g_2(x)$ for *III*; *III* for *IV* ($x\geqslant 1$); $g(1)\exp[-\beta\epsilon\gamma_L(x)]$ for *IV* if $x\leqslant 1$ and held constant during several cycles of iteration, starting from the above first approximation and using $\alpha^{(n)}$ of $\frac{1}{3}$ to $\frac{1}{2}$. When the difference $[\psi^{(n,\mathrm{OUT})}(x)-\psi^{(n,\mathrm{IN})}(x)]$ became small, a new kernel was prepared from $\psi^{(n+1,\mathrm{IN})}(x)$. Two or three repetitions of this process were enough to obtain the tabulated solutions.

A similar procedure, starting from $g_2(x)$, was applied at several other values of λ and $\beta\epsilon$, with the purpose both of estimating and of improving the accuracy of the solutions. Table IV shows the differences, $\psi^{(\mathrm{OUT})}(x)$

[9] A. Eisenstein and N. S. Gingrich, Phys. Rev. **62**, 261 (1942).
[10] J. de Boer, Reports on Progress in Physics. Phys. Soc. London, **XII**, 305 (1948–9).

TABLE I. ψ-functions[a, b] for small x.

	$\lambda=1$			$\lambda=5$				
x	ψ_0	I[c]	II[c]	ψ_0	ψ_1	ψ_2	III[c]	IV[c]
1.00	0.095	0.022	0.150	0.368	−0.586	0.078	0.088	0.075
1.02	···	0.263	0.547	···	−0.183	0.077	0.321	0.308
1.04	0.092	0.430	0.834	0.349	+0.099	0.075	0.479	0.466
1.06	···	0.541	1.017	···	0.290	0.074	0.584	0.572
1.08	0.088	0.613	1.138	0.329	0.414	0.073	0.649	0.637
1.12	0.083	0.674	1.243	0.305	0.529	0.069	0.691	0.679
1.16	0.079	0.670	1.239	0.283	0.534	0.067	0.671	0.659
1.20	0.074	0.631	1.180	0.260	0.486	0.065	0.618	0.606
1.24	0.069	0.575	1.095	0.236	0.411	0.063	0.547	0.536
1.32	0.059	0.455	0.900	0.188	0.250	0.058	0.401	0.391
1.40	0.048	0.346	0.740	0.141	0.109	0.053	0.265	0.257
1.48	0.037	0.260	0.590	0.091	+0.006	0.048	0.148	0.144
1.56	0.027	0.193	0.488	0.048	−0.064	0.045	+0.060	0.060
1.64	0.017	0.140	0.415	+0.011	−0.105	0.044	−0.004	+0.002
1.72	0.009	0.100	0.360	−0.020	−0.123	0.044	−0.048	−0.038
1.80	+0.002	0.074	0.330	−0.041	−0.120	0.046	−0.065	−0.053
1.88	−0.002	0.059	0.315	−0.051	−0.101	0.049	−0.062	−0.049
1.96	−0.004	0.059	0.325	−0.051	−0.070	0.055	−0.038	−0.022
2.00	−0.004	0.061	0.335	−0.040	−0.053	0.059	−0.016	+0.003
2.04	−0.003	0.063	0.345	−0.032	−0.030	0.062	+0.009	0.024
2.12	−0.002	0.065	0.366	−0.016	+0.014	0.069	0.055	0.065
2.20	−0.002	0.064	0.385	−0.003	0.041	0.067	0.087	0.095
2.28	−0.001	0.060	0.375	+0.003	0.051	0.057	0.098	0.104
2.36	−0.001	0.056	0.355	0.007	0.051	0.042	0.097	0.102
2.44	0.000	0.052	0.330	0.008	0.040	0.026	0.083	0.088
2.52		0.047	0.305	0.008	0.029	0.011	0.068	0.073
2.60		0.042	0.285	0.006	0.017	+0.001	0.053	0.059
2.68		0.037	0.265	0.004	+0.006	−0.006	0.040	0.046
2.76		0.033	0.242	0.003	−0.003	−0.008	0.032	0.039
2.84		0.029	0.222	+0.001	−0.007	−0.007	0.026	0.033
2.92		0.025	0.214	0.000	−0.009	−0.005	0.022	0.029
3.00		0.023	0.200	−0.001	−0.009	−0.001	0.019	0.027
Diff[d]	±0.001	0.003	0.008	0.002	0.002	0.001	0.004	0.004

	$\lambda=10$			$\lambda=20$				$\lambda=27.4$			$\lambda=33$
x	ψ_0	ψ_1	ψ_2	ψ_0	ψ_1	ψ_1(K)	ψ_2	ψ_0	ψ_1	ψ_2	ψ_0
1.00	0.587	−0.789	0.025	0.859	−0.920	−0.788	−0.038	0.980	−0.956	−0.048	1.040
1.02	0.570	−0.382	0 025	0.834	−0.508	−0.379	···	0.957	−0.542	−0.046	···
1.04	0.552	−0.095	0.024	0.808	−0.218	−0.091	−0.034	0.933	−0.247	−0.044	1.016
1.06	0.534	+0.100	0.024	0.780	−0.016	+0.109	···	0.907	−0.043	−0.042	···
1.08	0.515	0.230	0.024	0.751	+0.119	0.241	−0.031	0.879	+0.095	−0.041	0.980
1.12	0.476	0.353	0.023	0.691	0.253	0.363	−0.028	0.817	0.236	−0.038	0.928
1.16	0.436	0.367	0.021	0.627	0.280	0.374	−0.025	0.745	0.268	−0.036	0.861
1.20	0.392	0.330	0.019	0.556	0.255	0.324	−0.023	0.665	0.245	−0.034	0.778
1.24	0.350	0.266	0.018	0.483	0.203	0.242	−0.021	0.575	0.196	−0.033	0.673
1.32	0.261	0.127	0.015	0.329	+0.081	+0.046	−0.017	0.371	+0.079	−0.028	0.414
1.40	0.174	+0.008	0.013	0.170	−0.019	−0.141	−0.013	+0.148	−0.019	−0.022	+0.108
1.48	0.089	−0.074	0.011	+0.014	−0.085	−0.290	−0.008	−0.077	−0.082	−0.013	−0.204
1.56	+0.013	−0.123	0.010	−0.128	−0.115	−0.387	−0.002	−0.281	−0.109	−0.001	−0.491
1.64	−0.052	−0.142	0.010	−0.240	−0.120	−0.428	+0.003	−0.441	−0.108	+0.010	−0.709
1.72	−0.101	−0.139	0.012	−0.313	−0.105	−0.407	0.009	−0.536	−0.086	0.024	−0.828
1.80	−0.131	−0.117	0.015	−0.338	−0.077	−0.321	0.018	−0.548	−0.055	0.040	−0.816
1.88	−0.133	−0.084	0.020	−0.301	−0.045	−0.181	0.029	−0.460	−0.027	0.054	−0.657
1.96	−0.106	−0.046	0.027	−0.194	−0.019	+0.008	0.039	−0.264	−0.011	0.069	−0.341
2.00	−0.077	−0.026	0.030	−0.110	−0.010	0.118	0.043	−0.122	−0.009	0.074	−0.125
2.04	−0.051	+0.003	0.031	−0.030	+0.022	0.244	0.034	+0.021	+0.019	0.056	+0.094
2.12	−0.007	0.063	0.033	+0.089	0.106	0.431	0.020	0.227	0.127	0.025	0.412
2.20	+0.021	0.094	0.033	0.155	0.137	0.465	0.017	0.333	0.159	+0.014	0.580
2.28	0.037	0.092	0.023	0.175	0.116	0.380	+0.010	0.354	0.118	−0.002	0.600
2.36	0.041	0.073	+0.009	0.161	0.066	0.223	−0.005	0.305	+0.043	−0.024	0.493
2.44	0.039	0.044	−0.005	0.124	+0.008	+0.043	−0.017	0.207	−0.033	−0.039	0.302
2.52	0.030	+0.017	−0.015	0.069	−0.036	−0.117	−0.022	+0.083	−0.091	−0.046	+0.061
2.60	0.019	−0.008	−0.021	+0.013	−0.067	−0.241	−0.023	−0.042	−0.123	−0.038	−0.173
2.68	+0.008	−0.026	−0.002	−0.037	−0.082	−0.309	−0.017	−0.150	−0.125	−0.022	−0.369
2.76	−0.003	−0.035	+0.007	−0.074	−0.080	−0.322	−0.008	−0.221	−0.105	+0.001	−0.495
2.84	−0.010	−0.037	0.009	−0.093	−0.064	−0.276	+0.003	−0.247	−0.066	0.022	−0.552
2.92	−0.012	−0.033	0.005	−0.090	−0.041	−0.184	0.013	−0.222	−0.019	0.039	−0.448
3.00	−0.014	−0.022	0.001	−0.071	−0.009	−0.058	0.200	−0.155	+0.032	0.048	−0.283
Diff[d]	±0.002	0.002	0.002	0.002	0.002	0.003	0.003	0.002	0.004	0.004	0.007

[a] All ψ_1, ψ_2, and exact ψ-functions on Born-Green basis, except $\lambda=20$ column labeled ψ_1(K).
[b] $g(x)$ = radial distribution function; $\psi(x)=x\ln(x)+\beta\epsilon\gamma_0(x)$; $\psi(x)=\psi_0(x)+\beta\epsilon\psi_1(x)+(\beta\epsilon)^2\psi_2(x)+\cdots$.
[c] Exact; i.e., no expansion in powers of $\beta\epsilon$. Column headings: *I*, $\lambda=1$, $\beta\epsilon=0.6$; *II*, $\lambda=1$, $\beta\epsilon=1.0$; *III*, $\lambda=5$, $\beta\epsilon=0.6$; *IV*, $\lambda=5$, $\beta\epsilon=0.6$, $\gamma=\gamma_L$ instead of γ_m.
[d] Maximum difference between ψ-function and its iterate for any x.

TABLE II. ψ-functions[a] for large x.

	$\lambda=5$			$\lambda=10$		
	ψ_0	ψ_1	ψ_2	ψ_0	ψ_1	ψ_2
x_n[b]	2.92	3.32	3.02	2.74	3.14	2.99
ψ_e[b]	−0.002	0.004	0.011	−0.014	0.018	0.012
x_n	3.36	4.12	3.88	3.32	3.73	3.54
ψ_e	0.000	0.000	−0.001	0.005	−0.007	−0.006
x_n			4.20	3.92	4.30	3.84
ψ_e			0.002	−0.001	0.003	0.002
x_n			5.10	4.28	4.80	4.14
ψ_e			0.000	0.000	0.000	0.003
x_n						4.78
ψ_e						−0.001
x_n						5.33
ψ_e						+0.001
x_n						5.70
ψ_e						0.000
x_n						
ψ_e						
x_n						
ψ_e						
x_n						
ψ_e						
x_n						
ψ_e						
x_n						
ψ_e						
x_n						
ψ_e						

	$\lambda=20$				$\lambda=27.4$			$\lambda=33$
	ψ_0	ψ_1	ψ_1(K)	ψ_2	ψ_0	ψ_1	ψ_2	ψ_0
x_n[b]	3.17	3.02	3.04	2.82			2.76	3.10
ψ_e[b]	0.048	0.063	0.233	0.023			0.049	0.399
x_n	3.74	3.56	3.58	3.38	3.13	2.95	3.32	3.64
ψ_e	−0.025	−0.038	−0.143	−0.018	0.161	0.119	−0.043	−0.327
x_n	4.31	4.12	4.15	3.92	3.68	3.48	3.83	4.20
ψ_e	0.012	0.025	0.089	0.013	−0.108	−0.098	0.039	0.249
x_n	4.87	4.67	4.71	4.46				4.75
ψ_e	−0.007	−0.014	−0.051	−0.006				
x_n	5.44	5.23	5.26	5.00				
ψ_e	0.003	0.008	0.028	0.004				
x_n	6.02	5.80	5.82	5.58				
ψ_e	−0.001	−0.004	−0.016	−0.001				
x_n	6.36	6.43	6.40	6.10				
ψ_e	0.000	0.002	0.006	0.001				
x_n		7.02	6.96[c]	6.48	6.46	6.23	6.55	
ψ_e		0.000		0.000	0.009	0.020	−0.012	
x_n								
ψ_e								
x_n								
ψ_e								
x_n								
ψ_e								
x_n					8.80			
ψ_e					0.001			
x_n					9.04	9.18	9.34	
ψ_e					0.000	−0.001	0.001	
x_n						9.64[d]	9.68[d]	
ψ_e								

[a] See references a and b of Table I.
[b] To save space, we have here tabulated only the x-values (x_n) of successive nodes of the ψ-functions, and the intervening peaks (ψ_e) of the ψ-functions. More detailed tables are given in the thesis of B. J. Alder.
[c] Carried only to $x=7$.
[d] Carried only to $x=10$.

$-\psi^{(\mathrm{IN})}(x)$, between various ψ-functions and their iterates. The two rows for $\lambda=5$, $\beta\epsilon=1.0$ are of particular interest; the addition of $\psi_2(x)$ has improved the ψ-function somewhat, but not greatly. Table IV suggests that the ψ-functions are more accurate for $\lambda=27.4$ than for $\lambda=5$ or $\lambda=10$, since the differences are smaller and smaller corrections will have a greater influence [see Eq. (35)]. Naturally, $\psi_3(x)$ and higher terms are less important for lower $\beta\epsilon$, as confirmed by the first two and the last two rows.

TABLE III. Exact[a, b] ψ-functions for large x.

	$\lambda=1$		$\lambda=5$	
x	*I*	*II*	*III*	*IV*
3.50	0.012	0.145	0.024	0.030
4.00	0.007	0.100	0.017	0.020
4.50	0.004	0.070	0.011	0.014
5.00	0.003	0.048	0.009	0.011
5.50	0.001	0.032	0.006	0.008
6.00	0.000	0.020	0.004	0.006
7.00		0.009	0.000	0.002
8.00		0.000		

[a] See references a, b, and c of Table I.
[b] These do not oscillate.

It was not possible materially to improve the accuracy of the ψ-functions by the above process. The kernel is now not the simple, always negative $K_0(t)$, but a much more complicated function with positive peaks at $t=\pm1$ and a valley between where $K(t)$ may or may not become negative. Hence, $\alpha^{(n)}$ in (34) is no longer confined to the range $0<\alpha^{(n)}\leqslant 1$. Even if $\alpha^{(n)}$ is chosen systematically[11] so as to minimize

$$\Delta^{(n+1)}=\int_0^\infty [\psi^{(n+1,\mathrm{OUT})}(x)-\psi^{(n+1,\mathrm{IN})}(x)]^2dx, \quad (37)$$

it is found that $\alpha^{(n)}=0$ is the best choice, i.e., $\psi^{(n+1,\mathrm{IN})}(x)$ cannot be improved by linear combination with $\psi^{(n,\mathrm{OUT})}(x)$ before $\Delta^{(n+1)}$ becomes small.

TABLE IV. Differences between some ψ-functions and their iterates.

		Differences[a] at:				
λ	$\beta\epsilon$	$x=1.00$	$x=1.12$	$x=1.80$	$x=3.00$	$x=4.00$
5	0.6[b]	0.033	0.036	0.031	0.013	0.003
5	1.0[b]	0.147	0.159	0.170	0.069	0.015
5	1.0[c]	0.163	0.171	...	...	...
10	1.0[b]	0.111	0.118	0.111	0.047	0.003
27.4	0.8[b]	0.025	0.031	0.058	0.031	0.015
27.4	1.0[b]	0.089	0.101	0.110	0.053	0.015

[a] $\psi^{(\mathrm{OUT})}(x)-\psi^{(\mathrm{IN})}(x)$.
[b] $\psi^{(\mathrm{IN})}(x)=\psi_0(x)+\beta\epsilon\psi_1(x)+(\beta\epsilon)^2\psi_2(x)$.
[c] $\psi^{(\mathrm{IN})}(x)=\psi_0(x)+\beta\epsilon\psi_1(x)$.

Two of the tabulated ψ-functions deserve special mention. *IV* is a solution at $\lambda=5$, $\beta\epsilon=0.6$, for the unmodified LJ potential $\gamma_L(x)$ (11) without the hard core. For $0.8\leqslant x\leqslant 1.0$, the following expression for $\psi(x)$ was correct within ±0.001:

$$\psi(x\leqslant 1)=-0.6x\gamma(x)+0.655-0.580x. \quad (38)$$

When $x<0.8$, $g(x)$ is so small that even $x^3\gamma'(x)g(x)$ is negligible. By comparison with *III*, it will be seen that for $x\geqslant 1$, $\psi(x)$ is insensitive to the choice between $\gamma_L(x)$ and $\gamma_m(x)$. The pressure calculated from *IV*, however, is lower than that for *III* by about 10 percent (see Tables V and VI).

Equation (25) ($r=1$) was solved for $\lambda=20$ on the Kirkwood basis, to provide a comparison with the Born-Green formulation. The resulting function $\psi^{(\mathrm{K})}(x)$ is included in Tables I and II. Following (26) and (27), $\lambda^{(\mathrm{K})}=20$ corresponds to almost the same density as $\lambda^{(\mathrm{B})}=27.4$ ($\lambda_0=10.00$ and 10.28, respectively). In the important range of $0.6\leqslant\beta\epsilon\leqslant 1.0$, cancellation occurs so

[11] See reference (8), pp. 1044–1045.

TABLE V. Reduced equation of state.[a] $\Phi=(p^*v^*/T^*)$, *versus* v^* and T^*.

λ	v^*	Source of $g(x)$	$T^*=0.833$	1.000	1.250	1.667	2.500	5.000	∞
1	13.82	ψ_0, *I*, *II*[b]	...	0.629	0.768	0.883	...	...	1.167
5	3.632	g_1[c]	−0.610	−0.175	0.245	0.656	1.057	1.452	1.833
	3.632	g_2[d]	−0.594	−0.156	0.264	0.670	1.064	1.456	1.833
	3.632	*III*[b]	...	...	...	0.685	...	...	...
	3.632	*IV*[b]	...	...	...	0.620	...	...	...
10	2.260	g_1[c]	−1.460	−0.751	−0.050	0.640	1.320	1.998	2.667
	2.260	g_2[d]	−1.445	−0.734	−0.038	0.649	1.326	1.998	2.667
20	1.483	g_1[c]	−2.298	−1.167	−0.049	1.059	2.158	3.249	4.333
	1.483	g_2[d]	−2.433	−1.268	−0.115	1.018	2.139	3.242	4.333
$20^{(K)}$	1.257[a]	$g_1^{(K)}$[c]	...	−0.943	0.219	1.382	...	...	4.333
27.4	1.222	g_1[c]	...	−1.215	0.165	1.534	2.889	4.232	5.567
	1.222	g_2[d]	−2.829	−1.382	0.052	1.467	2.856	4.223	5.567
33	1.077	ψ_0	...	...	...	...	...	...	6.500

[a] All on Born-Green basis, except row $\lambda^{(K)}=20$, $v^*=1.257$.
[b] See Tables I, II, III.
[c] I.e., using $g_1(x)=\exp[-\beta\epsilon\gamma_0(x)+\{\psi_0(x)+\beta\epsilon\psi_1(x)\}/x]$.
[d] I.e., using $g_2(x)=\exp[-\beta\epsilon\gamma_0(x)+\{\psi_0(x)+\beta\epsilon\psi_1(x)+(\beta\epsilon)^2\psi_2(x)\}/x]$.

that $\psi^{(K)}(x)$ and $\psi^{(B)}(x)$ are not greatly different. This is shown in Fig. 4, where the dotted curve is $g^{(B)}(x)$ for $\lambda^{(B)}=27.4$, and the solid curve is $g^{(K)}(x)$ for $\lambda^{(K)}=20$, both at $\beta\epsilon=0.6$. The resulting difference in thermodynamic functions is not excessive (see Tables V and VI).

III. THERMODYNAMIC FUNCTIONS

Because of the dimensionless form of the potential (4) and integral equation (8), reduced or dimensionless thermodynamic functions may be computed from the radial distribution function. By appropriate choice of the parameters a and ϵ, these reduced functions may be compared with experimental values for various fluids. The reduced volume (v^*), pressure (p^*), and temperature (T^*) are

$$v^*=v/Na^3=4\pi/\lambda_0, \tag{39}$$

$$p^*=p(a^3/\epsilon), \tag{40}$$

$$T^*=T(k/\epsilon)=1/\beta\epsilon. \tag{41}$$

We shall take as fundamental the equation of state and the internal energy, calculating only the excess internal energy, defined by

$$E^E=E-\tfrac{3}{2}NkT. \tag{42}$$

TABLE VI. Reduced excess internal energy.[a] $-E^E/N\epsilon$ *versus* v^* and T^*.

v^*	Source of $g(x)$	$T^*=0.833$	1.000	1.250	1.667	2.500	5.000
13.82	ψ_0, *I*, *II*[b]	...	0.741	0.621	0.537	...	...
3.632	g_1[a]	2.143	2.059	1.981	1.908	1.842	1.782
3.632	g_2[a]	2.280	2.148	2.035	1.939	1.856	1.787
3.632	*III*[b]	...	...	...	1.992	...	...
3.632	*IV*[b]	...	...	...	1.910	...	...
2.260	g_1[a]						
2.260	g_2[a]	3.370	3.277	3.192	3.118	3.050	2.990
1.483	g_1[a]						
1.483	g_2[a]	5.073	5.024	4.974	4.925	4.873	4.822
1.257[a]	$g_1(K)$[a]	...	6.102	5.986	5.881	...	...
1.222	g_1[a]						
1.222	g_2[a]	6.313	6.280	6.232	6.181	6.125	6.066

[a] See Table V.
[b] See Tables I, II, III.

From these, the other thermodynamic functions can be computed; for example, the excess entropy:

$$S_v^E=S-R\ln v-S_v^*(T);\quad S_v^*=\lim_{v\to\infty}[S-R\ln v]. \tag{43}$$

The equation of state is

$$\Phi=\frac{p^*v^*}{T^*}=\frac{pv}{NkT}=1-\frac{2\pi}{3v^*T^*}\int_0^\infty x^3\frac{d\gamma(x)}{dx}g(x)dx, \tag{44}$$

and E^E and S^E are given by

$$\frac{E^E}{N\epsilon}=\frac{2\pi}{v^*}\int_0^\infty x^2\gamma(x)g(x)dx; \tag{45}$$

$$\frac{S_v^E}{R}=\int_\infty^{v^*}\left[\left(\frac{\partial p^*}{\partial T^*}\right)_{v^*}-\frac{1}{v^*}\right]dv^*. \tag{46}$$

These functions are tabulated in Tables V (p^*v^*/T^* *versus* v^* and T^*), VI ($-E^E/N\epsilon$), and VII ($-S_v^E/R$).

Using power-series interpolation formulas (See Appendix III), the critical point can easily be determined by the conditions $(\partial p/\partial v)_T=0$ and $(\partial^2 p/\partial v^2)_T=0$. The

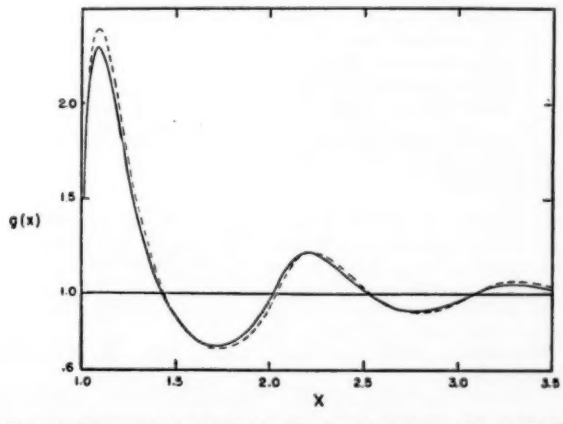

FIG. 4. Theoretical radial distribution function $g_1(x)$. Solid line, Kirkwood theory ($\lambda^{(K)}=20$, $v^*=1.26$; $\beta\epsilon=0.6$, $T^*=1.67$). Dashed, Born-Green theory ($\lambda^{(B)}=27.4$, $v^*=1.22$; $T^*=1.67$).

TABLE VII. Reduced excess entropy.[a] $-S^E/R$ *versus* v^* and T^*.

v^*	$T^*=1.000$	1.250	1.667	2.500	5.000
13.82	0.28	0.24	0.21	0.20	0.19
3.632	0.80	0.91	0.99	1.05	1.11
2.260	1.43	1.52	1.56	1.64	1.69
1.483	2.49	2.56	2.57	2.66	2.72
1.222	3.29	3.35	3.35	3.44	3.50

[a] Radial distribution functions used: *K*, *II*, and $g_2(x)$; see Tables I, II, and III, and reference d of Table V. All on Born-Green basis.

critical constants are

$$p_c^*=0.199; \quad v_c^*=2.585; \quad T_c^*=1.433. \tag{47}$$

The value Φ_c of the dimensionless quantity Φ (44) at the critical point is independent of the parameters a and ϵ, and so affords an absolute check of the theory. Several values of Φ_c are given in Table VIII; it will be seen that the best value from this research differs by only 23 percent from the experimental. As shown in Table V, Φ is somewhat decreased at $v^*=3.63$ and $T^*=1.67$ when $g_2(x)$ is replaced by the exact $g(x)$ corresponding to the unmodified potential $\gamma_L(x)$. Probably the same would be true of Φ_c, which would then be very close to the experimental value.

In Tables IX and X we compare the theoretical and experimental equation of state[12] and excess energy[13] for argon, for which excellent data are available. The values of a and ϵ used are those calculated by Michels[12] from second-virial-coefficient data,

$$\begin{aligned} \epsilon_L &= 1.653\times10^{-14} \text{ erg}, \\ a_L &= 3.405\times10^{-8} \text{ cm}, \end{aligned} \tag{48}$$

which differ only slightly from those of other authors.[14–17] Figure 5 displays the 0°C isotherm [curve *A*, experimental values; *B* (dashed), this research; *C*, free-volume theory[18]]. It will be seen that both theoretical isotherms are too flat (too large compressibility),

TABLE VIII. Φ, or (pv/NkT) at critical point.

Source	Φ_c
Van der Waals equation	0.375
Free-volume theory[a]	0.591
This research, using $g_1(x)$	0.404
This research, using $g_2(x)$	0.358
Experiment,[b] argon	0.292

[a] See reference 18.
[b] See reference 9.

[12] A. Michels, H. and H. Wijker, Physica **15**, 627 (1949).
[13] Michels, Lunbeck, and Wolkers, Physica **15**, 689 (1949).
[14] J. Corner, Trans. Faraday Soc. **44**, 914 (1948) (Second virial coefficient and data on solid argon).
[15] R. Buckingham, Proc. Roy. Soc. (London) **A168**, 264 (1938) (Second virial coefficient data).
[16] Hirschfelder, Bird, and Spotz, Chem. Rev. **44**, 205 (1949) (Viscosity data).
[17] It should be pointed out that this choice of a and ϵ is slightly arbitrary, for Michels used the unmodified Lennard-Jones potential γ_L. See Appendix IV.
[18] Wentorf, Jr., Buehler, Hirschfelder, and Curtiss, J. Chem. Phys. **18**, 1484 (1950).

the free-volume one being worse in this respect, and that the results of the present research agree better with experiment at the lower densities, whereas the free-volume agrees better at higher densities. Since this comparison is at a fairly high temperature ($T^*>2$), $g_2(x)$ should be a good approximation to $g(x)$, the correct solution of (8). The discrepancies must be ascribed either to the superposition approximation or to inadequacies in the form of the potential $\gamma_m(x)$.

The boundary of the two-phase region in the reduced equation of state (i.e., vapor pressure *vs* liquid and vapor volume) can be established by finding on each isotherm the two volumes v_e^* and v_g^* which have the same pressure p^* and the same chemical potential $\mu/N\epsilon$:

$$\begin{aligned} \frac{\mu}{N\epsilon} &= \frac{\mu^*(T)}{N\epsilon} - T^* \ln v^* + \int_{v^*}^{\infty}\left[p^* - \frac{T^*}{v^*}\right]dv^* + p^*v^* - T^*, \\ \frac{\mu^*(T)}{N\epsilon} &= \lim_{v^*\to\infty}\left[\frac{\mu}{N\epsilon} + T^* \ln v^*\right]. \end{aligned} \tag{49}$$

The integral was evaluated analytically, using the power-series equation of state (see Appendix II), and then the volumes v_e^* and v_g^* were found by successive approximations. The two-phase region and a number of isotherms are graphed, using reduced units, in Fig. 6. Here the theory reproduces very well the qualitative aspects of experimental fluid isotherms.

TABLE IX. Theoretical and experimental equation of state (pv/NkT) for argon.

Density d (amagats)	0°C isotherm Expt	Theoret	Error, %	150°C isotherm Expt	Theoret	Error, %
259.6	0.925	0.982	+6	1.161	1.290	+11
417.1	1.122	1.186	+6	1.486	1.713	+15
635.5	2.138	1.907	−11	2.556	2.776	+9
771.4	3.661	2.569	−30	···	3.644	···

In summary, one may say that the theory gives a correct qualitative description of the radial distribution function and thermodynamic functions of fluids. The quantitative results are good (±10 percent to 20 percent in the equation of state and the internal energy) for lower densities, up to about twice the density at the critical point. At the density of the liquid near its freezing point, however, the results are quantitatively poor. The large error may equally well be considered to be in the volume scale or in the pressure calculation. The volume $v^*=1.19$, for instance, corresponds experimentally to the liquid under 1-atmos vapor pressure ($T^*=0.70$, $p^*=0.0024$); the theory predicts the vapor pressure $p^*=0.074$ at $T^*=1.25$ for this volume. Or, alternatively, for $v^*=1.19$ and $T^*=0.70$, the theory predicts a *negative* pressure of about 1000 atmos. The equation of state, (15), is very sensitive: for pressures below 100 atmos, the right-hand side contains large

positive and negative contributions, of which p^*v^*/T^* is a small difference. What one might call a small "phase shift" of $g(x)$ relative to $\gamma(x)$ [i.e., using

$$\int_0^\infty x^3 \frac{d\gamma(x)}{dx} g(x+b)dx$$

instead of

$$\int_0^\infty x^3 \frac{d\gamma(x)}{dx} g(x)dx,$$

in (44), where b is of the order 0.02] produces a change of hundreds of atmospheres in the pressure. Perhaps some small inadequacy of the repulsive part of the potential might cause such a "phase shift." Further research on this project is now in progress, with these objectives: (1) to improve the accuracy of the radial distribution functions, since both the thermodynamic and the transport properties[19] depend sensitively on $g(x)$; (2) to study the effect of changes in the form of the potential; (3) to find, if possible, an alternative way to compute p^* from $g(x)$ so that the desired quantity will not be a small difference of large terms.

TABLE X. Theoretical and experimental excess internal energy ($-E^E$, calc) for argon.

Density	0°C isotherm			150°C isotherm		
d (amagats)	Expt	Theoret	Error, %	Expt	Theoret	Error, %
259.6	399	445	+11	359	431	+20
417.1	625	729	+17	560	717	+28
635.5	918	1162	+27	782	1152	+47

ACKNOWLEDGMENTS

The authors express their sincere thanks to Professor Stanley P. Frankel, for his assistance in preparing the calculations for the IBM equipment, and to Mr. Wm. C. Chaplin, of the Digital Computing Laboratory, who set up and carried out the IBM work. They are also grateful to Mrs. W. A. Alfonte, Jr. and to G. M. Nazarian and R. W. Zwanzig for assistance in the calculations.

APPENDIX I. EXPANSION OF KERNELS

There is no difficulty in the expansion of the Born-Green kernel, Eq. (10). From (12), for $\xi>0$,

$$(d/dx)e^{-\beta\epsilon\xi\gamma_0(x)} = -\beta\epsilon\xi[d\gamma_0(x)/dx]e^{-\beta\epsilon\xi\gamma_0(x)} = \delta(x-1), \quad \text{(I-1)}$$

and $g(x)$ contains the factor $e^{-\beta\epsilon\xi\gamma_0(x)}$. Equations (16), (19), (22), and (23) follow immediately.

To expand the Kirkwood kernel (3), we must go back to (9) and introduce two coupling parameters, ξ_0 for

[19] This is especially true of the heat capacity and the thermal conductivity, where differentiation with respect to temperature emphasizes the higher terms in the expansion (15).

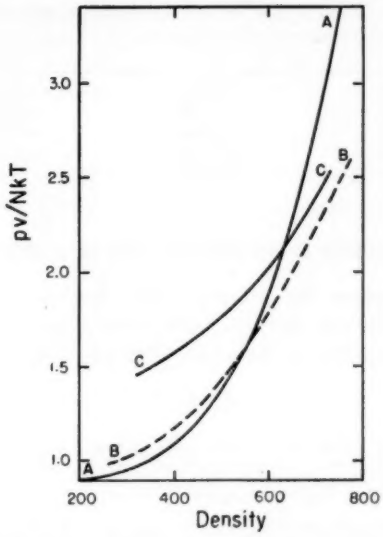

FIG. 5. 0°C isotherm for argon, pv/NkT *versus* density (amagats). *A*, experimental (see reference 12); *B* (dashed), this research; *C*, free-volume theory (see reference 18).

γ_0 and ξ for γ_1. Then (9) becomes

$$K^{(K)}(t, \xi_0, \xi) = -2\beta\epsilon\int_{|t|}^\infty ds \int_0^{\xi_0} d\xi' \cdot s\gamma_0(s)g_0(s, \xi', \xi=0) - 2\beta\epsilon\int_{|t|}^\infty ds \int_0^{\xi} d\xi' \cdot s\gamma_1(s)g(s, \xi_0, \xi'). \quad \text{(I-2)}$$

The first term is evaluated by previously described methods;[20] this derivation makes clear the difference between (18), where $k_0^{(K)}$ is independent of $\beta\epsilon$, and (19), where $k_0^{(B)}$ must be expanded in powers of $\beta\epsilon$. The second term of (I-2) is expanded in powers of $(\beta\epsilon\xi)$, starting with $(\beta\epsilon\xi)^1$, and then ξ is set equal to unity.

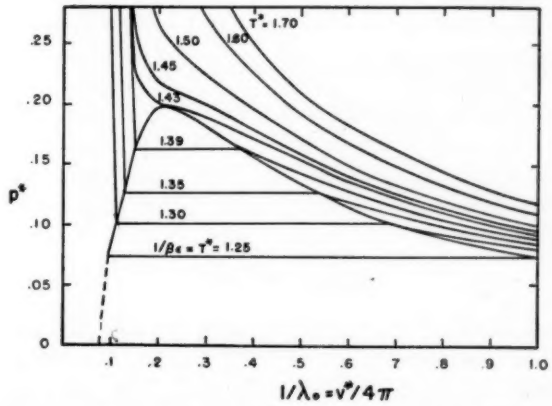

FIG. 6. Theoretical reduced isotherms of fluid, showing liquid-vapor transition.

[20] J. G. Kirkwood and E. M. Boggs, J. Chem. Phys. **10**, 394 (1942).

TABLE XI. Second virial coefficients.

β	$F_L/6$	$F_m/6$
0.20	0.0735	0.0406
0.40	−0.0290	−0.0521
0.60	−0.1426	−0.1607
0.80	−0.2689	−0.2840
1.00	−0.4100	−0.4231

APPENDIX II. INTERPOLATION FORMULAS

To compute the integrals and derivatives required for S^E (46), the critical point, and $\mu/N\epsilon$ (49), power-series interpolation formulas were prepared. Here

$$d=1/v^*. \tag{II-1}$$

(*A*) $5\leqslant\lambda\leqslant 27.4$; $0.6\leqslant\beta\epsilon\leqslant 1.0$; using $g_2(x)$:

$$p^*=p_0(v^*)+T^*p_1(v^*)+T^{*2}p_2(v^*); \tag{II-2}$$

$$p_0=-8.0782d^2+2.7487d^3-7.3144d^4+4.0070d^6; \tag{II-3}$$

$$p_1=0.101,307d+11.1551d^2-21.9676d^3+27.4701d^4 -9.652,97d^6; \tag{II-4}$$

$$p_2=-0.189,32d^2-0.278,82d^3+0.680,60d^4 -0.371,61d^6. \tag{II-5}$$

(*B*) $5\leqslant\lambda\leqslant 27.4$; $0.2\leqslant\beta\epsilon\leqslant 0.4$; using $g_2(x)$:

$$p^*=p_0(v^*)+T^*p_1(v^*); \tag{II-6}$$

$$p_0=-7.0393d^2+5.2986d^3-19.285d^4+15.861d^5; \tag{II-7}$$

$$p_1=0.101,306d+11.025d^2-27.447d^3+45.691d^4 -22.484d^5. \tag{II-8}$$

(*C*) $0\leqslant\lambda\leqslant 5$; $0.1\leqslant\beta\epsilon\leqslant 1.0$; using $g_2(x)$ at $\lambda=5$, "exact" solutions at $\lambda=1$, and second virial coefficients (see Appendix III) calculated for modified potential, γ_m:

$$p^*=T^*d+B^*(T^*)d^2+C^*(T^*)d^3; \tag{II-9}$$

$$B^*=2.0944T^*-5.60005-1.187,52/T^* -0.459,46/T^{*2}; \tag{II-10}$$

$$C^*=3.6876T^*-6.7375+8.6017/T^*-3.6611/T^{*2} +1.5794/T^{*3}. \tag{II-11}$$

(*D*) Excess internal energy, using $g_2(x)$,

$5\leqslant\lambda\leqslant 27.4$; $0.2\leqslant\beta\epsilon\leqslant 1.0$:

$$E^E/N\epsilon=e^0+e_1(\beta\epsilon)+e_2(\beta\epsilon)^2; \tag{II-12}$$

$$e_0=-0.447,10\lambda_0-0.017,277\lambda_0^2 +0.000,5912\lambda_0^3-0.000,0197\lambda_0^4; \tag{II-13}$$

$$e_1=-0.123,93-0.064,711\lambda_0+0.011,858\lambda_0^2 -0.000,7322\lambda_0^3; \tag{II-14}$$

$$e_2=0.214,07-0.628,44\lambda_0^{\frac{1}{2}}+0.246,19\lambda_0 -0.006,406\lambda_0^2. \tag{II-15}$$

APPENDIX III. SECOND VIRIAL COEFFICIENTS

Lennard-Jones[21] has shown how to reduce the expression for the second virial coefficient,

$$B=-\frac{2\pi a^3\beta\epsilon}{3}\int_0^\infty \frac{d\gamma(x)}{dx}e^{-\beta\epsilon\gamma(x)}x^3dx, \tag{III-1}$$

to an infinite series,

$$B=(2\pi a^3/3)F(y); \quad y^2=4\beta\epsilon. \tag{III-2}$$

If $\gamma=\gamma_L$, the unmodified Lennard-Jones potential, then

$$F_L(y)=\left[\Gamma(\tfrac{3}{4})-\tfrac{1}{4}\sum_{\tau=1}^{\infty}\frac{y^\tau}{\tau!}\Gamma\left(\frac{2\tau-1}{4}\right)\right]\cdot y^{\frac{1}{2}}. \tag{III-3}$$

If $\gamma=\gamma_m$, $F(y)$ has a slightly more complicated form:

$$F_m(y)=\left[\Gamma(\tfrac{3}{4},y^{\frac{1}{2}})-\tfrac{1}{4}\sum_{\tau=1}^{\infty}\frac{y^\tau}{\tau!}\Gamma\left(\frac{2\tau-1}{4},y^{\frac{1}{2}}\right)\right]\cdot y^{\frac{1}{2}} +\exp(-y^2) \tag{III-4}$$

$$\Gamma(\alpha,\beta)=\int_0^\beta t^{(\alpha-1)}e^{-t}dt. \tag{III-5}$$

Some values of F_L and F_m are given in Table XI. The two sets of second virial coefficients, B_L and B_m, can be brought into close coincidence over the range $0.3\leqslant\beta\epsilon\leqslant 1.0$ by means of the following relations among the parameters a and ϵ in the potential:

$$\epsilon_m/\epsilon_L=1.171 \quad (a_L/a_m)=1.086. \tag{III-6}$$

[21] J. E. Lennard-Jones, Physica **4**, 941 (1937).

The Chemical Effects of Ultrasonics*

VIRGINIA GRIFFING
Department of Chemistry, The Catholic University of America, Washington, D. C.
(Received February 5, 1952)

A study of the effects of ultrasonics on the inversion of sucrose was made and negative results were obtained. In the light of these results one can make the following conclusions.

Chemical reactions attributed to ultrasonics can be classified according to three mechanisms. (1) Reactions due to cavitation never occur without the formation of bubbles. All of these reactions take place in the gas phase, are primarily thermal and are due to the heat developed during adiabatic compression. Thus, only reactants with an appreciable vapor pressure are affected. (2) Many reactions in the liquid phase are of secondary origin due to reactions with dissolved products of the primary reaction in the gas phase. Luminescense is also a secondary effect. (3) Some reactions are due to the uniform temperature elevation caused by absorption of acoustic energy of very high intensity in a short path length.

AN extensive literature[1] now exists which reports a large variety of chemical reactions due to ultrasonics. Most authors agree that a gas must be present in the solutions before these reactions take place. On the assumption that a gas dissolved in the solution forms minute bubbles in the sound field, an explanation for many of these phenomena has been suggested in a previous note.[2] According to this hypothesis, the liquid transfers the energy of the sound wave from the source to the interfaces between the liquid and bubbles already present or actually formed in the sound field. The bubbles are then adiabatically compressed, producing high temperatures inside the bubble. The temperature changes are transmitted to the liquid surrounding the bubble by heat conduction and affect the reaction rate in solution purely thermally. However, this should occur only if the temperature changes in the liquid are appreciable ($\sim\pm 100°C$), otherwise the effect of the temperature increase and decrease due to periodic expansion of the bubble will cancel out. According to this idea, two thermal properties of the gas content of the bubbles are important. Firstly, $(\gamma-1)$ will determine the temperature reached in the compressed bubble. This is in agreement with the results of experiments carried out in this laboratory.[3] Solutions saturated with rare gases gave significantly greater yields of free chlorine in a study of the action of ultrasonics on the hydrolysis of carbon tetrachloride than if the solutions were saturated with oxygen or nitrogen. Furthermore, solutions saturated with nitrogen and oxygen, $\gamma=1.4$, were much more effective than solutions saturated with SF_6 or freon 114 ($C_2Cl_2F_4$). This will also explain the fact that ethers and other liquids with a high vapor pressure inhibit chemical reactions even though bubble formation persists, since these vapors will diffuse into the bubble and reduce the average γ of the mixture in the bubble. Secondly, the thermal conductivity of the gas will determine how long the heat stays in the gas bubble and how much gets into the liquid. One would expect that for gases having the same value of γ (e.g., all the rare gases), a gas having a higher heat conductivity should give larger reaction rates, since the surrounding liquid would get hotter. However, the experiments[3] mentioned previously gave the opposite effect, namely a greater reaction rate for the gas with smaller conductivity. They gave a greater yield for solutions saturated with argon than for solutions saturated with neon. This dependence suggested that the primary reactions actually took place in the gas bubble. This assumption was strengthened by numerical calculations made at our request by Mr. N. MacDonald. According to these, the temperature variation of the liquid surrounding the bubble is, under reasonable conditions, far from resonance, only $+4°C$, too small to affect the reaction rate appreciably. The following experiments on the rate of inversion of sucrose in acid solution were undertaken to determine if there was any significant direct effect of the heating of the liquid at the bubble boundary.

Conflicting observations on the effect of ultrasonics on this reaction have been reported in the literature. This reaction was chosen because it goes at a measurable rate at room temperature and has a high temperature coefficient. A ten-degree rise in temperature would bring about a threefold increase in rate. In addition, sugar has a negligible vapor pressure so that the hydrolysis of the sugar must take place in the liquid phase. Thus, any appreciable heating at the bubble-liquid interface would increase the rate of inversion.

EXPERIMENTAL

All experiments were carried out with a 2-mc quartz crystal mounted in a Lucite holder in one end of a glass tank The glass tank was filled with water to transmit the high intensity sound wave from the source to the reaction vessel which was immersed in the water. The temperature of the water was controlled to $\pm 0.1°C$. The crystal was driven by an oscillator from a radio

* This work was supported by ONR Contract Nonr-331(00).

[1] R. Prudhomme and P. Grabar, Ann. inst. Pasteur **76**, 460 (1949); Compt. rend. **226**, 1821 (1948); J. chim. phys. **46**, 323 (1949). N. S. Marinesco, Chimie & Industrie **55**, 263–268 (1946). Weissler, J. Am. Chem. Soc. **70**, 1634 (1948); **71**, 93, 418 (1949).

[2] V. Griffing, J. Chem. Phys. **18**, 997 (1950).

[3] M. E. Fitzgerald, Ph.D. thesis, The Catholic University of America, Washington, D. C. (to be published).

TABLE I.

Without ultrasonics		With ultrasonics (intensity = 6.5 watts/cm, frequency 2 Mc)	
Temp. °C	% inversion	Temp. °C[a]	% inversion
30.2	12.6	29.8	12.8
30.2	13.5	29.8	12.9
30.2	13.5	29.0	13.5
30.2	12.5	30.0	13.2
		30.0	11.9
		30.1	12.6
		30.1	11.9
		30.1	11.9
		30.3	15.7

[a] This is the arithmetic mean of the recorded temperatures in the reaction vessel.

transmitter and the intensity was kept constant over a given run by keeping the voltage across the crystal constant. The voltage was measured with a vacuum tube voltmeter with a range of 0- to 1500-volts rms. The actual intensity of the sound was measured by observing the radiation pressure[4] on a rubber disk, suspended by two Nylon threads from a rod about a meter above the tank. The reaction was carried out in a tube one-inch inside diameter and six inches long, closed at one end and supported horizontally in the bath. Three sidearms were sealed to the tube, one for a thermometer, and the other two were equipped with stopcocks to facilitate the filling and emptying of the tube. The ultrasonic radiation entered the open end of the tube which was closed with a Nylon film (thickness 0.001 in.) supplied by DuPont. This Nylon was nonreactant and allowed at least 99 percent of the sound energy to pass into the reaction mixture.

Preliminary experiments were carried out with the Nylon at both open ends of a cylindrical tube and an absorbing rubber disk suspended at the end of the tube farthest from the crystal. This set-up was designed to eliminate reflections and to enable us to keep a constant intensity by keeping the radiation pressure on the disk constant throughout a run. However, this method was unsuccessful because as soon as cavitation begins, many small bubbles are produced in the sound field and most of the sound energy is scattered by the bubbles so that no measurement of intensity can be made in this manner. Therefore, we modified this method by adjusting the intensity (as measured by the radiation pressure) of the sound beam entering the reaction vessel at the beginning of the run so that the intensity was the same in all runs. During the run the intensity was continually monitored by maintaining a constant voltage on the crystal.

The presence of cavitation was observed by passing a Tyndall beam through the solution in each experiment. Any experiments in which cavitation ceased during the run were discarded.

[4] F. E. Fox and V. Griffing, J. Acoust. Soc. Am. **21**, 352 (1949).

(a) The Hydrolysis of Sucrose

All the following experiments were done using a 0.1 M sucrose solution in 0.78 N sulfuric acid. After preparing this solution it was rapidly transferred from the volumetric flask into the reaction vessel and irradiated. The reaction vessel was kept in a constant temperature bath (±0.1°C) throughout the irradiation period. The temperature inside the reaction vessel was recorded every 15 seconds during irradiation. The stationary temperature rose about 2° above that of the bath. This temperature was averaged and blank runs were made at this average temperature. The blanks were treated in exactly the same way as described above except for the irradiation itself. After irradiation, the sucrose solution was transferred to a stoppered flask neutralized with sodium bicarbonate in order to stop the reaction. The samples were allowed to stand for 12 hours in order to attain equilibrium in the mutarotation. The optical rotation was then measured, with a Franz-Schmidt and Haensch polarimeter No. 4661 with a triple field.

The final experiments were carried out on 90 ml samples, irradiated with an ultrasonic intensity of 6.5 watts/cm² for 20 minutes and the results are given in Table I. The Nylon was tested for the diffusion of sucrose and its reaction products and no detectable diffusion was observed.

It is apparent from the results of Table I that there is no significant increase in the rate of inversion of sucrose in acid solution due to the action of ultrasonics. In all cases there was vigorous cavitation. A few observations were made on the inversion of sugar in neutral solution and a slight increase in rate was observed. The *p*H of these solutions after irradiation were measured and the blanks then run for solutions with this *p*H, and the rates were found to be the same. Thus, there is a slight increase in rate for the neutral solution due to the change in *p*H of the solution; however, there is no increase in rate due to heating at the liquid-bubble surface. This would indicate that any thermal effects must take place in the gas phase rather than the liquid.

Some experiments were made in which 5 percent solutions of acetone and water saturated with air were irradiated. A small increase in *p*H resulted and the

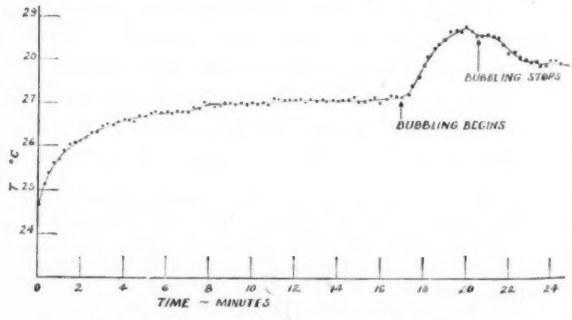

FIG. 1. Temperature *vs* time when H_2O saturated with air is irradiated with U. S.

mixture had the distinct odor of ketene. Since this reaction could not go in the liquid phase, this is also evidence that the primary reaction due to ultrasonics takes place in the gas phase.

(b) Temperature Elevation Produced by Ultrasonic Radiation

Another set of experiments was undertaken to determine the effect of bubbles on the observed increase in temperature of the liquid. A sample of water saturated with air was placed in the reaction vessel. The reaction vessel was placed in the constant temperature bath and brought to the temperature of the bath. The sound beam was then turned on but no cavitation was observed and the temperature began to rise as shown in Fig. 1. The temperature rose to an almost constant value after four to five minutes. At 7 minutes a slight increase in temperature was observed and a few small bubbles could be seen in the vessel. However, at 17 minutes vigorous bubbling started and the temperature increased sharply about one and a half degrees. When bubbling stopped at about 21 minutes the temperature decreased again.

In order to be sure that no appreciable amount of sound energy was lost through the end of the reaction vessel when there was no bubbling, the foregoing experiment was repeated, keeping the intensity the same as before but with an absorbing plug of glass wool at the far end of the tube. The results are shown in Fig. 2. Curve *A* shows the temperature rise in degassed water. The temperature rises about 1°C above the temperature of the bath and remains constant except for slight increases at *x* and *y*. These rises are correlated with the appearance of a few bubbles in the reaction tube. Curve *B* shows the temperature rise in water saturated with air in which there was vigorous bubbling throughout the experiment. Thus, there is greater increase in temperature with bubbling than without. The steady state temperature did not rise as high in the cases where the glass wool was used as when bubbling persisted without the glass wool. The same effect was also noted in the comparison of the amount of free chlorine produced in the ultrasonic induced hydrolysis of carbon tetrachloride. The yield without glass wool was four or five times as great as those with glass wool even though bubbling persisted. This is probably caused by a decreased intensity due to the elimination of standing waves.

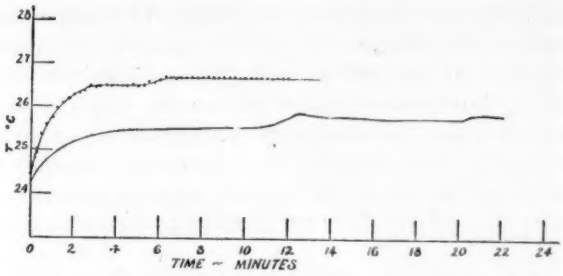

FIG. 2. Temperature variation for water with glass-wool plug.

DISCUSSION

The experiments in our laboratory and those reported in the literature lead to the conclusion that chemical reactions attributed to ultrasonics can be classified according to three mechanisms.

(1) Reactions due to cavitation. These have been more extensively studied both in our laboratory and by other investigators.

(a) A gas in the form of minute bubbles must either be suspended in the sample or formed as the sound wave passes through the liquid, in order for these chemical reactions to take place. These bubbles grow under the action of the sound wave and can be observed visually by the Tyndall beam. No chemical reactions of this type have been observed without the accompanying bubble formation.

(b) All primary reactions due to the ultrasonic waves take place inside the gas bubbles. Thus, no reactant is affected directly by the sound field unless it has an appreciable vapor pressure.

(c) The reactions which take place in the gas phase are primarily thermal,† and are due to the heat developed during adiabatic compression. This is demonstrated by the observed dependence of the rate of hydrolysis of CCl_4 on the thermal properties of the dissolved gases; also by the inhibition of these reactions by the addition of small quantities of ether or other liquid with a high vapor pressure.

(2) Many reactions in the liquid phase have been reported as due to ultrasonics which now appear to be secondary reactions. For example, oxidizing agents, such as H_2O_2, which have been formed in the gas bubbles in the presence of oxygen may dissolve in the liquid and cause further reaction. Examples of these are the decomposition of KI and the oxidation of Na_2SO_3 to Na_2SO_4. The change in *p*H of the solution brought about by reactions in the gas bubbles is responsible for other reactions that have been attributed directly to cavitation. An example of this is increase in rate of the inversion of sucrose. Luminescence observed in some solutions is also a secondary effect of the cavitation process.

(3) Some reactions are due to the temperature elevation caused by the absorption of acoustic energy of very high intensity in a short path length. An example of such a reaction is the denaturization of proteins.[5] In these experiments ox eyes were irradiated with ultrasonics until cataracts were produced. That this was due to absorption heating was conclusively demonstrated by placing a thermocouple in the center of the lens of

† This type of heating is often called "local heating" or "hot spots" in the literature.

[5] Lavine, Langenstraus, Bourger, Fox, Griffing and Thaler, Arch. of Opthalmol., Chicago (1952).

the eye and recording the temperature. The temperature reached was sufficient to produce opacities by heating in a constant temperature bath. The opacities were more quickly produced at higher frequencies, which is to be expected, since the absorption varies as the square of the frequency. This suggests that frequency dependence would enable one to distinguish between reactions of types (1) and (3). It is not possible at present to conclude definitely the mechanism of the depolymerization of polymers by ultrasonics but a study of the dependence on frequency and the dissolved gases should conclusively settle the matter.

The author wishes to thank Miss Alicia Contreras and Miss Patricia Marshall for doing much of the experimental work reported and Professors F. O. Rice and K. F. Herzfeld for many helpful discussions.

THE JOURNAL OF CHEMICAL PHYSICS VOLUME 20, NUMBER 6 JUNE, 1952

A Mechanical Theory of Spinning Detonation*

JAMES A. FAY
Cornell University, Ithaca, New York
(Received November 29, 1951)

A review of published experimental data and theoretical discussions of spinning detonation reveals that there does not exist a consistent explanation of all the characteristics of such a phenomenon, particularly the dependence of spinning frequency upon tube diameter. In view of this, it is proposed to treat the problem principally from a hydrodynamic viewpoint by considering a possible periodic fluid motion with a characteristic frequency.

It is found that the calculated natural frequencies of vibration of the gaseous products behind a detonation wave agree closely with the measured frequencies of spinning detonation previously published in the literature. An analysis of such vibrations in the light of experimental evidence indicates that the vibratory motion is principally transverse. Of the various possible modes of vibration, the one which is observed depends upon the mixture composition and the tube size.

The observed existence of pressure waves in the wake of a spinning detonation wave is probably due to nonuniform combustion at the detonation front. It is shown how the initiation or cessation of combustion in a plane wave gives rise to compression or expansion waves respectively, and how a nonplanar disturbance excites a transverse vibration of characteristic frequency.

It is proposed that the uneven combustion of the spinning detonation wave is sustained by the heating and cooling effects of the vibratory pressure waves, which are themselves generated by such irregular combustion; i.e., spinning detonation is a self-excited vibratory phenomenon. Its appearance may thus be attributed to the susceptibility of the reaction rate to the heating or cooling effects of pressure waves.

I. CHARACTERISTICS OF SPINNING DETONATION

WHILE investigating the detonation characteristics of carbon monoxide-oxygen mixtures, Campbell and Woodhead[1] first observed the phenomenon of what is commonly known as spinning detonation. Flame photographs made on a moving film showed an undulating wave front and noticeable striations in the wake of the detonation (see Fig. 1, reproduced from reference 4), unlike the uniform propagation of most detonation waves. Further experiments by these and other investigators have succeeded in establishing the following principal characteristics of spinning detonation:

1. In round tubes, the luminous head of the detonation wave appears to move in a spiral path along the wall of the tube, as evidenced by phasing photographs[2] and deposits on the tube wall.[2,3]

2. For a given combustible mixture, the pitch† of the spin is proportional to the diameter of the tube,[1] although in larger tubes multiple heads may appear.[4] For many mixtures, the pitch is approximately three times the tube diameter for the single-headed wave.

3. Spinning detonation occurs principally in mixtures near the limits of detonation or mixtures difficult to detonate.[5,6] Spin has also been observed in mixtures which cannot support an unattenuating detonation when detonation is initiated by a strong shock. In such cases spin appears when the slowing detonation reaches the velocity which, according to the Chapman-Jouquet theory, is the normal velocity for such a mixture.[5]

4. Photographs of spinning mixtures detonated in noncircular tubes show the usual spinning characteristics, but no more direct evidence has been obtained that the wave head propagates in a more or less spiral path.[6]

5. The average velocity of propagation of the spinning detonation wave is very close to the theoretical velocity of the normal detonation calculated according to the Chapman-Jouquet theory.[5]

6. Pressure measurements made during spinning detonation

* This material is taken from a thesis submitted to the Graduate School of Cornell University for the degree of Doctor of Philosophy (September, 1951). The research was sponsored by a du Pont Graduate Fellowship in Mechanical Engineering.

[1] C. Campbell, and D. W. Woodhead, J. Chem. Soc. **129**, 3010 (1926); **130**, 1572 (1927).

[2] C. Campbell and A. C. Finch, J. Chem. Soc. 2094 (1928).

[3] W. A. Bone, and R. P. Fraser, Phil. Trans. Roy. Soc. (London) **A228**, 197 (1929).

† Pitch is defined as the distance along the tube axis which the detonation wave travels during one cycle of events at the wave front. Similarly, the spin frequency is the time rate at which events are repeated at the detonation front.

[4] W. A. Bone, and R. P. Fraser, Phil. Trans. Roy. Soc. (London) **A230**, 371 (1932).

[5] A. J. Mooradian, and W. E. Gordon, J. Chem. Phys. **19**, 1166 (1951).

[6] Bone, Fraser, and Wheeler, Phil. Trans. Roy. Soc. (London) **A235**, 29 (1936).

show appreciable pressure fluctuations, the pressure peaks on opposite sides of the tube being 180° out of phase.[5]

7. Transient spinning may occur during the initiation of detonation in many mixtures which do not normally spin.[4]

8. Flame photographs of spinning detonation show that the prominent striations visible in the wake of the detonation wave persist even after the latter emerges from an open end of the tube.[2]

II. EXISTING THEORIES OF SPIN

Campbell and Finch[2] proposed the theory that the luminous head of the spinning detonation wave progressed along a helical path, followed by a luminous tail which was the track of heated particles streaming through the head. In order to account for the striations in the wake of the detonation, it was necessary to assume that the product gas as a whole rotated in the tube. Since there is no mechanism by which a net angular momentum could be imparted to the fluid by the passage of a detonation wave, such an hypothesis would violate the laws of motion. A subsequent experiment by Bone and Fraser,[4] in which a longitudinal fin projecting radially inward from the wall of a circular tube had no effect on the spin, indicated that no such rotation of the gas occurred.

Jost[7] and Becker[8] give slightly different variations of an essentially one-dimensional theory. Both conceive of spinning detonation as a cyclic process in which the combustion zone falls behind the shock wave forming the front of the detonation as a whole, but which subsequently overtakes the slowed shock or generates a new combusion zone behind the shock by means of compression waves. Both the shock wave and the combustion zone are essentially plane, so that admittedly such a theory fails to account for the spiral propagation character of the wave (although on a flame photograph such a hypothetical wave would exhibit the undulating front of a spinning detonation). Furthermore, the dependence of pitch on tube diameter is not accurately explained. (Doering[9] attempts a qualitative explanation.) Nevertheless, the theories of Jost and Becker may be an accurate description of the nonuniform propagation of detonation waves in very small tubes.[6]

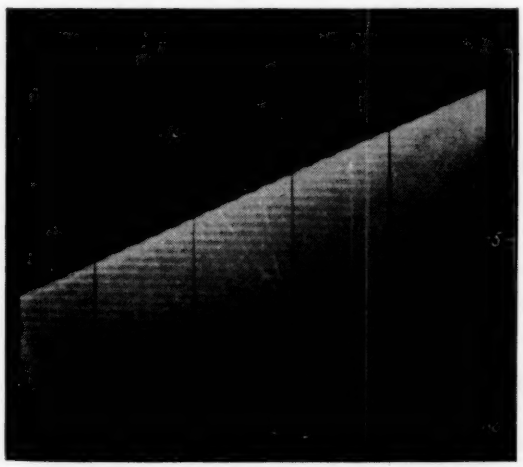

FIG. 1. Moving film photograph of spinning detonation in a $2CO+O_2$ mixture (Bone and Fraser[4]).

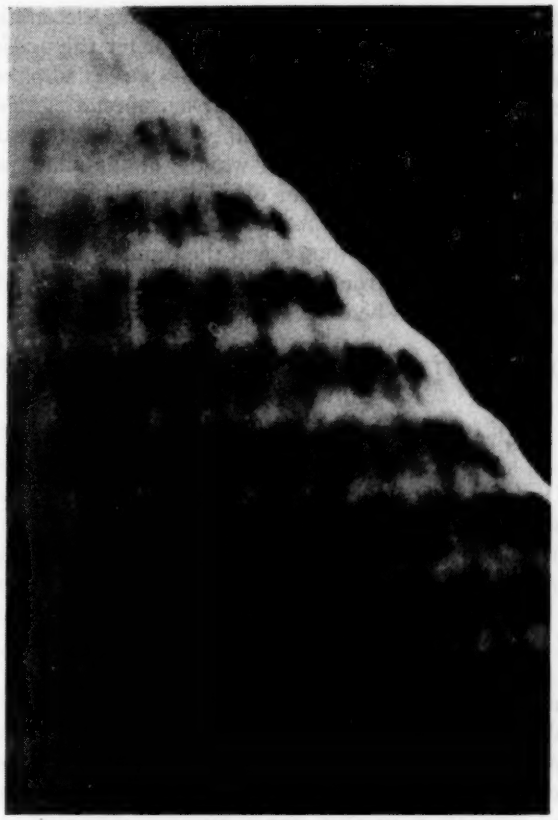

FIG. 2. Moving film photograph of spinning detonation in a $2CO+O_2$ mixture (Bone, Fraser, and Wheeler[6]). Especially evident are patterns of forward and backward moving luminous tracks, the ratio of such occurrence to spin frequency being about 1.8.

Bone, Fraser, and Wheeler[6] make an interesting observation in connection with one of their photographs taken with a high speed rotating mirror camera (reproduced in Fig. 2). In addition to the nearly horizontal and rather prominent striations normally present in spin pictures, two other systems of luminous paths are evident. One runs forward in the direction of detonation and evidently is the path of the burned particles accelerated by the detonation wave; the other runs backward and is considered to be the familiar retonation wave observable during the initiation of detonation. Bone, Fraser, and Wheeler state that two such pairs of forward and backward running traces originate with each spin, and that the intersection of these on the film form the prominent nearly-horizontal striations commonly seen on spin photographs. Accordingly, the latter would not be physically meaningful.

Such an interpretation of the spin photograph fails completely to account for the type of striation obtained

[7] W. Jost, *Explosion and Combustion Processes in Gases* (McGraw-Hill Book Company, Inc., New York, 1946).

[8] R. Becker, Z. Elektrochem **42**, 457 (1936).

[9] W. Doering, Ann. Physik **43**, 421 (1943).

by Campbell and Finch when a spinning detonation wave passed through a conical tube, or for the persistence of the striation after a detonation wave had passed out an open end of the tube.[2] Furthermore, a close examination of Fig. 2 unmistakeably shows that the ratio of the number of retonation waves (or luminous particle paths) to the number of spin undulations is not two but more nearly 1.8. Accordingly, the number of striations would not then equal the number of undulations of the wave front. (A possible explanation for this phenomenon will be discussed in Sec. VI.)

III. VIBRATIONAL FREQUENCY IN DETONATION WAKE

Of all the characteristics of spinning detonation, the most striking are its periodic nature and the dependence of spin frequency on tube diameter. These properties suggest that spinning detonation is closely associated with a natural vibration of the gas particles behind the detonation wave such that the characteristic frequency is principally determined by the transverse dimensions of the tube.

The general case of three-dimensional vibrations in the wake of the detonation will be considered. For the sake of simplicity, it will be assumed that the wake is uniform in temperature and pressure (except for vibrational effects). Actually, a plane expansion wave follows the detonation, cooling the combustion products, but this effect will be ignored for the present.

In order to determine the natural vibrational frequency of the combustion products behind a detonation wave, it is necessary to consider the vibrations to be sound waves; that is, waves of very small amplitude. Pressure measurements of spinning detonation[5] show that such waves have a considerable amplitude so that sound wave theory would appear to be inapplicable. The lack of a three-dimensional finite amplitude wave theory leaves no alternative but to use the linear sound theory, gauging its accuracy by comparison with experimental observations. It is probable that the error in the natural frequency as determined from the approximate (sound) theory is not so great as that in the wave form and amplitude. Where the frequency is of principal interest, the approximation may be acceptable.

TABLE I. Comparison of measured and calculated ($Z=\infty$) pitch-diameter ratios for the fundamental mode ($n=1$) of spinning detonation in circular pipes (measurements by Bone, Fraser, and Wheeler[6]).

Mixture	Tube diam (mm)	Pitch/Diam measured	Ratio calculated
$2CO+O_2$	3.62	3.28	3.08
$2CO+O_2$	4.15	3.23	3.08
$2CO+O_2$	12.8	3.00	3.08
$2CO+O_2$	13.0	3.04	3.08
$2CO+O_2$	15.2	2.90	3.08
$2CO+O_2$	25.4	2.95	3.08
$3CO+O_2$	25.5	3.15	3.04
$CO+N_2O$	12.8	2.97	3.05

The theory of the natural vibrations of a uniform gas in a cylindrical duct was treated by Rayleigh.[10] Under the usual assumptions of sound theory, the equation for the velocity potential ϕ (in cylindrical coordinates) is

$$\frac{\partial^2\phi}{\partial r^2}+\frac{1}{r}\frac{\partial\phi}{\partial r}+\frac{1}{r^2}\frac{\partial^2\phi}{\partial\theta^2}+\frac{\partial^2\phi}{\partial z^2}=\frac{1}{a^2}\frac{\partial^2\phi}{\partial t^2}, \tag{1}$$

where $a=$velocity of sound.

The space derivatives of the velocity potential ϕ define the vibrational velocities of the gaseous products behind the detonation wave with respect to axes which move with the mean velocity of such gases. The normal detonation front, therefore, moves in the z direction with a velocity a (this velocity being determined by the Chapman-Jouquet condition.[11])

An appropriate solution of the wave equation is

$$\phi_n=\cos\left\{n\theta+2\pi\left(\nu-\frac{a}{l}\right)t+\frac{2\pi z}{l}\right\}\times J_n\left[\frac{2\pi r}{a}\left(\nu\left(\nu-2\frac{a}{l}\right)\right)^{\frac{1}{2}}\right]. \tag{2}$$

This solution describes a wave whose crest rotates at a uniform angular velocity about the tube axis and has a wave length l in the z direction. At the detonation front ($z=at$) the characteristic frequency is ν. The frequency at a fixed point of the tube is less than that at the detonation front, which is characteristic of the striation frequency observed on photographs. The number of circumferential crests or wavelengths is given by the modal number n.

The wavelength l and the frequency ν must be chosen so as to satisfy the two boundary conditions:

1. At the tube wall ($r=r_0$) the radial component of vibrational velocity must be zero.

2. At the detonation front, the changes in pressure and velocity due to the gaseous vibration must satisfy the conditions imposed by the combustion process, which is the energy source of the vibration.

From the first boundary condition there is obtained

$$\partial\phi/\partial r=0 \quad \text{at} \quad r=r_0$$

or

$$\frac{2\pi r_0}{a}\left[\nu\left(\nu-2\frac{a}{l}\right)\right]^{\frac{1}{2}}=k_{nm}, \tag{3}$$

where

$$J_n'(k_{nm})=0. \tag{4}$$

k_{nm} is the mth zero of the first derivative of the Bessel function J_n, the index m being the number of radial

[10] Lord Rayleigh, *Theory of Sound* (Dover Publications, New York, 1945).

[11] W. Doering and G. Burkhardt, "Contributions to the theory of detonation," transl. Technical Report No. F-TS-1227-IA (GDAM A9-T 46), Air Material Command (1949).

nodes (point of no radial velocity). Since spinning detonations in circular tubes apparently have a "head" (node) only at the wall, m will subsequently be considered to be unity. The values of $k_n = k_{n1}$ for the first few modes are

n	1	2	3	4	5
k_n	1.841	3.054	4.201	5.35	6.35.

The second boundary condition will determine the relation between the vibrational pressure and velocity at the detonation wave. By defining a dimensionless quantity Z called the "specific acoustic impedance" as

$$Z=\frac{1}{\rho a}\left\{\frac{\text{vibrational wave pressure}}{\text{vibrational velocity}}\right\}_{z=at}$$
$$=\frac{1}{\rho a}\left\{\frac{-(1/\rho)(\partial\phi/\partial t)}{\partial\phi/\partial z}\right\}_{z=at}, \tag{5}$$

where ρ = density, then by using Eq. (2) in (5) there results

$$Z=1-\nu l/a. \tag{6}$$

Equation (3) for the vibrational frequency at the detonation front becomes

$$\nu=(ak_n/2\pi r_0)[(Z-1)/(Z+1)]^{\frac{1}{2}}, \tag{7}$$

where r_0 = tube radius.

By combining the above two equations, Z can also be given as

$$Z=-[(k_n l/2\pi r_0)^2+1]^{\frac{1}{2}}. \tag{8}$$

The negative sign of Z results from Eq. (6), if account is taken of the fact that photographic measurements show that ν is greater than a/l (see Fig. 1). l is usually at least 30 tube diameters, so that Z is approximately -20. The value of ν in Eq. (7) is only slightly changed if Z is considered to be infinite, rather than equal to -20. An infinite value of Z would result from no axial velocity, so that the vibrational motion would be only two dimensional. *The experimental evidence thus indicates that the vibrational motion is almost entirely transverse.*

IV. COMPARISON WITH EXPERIMENT

By virtue of the foregoing analysis, it is possible to compare the natural vibrational frequency in a detonation wave with the measured frequency of spin. For this comparison Z will be assumed infinite; i.e., the vibration will be considered transverse (two-dimensional).

It is customary to describe the spinning detonation in terms of the ratio of spin pitch to tube diameter rather than to give the spin frequency. The pitch P is related to the frequency ν and the velocity of propagation D of the detonation wave by

$$P=D/\nu. \tag{9}$$

TABLE II. Comparison of measured and calculated ($Z=\infty$) "apparent" pitch-diameter ratios for both fundamental ($n=1$) and higher modes of spinning detonation in circular pipes (measurements by Bone, Fraser, and Wheeler[6]).

Mixture	Tube diam (mm)	Apparent pitch/diam ratio Measured	Calculated	n
$2CO+O_2$	13	3.04	3.08	1
$2CO+O_2+\frac{1}{22}(2H_2+O_2)$	13	2.96	3.08	1
$2CO+O_2+\frac{1}{16}(2H_2+O_2)$	13	1.11	1.06	4
$2CO+O_2+\frac{1}{8}(2H_2+O_2)$	13	0.86	0.89	5
$2CO+O_2$	41	1.10	1.06	4
CH_4+O_2	13	1.92	1.89	2
CH_4+O_2	13	1.74	1.89	2
CH_4+O_2	13	0.87	0.91	5

The pitch-diameter ratio is accordingly

$$P/d=P/2r_0=(\pi D/ak_n)[(Z+1)/(Z-1)]^{\frac{1}{2}}. \tag{10}$$

Doering and Burkhardt[11] give the following expression for the specific volume change across the normal detonation wave:

$$\frac{v_1}{v_0}=\frac{\gamma_0+1}{2\gamma_0}+\left[\left(\frac{\gamma_0+1}{2\gamma_0}\right)^2-\frac{M_2T_1}{\gamma_0M_1T_2}\right]^{\frac{1}{2}}, \tag{11}$$

where v = specific volume, T = temperature, γ = ratio of specific heats, M = molecular weight, 1 = state before detonation wave, and 0 = state behind normal detonation wave. From the Chapman-Jouquet condition, the equation of continuity becomes

$$a_0/v_0=D/v_1. \tag{12}$$

Substituting this and Eq. (11) in (10),

$$\frac{P}{d}=\frac{\pi}{k_n}\cdot\frac{\gamma_0+1}{\gamma_0}\left[\frac{Z+1}{Z-1}\right]^{\frac{1}{2}}\left\{\frac{1}{2}+\left[\frac{1}{4}-\frac{\gamma_0M_2T_1}{(\gamma_0+1)^2M_1T_2}\right]^{\frac{1}{2}}\right\}. \tag{13}$$

Since T_0 is much greater than T_1, and assuming Z is infinite, the pitch diameter ratio should be given approximately for all gases by

$$P/d\approx[\pi(\gamma_0+1)/\gamma_0k_n]. \tag{14}$$

For $\gamma_0=1.2$ and $n=1$, the pitch-diameter ratio is 3.13 which is close to the value of 3 measured by Campbell and Woodhead.[1]

Table I compares the calculated pitch-diameter ratio for the fundamental mode of spin in circular pipes (assuming infinite Z) with those values measured by Bone, Fraser, and Wheeler.[6]

If a higher harmonic of the transverse pressure wave predominates, a multiple-headed spin will appear, a phenomenon which is sometimes observed. A comparison of the theoretical and measured "apparent" pitch/diameter ratios is given in Table II, the "apparent" pitch being defined as the detonation velocity divided by the spin frequency. (The actual pitch of each head is n times the apparent pitch, where n is the number of heads.)

Bone, Fraser, and Wheeler[6] have investigated spinning detonation in a $2CO+O_2$ mixture in ducts of triangular, square, and rectangular cross sections. The flame photographs have an appearance similar to that of a spinning detonation in a circular tube, so that it is claimed that the luminous head still follows a more or less spiral track in the noncircular ducts. No phasing photographs, such as those made by Campbell and Finch,[2] were obtained so that it is not certain that a spiral progression of the detonation wave actually exists. On the contrary, it will be seen that, according to the hydrodynamic theory previously advanced, no such spiral propagation would exist.

For a rectangular cross section, of width w and height h, the sound theory velocity potential equation becomes

$$\frac{\partial^2\phi}{\partial x^2}+\frac{\partial^2\phi}{\partial y^2}+\frac{\partial^2\phi}{\partial z^2}=\frac{1}{a^2}\frac{\partial^2\phi}{\partial t^2}. \tag{15}$$

The boundary condition which defines zero normal velocity at the walls of the tube is

$$\partial\phi/\partial x=0 \quad \text{at} \quad x=0, \quad x=w$$
$$\partial\phi/\partial y=0 \quad \text{at} \quad y=0, \quad y=h.$$

A solution of (15) satisfying these boundary conditions is

$$\phi_{nm}=\cos\frac{n\pi x}{w}\cos\frac{m\pi y}{h}\cos 2\pi\left\{\left(\nu-\frac{a}{l}\right)t+\frac{z}{l}\right\}, \tag{16}$$

where

$$\nu=\frac{a}{2}\left[\frac{n^2}{w^2}+\frac{m^2}{h^2}+\frac{4}{l^2}\right]^{\frac{1}{2}}-\frac{a}{l}, \tag{17}$$

n, m = integer.

The boundary condition at the detonation wave gives the same relation [Eq. (6)] as for the circular duct, so that (17) becomes

$$\nu=\frac{a}{2}\left[\frac{n^2}{w^2}+\frac{m^2}{h^2}\right]^{\frac{1}{2}}\left[\frac{Z-1}{Z+1}\right]^{\frac{1}{2}}. \tag{18}$$

TABLE III. Comparison of measured and calculated ($Z=\infty$) "apparent" pitch of spinning detonation in ducts of noncircular cross section (measurements by Bone, Fraser, and Wheeler[6]).

Section	Size (cm)	Apparent pitch (cm) Measured	Calculated	Adjacent modes	n	m
Square	1.2 ×1.2	4.10	4.33	3.06	0	1
Rectangle	0.98×1.2	4.20	4.33	3.54	0	1
Rectangle	1.1 ×2.2	3.75	3.96	3.54	1	0
Rectangle	1.35×2.2	7.28	7.94	4.15	0	1
Rectangle	2.4 ×3.0	3.23	3.37	3.59	2	2
				2.87		
		4.5	4.59	5.39	1	2
				4.31		
Equilateral triangle	1.7 (side)	5.08	4.60	2.66	1	0
Equilateral triangle	2.3 (side)	6.7–8.0	6.21	3.59	1	0

Such a solution [Eq. (16)] is a standing wave similar to that obtained in the transverse vibration of a plate or membrane. On the other hand, in a circular cross section a progressive wave is possible, in which the crest rotates at constant angular velocity about the axis of tube (actually, a superposition of many standing waves slightly phased with respect to each other). In the former case, the "head" of the detonation would appear and disappear regularly at the pressure antinodes, but would not progress regularly from one to another. If w and h are commensurate so that more than one mode is possible for the same frequency, and if all modes are present, then the "head" will appear to progress more regularly. In any case, a flame photograph would show all the characteristics of a spinning detonation in a circular tube.

The theoretical pitch of the spin (assuming infinite Z) in noncircular ducts is compared in Table III with the experiments of Bone, Fraser, and Wheeler.[6] The mode is specified by the numbers n and m, those modes being chosen which gave the closest agreement with experiment. Note that in most cases only the "unmixed" modes appear (n or m equals zero). The next higher and lower mode is also given for comparison. The pitch for the duct of triangular cross section was calculated following the solution of Lamé[12] for a vibrating membrane.

A series of interesting experiments was performed by Campbell and Finch[2] who suspended a circular rod along the axis of a circular tube. A spinning detonation wave in such an annulus possessed a greater pitch than one in the unobstructed tube (ascribed by Campbell and Finch to frictional effects). Such an effect is readily accounted for by the hydrodynamic theory in the solution of the wave equation for an annulus.

Choosing the following solution of the wave equation (1) in cylindrical coordinates,

$$\phi_n=\cos\left[n\theta+2\pi\left(\nu-\frac{a}{l}\right)t+2\pi\frac{z}{l}\right]\times\left\{c_1J_n\left\{\frac{2\pi r}{a}\left[\nu\left(\nu-2\frac{a}{l}\right)\right]^{\frac{1}{2}}\right\}+c_2N_n\left\{\frac{2\pi r}{a}\left[\nu\left(\nu-2\frac{a}{l}\right)\right]^{\frac{1}{2}}\right\}\right\}, \tag{19}$$

the vanishing of the radial velocity at the walls results in the following conditions:

$$c_1\frac{d}{dr}J_n\left\{\frac{2\pi r}{a}\left[\nu\left(\nu-2\frac{a}{l}\right)\right]^{\frac{1}{2}}\right\}+c_2\frac{d}{dr}N_n\left\{\frac{2\pi r}{a}\left[\nu\left(\nu-2\frac{a}{l}\right)\right]^{\frac{1}{2}}\right\}=0 \tag{20}$$

at $r=r_i$ and $r=r_0$.

[12] Lamé, *Lecons sur la théorie mathématique de l'élasticité des corps solides* (Bachelier, Paris, 1859).

Since c_1 and c_2 are both not zero, it is necessary that

$$J_n'\left\{\frac{2\pi r_i}{a}\left[\nu\left(\nu-2\frac{a}{l}\right)\right]^{\frac{1}{2}}\right\}\cdot N_n'\left\{\frac{2\pi r_0}{a}\left[\nu\left(\nu-2\frac{a}{l}\right)\right]^{\frac{1}{2}}\right\}=J_n'\left\{\frac{2\pi r_0}{a}\left[\nu\left(\nu-2\frac{a}{l}\right)\right]^{\frac{1}{2}}\right\}\cdot N_n'\left\{\frac{2\pi r_i}{a}\left[\nu\left(\nu-2\frac{a}{l}\right)\right]^{\frac{1}{2}}\right\}. \quad (21)$$

This condition, together with Eq. (6), determines ν as a function of r_0/r_i and the modal number n.

Figure 3 shows the relation between the pitch/outer diameter ratio and the inner diameter/outer diameter ratio for $n=1$ and $Z=\infty$ with radial nodes at the two walls only. The experimental measurements of Campbell and Finch[2] are shown for comparison.

An examination of the calculated and experimental values of spin pitch in Tables I through III, and in Fig. 3, shows that the calculated values are, on the average, 3 percent to 6 percent higher than those measured. If, instead of assuming Z to be infinite, a value of -20 or -30 were used (as determined in section C) better agreement would be obtained. Considering the fact that spin measurements are not exactly reproducible, the calculations modified for a finite Z may agree within the limits of experimental error.

For all the foregoing examples it can be seen that there is good agreement between experiment and the hydrodynamic theory. However, there are two exceptions which require further explanation:

(a) A detonation wave "forced" in pure acetylene has a pitch diameter ratio 4 or greater.[4] The fact that acetylene cannot support a normal detonation wave and that large quantities of solid carbon are precipitated may have some effect.

(b) Spinning detonation in certain helium diluted hydrogen-oxygen mixtures has a pitch of more than six tube diameters.[13] This may be a purely radial (axially symmetric) vibration, whose theoretical pitch is slightly more than six tube diameters. Unfortunately, no further information on this type of spinning detonation is available.

There are several indications that plane longitudinal waves can propagate through the region of predominantly transverse vibration without appreciably affecting the latter. When a spinning detonation wave passes out of an open end, the striations in the wake are not destroyed by the expansion wave which is reflected from the end.[2] Also, the persistence of the striations for some distance behind a spinning detonation shows that the expansion wave following the latter has very little effect upon the predominantly transverse motion.

[13] From a private communication from W. E. Gordon.

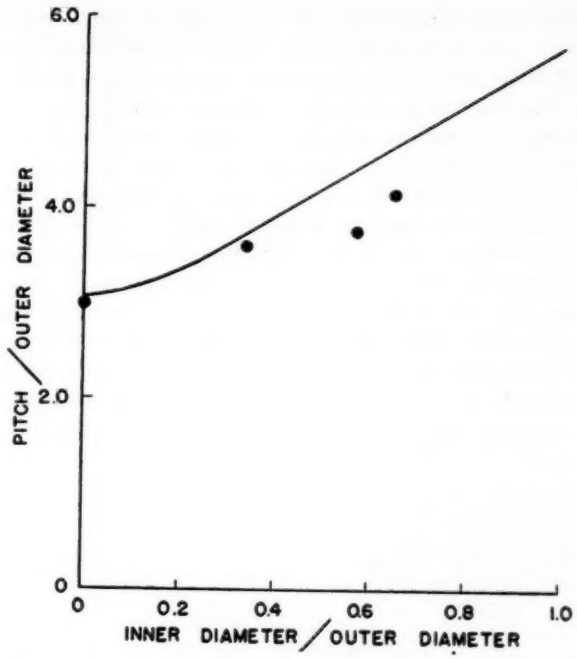

FIG. 3. Comparison of measured and calculated pitch/diameter ratios of spinning detonation in a circular annulus. (Measurements by Campbell and Finch[2]).

V. DETERMINATION OF IMPEDANCE

Although experimental evidence shows that the impedance Z is large and that the vibratory motion is principally transverse, there is no obvious reason for such a condition to exist. Some explanation is possible, however, if we consider the case of forced three-dimensional oscillations of a gas in a pipe.

Following Morse,[14] suppose that a three-dimensional wave is generated by a piston at $z=0$ such that its velocity potential ϕ is given by

$$\phi_n=\cos[n\theta+(2\pi z/l)+2\pi\omega t]J_n(\alpha r). \quad (22)$$

Such a wave satisfies the wave Eq. (1) if the following condition holds:

$$\alpha^2+(2\pi/l)^2=(2\pi\omega/a)^2. \quad (23)$$

Also, from the condition of zero radial velocity at the wall,

$$\alpha r_0=k_n. \quad (24)$$

Substituting these conditions in Eq. (5),

$$Z=-\omega/(\omega^2-\omega_n^2)^{\frac{1}{2}} \quad (25)$$

where

$$\omega_n=k_n a/2\pi r_0. \quad (26)$$

If the frequency of the forced motion is the same as one of the natural frequencies of transverse vibration (ω_n), then Z becomes infinite; that is, the vibrational energy is stored in transverse rather than longitudinal motion. If the exciting disturbance has harmonic components of many frequencies, then the nonresonant

[14] P. M. Morse, *Vibration and Sound* (McGraw-Hill Book Company, Inc., New York, 1948).

frequency components will propagate as three-dimensional waves down the tube, while the resonant components will produce only transverse motion. The effect of the pipe walls is thus to convert three-dimensional waves of certain frequencies into two-dimensional (transverse) waves of the same (natural) frequency.

If the pipe walls are not rigid, so that the radial velocity is not zero at the wall, then Z will be finite (see reference 14). If the pipe wall frequency is much higher than the spin frequency,[15] then it can be shown that for the fundamental mode Z becomes negative and is of the proper order of magnitude. Because of lack of exact data, it cannot be said with certainty that the finiteness of Z is due to the elasticity of the walls.

VI. NATURE AND STRUCTURE OF SPINNING DETONATION WAVE

Having shown the close correspondence between the frequency of spinning detonation and that of gaseous vibrations in the detonation wake, it is desirable to show how and why such vibrations could arise in light of what is believed to be true regarding the process of combustion.

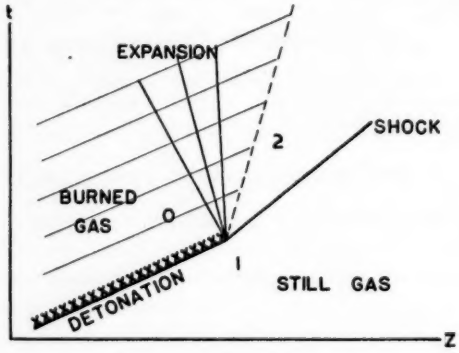

FIG. 4. Space-time diagram illustrating the degeneration of a plane detonation wave into a shock and an expansion wave when combustion ceases abruptly. The shock is propagated forward into unburned bas and an expansion wave travels backward through the burned gases.

It is universally acknowledged that the combustion in the detonation wave is a spontaneous reaction induced by the heat generated in the shock wave which precedes it; that is, the propagation of the reaction is little affected by conduction or diffusion. From a hydrodynamic viewpoint, any mixture capable of an exothermic change can support a detonation wave. However, weak mixtures would only generate a weak shock with insufficient heating to maintain a spontaneous chemical reaction, hence the existence of detonation limits.

It is also believed, although not quite so generally, that two other effects are present in a detonation wave: (a) an ignition lag between the time the reactant passes through and is heated in the shock wave and the time when combustion begins and (b) the loss of energy by heat conduction and friction. The latter only affects the detonation process if it occurs in the zone between the shock plane and the plane where combustion is just complete (Chapman-Jouquet plane). The experimentally observed effects of tube diameter and wall roughness on the detonation velocity are usually explained[11] by taking into account the energy losses which are thus determined by thermal conductivity, viscosity, and thickness of zone between shock and Chapman-Jouquet planes (as affected by ignition lag, and reaction rate).

Similar considerations are also present in the question of detonation limits. An energy loss in the combustion zone tends to reduce the detonation velocity and hence the shock wave heating. In turn the ignition lag (if any) increases and the reaction rate decreases due to the lower temperature, lengthening the combustion zone and increasing the energy loss. It can be seen that a detonation wave becomes unstable near the detonation limit since a slight increase in energy loss precipitates a chain of events which stops the combustion. Furthermore, it is probable that in any mixture near the limit of stability in this respect, the combustion rate could be increased and decreased with great rapidity by alternately cooling and heating the reactants immediately behind the shock plane.

It is interesting to show how, in a purely plane wave, an abrupt change in combustion rate can result in the generation of compression and expansion waves. Assuming that expansion and compression waves arise from the cessation and initiation of combustion, respectively, consider the following two cases:

(a) A normal detonation wave, progressing uniformly, suddenly ceases to produce combustion. It degenerates into a shock wave moving forward and an expansion wave moving backwards into the burned mixture (see Fig. 4).

(b) A shock wave propagating in a combustible mixture suddenly causes ignition. A detonation wave moving forward and a retonation moving backwards are both generated (see Fig. 5).

Case A

In order to determine the velocities and pressures involved, it is necessary to know the changes in pressure and particle velocity across the detonation, expansion, and shock waves. The uniformity of pressure and particle velocity in each of the regions *0*, *1*, and *2* (Fig. 4) then supplies sufficient conditions to enable the determination of all the quantities.

Assuming that the conditions behind the detonation wave *0* are given, as well as the initial conditions in region *1*, for the expansion and shock waves, respectively (from reference 11),

$$\frac{u_0-u_2}{a_0}=\frac{2}{\gamma_0-1}\left\{\left(\frac{P_2}{P_0}\right)^{\gamma_0-1/2\gamma_0}-1\right\} \tag{27}$$

$$\frac{u_2}{a_1}\approx\left[\frac{2}{\gamma_1(\gamma_1+1)}\frac{P_2}{P_1}\right]^{\frac{1}{2}}, \tag{28}$$

where u=particle velocity and P=pressure.

[15] For a thin-walled tube, the natural frequency of radial vibration is calculated to be about ten times the spin frequency.

For many detonation waves, the resulting expansion wave is weak. For a $2CO+O_2$ mixture, the author calculated the ratio P_2/P_0 to be 0.87.

Case B

If the initial shock strength is known so that the state 2 (Fig. 5) is also known, then the following conditions hold across the retonation wave (from reference 11):

$$u_2-u_0=a_0\{v_2/v_0)-1\} \tag{33}$$

$$P_0/P_2=(a_0/a_2)^2(\gamma_2/\gamma_0)(v_2/v_0) \tag{34}$$

$$\frac{v_2}{v_0}=\frac{\gamma_0+1}{2\gamma_0}+\left[\left(\frac{\gamma_0+1}{2\gamma_0}\right)^2-\frac{M_0T_2}{\gamma_0M_2T_0}\right]^{\frac{1}{2}} \tag{35}$$

$$\frac{T_0}{T_2}=\left(\frac{a_0}{a_2}\right)^2\left(\frac{\gamma_2M_0}{\gamma_0M_2}\right)$$

$$=\frac{(Q/\bar{C}_vT_2)+1}{1+(\bar{\gamma}-1/2)[\gamma_0(v_2/v_0)^2-2(\gamma_0+1)(v_2/v_0)+\gamma_0+2]}, \tag{36}$$

where $\bar{C}_v$ = average value of specific heat at constant volume, $\bar{\gamma}$ = ratio of average values of specific heats, Q = heat of reaction at constant volume, M = molecular weight, 2 = state before retonation wave, and 0 = state after retonation wave.

For a $2CO+O_2$ mixture, the author calculated the ratio P_0/P_2 to be 4.6, when P_2/P_1 is 17.7.

There are other possible mechanisms giving a reaction of the same nature as case *B*. For example, detonation and retonation waves may originate some distance behind the shock front. Also, combustion may occur simultaneously over a large region (constant volume combustion), so that a backward moving compression wave is formed much like the action of a shock tube. In any case, the qualitative picture is the same.

It can thus be seen that there are two possible mechanisms at work in a spinning detonation wave: (a) the variation of reaction rate by pressure waves and (b) the generation of pressure waves by a changing reaction rate. Under the proper conditions, a self-excited vibration could easily be sustained.

From these considerations and those resulting from the analysis of the spin frequency, the following description of a spinning detonation wave appears to be the most likely:

1. A periodic pressure wave alternately heats and cools the combustible gases passing through the shock wave forming the front of the detonation.
2. During the low pressure period of the cycle a quantity of slowly reacting combustible accumulates behind the shock. During the high pressure period, the reaction rate increases sufficiently to burn quite rapidly this unburned gas, thereby generating a strong compression (or retonation) wave.
3. The compression wave excites natural vibrations of the product gases in the tube, reinforcing that vibrational mode whose frequency corresponds to the rate at which combustion may be advanced or retarded by heating or cooling.

This describes a self-excited vibration which can only persist when the changes in reaction rate due to the heating and cooling by pressure waves are sufficiently great to allow the accumulation of unburned gas behind the shock front which is then followed by a very rapid ignition. Such a condition is generally considered to exist near the limit of detonation.

The transient spinning detonation which sometimes appears at the initiation of detonation in nonspinning mixtures[4] aptly illustrates how this effect, although present in normal mixtures when excited by uneven combustion, is not self-perpetuating.

The role of energy losses by friction or cooling is not a necessary one for the spinning process described above, although it may affect the appearance of spinning in the same manner as it affects the limits of detonation. It may, however, be important in initiating spin, if it is assumed that the energy losses are not uniform around the circumference of the tube, thereby giving rise to transverse disturbances which excite the spinning process.

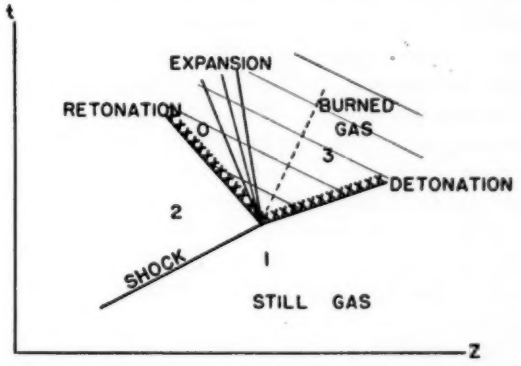

FIG. 5. Space-time diagram showing the initiation of combustion immediately behind a plane shock wave. A detonation wave propagates forward, and a retonation wave backward, into unburned gas.

There is also a possibility that wall friction or cooling is instrumental in causing the purely radial mode since the latter appears in helium diluted mixtures not too close to the detonation limits. In this connection, one might advance the following hypotheses concerning spinning detonation:

1. Helical spin ordinarily appears in a mixture in which a plane detonation could not propagate because its shock-heating would be insufficient to induce combustion in a reasonable length of time.
2. If wall effects are sufficiently strong, they may induce spin in mixtures in which plane detonation waves could propagate in the absence of wall effects.

The number of heads which appear in a spinning detonation is probably closely associated with the frequency with which the chemical reaction rate can be advanced and retarded by the pressure wave. This is apparent from a study of Table II, from which it can be seen that the addition of increasing amounts of

$2H_2+O_2$ to a moist $2CO+O_2$ mixture caused the development of higher harmonic spins in the same tube. (When sufficient $2H_2+O_2$ was added, the spin disappeared.) Again, by increasing the tube diameter for a $2CO+O_2$ mixture, a higher harmonic spin developed whose frequency was very nearly the same as that for the fundamental spin in the smaller tube (Table II).

The development of a progressive, rather than a standing, wave in the circular tube is probably due to the more continuous propagation of the combustion zone afforded by the former. A standing wave is not precluded, however, and the peculiar secondary wave in Fig. 2 is probably a standing wave of the second mode. (Its frequency is theoretically 1.65 times the fundamental, which compares favorably with that of 1.8 measured). For a standing wave, the retonation and particle paths are the same as those seen in nonspinning photographs. The nearly horizontal striations of spinning photographs could be called "progressive retonations."

The periodic nature of combustion during spinning will result in a distortion of the detonation shock front so that it is no longer plane, although it must always be normal to the tube walls at the boundary. A private communication from G. B. Kistiakowsky of Harvard University states that comparison of flame photographs and pressure records shows that the shock wave and the luminous head (measured at points 90 degrees apart in the same cross section) are not in the same plane. A spark photograph by Bone, Fraser, and Wheeler[6] also indicates that the shock wave preceding a spinning detonation is far from plane.

If the negative portion of the pressure wave results from the process pictured in Case *A* above, and if it is assumed that such a condition exists for half of the cycle, then an average slope of the shock front (with respect to a plane normal to the tube axis) may be estimated by considering the difference in propagation rates during one quarter of the cycle:

$$\text{slope}=D-M/4\nu r_0=\pi(D-M)/2ak_n,$$

where ν was obtained from Eq. (11) for $Z=\infty$ and M is the shock wave velocity.

For a $2CO+O_2$ mixture, the slope was calculated to be 0.4.

AUTHOR'S NOTE

After preparing the above for publication, the author's attention was called to a book by N. Manson entitled: "Propagation des détonations et des déflagrations dans les mélanges gaseux" published jointly by L'Office National d'Etudes et des Recherches Aeronautiques and L'Institut Français des Pétroles (Paris, 1947). This latter contains a treatment of spinning detonation which is similar to that above in some respects, but there are major differences in interpreting the nature of the phenomenon.

Manson considers a purely transverse vibratory motion in the wake of the detonation wave, obtaining good agreement with the measured values of spin frequency. In interpreting the potential solution, it is claimed that the gas particles move across the tube, those near the walls tracing a helicoidal path along its surface. However, the potential solution describes only small vibratory motions about a mean position, so that a particle does not wander far from its mean (coaxial) path in the detonation wake. The crest of the wave (pressure peak and luminous region) does follow a helical path, yet it is not necessary for the medium as a whole to follow such a path. Furthermore, it can be shown that the net angular momentum of the motion described by the potential solution is zero, so that such a motion does not violate the laws of mechanics.

According to Manson, the vibratory motion is transverse since the wave front moves at sonic speed with respect to the wake and cannot be influenced by the latter. Such a viewpoint requires that the exciting disturbance also be transverse, which is a severe restriction. In the author's analysis it is shown how a general three-dimensional disturbance can give rise to predominantly transverse motion.

The analysis of Fig. 2 above as given by Bone, Fraser, and Wheeler[6] to the effect that a double series of forward and backward running luminous tracks form the prominent features of the spin photograph is accepted by Manson. In his interpretation the luminous front is visible twice in a cycle, once on the near side and once on the far side of the tube, resulting in a double series of "paths." However, the phasing photographs of Campbell and Finch[2] definitely show that only events on the near side of the tube are clearly seen. From the description afforded by the potential solution, the interpretation of the spinning photographs is unambiguous: the undulating front and nearly horizontal striae are due to the passage of the point of peak pressure in the wave (made luminous by the higher temperature existing in the wave "crest") across the near side of the tube (window).

From the author's point of view, the source of energy for the vibratory motion is the sudden combustion of partially burned material which accumulates behind the front during the low pressure portion of the cycle. Such uneven heat release cannot arise without the heating and cooling effects of the pressure wave which it excites. On the other hand, Manson considers the energy source of vibratory motion to be the exchange of internal molecular energy as a state of equilibrium is established, irrespective of the presence of a pressure wave. While such may be a part, or the whole of the energy source, it is the author's opinion that the exciting effect of the pressure wave is essential to the existence of spinning detonation.

In computing the natural frequencies in the detonation wake, Manson obtained better agreement by assuming, in some instances, the existence of more than one radial node (m greater than one). Because of the close spacing of the roots k_{nm} for the higher modes, it would be difficult to distinguish among them on the basis of frequency alone. In the above analysis it is merely shown that satisfactory agreement is possible under the assumption that only one radial node exists.

Calculation of Some Electronic Energy Levels of Sulfur Hexafluoride*

A. B. F. DUNCAN
University of Rochester, Rochester, New York
(Received July 24, 1950)

An attempt has been made to calculate the coefficients in LCAO molecular orbital functions of SF_6, and ionization and excitation energies of this molecule, using a self-consistent field method. The lowest ionization potential computed is 20.1 ev. Excitation energies to some forbidden and allowed levels are obtained, but are too large to be considered trustworthy. The present treatment was restricted in detail to twelve electrons, six from the sp^3d^2 valence configuration of sulfur, and six $2p\sigma$ of fluorine. The other electrons were treated in smoothed-out core potentials of the sulfur and fluorine atoms. It is believed that unexpectedly large errors may have been introduced by the neglect of detailed interactions of these electrons, and that the molecular orbitals in which they might be put are of importance.

The present calculation is purely theoretical and only the empirical value of the S–F bond distance has been used. All necessary integrals have been evaluated, most of them for the first time, and are collected in tables.

SULFUR hexafluoride is one of the few molecules known definitely to have octahedral symmetry, and and the possibility of theoretical treatment appeared to be somewhat promising because of this high symmetry, in spite of the large number of electrons present. Calculations on some of the ground-state molecular orbitals and on some excitation energies are reported here, based on a self-consistent field molecular orbital method. The molecular orbitals are approximated by linear combinations of atomic orbitals (LCAO), as is usual.

The octahedral structure of SF_6 was shown directly by electron diffraction in the vapor.[1] According to this investigation, the S–F distance is 1.58A, which is the only empirical data used in these computations. The geometrical structure of a regular octahedron is confirmed amply by spectroscopic evidence.[2]

Since these computations were begun, a theoretical treatment of the ground state of the CO_2 molecule by Mulligan[3] has appeared, which is based on the general self-consistent field methods developed by Mulliken[4] and Roothaan.[5] Exactly the same method has been followed in the present paper. Mulligan has given an excellent review of previous molecular orbital calculations, with many references, as well as a clear outline of LCAO self-consistent field theory. In view of Mulligan's paper, it does not appear necessary to refer extensively to previous work. For the same reason it is not necessary to discuss the general theory in detail but instead the discussion will be confined to points of specific interest in connection with SF_6.

ELECTRONIC STRUCTURE OF SULFUR HEXAFLUORIDE. STATEMENT OF THE PRESENT PROBLEM

A general treatment would consider 70 electrons. Of these, 22 will be in the inner shells of sulfur (10) and the six fluorines (12). It will be assumed that the 22 inner shell electrons will move essentially in atomic orbitals, or linear combinations of these, which will have energies high in comparison with the other molecular orbitals of the molecule. Consequently (as a doubtful approximation), we neglect interaction energy between inner shell and valence shell orbitals.

The remaining 48-electron problem is still far too complicated, principally because of the 42 fluorine valence electrons in $2s$ and $2p$ orbitals. At this point we shall discuss briefly the bonding properties of these electrons.

The usual valence state of fluorine belongs to the configuration[6] $s^2\pi_x^2\pi_y^2\sigma$. Local axes attached to each fluorine may be chosen so that each σ is directed toward the central atom along one of the fourfold axes of the molecule, along which we suppose the principal bonding occurs. We consider next the construction of "bonding" molecular orbitals. Such orbitals will not, of course, be concentrated along the bonds of valence-bond theory, but will be spread out through the molecule. There will occur, however, a greater overlapping of charge distributions in the regions between S and F for these bonding orbitals. The molecular orbitals (φ_l) must conform to the symmetry properties of the molecule, and transform like the representations of the group O_h.

We begin with six linear combinations of σ_i which transform like the representations of O_h. The linear combinations (ρ_l) were found with the aid of group theory, and are (with transformation properties indicated):

$$\begin{aligned}
\rho_1(A_{1g}) &= (6)^{-\frac{1}{2}}(\sigma_1+\sigma_2+\sigma_3+\sigma_4+\sigma_5+\sigma_6)\\
\rho_2(E_g) &= (12)^{-\frac{1}{2}}(2\sigma_1-\sigma_2-\sigma_3-\sigma_4-\sigma_5+2\sigma_6)\\
\rho_3(E_g) &= (2)^{-1}(\sigma_2-\sigma_3+\sigma_4-\sigma_5)\\
\rho_4(F_{1u}) &= (2)^{-\frac{1}{2}}(\sigma_1-\sigma_6)\\
\rho_5(F_{1u}) &= (2)^{-\frac{1}{2}}(\sigma_2-\sigma_4)\\
\rho_6(F_{1u}) &= (2)^{-\frac{1}{2}}(\sigma_3-\sigma_5).
\end{aligned} \tag{1}$$

Subscripts on σ correspond to a numbering of fluorine atoms. The fluorine atoms are numbered $1\cdots6$, re-

* This work was supported in part by the ONR, Contract N6onr-241, Task Order 10, with the University of Rochester.

[1] L. Pauling and L. O. Brockway, Proc. Natl. Acad. Sci. U. S. 19, 68 (1933).

[2] G. Herzberg, *Infrared and Raman Spectra* (D. Van Nostrand Company Inc., New York, 1945), p. 336.

[3] J. F. Mulligan, J. Chem. Phys. 19, 347 (1951).

[4] R. S. Mulliken, J. chim. phys. 46, 497 (1949); 46, 675 (1949).

[5] C. C. J. Roothaan, Revs. Modern Phys. 23, 69 (1951).

[6] R. S. Mulliken, J. Chem. Phys. 2, 782 (1934).

ferring to a Cartesian coordinate system, where positive z, x, y are directed from the central S atom at the origin toward F atoms 1, 2, 3 and $-x, -y, -z$ are directed toward F atoms 4, 5, 6. The choice of linear combinations is not unique, of course, in the degenerate cases E_g and F_{1u}.

The ρ_l are to be combined with atomic orbitals of sulfur (χ_l) which have corresponding transformation properties. The orbitals are

$$\chi_1(A_{1g})=(3s) \qquad \chi_4(F_{1u})=(3p_z)$$
$$\chi_2(E_g)=(3d_{z^2}) \qquad \chi_5(F_{1u})=(3p_x)$$
$$\chi_3(E_g)=(3d_{x^2-y^2}) \qquad \chi_6(F_{1u})=(3p_y).$$

The resulting linear combinations of the ρ_l and χ_l will be the molecular orbitals, and will be of the form $\varphi_l=a_l\chi_l+b_l\rho_l$. They will of necessity be symmetry orbitals and belong to representations of the group O_h. The molecular orbitals are normalized and orthogonal; the ρ_l are not normalized.

But these are not the only bonding orbitals possible in SF_6, for the twelve $(2s)_F$ orbitals and the 24 $(2p\pi)_F$ orbitals have to be considered. Bonding orbitals made from linear combinations of $(2s)_F$ with atomic orbitals of S may be as strong, if not stronger, than those made with $(2p\sigma)$ orbitals. If molecular orbitals are constructed from linear combinations of the $(2s)_F$ functions and the above sulfur functions, they will have exactly the same form, but *different* coefficients. It is to be expected that molecular orbitals with $(2s)$ linear combinations will have different orbital energies from those with $(2p\sigma)$ combinations. A satisfactory solution of this difficulty might possibly be reached if the $2s$, $2p\sigma$ functions were hybridized from the beginning, with coefficients to be determined in the course of solution of the problem.

The treatment of the π-electrons could be made as follows. According to Kimball,[7] they will transform in O_h symmetry like $(F_{1u}+F_{2u}+F_{1g}+F_{2g})$. The proper linear combinations of $(2p\pi)_F$ could be found which transformed like the corresponding representations. The F_{2u} and F_{2g} molecular orbitals would contain only $(2p\pi)_F$, since there are no sulfur orbitals of these species with which they can be combined. The F_{1g} combinations of $(2p\pi)$ could be combined with the unfilled $(3d_{xy}, 3d_{xz}$ and $3d_{yz})$ orbitals of sulfur to form acceptable molecular orbitals. A detailed investigation would have to be made of the possibility of combining the F_{1u} $(2p\pi)$ combinations with $(3p)$ of sulfur, which latter have already been used with the $(2p\sigma)$ combinations. Possibly here also a satisfactory solution could be reached by hybridization of the fluorine functions from the beginning.

The above qualitative sketch of possible treatment of all the atomic orbitals of the fluorines indicates that a comprehensive treatment would be exceedingly complex. As a first approach to the problem, we are attempting a quantitative calculation based on a highly simplified picture of the electronic structure of SF_6.

In the present treatment, we replace the bare octahedral potential field of the seven nuclei in which 70 electrons move by a field of the same symmetry, but which now is made up of a S^{+6} core and six F^{+1} cores. The S^{+6} core contains within it the 10 inner shell electrons of S and each F^{+1} core contains eight electrons $(1s^22s^2\pi^4)$ which are supposed to move in a local field of approximately spherical symmetry. The six valence electrons of sulfur (one $3s$, three $3p$ and two $3d$) and six $(2p\sigma)_F$, one from each fluorine, move in this attractive field, subject to mutual Coulomb and exchange repulsions. Note that the cores are not equivalent to ions formed from S and F atoms in their normal states, but to ions formed by stripping off valence electrons from atoms while they are in their appropriate valence states in molecular formation.

A suitable LCAO Hamiltonian operator (L) for an electron (ν) in the field described above may be written

$$L=T+U_{S^{+6}}+U_{F_i^{+1}}+4U_{F_j^{+1}}+U_{F_k^{+1}}$$
$$+2\sum_{l=1}^{6}\varphi_l^2:\ -\sum_{l=1}^{6}\varphi_l:\varphi_l. \quad (2)$$

In Eq. (2), T is the kinetic energy operator $-h^2\nabla^2/8\pi^2m$. The next four terms are potential energy operators for the electron in the field of the cores. It is evident from the geometrical structure of SF_6 that any particular core F_i is related similarly to four other cores F_j, but differently to the (opposite) core F_k. The last two terms are sums of Coulomb operators and exchange operators. These are defined by the following equations, which show the results of their operation on an arbitrary atomic orbital $\chi_p(\nu)$,

$$\varphi_l^2:\chi_p(\nu)=\left[\int\varphi_l(\mu)\varphi_l(\mu)(e^2/r_{\mu\nu})dv_\mu\right]\chi_p(\nu)$$

$$\varphi_l:\varphi_l\chi_p(\nu)=\left[\int\varphi_l(\mu)\chi_p(\mu)(e^2/r_{\mu\nu})dv_\mu\right]\varphi_l(\nu).$$

(The functions φ_l are real, so there is no need for a complex notation here.) In these equations, (μ) is another electron and $r_{\mu\nu}$ is the distance between the two electrons. With two orbitals, $\chi_p(\nu)$ and $\chi_q(\nu)$ we have

$$\varphi_l^2:\chi_p(\nu)\chi_q(\nu)=\varphi_l^2:pq$$
$$=\int\varphi_l(\mu)\varphi_l(\mu)(e^2/r_{\mu\nu})\chi_p(\nu)\chi_q(\nu)dv_\mu dv_\nu$$

$$\varphi_l\chi_p:\varphi_l\chi_q=\varphi_lp:\varphi_lq$$
$$=\int\varphi_l(\mu)\chi_p(\mu)(e^2/r_{\mu\nu})\varphi_l(\nu)\chi_q(\nu)dv_\mu dv_\nu$$

The object of the present problem is to find the orbital energies and coefficients of molecular orbitals of the

[7] G. E. Kimball, J. Chem. Phys. 8, 188 (1940).

form

$$\varphi_l = a_l\chi_l + b_l\rho_l,$$

which move in a field specified by the potential in Eq. (2).

METHOD OF CALCULATION

General Theory

Roothaan and others have shown [3-5] that when the molecular wave function of the normal state is expressed as an antisymmetrized product of LCAO molecular orbitals (including spin), and when this function is made a minimum by a variational procedure, the following matrix equation results,

$$\mathbf{L}a_i = \epsilon_i \mathbf{S}a_i. \tag{3}$$

In our case, a_i is a column matrix with twelve elements which are the coefficients a_l and b_l in the molecular orbitals $\varphi_1 \cdots \varphi_6$. The parameters ϵ_i are the orbital energies of the MO's. $\mathbf{L}$ is a matrix with elements $L_{pq} = \int \chi_p L \chi_q dv$, where χ_p and χ_q are χ_l and/or ρ_l and L is given by Eq. (2). $\mathbf{S}$ is a matrix whose elements are overlap integrals $S_{pq} = \int \chi_p \chi_q dv$. $\mathbf{L}$ and $\mathbf{S}$ are in our case twelve by twelve matrices. The desired energies $\epsilon_1 \cdots \epsilon_6$ and coefficients a_l, b_l $(l = 1 \cdots 6)$ are obtained by solving the general Eq. (3).

The matrix elements of $\mathbf{L}$ depend, however, on the vectors a_i, (in our case through the last two terms of (2)) and it is necessary to use an iterative process of solution, whereby the a_i are assumed, $\mathbf{L}$ computed and (3) solved for the ϵ_i, and the latter used to compute a new set of a_i. This procedure is repeated until the set of a_i thus computed agrees with the set assumed. At this point "self-consistency" is said to be attained.

Details of the Calculations

In the case of SF_6, molecular symmetry is used to factor the matrix Eq. (3) into smaller (two by two) matrix equations associated with particular representations of the group O_h. These equations of the type

$$\begin{cases} a_l(L_{\chi_l\chi_l} - \epsilon_l) + b_l(L_{\chi_l\rho_l} - S_{\chi_l\rho_l}\epsilon_l) = 0 \\ a_l(L_{\chi_l\rho_l} - S_{\chi_l\rho_l}\epsilon) + b_l(L_{\rho_l\rho_l} - S_{\rho_l\rho_l}\epsilon_l) = 0 \end{cases} \qquad (l = 1 \cdots 6)$$

may then be conveniently expanded into sets of linear equations expressed in terms of atomic orbitals. For the ground state of SF_6, we have specifically the sets (with symmetry representations noted)

$$(A_{1g}) \begin{cases} a_1(\alpha_1 - \epsilon_1) + b_1(6)^{\frac{1}{2}}(\gamma_1 - S_1\epsilon_1) = 0 \\ a_1(6)^{\frac{1}{2}}(\gamma_1 - S_1\epsilon_1) + b_1[(\alpha_{ii} + 4\gamma_{ij} + \gamma_{ik}) \\ \qquad - (1 + 4S_{ij} + S_{ik})\epsilon_1] = 0 \end{cases}$$

$$(E_g) \begin{cases} a_2(\alpha_2 - \epsilon_2) + b_2(4)(3^{-\frac{1}{2}})(\gamma_2 - S_2\epsilon_2) = 0 \\ a_2(4)(3^{-\frac{1}{2}})(\gamma_2 - S_2\epsilon_2) + b_2[(\alpha_{ii} - 2\gamma_{ij} + \gamma_{ik}) \\ \qquad - (1 - 2S_{ij} + S_{ik})\epsilon_2] = 0 \end{cases} \tag{4}$$

$$(E_g) \begin{cases} a_3(\alpha_3 - \epsilon_3) + b_3(2)(\gamma_3 - S_3\epsilon_3) = 0 \\ a_3(2)(\gamma_3 - S_3\epsilon_3) + b_3[(\alpha_{ii} - 2\gamma_{ij} + \gamma_{ik}) \\ \qquad - (1 - 2S_{ij} + S_{ik})\epsilon_3] = 0 \end{cases}$$

$$(F_{1u}) \begin{cases} a_4(\alpha_4 - \epsilon_4) + b_4(2)^{\frac{1}{2}}(\gamma_4 - S_4\epsilon_4) = 0 \\ a_4(2)^{\frac{1}{2}}(\gamma_4 - S_4\epsilon_4) \\ \qquad + b_4[(\alpha_{ii} - \gamma_{ik}) - (1 - S_{ik})\epsilon_4] = 0, \end{cases}$$

and two other (F_{1u}) sets of identical form corresponding to ϵ_5 and ϵ_6. The matrix elements α, γ, and S_{pq} are defined as follows:

$$\begin{aligned} \alpha_l &= \int \chi_l L \chi_l dv \qquad \gamma_{ik} = \int \sigma_i L \sigma_k dv \\ \gamma_l &= \int \chi_l L \sigma_i dv \qquad S_l = \int \chi_l \sigma_i dv \\ \alpha_{ii} &= \int \sigma_i L \sigma_i dv \qquad S_{ij} = \int \sigma_i \sigma_j dv \\ \gamma_{ij} &= \int \sigma_i L \sigma_j dv \qquad S_{ik} = \int \sigma_i \sigma_k dv. \end{aligned} \tag{4a}$$

The ϵ_l in Eqs. (4) are solutions of the equations:

$$\begin{aligned} &(\alpha_1 - \epsilon_1)[(\alpha_{ii} + 4\gamma_{ij} + \gamma_{ik}) - (1 + 4S_{ij} + S_{ik})\epsilon_1] \\ &\qquad - 6(\gamma_1 - S_1\epsilon_1)^2 = 0 \\ &(\alpha_3 - \epsilon_3)[(\alpha_{ii} - 2\gamma_{ij} + \gamma_{ik}) - (1 - 2S_{ij} + S_{ik})\epsilon_3] \\ &\qquad - 4(\gamma_3 - S_3\epsilon_3)^2 = 0 \\ &(\alpha_4 - \epsilon_4)[(\alpha_{ii} - \gamma_{ik}) - (1 - S_{ik})\epsilon_4] - 2(\gamma_4 - S_4\epsilon_4)^2 = 0. \end{aligned} \tag{5}$$

Because of the degeneracy of the E_g and F_{1u} orbitals, $\epsilon_2 = \epsilon_3$ and $\epsilon_4 = \epsilon_5 = \epsilon_6$, it is not necessary to solve additional equations of type (5) for ϵ_2, ϵ_5, and ϵ_6. It is necessary, however, to solve the ϵ_2 set in Eqs. (4) for a_2 and b_2, which will not be the same as a_3 and b_3. We have $a_5 = a_6 = a_4$ and $b_5 = b_6 = b_4$, however, and one solution for the coefficients of the (F_{1u}) orbitals is sufficient.

As a starting point in the solutions of Eqs. (5), we assumed a set of coefficients thought to be in harmony with the relative empirical electronegativities of S and F. Subsequent solution of (4) for the coefficients showed that this was a very poor guess, but a second solution of (5) using the coefficients from the previous trial indicated the direction of change of coefficients for self-consistent solution. Many trials were necessary, however, before approximate convergence was found. In the present work, final agreement of assumed to computed coefficients to within 0.1 percent was obtained (except a_4/b_4 to 0.6 percent), as is shown in Table II. The lowest roots of Eqs. (5) are the energies of molecular orbitals occupied in the ground state of the molecule, each orbital being occupied by two electrons with opposed spins. The other roots correspond to

orbital energies of unoccupied orbitals, which we call $\epsilon_7 \cdots \epsilon_{12}$. We have not specified the forms of the orbitals, but they must be orthogonal to the ground state orbitals, and we suppose that they must satisfy the Eqs. (4). On this supposition, they should also have the form $\varphi_l = a_l\chi_l + b_l\rho_l$ $(l=7\cdots12)$, and their coefficients can therefore be found immediately from orthogonality with normal state orbitals. Using these coefficients and the energies from (5), it is easy to show that Eqs. (4) are satisfied.

Since the b_l in these excited orbitals turns out to be negative, it is evident that they are antibonding orbitals. We cannot be sure, from the discussion in the previous section, that these will be the unoccupied orbitals of lowest energy. We shall assume this to be the case provisionally, and use these orbital energies as a basis for computations of excitation energies, to be described in a later section.

The evaluation of the matrix elements and the numerous integrals over atomic orbitals will be discussed in an Appendix. It is appropriate to discuss now the atomic orbitals which have been used in the previous computations.

Forms of the Atomic Orbitals

The forms of atomic orbitals are of great importance for numerical computations, since all integrals are evaluated ultimately in terms of these orbitals. The advantages and disadvantages of the simple Slater forms have been discussed adequately elsewhere.[3,4] We have chosen these orbitals as given in their original form[8] without any attempt to make them mutually orthogonal. The orbitals are of the form $Nr^{n^*-1} \times \exp(-cr)Y_{lm}$, with $c=Z^*/na_0$ $(a_0=0.5292\text{A})$. The parameters Z^* and n^* were computed by the rules given by Slater and appear in Table I, with the normalization factors N and the angular factors Y_{lm}.

DISCUSSION

General Considerations

The final results are given in Table II. Before discussion of these results in detail, it should be emphasized, if this is not already clear, that the results are obtained by a severely restricted treatment. Only 12 of the 70 total electrons in the molecule have been considered in detail; the others have been included in smoothed-out core potentials, and no interactions between these core electrons have been admitted.

As a result we have been able to obtain only part of the total energy of the normal state, that part which may be associated with molecular wave functions which may be called "bonding" functions. The principal quantitative results which may be expected are the ionization potentials of electrons from these bonding orbitals. Provided that the computations are correct, this is a positive result. In the process of computation, the coefficients in the molecular functions have been obtained, and these coefficients serve to define self-consistent functions, which are presumably the best LCAO functions which can be obtained. Hence, these functions should be useful in other computations.

When the excitation energies are considered, which were the principal object of the computations, the calculation may be regarded as a failure. The numerical values obtained appear to be unreasonable and cannot be identified with any observed electronic spectra. This situation will be discussed in detail in a later section.

TABLE I. Parameters and factors for the atomic functions.

Orbital	n^*	Z^*	N	Y_{lm}
χ_1	3	6.15	$(2c_1^7/45\pi)^{\frac{1}{2}}$	1
χ_2	3	1.65	$(c_2^7/18\pi)^{\frac{1}{2}}$	$3\cos^2\theta-1$
χ_3	3	1.65	$(c_3^7/6\pi)^{\frac{1}{2}}$	$\sin^2\theta\cos2\varphi$
χ_4	3	6.15	$(2c_4^7/15\pi)^{\frac{1}{2}}$	$\cos\theta$
σ_i	2	5.20	$(c_F^5/\pi)^{\frac{1}{2}}$	$\cos\theta$

[8] J. C. Slater, Phys. Rev. **36**, 57 (1930).

Ionization Energies

According to well-established self-consistent field theory, the energies $\epsilon_1 \cdots \epsilon_6$ of orbitals occupied in the normal state of the molecule should be the negatives of the ionization potentials of the molecule. The lowest ionization potential for an electron in the orbitals treated here is seen to be 20 ev.

The direct evidence on ionization potentials of SF_6 is somewhat conflicting. Goldstein[9] found a value of 19.3 ev for the lowest potential by the method of Franck and Hertz. He did not however, examine the mass of the species ionized. Goldstein observed further that SF_6 decomposed on continued bombardment with 8 ev electrons. The mass spectrum of SF_6 decomposition products was examined recently by Dibeler and Mohler.[10] They found *no* SF_6^+ in the mass spectrum, but there is a possibility that SF_6 may have been almost completely decomposed in their intense electron beam, which had a minimum energy of 50 ev, and the 20 ev ionization potential may have been missed.

A lowest ionization potential of 20 ev is in reasonable agreement with an estimate (16 ev) obtained from thermal and spectroscopic data.[11] It is evident from the spectrum that there are resolved electronic levels as high as 14.93 ev above the normal level, and a high value of the lowest potential is to be expected.

Excitation Energies

The excitation energies were computed on the assumption that the electron is excited from φ_2 or

[9] L. Goldstein, Ann. Phys. **9**, Series 1, 723 (1938).
[10] V. H. Dibeler and F. L. Mohler, J. Research Natl. Bur. Standards **40**, 25 (1948).
[11] Liu, Moe, and Duncan, J. Chem. Phys. **19**, 71 (1951).

φ_3 (E_g) to φ_6 or φ_9 (E_g) or to a higher degenerate orbital φ_{10}, φ_{11} or φ_{12} (F_{1u}). The lower excitation gives configurations which result in triplet and singlet A_{1g}, A_{2g}, and E_g states. Transitions to all these states are forbidden from the normal state (A_{1g}) with dipole radiation. The higher excitation corresponds to forbidden transitions to F_{2u} states and allowed transitions to F_{1u} states.

We have computed the excitation energies to all of the singlet states. The energies (E) of these states measured above the normal state were obtained by the general method of Roothaan.[5] All possible antisymmetric product functions for the singlet states were written out and linear combinations of these with the correct symmetry were found. The state energies and excitation energies may be expressed in terms of the orbital energies (Table II) and certain molecular orbital interaction terms (see Table X), and are:

$$E(^1E_g) = \epsilon_8 - \epsilon_2 - \varphi_2\varphi_2 : \varphi_8\varphi_8 + 2\varphi_2\varphi_8 : \varphi_2\varphi_8 + \varphi_2\varphi_3 : \varphi_8\varphi_9 - 2\varphi_2\varphi_9 : \varphi_3\varphi_8$$

$$E(^1A_{1g}) = \epsilon_8 - \epsilon_2 - \varphi_2\varphi_2 : \varphi_8\varphi_8 + 2\varphi_2\varphi_8 : \varphi_2\varphi_8 - \varphi_2\varphi_3 : \varphi_8\varphi_9 + 2\varphi_2\varphi_8 : \varphi_3\varphi_9$$

$$E(^1A_{2g}) = \epsilon_8 - \epsilon_2 - \varphi_2\varphi_2 : \varphi_9\varphi_9 + 2\varphi_2\varphi_8 : \varphi_2\varphi_8 - \varphi_2\varphi_3 : \varphi_8\varphi_9 + 2\varphi_2\varphi_9 : \varphi_3\varphi_8$$

$$E(^1F_{1u}) = \epsilon_{11} - \epsilon_2 - \varphi_2\varphi_2 : \varphi_{11}\varphi_{11} + 2\varphi_2\varphi_{11} : \varphi_2\varphi_{11} - \varphi_2\varphi_3 : \varphi_{11}\varphi_{11} + 2\varphi_2\varphi_{11} : \varphi_3\varphi_{11}.$$

The energies of $^1F_{2u}$ and $^1F_{1u}$ were identical in this approximation. The excitation energies are shown in Table II. The energies of the triplet states were not computed, but they are not expected to be substantially lower than the corresponding singlet state energies, since the interaction integrals are small in comparison with the differences between orbital energies.

It is evident that these excitation energies are very much larger than any observed experimentally. What is worse, the excitation energies are all considerably higher than the corresponding ionization potential. While there are many possible sources of error in the details of the computations, even in the basic integrals, we find it difficult to locate any basic error or combination of errors which accounts for these high excitation energies. Mulliken[12] has discussed reasons why the LCAO—MO method may be unreliable for large excitation energies. One reason suggested is that the LCAO approximation itself may be poor in this case, and that a united atom approximation of a MO of high energy may be better. This suggests that in our case, the excited orbitals may be better approximated by $4s$, $4p$ or $4d$ united atom functions, depending on the symmetry of the orbital involved.

The possible existence of energy states corresponding to configurations which contain united atom MOs, would lead to configuration interaction with the anti-

[12] See reference (4), p. 711.

TABLE II. Final results of computation.

Orbital energies and coefficients

		a_l		b_l	
l	ϵ_l	assumed	found	assumed	found
1	−60.749	0.66572	0.66528	0.48950	0.48998
2	−20.10062	0.88764	0.88760	0.35505	0.35513
3	−20.10062	0.89296	0.89294	0.35718	0.35726
4, 5, 6	−50.46891	0.76720	0.76592	0.40379	0.40543
7	95.634		0.90788		−0.98600
8	9.20035		0.48431		−0.95822
9	9.20035		0.46860		−0.95460
10, 11, 12	62.5771		0.77670		−1.01474

Excitation energies to antibonding states

State	E (in ev above ground state)
^1E_g	25.776
$^1A_{1g}$	28.985
$^1A_{2g}$	30.042
$^1F_{1u}$	73.214
$^1F_{2u}$	73.214

bonding states whose energy we have computed. The interaction would be strong, since it is expected that the absolute energies of the two types of states will be similar. If this factor were taken into account, it would lead to a lowering of excitation energies, perhaps by a large amount.

Finally, the experimental excitation energies[11] may not correspond to those which have been computed, but may correspond to excitation between the neglected π-type bonding MOs. A decision between the large number of possibilities could be made only on the basis of further energy computations, which appear to be decidedly unpromising and impracticable at the present time.

Polarity

In the present treatment, only coefficients in some bonding molecular orbitals have been obtained, and no definite conclusion should be drawn about the total internal polarity of SF_6. As far as this treatment goes, the coefficients lead to the view that S in the valence state sp^3d^2 is considerably more electronegative than F. If Mulliken's[13] procedure of dividing the charge in a molecular orbital is carried through for this case, we obtain an average charge distribution $S^{-.47}$ $(F_6)^{+.47}$ for the six molecular orbitals occupied in the normal state. We might have expected about the same charge distribution *with reversed signs* on the basis of empirical electronegativity scales. It is possible, however, that the unusual valence state of SF_6 may have something to do with the result, and that the electronegativity of S in this state may be quite different from that of S in the compounds from which its place in the usual scales is determined.

Errors and Conclusion

The general errors which are inherent in a calculation of this type have been summarized adequately by

[13] R. S. Mulliken, J. Chem. Phys. 3, 573, 586 (1935).

Mulligan.[3] There will be discussed here briefly (and more fully in the Appendix) what is regarded as one of the chief specific errors in this computation. This is the use of "core" potentials for the inner electrons in the present work. The alternative method would have been to use a Hamiltonian in which the core potentials (terms 2, 3, 4, 5 in Eq. (2)) were replaced by the field of the bare nuclei and the interaction of all (70) electrons included explicitly in the last two terms of Eq. (2). But the treatment of the complete 70 electron problem is what we tried to avoid.

Consideration of the alternate methods shows that the core potentials at least partly include the Coulomb repulsions of the inner electrons but neglect exchange repulsions. This neglect has only a small effect on most penetration integrals, but is expected to have a rather large effect on other (self-penetration) integrals. A numerical illustration of this point is made in the Appendix (B, 2), where an attempt will be made to estimate the error, but unfortunately no definite conclusions can be drawn without repeating the entire self-consistent procedure.

In conclusion, it should be emphasized that this a first attempt to treat quantitatively a rather complicated problem. It is still felt, as at the beginning of the attempt, that only a quantitative treatment will be of significance in a final solution of the problem. Essentially, this is because we are sure experimentally that there are no low lying electronic energy levels in SF_6, and there may not be large differences between excitation energies from the bonding orbitals considered and from other orbitals not considered. It is suggested that attempts should be made to compute the energies of some of the neglected orbitals and the resulting excitation energies, especially the orbitals made with $(2p\pi)_F$ atomic orbitals, and the energies of the united atom orbitals discussed previously.

The writer expresses his appreciation to Mr. Norman Gunderson, Mr. Peter Lyman, and Mr. Robert Greenler for aid in numerical calculations.

APPENDIX

Evaluation of Integrals

All two and higher centered integrals were evaluated at distances based on the electron diffraction value of 1.58A for the S−F distance.

A. *Overlap Integrals*

There are only six basic integrals of this type. $S_1=\int\chi_1\sigma_i dv$, $S_4=\int\chi_4\sigma_i dv$, and $S_{ik}=\int\sigma_i\sigma_k dv$ might have been obtained from existing tables,[14] but had been computed before publication of these tables. $S_2=\int\chi_2\sigma_i dv$ and $S_3=\int\chi_3\sigma_i dv$ were computed with Slater functions in the usual ellipsoidal coordinate system. In the integral S_3, the positive part of χ_3 (transforming like x^2) with angular factor $\sin^2\theta\cos^2\varphi$, was used with σ_2 and σ_4, which lie on the x axis of the molecule, while the negative part with $\sin^2\theta\sin^2\varphi$ was used with σ_3 and σ_5. In the integral $S_{ij}=\int\sigma_i\sigma_j dv$, the internuclear F_i-F_j axis makes an angle of 45° with the direction of the $2p\sigma$ orbitals. Hence, $S_{ij}=(2)^{-1}\int(2p\sigma_i)(2p\sigma_j)dv$.

B. *Matrix Elements α and γ*

The expansions of these integrals, defined in Eqs. (4a), in terms of the Hamiltonian (Eq. (2)), result in four types of integrals:

(1) $$pTq=\int p(-h^2\nabla^2/8\pi^2m)qdv$$

(kinetic energy integrals)

(2) $$\text{S: } pq=\int p(e^2U_S^{+6}/r_S)qdv$$

(sulfur penetration integrals)

$$\text{F: } pq=\int p(e^2U_F^{+1}/r_F)qdv$$

(fluorine penetration integrals)

(3) $$\varphi_l^2\text{: } pq=\varphi_l^2\text{: } qp$$
$$=\int\varphi_l(\mu)\varphi_l(\mu)(e^2/r_{\mu\nu})p(\nu)q(\nu)dv_\mu dv_\nu$$

(Coulomb integrals)

(4) $$\varphi_l p\text{: } \varphi_l q=\varphi_l q\text{: } \varphi_l p$$
$$=\int\varphi_l(\mu)q(\mu)(e^2/r_{\mu\nu})\varphi_l(\nu)p(\nu)dv_\mu dv_\nu$$

(exchange integrals).

In the above notation r_S, r_{Fi}, r_{Fj}, r_{Fk} are distances of the electron from the centers indicated by subscripts; $r_{\mu\nu}$ is an interelectronic distance; dv_μ and dv_ν are the volume elements of the two electrons, and $p=\chi_p$, $q=\chi_q$ are two atomic orbitals. Note that in the two-electron integrals, the functions for one electron are written on the same side of the colon. In the expansion of integrals of types (3) and (4), atomic integrals designated $pr:ql=\int p(\mu)r(\mu)(e^2/r_{\mu\nu})q(\nu)t(\nu)dv_\mu dv_\nu$ are obtained, where the four different letters refer in general to functions located on four different centers. Conventionally $pp:pp$, $pp:qq$, $pp:rr$, etc., are called Coulomb integrals and are sometimes designated by J (with appropriate subscripts). Integrals $pp:pq$ are called Coulomb-exchange integrals and $pq:pq=pq:qp$ is an exchange integral, frequently designated by K. All integrals where two electrons are distributed in three or four functions are called exchange integrals, regardless of the number of centers to which the functions are referred. Each

[14] Mulliken, Rieke, Orloff, and Orloff, J. Chem. Phys. **17**, 1248 (1949).

type of integral will be discussed briefly and tables will be given of numerical values.

1. Kinetic energy integrals.—One-centered integrals were easily evaluated in spherical polar coordinates after ∇^2 was expanded in these coordinates. Two-centered integrals of this type reduced to overlap integrals and other integrals, some of which were evaluated with the help of formulas given by Coulson,[15] others were computed directly in ellipsoidal coordinates. The two-centered integrals were found to be negative. The numerical values appeared to be sensitive to absence of nodes in the atomic functions, and integrals involving χ_1 and χ_4 may be in error for this reason.

2. Penetration integrals.—The detailed forms of U_S^{+6} and U_F^{+1} have to be specified. We employed an extension of the approximation made originally by Goeppert-Mayer and Sklar[16] for carbon in benzene. The ion potentials were replaced by potentials of the atoms from which they were derived, in their proper valence states, minus the potentials of the electrons added to the ion to form the atom. In the case of the S ion, this approximation leads to

$$U_S^{+6}(\nu)=V_S^0(\nu)-\sum_{l=1}^{6}\int(e^2/r_{\mu\nu})\chi_l^2(\mu)dv_\mu. \qquad (6)$$

The potential V_S^0 of the neutral atom is fairly complicated, because it appeared to be necessary to consider the penetration of a charge distribution (pq) into the inner shells as well as into the valence shell. Furthermore, the Slater rules assign different effective nuclear charges to electrons in $1s$, $2(s, p)$, $3(s, p)$ and $3d$ orbitals. We write

$$V_S^0=-Ze^2/r_S+\int\sigma(r)r^2dr \quad (Z=16),$$

where the first term is the attraction of the bare nucleus and $\sigma(r)$ in the second term is the total charge density of all the electrons. The electron density term may be separated into four integrals, each containing functions with the same nuclear charge. The term $(-16e^2/r_S)$ is divided also according to the number of electrons in the shells. Consequently, we may write the potential V_S^0 in four parts as

$$V_S^0=V_S^0(1s)+V_S^0(2s, 2p)+V_S^0(3s, 3p)+V_S^0(3d).$$

Each of the potentials was computed separately by the method of Goeppert-Mayer and Sklar (except the $1s$ electrons were not assumed to be located in the nucleus), with the following nuclear charges computed from Slater's rules: $Z_S^*(1s)=15.7$; $Z_S^*(2s, p)=11.85$; $Z_S^*(3s, p)=6.15$; $Z_S^*(3d)=1.65$. The potential $V_S^0(3d)$ was not spherical with one electron in each of the two d functions, but it was made almost so by taking a linear combination of the two functions. As might have been anticipated, contributions of $V_S^0(1s)$ to all integrals S:pq were negligible. Those from $V_S^0(2s, p)$ were small, but not negligible. The analytical expressions for the potentials are (with $r=r_S$ and $h_i=Z^*/n^*a_0$)

$$V_S^0(1s) \quad =-(2e^2/r)[h_1r+1]\exp(-2h_1r);$$

$$V_S^0(2s, p)=-(8e^2/3r)[2(h_2r)^3+6(h_2r)^2+9h_2r+6]\exp(-2h_2r);$$

$$V_S^0(3s, p)=-(4e^2/45r)[2(h_3r)^5+10(h_3r)^4+30(h_3r)^3+60(h_3r)^2+75h_3r+45]\exp(-2h_3r);$$

$$V_S^0(3d) \quad =-(e^2/48)[2(h_4r)^5+10(h_4r)^4+30(h_4r)^3+60(h_4r)^2+75h_4r+45]\exp(-2h_4r).$$

The potential U_F^{+1} was treated in a similar way and expanded into

$$U_F^{+1}+\int(e^2/r_{\mu\nu})\sigma_i^2(\mu)dv_\mu=V_F^0=V_F^0(1s)+V_F^0(2s, p),$$

with

$$V_F^0(1s) \quad =-(2e^2/r)[h_1r+1]\exp(-2h_1r) \quad (r=r_F)$$

$$V_F^0(2s, p)=-(7e^2/6r)[2(h_2r)^3+6(h_2r)^2+9h_2r+6]\exp(-2h_2r).$$

The latter potential is not quite spherical, but the angular factor neglected is small. The contribution to any integral from the $(1s)$ shell is negligible. The penetration integrals were evaluated term by term with the use of the above potentials.

Two-centered penetration integrals were evaluated in ellipsoidal coordinates. Because of the numerous terms in the potentials, this proved to be one of the most laborious parts of the computation. Three-centered integrals, with centers m_1, m_2, m_3, were evaluated by the approximate formula

$$V_{m1}^0: p(m_2)q(m_3)=S_{pq}[V_{m1}: pq(m_4)],$$

where the center m_4 is at the midpoint of a line joining m_2 and m_3.

The one-centered integrals require special comment. It is convenient to call these "self-penetration" integrals, because the charge distribution of the electron (pp) is penetrating the charge density of the atom to which its center is referred. It is here that the absence of exchange terms in the potentials V_S^0 and V_F^0 assumes importance, because it is reasonable to suppose that the penetration is large, as is apparent from the numerical values of the integrals without exchange. A numerical example may serve to illustrate a difficulty caused, we believe, by the form of the potentials. Consider the integral $F_i:\sigma_i\sigma_i$, for which we have obtained a value -67.69117 ev. Now since σ_i is an atomic orbital we have

$$[T(\nu)+U_{F_i}^{+1}(\nu)]\sigma_i=\epsilon(\sigma_i)\sigma_i$$

[15] C. A. Coulson, Proc. Cambridge Phil. Soc. **38**, 210 (1941).
[16] M. Goeppert-Mayer and A. L. Sklar. J. Chem. Phys. **6**, 645 (1938).

TABLE III. Expansions of matrix elements (see Eq. 4a).

$$\alpha_p=\chi_pT\chi_p+V_{S^0}:\chi_p^2+6V_{F^0}:\chi_p^2-J_{p_1}-2J_{p_2}-3J_{p_4}-6J_p+2\sum_{l=1}^{6}\varphi_l^2:\chi_p-\sum_{l=1}^{6}\varphi_l\chi_p:\varphi_l\chi_p;\quad (p=1,3,4)$$

$$\gamma_p=\chi_pT\sigma_i+V_{S^0}:\chi_p\sigma_i+V_{F_i^0}:\chi_p\sigma_i+4V_{F_j^0}:\chi_p\sigma_i+V_{F_k^0}:\chi_p\sigma_i-S_p(J_1+2J_3+3J_4+J_{p_1}+2J_{p_3}+3J_{p_4}+$$
$$+6J_p+J_{ii}+4J_{ij}+J_{ik})/2+2\sum_{l=1}^{6}\varphi_l^2:\chi_p\sigma_i-\sum_{l=1}^{6}\varphi_l\chi_p:\varphi_l\sigma_i;\quad (p=1,3,4)$$

$$\alpha_{ii}=\sigma_iT\sigma_i+V_{S^0}:\sigma_i^2+V_{F_i^0}:\sigma_i^2+4V_{F_j^0}:\sigma_i^2+V_{F_k^0}:\sigma_i^2-J_1-2J_3-3J_4-J_{ii}-4J_{ij}-J_{ik}+2\sum_{l=1}^{6}\varphi_l^2:\sigma_i^2-\sum_{l=1}^{6}\varphi_l\sigma_i:\varphi_l\sigma_i$$

$$\gamma_{ij}=\sigma_iT\sigma_j+V_{S^0}:\sigma_i\sigma_j+V_{F_i^0}:\sigma_i\sigma_j+4V_{F_j^0}:\sigma_i\sigma_j+V_{F_k^0}:\sigma_i\sigma_k-S_{ij}(J_1+2J_3)-S_{ij}(5J_{ii}+6J_{ij}+J_{ik})/2+2\sum_{l=1}^{6}\varphi_l^2:\sigma_i\sigma_j-\sum_{l=1}^{6}\varphi_l\sigma_i:\varphi_l\sigma_j$$

$$\gamma_{ik}=\sigma_iT\sigma_k+V_{S^0}:\sigma_i\sigma_k+V_{F_i^0}:\sigma_i\sigma_k+4V_{F_j^0}:\sigma_i\sigma_k+V_{F_k^0}:\sigma_i\sigma_k-S_{ik}(J_1+2J_3+3J_4+J_{ii}+4J_{ij}+J_{ik})+2\sum_{l=1}^{6}\varphi_l^2:\sigma_i\sigma_k-\sum_{l=1}^{6}\varphi_l\sigma_i:\varphi_l\sigma_k$$

and

$$\epsilon(\sigma_i)=\int\sigma_iT\sigma_idv+\int U_{F_i^{+1}}\sigma_i^2dv$$
$$=\sigma_iT\sigma_i+F_i:\sigma_i^2-\sigma_i^2:\sigma_i^2$$
$$=-3.43\text{ ev.}$$

But $\epsilon(\sigma_i)$ should be equal to the energy of a $2p\sigma$ electron in the valence state $s^2\pi^4\sigma$ of the fluorine atom, which is not very different from the negative of the lowest ionization potential of F in its normal configuration s^2p^5. Thus $\epsilon(\sigma_i)$ should have the value -17.42 ev. This discrepancy should be discussed in some detail.

It is difficult to believe that either the integrals $\sigma_iT\sigma_i$ or $\sigma_i^2:\sigma_i^2$ are in error, the former is just $(Z^*)^2e^2/4a_0$ and the latter integral is given by Parr and Crawford[17] and was computed independently for this work, with complete agreement. The discrepancy appears to lie in the self-penetration integral, and we believe that this is caused by the lack of exchange terms in the potential. We ask next what is the possible error in the final results caused by this integral? An error will have the largest effect on the matrix element α_{ii}, which appears in all the Eqs. (4) and (5) and accordingly may affect all the orbital energies, and consequently all the coefficients. Some study was made of this effect by arbitrarily making α_{ii} about 14 ev more negative. This caused the ratios of the coefficients a_4/b_4 and a_3/b_3 to be decreased, but not greatly, while the excited orbital energies were raised relative to the occupied orbital energies. The results indicated that the final values would not be changed greatly, although self-consistency was not attained. Errors resulting from the same fundamental cause must also be present in other matrix elements, notably in γ_l which must compensate to some extent for the error in α_{ii}, so that a large change in the final result is not expected.

TABLE IV. Final values of matrix elements (ev) from expansions (Table III) and integrals (Tables VI–IX).

	H_{pq}	G_{pq}	L_{pq}
α_1	−112.34361	82.54538	−29.79823
α_3	− 58.71734	42.21278	−16.50456
α_4	−125.97853	91.08858	−34.88995
α_{ii}	− 85.36210	87.84671	+ 2.48461
γ_1	− 43.73598	14.92830	−28.80768
γ_3	− 8.98590	3.24577	− 5.74013
γ_4	− 58.33328	23.20923	−35.12405
γ_{ij}	− 1.88812	0.38627	− 1.50185
γ_{ik}	− 0.10143	−2.58441	− 2.68584

Definitions:

$\alpha_l=\int\chi_lL\chi_ldv$ $\quad L\text{ (Eq. (2))}=H+G$

$\alpha_{ii}=\int\sigma_iL\sigma_idv$ with $H=T+U_{S^{+6}}+U_{F_i^{+1}}+4U_{F_j^{+1}}+U_{F_k^{+1}}$

$\gamma_l=\int\chi_lL\sigma_idv$ $\quad G=2\sum_{l=1}^{6}\varphi_l^2:-\sum_{l=1}^{6}\varphi_l:\varphi_l$

$\gamma_{ij}=\int\sigma_iL\sigma_jdv$

$\gamma_{ik}=\int\sigma_iL\sigma_kdv$

3. Coulomb integrals.—One-center integrals Coulomb integrals were evaluated by the usual expansion of $(1/r_{\mu\nu})$ in Legendre polynomials with subsequent integration over the coordinates of the two electrons in spherical polar coordinates. No approximations had to be made.

Two-centered integrals with equal nuclear charge ($\sigma_i\sigma_i:\sigma_j\sigma_j$ and $\sigma_i\sigma_i:\sigma_k\sigma_k$) were obtained graphically by extrapolating curves drawn from the data of Parr and Crawford[17] at small internuclear distance to Coulomb point-charge values of these integrals, which must be valid at large distances. Actually, at the F_i-F_j distance of 2.23A the overlapping of the charge densities σ_i^2 with σ_j^2 is small and the point-charge values could have been used directly with little error. There should be even less error in the case of $\sigma_i\sigma_i:\sigma_k\sigma_k$.

The remaining Coulomb integrals involved electrons on S and F so the nuclear charges were unequal. In the integral $\chi_1^2:\sigma_i^2$, when $(1/r_{\mu\nu})$ was expanded about the S atom, only the polynomial P_0^0 appeared. Integration over the coordinates of the electron on sulfur resulted in a lengthy expression, which was then transformed to

[17] R. G. Parr and B. L. Crawford, Jr., J. Chem. Phys. **16**, 1049 (1948).

TABLE V. Expansions of molecular-atomic integrals.

$\varphi_p^2:\chi_l^2 = m_p J_{pl} + n_p J_l$; $\quad \varphi_p^2:\bar{\sigma}_i^2 = m_p J_l + n_p(J_{ii}+4J_{ij}+J_{ik})/6$

$\varphi_p^2:\chi_l\sigma_i = S_l[\varphi_p^2:\chi_l^2 + \varphi_p^2:\bar{\sigma}_i^2]/2$; $\quad \varphi_p^2:\sigma_i\sigma_j = S_{ij}(\varphi_p^2:\bar{\sigma}_i^2)$; $\quad \varphi_p^2:\sigma_i\sigma_k = S_{ik}(\varphi_p^2:\bar{\sigma}_i^2)$

($\bar{\sigma}_i$ = average $\sigma_1\cdots\sigma_6$; $\quad l=1\cdots6$; $\quad p=1\cdots6$)

p	m_p	n_p
1	$a_1^2+(6)^{\frac{1}{2}}a_1b_1S_1$	$(6)^{\frac{1}{2}}a_1b_1S_1+b_1^2(1+4S_{ij}+S_{ik})$
2	$a_2^2+4(3^{-\frac{1}{2}})a_2b_2S_2$	$4(3^{-\frac{1}{2}})a_2b_2S_2+b_2^2(1-2S_{ij}+S_{ik})$
3	$a_3^2+2a_3b_3S_3$	$2a_3b_3S_3+b_3^2(1-2S_{ij}+S_{ik})$
4, 5, 6	$a_4^2+(2)^{\frac{1}{2}}a_4b_4S_4$	$(2)^{\frac{1}{2}}a_4b_4S_4+b_4^2(1-S_{ik})$

$\varphi_1\chi_1$: $\varphi_1\chi_1=[a_1^2+(6)^{+\frac{1}{2}}a_1b_1S_1^{SF}+1.5b_1^2(S_1)^2]J_{11}^{88}+[(6)^{\frac{1}{2}}a_1b_1S_1+3b_1^2(S_1)^2]J_1+b_1^2(S_1)^2(J_{ii}+4J_{ij}+J_{ik})/4$

$\varphi_1\chi_2$: $\varphi_1\chi_2=a_1^2K_{13}+b_1^2(S_3)^2[6J_{33}+12J_3+J_{ii}+4J_{ij}+J_{ik}]/4$

$\varphi_1\chi_4$: $\varphi_1\chi_4=a_1^2K_{14}+b_1^2(S_4)^2[6J_{44}+12J_4+J_{ii}+4J_{ij}+J_{ik}]/4$

$\varphi_2\chi_1$: $\varphi_2\chi_1=a_2^2K_{12}+b_2^2(S_1)^2[J_{ii}-2J_{ij}+J_{ik}]/4$

$\varphi_2\chi_3$: $\varphi_2\chi_3=a_2^2K_{23}+b_2^2(S_3)^2(J_{ii}-2J_{ij}+J_{ik})/4$

$\varphi_2\chi_4$: $\varphi_2\chi_4=a_2^2K_{24}+b_2^2(S_4)^2(J_{ii}-2J_{ij}+J_{ik})/4$

$\varphi_3\chi_1$: $\varphi_3\chi_1=a_3^2K_{13}+b_3^2(S_1)^2(J_{ii}-2J_{ij}+J_{ik})/4$

$\varphi_3\chi_3$: $\varphi_3\chi_3=a_3^2J_{33}+a_3b_3S_3(J_{33}+J_3)+b_3^2(S_3)^2(J_{ii}-2J_{ij}+J_{ik})/4$

$\varphi_3\chi_4$: $\varphi_3\chi_4=a_3^2K_{34}+b_3^2(S_4)^2(J_{ii}-2J_{ij}+J_{ik})/4$

$\varphi_4\chi_1$: $\varphi_4\chi_1=a_4^2K_{14}+b_4^2(S_1)^2(J_{ii}-J_{ik})/4$

$\varphi_4\chi_3$: $\varphi_4\chi_3=a_4^2K_{34}+b_4^2(S_3)^2(J_{ii}-J_{ik})/4$

$\varphi_4\chi_4$: $\varphi_4\chi_4=a_4^2J_{44}+b_4^2(S_4)^2(J_{ii}-J_{ik})/4+(2)^{-\frac{1}{2}}(S_4)a_4b_4(J_{44}+J_4)$

$\varphi_1\sigma_i$: $\varphi_1\sigma_i=a_1^2S_1^2(J_{11}+2J_1+J_{ii})/4+[(6)^{-\frac{1}{2}}S_1a_1b_1/2][2J_1(1+4S_{ij}+S_{ik})+J_{ii}(2+4S_{ij}+S_{ik})+S_{ij}J_{ij}+S_{ik}J_{ik}/4]$
$+(b_1^2/6)[J_{ii}+4S_{ij}(J_{ii}+J_{ij})+S_{ij}^2(5J_{ii}+10J_{ij}+J_{ik})+2S_{ij}S_{ik}(J_{ii}+2J_{ij}+J_{ik})+(2S_{ik}+S_{ik}^2)(J_{ii}+J_{ik})/2]$

$\varphi_2\sigma_i$: $\varphi_2\sigma_i=a_2^2S_2^2(J_{22}+J_2+J_{ii})/4+[(12)^{-\frac{1}{2}}S_2a_2b_2/2][2J_2(2+2S_{ij}+S_{ik})+J_{ii}(2+2S_{ij}+S_{ik})+S_{ij}J_{ij}/2+S_{ik}J_{ik}/4]$
$+(b_2^2/6)[J_{ii}-2S_{ij}(J_{ii}+J_{ij})+S_{ij}^2(J_{ii}-2J_{ij})+S_{ij}S_{ik}(J_{ii}+2J_{ij}+J_{ik})+(S_{ik}^2-2S_{ij})(J_{ii}+J_{ik})/2]$

$\varphi_3\sigma_i$: $\varphi_3\sigma_i=a_3^2S_3^2(J_{33}+2J_3+J_{ii})/4+(S_3a_3b_3/2)[J_3+J_{ii}-S_{ij}(2J_3+J_{ii}+J_{ij})+S_{ik}(2J_3+J_{ii}+J_{ik})/2]$
$+(b_3^2/4)[J_{ii}+(S_{ik}-S_{ij}+2S_{ik}^2)(J_{ii}+J_{ik})+2S_{ij}S_{ik}(J_{ii}+2J_{ij}+J_{ik})+S_{ij}^2(3J_{ii}+4J_{ij}+J_{ik})/2]$

$\varphi_4\sigma_i$: $\varphi_4\sigma_i=a_4^2S_4^2(J_{44}+2J_4+J_{ii})/4+(2)^{\frac{1}{2}}a_4b_4S_4[2(1-S_{ik})J_4+2J_{ii}-S_{ik}(J_{ii}+J_{ik})]/2+(b_4^2/2)[J_{ii}+(S_{ik}^2-S_{ik})(J_{ii}+J_{ik})/2]$

$\varphi_1\chi_1$: $\varphi_1\sigma_i=a_1^2S_1(J_{11}^{88}+J_1^{SF})/2+(6)^{-\frac{1}{2}}a_1b_1S_1^2(6J_{11}+12J_1+J_{ii}+4J_{ij}+J_{ik})/4+(6)^{-\frac{1}{2}}a_1b_1J_1(1+4S_{ij}+S_{ik})$
$+(b_1^2/6)S_1(1+4S_{ij}+S_{ik})[3J_1+(J_{ii}+4J_{ij}+J_{ik})/2]$

$\varphi_2\chi_1$: $\varphi_2\sigma_i=(b_2^2S_1^{SF})(1+S_{ij}+S_{ik})(J_{ii}-2J_{ij}+J_{ik})/6$

$\varphi_3\chi_1$: $\varphi_3\sigma_i=(a_3b_3S_3^2/8)(4J_{13}+4J_3+4J_1+J_{ii}+2J_{ij}+J_{ik})+b_3^2(1+2S_{ij}+S_{ik})S_1^{SF}(4J_1+J_{ii}+2J_{ij}+J_{ik})/8$

$\varphi_4\chi_1$: $\varphi_4\sigma_i=[a_4b_4S_1S_4(2)^{-\frac{1}{2}}/4][2J_{14}+J_1+J_4+J_{ii}+J_{ik}]+b_4^2S_1(1+S_{ik})(2J_1+J_{ii}+J_{ik})/4$

$\varphi_1\chi_3$: $\varphi_1\sigma_i=(6)^{-\frac{1}{2}}a_1b_1S_1S_3(6J_{13}+6J_1+6J_3+J_{ii}+4J_{ij}+J_{ik})/4+(b_1^2S_3/6)(1+4S_{ij}+S_{ik})[3J_3+(4J_{ij}+J_{ik}+J_{ii})/2]$

$\varphi_2\chi_3$: $\varphi_2\sigma_i=b_2^2S_3(1+S_{ik}+S_{ij})(J_{ii}-2J_{ij}+J_{ik})/6$

$\varphi_3\chi_3$: $\varphi_3\sigma_i=a_3^2S_3^{SF}(J_{33}+J_3)/2+a_3b_3J_3(1-2S_{ij}+S_{ik})/2+a_3b_3S_3^2(4J_{33}+8J_3+J_{ii}+2J_{ij}+J_{ik})/8$
$+b_3^2S_3(1+2S_{ij}+S_{ik})(4J_3+J_{ii}+2J_{ij}+J_{ik})/8$

$\varphi_4\chi_3$: $\varphi_4\sigma_i=(2)^{-\frac{1}{2}}a_4b_4S_3S_4(J_{34}+J_3+J_4+J_{ii}+J_{ik})/4+b_4^2S_3(1+S_{ik})(2J_3+J_{ii}+J_{ik})/4$

$\varphi_1\chi_4$: $\varphi_1\sigma_i=(6)^{-\frac{1}{2}}a_1b_1S_1S_4(6J_{14}+6J_1+6J_4+J_{ii}+4J_{ij}+J_{ik})/4+b_1^2S_4(1+4S_{ij}+S_{ik})[3J_4+(J_{ii}+4J_{ij}+J_{ik})/2]/6$

$\varphi_2\chi_4$: $\varphi_2\sigma_i=b_2^2S_4(1+S_{ij}+S_{ik})(J_{ii}-2J_{ij}+J_{ik})/6$

$\varphi_3\chi_4$: $\varphi_3\sigma_i=a_3b_3S_3^2(4J_{34}+4J_3+4J_4+J_{ii}+2J_{ij}+J_{ik})/8+b_3^2S_4(1+2S_{ij}+S_{ik})(4J_4+J_{ii}+2J_{ij}+J_{ik})/8$

$\varphi_4\chi_4$: $\varphi_4\chi_4=a_4^2S_4(J_{44}+J_4)/2+a_4b_4(2)^{-\frac{1}{2}}S_4^2(2J_{44}+4J_4+J_{ii}+J_{ik})/4+b_4^2S_4(1+S_{ik})(2J_4+J_{ii}+J_{ik})/4$

$\varphi_1\sigma_i$: $\varphi_1\sigma_j=a_1^2S_1^2(J_{11}+2J_1+J_{ij})/4+(6)^{-\frac{1}{2}}a_1b_1[S_1(1+S_{ik})(J_1+J_{ij})+S_{ij}(J_{ii}+6J_{ij}+J_{ik})/2]$
$+(b_1^2/24)[(1+2S_{ik}+S_{ik}^2)4J_{ij}+4(S_{ij}+S_{ik})(J_{ii}+2J_{ij}+J_{ik})+2S_{ij}^2(5J_{ii}+5J_{ik}+22J_{ij})]$

$\varphi_2\sigma_i$: $\varphi_2\sigma_j=a_2^2S_2^2(J_{22}+2J_2+J_{ij})/4-b_2^2J_{ij}/12+b_2^2[(4S_{ij}-3S_{ij}^2+6S_{ij}S_{ik})(J_{ii}+J_{ij})+(7S_{ik}+5S_{ik}^2)J_{ik}]/36$

$\varphi_3\sigma_i$: $\varphi_3\sigma_j=a_3^2S_3^2(J_{33}+2J_3+J_{ij})/4+a_3b_3S_3(1+S_{ik})(J_3+J_{ij})/2+a_3b_3S_3S_{ij}(4J_3+J_{ii}+2J_{ij}+J_{ik})/4$
$-b_3^2J_{ij}/4+b_3^2S_{ij}(1+S_{ik}-S_{ij})(J_{ii}+2J_{ij}+J_{ik})/4+b_3^2S_{ik}^2J_{ij}/4$

$\varphi_4\sigma_i$: $\varphi_4\sigma_j=0$; (all a_4b_4 terms cancel; all b_4^2 terms cancel; $a_4S_4^2$ term is zero because either σ_i or σ_j must be orthogonal to χ_4).

$\varphi_1\sigma_i$: $\varphi_1\sigma_k=a_1^2S_1^2(J_{11}+2J_1+J_{ik})/4+a_1b_1(6)^{-\frac{1}{2}}S_1[4J_{ik}+8S_{ij}(J_{ij}+J_{ik})+2S_{ik}(J_{ii}+J_{ik})]/4$
$+(b_1^2/6)[(1+4S_{ij}+2S_{ik}+2S_{ij}S_{ik}+5S_{ij}^2+S_{ik}^2/2)J_{ik}+(4S_{ij}+4S_{ij}S_{ik}+10S_{ij}^2)J_{ij}+(S_{ik}+2S_{ij}S_{ik}+5S_{ij}^2+S_{ik}^2/2)J_{ii}]$

$\varphi_2\sigma_i$: $\varphi_2\sigma_k=a_2^2S_2^2(J_{22}+2J_2+J_{ik})/4+b_2^2J_{ik}/6+(b_2^2/36)[(6S_{ik}-12S_{ij}+12S_{ij}^2+3S_{ik}^2-2S_{ij}S_{ik})J_{ik}$
$+(6S_{ik}+6S_{ij}^2+3S_{ik}^2-2S_{ij}S_{ik})J_{ii}+(-12S_{ij}-6S_{ij}^2-4S_{ij}S_{ik})J_{ij}]$

$\varphi_3\sigma_i$: $\varphi_3\sigma_k=a_3^2S_3^2(J_{33}+2J_3+J_{ik})/4+a_3b_3S_3[J_3+J_{ik}-3S_{ij}(2J_3+J_{ij}+J_{ik})+S_{ik}(2J_3+J_{ii}+J_{ik})]/2$
$+b_3^2[(2S_{ik}+2S_{ij}S_{ik}+S_{ij}^2+S_{ik}^2)J_{ii}+(4S_{ij}^2+4S_{ij}S_{ik}-4S_{ij})J_{ij}+(2-4S_{ij}+2S_{ik}+2S_{ij}S_{ik}+3S_{ij}^2+S_{ik}^2)J_{ik}]/8$

$\varphi_4\sigma_i$: $\varphi_4\sigma_k=a_4^2S_4^2(J_{44}+J_4+J_{ik})/4+a_4b_4(2)^{-\frac{1}{2}}S_4[(1+S_{ik})J_4+S_{ik}(J_{ii}+J_{ik})/2+J_{ik}]+b_4^2[S_{ik}(J_{ii}+J_{ik})-J_{ik}]/2$

TABLE VI. Molecular-atomic integrals. (ev).

$\varphi_l^2:pq$	$l=1$	$l=2$	$l=3$	$l=4,5,6$	$2\sum_{l=1}^{6}\varphi_l^2:pq$
$\varphi_l^2:\chi_1^2$	9.78733	5.34294	5.33385	8.73332	93.32816
$:\chi_3^2$	4.55258	3.35432	3.24250	3.99251	46.25388
$:\chi_4^2$	11.13627	5.98204	5.95998	9.62185	103.88768
$:\sigma_i^2$	8.16162	4.88230	4.85993	10.27289	97.44508
$:\chi_1\sigma_i$	1.72130	0.98060	0.97758	1.82270	18.29516
$:\chi_3\sigma_i$	0.39414	0.25533	0.25118	0.44223	4.45528
$:\chi_4\sigma_i$	2.73644	1.54056	1.53426	2.82108	28.54898
$:\sigma_i\sigma_j$	0.09223	0.05517	0.05492	0.11608	1.10112
$:\sigma_i\sigma_k$	0.00612	0.00366	0.00364	0.00770	0.07304
$\varphi_l p:\varphi_l q$	$l=1$	$l=2$	$l=3$	$\sum_{l=1}^{6}\varphi_l p:\varphi_l q$	$\sum_{l=1}^{6}\varphi_l p:\varphi_l q$
$\varphi_l\chi_1:\varphi_l\chi_1$	8.44374	0.06877	0.06959	2.20060	10.78270
$\chi_3:\chi_3$	0.05467	1.25745	2.72411	0.00487	4.04110
$\chi_4:\chi_4$	2.85906	0.05904	0.05101	9.82991	12.79902
$\sigma_i:\sigma_i$	2.30080	0.79142	1.21043	5.29581	9.59846
$\chi_1:\sigma_i$	2.46459	0.07852	0.24670	0.57705	3.36686
$\chi_3:\sigma_i$	0.16570	0.02537	0.86758	0.15025	1.20890
$\chi_4:\sigma_i$	1.13658	0.11613	0.42073	3.66636	5.33980
$\sigma_i:\sigma_j$	0.80641	−0.04782	−0.04374	0	0.71485
$\sigma_i:\sigma_k$	0.42680	0.10467	0.22996	1.89606	2.65749

ellipsoidal coordinates. After this, integration over the other electron was carried out. The exact evaluation of the other integrals is considerably more difficult because of the presence of additional terms arising from the polynomials P_2^0 and P_2^2. After transformation to ellip-

TABLE VII. Kinetic energy integrals (in ev) and overlap integrals.

$\chi_1T\chi_1$	11.43249	S_1	0.1918
$\chi_3T\chi_3$	4.11460	S_2	0.062
$\chi_4T\chi_4$	26.67576	S_3	0.062
$\sigma_iT\sigma_i$	91.949	S_4	0.2836
$\sigma_iT\sigma_j$	−0.48549	S_{ij}	0.0113
$\sigma_iT\sigma_k$	−0.0185	S_{ik}	0.00075
$\chi_1T\sigma_i$	−6.69225		
$\chi_3T\sigma_i$	−1.76581		
$\chi_4T\sigma_i$	−8.83858		

tical coordinates, some of the resulting integrals would have required too much labor to evaluate. It was possible to estimate the relative contribution of the terms from P_2^m in comparison with the terms from P_0^0, by expanding the relatively small exponentials and considering average nuclear charges. As a result it was con-

TABLE VIII. Penetration integrals (ev).
(Computed at 1.58A, except as noted.)

VS^0	$:\chi_1^2$	−16.77369($R=0$)	
	$:\chi_3^2$	− 1.31847($R=0$)	
	$:\chi_4^2$	−16.77369($R=0$)	
	$:\sigma_i^2$	− 5.580	
	$:\chi_1\sigma_i$	−12.41490	
	$:\chi_3\sigma_i$	− 1.54498	
	$:\chi_4\sigma_i$	−10.67990	
	$:\sigma_i\sigma_j$	− 0.063(1.11A)	
	$:\sigma_i\sigma_k$	− 0.026($R=0$)	
VF_i^0	$:\sigma_i^2$	−67.69117($R=0$)	
	$:\sigma_i\sigma_j$	− 0.0396(2.23A)	
	$:\sigma_i\sigma_k$	− 0.00026(3.16A)	
	$:\sigma_j\sigma_j$	− 0.00146(2.23A)	
	$:\sigma_k\sigma_k$	-2.4×10^{-6}(3.16A)	
VF_i^0	$:\chi_1^2$	−1.2715	
	$:\chi_3^2$	−1.8729	
	$:\chi_4^2$	−2.5494	
	$:\chi_1\sigma_i$	−4.4723	
	$:\chi_3\sigma_i$	−0.6010	
	$:\chi_4\sigma_i$	−5.1329	
VF_1^0	$:\sigma_2\sigma_3$	−0.00016(1.93A)	
VF_j^0	$:\chi_1\sigma_i$	−0.1273 (1.77A)	
	$:\chi_3\sigma_i$	−0.05811(1.77A)	
	$:\chi_4\sigma_i$	−0.3671 (1.77A)	
VF_k^0	$:\chi_1\sigma_i$	−0.12193(2.37A)	
	$:\chi_3\sigma_i$	−0.05806(2.37A)	
	$:\chi_4\sigma_i$	−0.3615 (2.37A)	

TABLE IX. Two-electron integrals over atomic orbitals (ev).

One-centered integrals ($\chi_l\chi_l:\chi_{l'}\chi_{l'}=J_{ll'}$; $\chi_l\chi_{l'}:\chi_l\chi_{l'}=K_{ll'}$).	
J_{11}	11.517
$J_{22}=J_{33}$	3.2353
$J_{44}=J_{55}=J_{66}$	11.844
$J_{12}=J_{13}$	4.9627
$J_{14}=J_{15}=J_{16}$	11.517
$J_{24}=J_{25}=J_{26}$	5.0576
$J_{34}=J_{35}=J_{36}$	5.0576
$K_{12}=K_{13}$	0.05895
K_{23}	1.598
$K_{14}=K_{15}=K_{16}$	3.678
$K_{24}=K_{25}=K_{26}$	0.013
$K_{34}=K_{35}=K_{36}$	0.00203
$J_{ii}=\sigma_i\sigma_i:\sigma_i\sigma_i$	27.684
Two-centered integrals ($\chi_l\chi_l:\sigma_i\sigma_i=J_l$).	
J_1	7.230
$J_2=J_3$	3.945
$J_4=J_5=J_6$	10.570
$J_{ij}=\sigma_i\sigma_i:\sigma_j\sigma_j$ (at 2.23A)	6.325
$J_{ik}=\sigma_i\sigma_i:\sigma_k\sigma_k$ (at 3.16A)	4.220

cluded that the higher polynomial terms contributed only about 1 percent to the total value of the integral with these terms omitted, so the terms were neglected. After the paper of Mulligan[3] appeared, it was apparent that these approximations were closely similar to his asymptotic approximations. It is also clear that the approximations will not be bad at the S−F distance.

4. Exchange integrals.—One-centered integrals were treated in the same way as Coulomb integrals, and no approximations were made.

All other exchange integrals (and hybrid Coulomb-exchange integrals of type $pp:pq$ are included) were

TABLE X. Molecular interaction integrals (ev).

$\varphi_2\varphi_2:\varphi_8\varphi_8$	6.6616
$\varphi_2\varphi_8:\varphi_2\varphi_8$	1.80135
$\varphi_2\varphi_2:\varphi_9\varphi_9$	3.15887
$\varphi_2\varphi_9:\varphi_2\varphi_9$	1.71812
$\varphi_2\varphi_2:\varphi_{11}\varphi_{11}=\varphi_2\varphi_2:\varphi_{10}\varphi_{10}$	6.77313
$\varphi_2\varphi_{11}:\varphi_2\varphi_{11}=\varphi_2\varphi_{10}:\varphi_2\varphi_{10}$	0.01354
$\varphi_2\varphi_3:\varphi_8\varphi_9$	0.46334
$\varphi_2\varphi_8:\varphi_3\varphi_9$	1.60329
$\varphi_2\varphi_9:\varphi_3\varphi_8$	0.46334
$\varphi_2\varphi_3:\varphi_{11}\varphi_{11}=\varphi_2\varphi_3:\varphi_{10}\varphi_{10}$	0.62144
$\varphi_2\varphi_{11}:\varphi_3\varphi_{11}=\varphi_2\varphi_{10}:\varphi_3\varphi_{10}$	0

evaluated by an approximation suggested by Mulliken.[4] This approximation gives

$$pq:st=(S_{pq}S_{st}/4)(pp:ss+qq:ss+pp:tt+qq:tt).$$

In the case of integrals like $\sigma_1\sigma_2:\sigma_3\sigma_4$ the approximation is probably good, in view of the large distances involved and consequently small overlap of the charge distribution pq with st. The approximation is expected to be less good when one of the orbitals is on S, because of the reduced distance and the very large size and overlap of S orbitals. The three and four-center exchange integrals are extremely numerous, and they are not listed, but their magnitudes may be easily estimated from the formula above, with values of S (Table VII) and Coulomb integrals (Table IX).

Isotopic Composition of Oxygen in the Catalytic Decomposition of Hydrogen Peroxide*

MALCOLM DOLE, DEFOREST P. RUDD, GORDON R. MUCHOW AND CHARLES COMTE
Department of Chemistry, Northwestern University, Evanston, Illinois

(Received November 6, 1951)

The isotopic composition of oxygen liberated in the catalytic decomposition of hydrogen peroxide using MnO_2, Fe_2O_3, colloidal gold, metallic platinum, and soluble catalase as catalysts has been measured. All the catalysts except catalase produced a measurable fractionation of the oxygen isotopes in the case of complete decomposition. A few rate experiments were also carried out, and the kinetics studied from the standpoint of isotope separation as a function of fraction of hydrogen peroxide decomposed. It is demonstrated that none of the liberated oxygen comes from the substrate water or from the potassium permanganate when hydrogen peroxide is oxidized. Observed fractionation factors are somewhat smaller than the maximum values calculated on the basis of Bigeleisen's equations. A minimum in the O^{18} percentage of the evolved oxygen in the case of the catalase experiments suggests that two mechanisms are operative for this type of catalysis.

The initial enhancement of the O^{18} percentage of the evolved oxygen over that in the peroxide remains unexplained.

I. INTRODUCTION

THIS research was initiated for the purpose of finding out whether the isotopic composition of oxygen, evolved from the decomposition of hydrogen peroxide in water, bore any relation to the isotopic composition of the oxygen in the solvent water. Partly because of the fact that it is inadvisable to admit water vapor into most mass spectrometers, and partly because of difficulties due to the H_3O^+ ion, the isotopic composition of oxygen in the water has to be determined indirectly if the standard type mass spectrometer is used—usually by the isotopic study of carbon dioxide which has been equilibrated with the unknown water sample. The water-carbon dioxide equilibrium is relatively more sensitive to temperature than the water-oxygen equilibrium,[1] and for this reason there would be a slight advantage in using the latter, if it were possible to promote isotopic exchange and equilibration between molecular oxygen and water. In a paper published by Winter and Briscoe[2] while this work was in progress, evidence was given showing that no exchange of oxygen atoms occurred either during the time that hydrogen peroxide remained dissolved in the water, or during the decomposition of hydrogen peroxide by inorganic catalysts. These results are confirmed by our work presented below; so it would appear that the oxygen evolved in the decomposition of hydrogen peroxide cannot be used in a study of the isotopic composition of the substrate water. Even more recently Kolthoff and Miller[3] have demonstrated that in the uncatalyzed decomposition of persulfate in water, all the oxygen liberated comes from the water if the *p*H is 7 or higher. This finding suggests a method of obtaining the oxygen from water in the form of molecular oxygen, which is suitable for study in the mass spectrometer, but Kolthoff and Miller did not investigate any slight variations of isotopic composition due to rate effects, nor did they discover whether or not the evolved oxygen was in isotopic equilibrium with the solvent water.

There has been no previous studies of rate effects on the isotopic composition of oxygen evolved from hydrogen peroxide, nor of the isotopic composition of oxygen using organic catalysts such as catalase.[4]

II. THEORY OF THE EXPERIMENT

When hydrogen peroxide decomposes catalytically, half of its oxygen is liberated as molecular oxygen and half as water.

$$2H_2O_2 \rightarrow O_2 + 2H_2O. \quad (1)$$

If hydrogen peroxide is oxidized by excess manganese dioxide, let us say, a yield of molecular oxygen chemically equivalent to all the oxygen in the hydrogen peroxide is obtained.

$$H_2O_2 + MnO_2 + H_2SO_4 \rightarrow MnSO_4 + O_2 + 2H_2O. \quad (2)$$

Let

n_0 = original number of gram atoms of the oxygen in H_2O_2 before decomposition,
n_1 = gram atoms of oxygen in H_2O_2 remaining undecomposed at time t,
n_2 = gram atoms of oxygen in evolved oxygen,
n_3 = gram atoms of oxygen in water formed in reaction (1),
x = atom fraction of O^{18} in H_2O_2 remaining undecomposed at time t,
y = atom fraction of O^{18} in evolved oxygen at time t,
z = atom fraction of O^{18} in oxygen of water formed in reaction (1) at time t,

* This work was partially supported by the Air Force Cambridge Research Center under contract AF19(122)-157 with Northwestern University.

[1] See, for example, the calculations of H. C. Urey, J. Chem. Soc. 562 (1947), and of J. M. McCrea, J. Chem. Phys. **18**, 849 (1950).

[2] E. R. S. Winter and H. V. A. Briscoe, J. Am. Chem. Soc. **73**, 496 (1951).

[3] I. M. Kolthoff and I. K. Miller, J. Am. Chem. Soc. **73**, 3055 (1951).

[4] A. E. Cahill and H. Taube described some experiments in progress along these lines at the Diamond Jubilee Meeting of the Am. Chem. Soc., New York, Sept. 7, 1951. We are indebted to Professor Taube for discussing his results with us.

α=fractionation factor of oxygen isotope of mass 18 in the evolved oxygen with respect to the undecomposed hydrogen peroxide of reactions (1) and (2), or
$\alpha=y/x$,
β=fractionation factor of oxygen isotope of mass 18 in the evolved oxygen with respect to the oxygen of the water formed in reaction (1), or
$\beta=y/z$,
γ=average fractionation factor of oxygen isotope of mass 18 in the oxygen and water formed in reaction (1) with respect to the undecomposed hydrogen peroxide or

$$\gamma=\frac{y+z}{2x} \quad \text{or} \quad \gamma=\alpha\left(\frac{\beta+1}{2\beta}\right).$$

$$x_0 \cdot n_0 = x_1 \cdot n_1 + y \cdot n_2 + z \cdot n_3, \tag{3}$$

$$n_0 = n_1 + n_2 + n_3, \tag{4}$$

$$n_2 = n_3 \text{ (for catalytic decomposition)}, \tag{5}$$

whence

$$x=\frac{x_0 \cdot n_0 - n_2 \cdot y[(\beta+1)/\beta]}{n_1},$$

or

$$x=\frac{x_0 - fy[(\beta+1)/2\beta]}{1-f}, \tag{6}$$

where f is the fraction of peroxide decomposed. Equation (6) enables us to calculate x from the measured y provided that x_0 and β are known. At infinite time when the hydrogen peroxide has been completely decomposed, n_1 is zero and

$$\beta_\infty = y_\infty/(2x_0 - y_\infty). \tag{7}$$

If β is independent of the time, the β of Eqs. (7) and (6) will be identical. This point is discussed further below.

Let us now consider at any time t an additional amount, dn_1, of hydrogen peroxide decomposed; by virtue of the material balance we can write

$$n_1 \cdot x = -y\frac{dn_1}{2} - z\frac{dn_1}{2} + (x+dx)(n_1+dn_1) \tag{8}$$

(dn_1 is essentially negative, but dx is positive). Rearranging and integrating between limits of t' and t'', we obtain

$$\left[\alpha\left(\frac{\beta+1}{2\beta}\right)-1\right]\ln\frac{n_1''}{n_1'} = \ln\frac{x''}{x'}$$

or

$$(\gamma-1)\ln n_1''/n_1' = \ln x''/x'. \tag{9}$$

From the slope of a plot of $\log x_1$ as a function of $\log n_1$, it is possible to calculate $[\alpha(\beta+1/2\beta)-1]$ and knowing β to calculate α. The integration of (8) involves the assumption of the constancy of γ with the time.

In the case of reaction (2), n_3 is equal to zero, and Eqs. (6) and (9) become, respectively,

$$x=(x_0 \cdot n_0 - yn_2)/n_1 \tag{10}$$

and

$$(\alpha-1)\ln n_1''/n_1' = \ln x''/x'. \tag{11}$$

III. EXPERIMENTAL PROCEDURES

Source of Materials

Most of the sodium peroxide used was taken from one sample of J. T. Baker Company's calorific grade sodium peroxide, having an equivalent peroxide content of 97.0 percent on October 12, 1950 and a 96.8 percent content on December 24. This peroxide was manufactured by the Electrochemicals Division of E. I. du Pont de Nemours by air oxidation of sodium to Na_2O followed by oxidation to Na_2O_2 using pure oxygen from liquid air. The isotopic composition of the oxygen of this sodium peroxide must have been very close to that of atmospheric oxygen. A second sample of Na_2O_2 was supplied by the Parr Instrument Co. This peroxide gave oxygen of the same isotopic composition as that from the J. T. Baker Company sodium peroxide.

Two samples of manganese dioxide were used, one of them of unknown origin and the second, a sample of electrolytic manganese dioxide, WHM No. 3, from the Squier Signal Laboratory, Signal Corps, kindly supplied by Professor P. W. Selwood. Platinum wire, $FeSO_4$, and colloidal gold, the latter prepared by reduction of a one percent solution of gold chloride by tannin, were other inorganic catalysts used. The organic catalyst, catalase, was powdered soluble catalase from Armour and Company, their "Catalase 30."

Water, enhanced in O^{18} content by a factor of 1.025 relative to the oxygen of water, was obtained by reducing with hydrogen, carbon dioxide previously equilibrated with water.

Apparatus and Methods for the Decomposition of Peroxide

Sodium peroxide, dried in a desiccator, was weighed out into a small thin-wall glass bulb which was sealed off while the bulb was evacuated. The sodium peroxide bulb was then inserted into a mixing flask into the water or solution of desired *p*H and the whole evacuated and closed off to the atmosphere. By judicious shaking, the thin-walled bulb could be broken and the sodium peroxide dissolved in the distilled water or solution and allowed to stand as long as desired at a selected temperature. The concentration of the sodium peroxide was about one percent, the total volume of the solution about 100 ml.

This mixing flask was then inserted into the rest of the apparatus, a vacuum line, by means of a standard tapered joint. The catalyst tube, into which had been weighed the catalyst for the experiment, was inserted into the catalyst flask in a vertical position so that the

TABLE I. Isotopic composition of evolved oxygen in the catalytic decomposition of H_2O_2.

Water	Catalyst	% decomposition	% O^{18} in evolved oxygen
Normal	MnO_2 10 mg	103	0.2073
		106	0.2082
		107	0.2077
		103	0.2075
		100	0.2075 Av 0.2076
Enriched in O^{18}	MnO_2 10 mg	101	0.2073
Normal	Pt	101	0.2076
Normal	Colloidal Au	102	0.2078
Normal	$Fe(OH)_3$ 12 mg	102	0.2090
		108	0.2087 Av 0.2089
Normal	Catalase 10 mg	101	0.2041
		101	0.2045
		107	0.2044
		100	0.2043 Av 0.2043
Enriched in O^{18}	Catalase 10 mg	101	0.2043
		101	0.2040 Av 0.2042

peroxide solution could be delivered to the catalyst flask from the mixing flask without coming into contact with the catalyst until most of the solution had been transferred. In some experiments, the sodium peroxide bulb was broken under water containing the catalyst; in this case, the decomposition began the moment the sodium peroxide dissolved in the water. The oxygen evolved was collected in a flask for later insertion onto the mass spectrometer and the pressure measured so as to calculate oxygen yields. The decompositions took place at room temperature, 22–24°C.

Method of Measuring Isotope Ratios

A Consolidated-Nier isotope ratio mass spectrometer was used to determine percentages of O^{18} in the oxygen samples. The O^{18} abundance in the oxygen of water was calculated from O^{18} percentages of carbon dioxide brought into isotopic equilibrium with the water. All O^{18} percentages in this paper have been calculated with reference to the percentage of O^{18} in air, 0.2039 percent, as given by Nier.[5]

IV. DISCUSSION OF DATA

The data obtained in the catalytic decomposition of H_2O_2, reaction (1), are given in Table I and the data for the isotopic composition of the evolved oxygen in the total oxidation of the H_2O_2, reaction (2), are given in Table II. In agreement with the findings of Winter and Briscoe,[2] the O^{18} content of the evolved oxygen bore no relation to that of the substrate water. We also found that prolonged contact of gaseous oxygen with liquid water produced no exchange of oxygen isotopes in the presence of catalase or of hemoglobin. There is, however,

[5] A. O. Nier, Phys. Rev. **77**, 789 (1950).

TABLE II. Isotopic composition of evolved oxygen in total oxidation of H_2O_2.

Water	Oxidizing agent in excess	% yield	% O^{18} in evolved oxygen
Normal	MnO_2	98.0	0.2041
		96.2	0.2038
Normal	MnO_2 (Electrolytic)	76	0.2040
Enriched in O^{18}	MnO_2	92.2	0.2044
Normal	$KMnO_4$	90	0.2041

a marked difference in the percentage of O^{18} in the oxygen in the catalytic decomposition of H_2O_2 in the presence of inorganic catalysts as compared to the enzymatic catalyst, catalase. The experiments listed in Table II demonstrate that the O^{18} content of the evolved oxygen in the catalase experiments (Table I) was the same as the O^{18} content of the original sodium peroxide. In other words, there was no fractionation of the oxygen isotopes when catalase was used as the catalyst, in contrast to the small, but real, separation observed when platinum, colloidal gold, manganese dioxide (initially introduced in the form of manganous sulfate) and ferric hydroxide (initially introduced as ferrous sulfate) were used as the catalyst. Inasmuch as all the oxygen atoms in potassium permanganate are known to exchange with water,[6,7] the data of the last experiment of Table II prove that all the evolved oxygen in that experiment came from the peroxide, because if it had come from permanganate, the percentage of O^{18} would have been that of the substrate water or 0.1980 percent.[8] This conclusion is substantiated by the close agreement of the percent of O^{18} in the peroxide, 0.2041, with that expected due to oxidation by air, 0.2039, and by pure oxygen whose O^{18} percentage is usually slightly greater than that of air. It is further substantiated by the experiment using electrolytic MnO_2 whose oxygen derives from water.

The fact that the oxygen produced in the decomposition of hydrogen peroxide using catalase as the catalyst has the same O^{18} percentage as the original peroxide is in good agreement with the mechanism of the catalytic action of catalase postulated by Chance.[9] The first step in the reaction is probably the substitution of OH^- by OOH^- attached to the Fe-atom of the hematin group, or

$$\begin{array}{c}|\\ -\mathrm{FeOH}\\ |\end{array}+\mathrm{H_2O_2}\rightarrow\begin{array}{c}|\\ -\mathrm{FeOOH}\\ |\end{array}+\mathrm{H_2O}. \qquad (12)$$

The second step is the formation of molecular oxygen

[6] N. F. Hall and O. R. Alexander, J. Am. Chem. Soc. **62**, 3455 (1940).
[7] G. A. Mills, J. Am. Chem. Soc. **62**, 2833 (1940).
[8] M. Dole, J. Chem. Phys. **4**, 268 (1936); J. Am. Chem. Soc. **61**, 2025 (1939); Science **109**, 77 (1949).
[9] B. Chance, Nature, **161**, 914 (1948); J. Biol. Chem. **179**, 1299 (1949); **180**, 947 (1949).

according to the suggested mechanism

$$-\mathrm{FeOOH}+\mathrm{HOOH}\rightarrow\mathrm{O_2}+-\mathrm{FeOH}+\mathrm{H_2O}. \quad (13)$$

In process (12) there is no breaking of the O—O bond in the peroxide, nor is there in the reaction (13) as far as the molecular oxygen is concerned, according to the mechanism of Chance. The O—O bond is broken in the destruction of the $-\mathrm{FeOOH}$ group, but as all the oxygen of this group appears as water or exchanges with it, there can be no fractionation of the isotopes of oxygen in the separation of these oxygen atoms. The mechanism postulated by Chance does not permit any exchange of oxygen isotopes between the peroxide and water or between the molecular oxygen formed and the water, and is, therefore, in agreement with the observations of this paper. There might, of course, be a rate effect in either reaction (12) or (13); that is, the molecule $\mathrm{HO^{16}O^{16}H}$ might react with the catalase at a rate different from that of the molecule $\mathrm{HO^{16}O^{18}H}$. We consider the results of some rate experiments below.

Chance[9] suggests the possibility of two other mechanisms, one in which the second peroxide group adds to another Fe-atom of the hematin group after reaction (12) has taken place, followed by the splitting out of oxygen, or

$$\begin{array}{l} -\mathrm{Fe-OOH} \\ \quad | \\ -\mathrm{Fe-OH} \end{array} \quad +\mathrm{H_2O_2}\rightarrow \quad \begin{array}{l} -\mathrm{Fe-OOH} \\ \quad | \\ -\mathrm{Fe-OOH} \end{array} \quad +\mathrm{H_2O},$$

$$\begin{array}{l} -\mathrm{Fe-OOH} \\ \quad | \\ -\mathrm{Fe-OOH}\rightarrow -\mathrm{Fe-OH} \\ \quad | \qquad\quad | \\ \qquad\quad -\mathrm{Fe-OH}+\mathrm{O_2}; \end{array} \quad (14)$$

and the second in which hydroxyl radicals are produced by the hematin-peroxide complex, or

$$\begin{array}{l} -\mathrm{Fe-OOH} \\ \quad | \\ -\mathrm{Fe-OH}+\mathrm{H_2O_2}\rightarrow 2\mathrm{OH}+-\mathrm{FeOOH} \\ \quad | \qquad\qquad\qquad\quad | \\ \qquad\qquad\qquad\qquad -\mathrm{FeOH}. \end{array} \quad (15)$$

In the latter case, the hydroxyl radicals must react further, but the necessary additional reactions were not discussed by Chance.

We are inclined to reject processes (14) and (15) because of the possibility of fractionation of the oxygen isotopes in the splitting of the O—O bond in the peroxide group.

Turning now to the inorganic catalysts we see that $\mathrm{MnO_2}$, solid platinum and colloidal gold catalyze the decomposition of hydrogen peroxide to yield the same fractionation factor of the oxygen isotopes. This suggests that the mechanism of decomposition in each case may be the same, but at the present time the details of the heterogeneous catalysis of the decomposition of hydrogen peroxide have not been satisfactorily determined. Broughton and Wentworth[10] and Broughton, Wentworth, and Laing[11] demonstrated that the oxidation step of the cycle (oxidation of $\mathrm{Mn^{++}}$ to $\mathrm{Mn^{++++}}$) does not take place unless the solution is saturated with $\mathrm{Mn(OH)_2}$. Studies using radioactive manganese as tracer indicate that catalysis takes place by alternate oxidation and reduction of manganese. They suggest the following reactions as the probable mechanism:

$$\mathrm{MnO_2}+\mathrm{H_2O_2}+2\mathrm{H^+}\rightarrow\mathrm{Mn^{++}}+2\mathrm{H_2O}+\mathrm{O_2}, \quad (16)$$

$$\mathrm{Mn^{++}}+2\mathrm{H_2O}\rightleftarrows\mathrm{Mn(OH)_2}+2\mathrm{H^+}, \quad (17)$$

$$\mathrm{Mn(OH)_2}+\mathrm{H_2O_2}\rightarrow\mathrm{MnO_2}+2\mathrm{H_2O}. \quad (18)$$

Reaction (16) cannot represent in detail the path of the reaction for three reasons: first, there are too many reacting molecules in the reaction; second, the reaction does not clearly demonstrate that the evolved oxygen comes entirely from the peroxide as our experiments suggest, and third, no free radical is indicated (see below). Mooi and Selwood[12] have made an interesting magneto-chemical study of the catalytic decomposition of hydrogen peroxide by supported manganese oxides. From their observations, they have been led to suggest that the decomposition occurs in one electron steps and that the oxides involved are the dioxide and sesquioxide, or

$$\mathrm{Mn_2O_3}+\mathrm{H_2O_2}\rightarrow 2\mathrm{MnO_2}+\mathrm{H_2O} \quad (19)$$

$$2\mathrm{MnO_2}+\mathrm{H_2O_2}\rightarrow\mathrm{O_2}+\mathrm{Mn_2O_3}+\mathrm{H_2O}. \quad (20)$$

Mooi and Selwood believe furthermore that the decomposition proceeds at the interfaces between the dioxide and the sesquioxide, because the formation of either of these oxides should be facilitated by the nearby crystal of the other oxide into which the reduced or oxidized ions could fit. These reactions, like (16), (17), and (18) do not show the detailed path of the decomposition. If reaction (19) proceeds by the splitting of the O—O bond in the peroxide, a fractionation of isotopes would probably occur.

[10] D. B. Broughton and R. L. Wentworth, J. Am. Chem. Soc. **69**, 741 (1947).

[11] Broughton, Wentworth, and Laing, J. Am. Chem. Soc. **69**, 744 (1947).

[12] J. Mooi and P. W. Selwood, J. Am. Chem. Soc. **74**, 1750 (1952). We are indebted to Professor Selwood for the opportunity of reading this paper in advance of publication. A preliminary note appeared in J. Am. Chem. Soc. **72**, 4333 (1950).

The mechanism of the action of ferric and ferrous ions on the decomposition of hydrogen peroxide has been studied in much greater detail than that of the manganous, manganic or manganate ions. In 1934, Haber and Weiss[13] proposed the following mechanism:

$$Fe^{++}+H_2O_2\rightarrow Fe^{+++}+OH^-+OH, \quad (21)$$

$$OH+H_2O_2\rightarrow H_2O+HO_2, \quad (22)$$

$$HO_2+H_2O_2\rightarrow O_2+H_2O+OH, \quad (23)$$

$$OH+Fe^{++}\rightarrow Fe^{+++}+OH^-, \quad (24)$$

$$HO_2+Fe^{+++}\rightarrow Fe^{++}+O_2+H^+. \quad (25)$$

Baxendale, Evans, and Park,[14] demonstrated the existence of free radicals in the catalytic decomposition of H_2O_2 by observing the polymerization of vinyl compounds in this system. They found that chromous, mercury, cuprous, titanous, and manganous ions, as well as ferrous are effective in initiating vinyl polymerization in the aqueous solution decomposition of hydrogen peroxide.

Other mechanisms have been suggested: For example, Andersen[15] proposed that the decomposition of H_2O_2 in solutions of nitric acid and ferric nitrate proceeds according to the scheme

$$Fe^{+++}+HO_2^-\rightarrow FeOH^{++}+O \quad (26)$$

$$O+HO_2^-\rightarrow OH^-+O_2. \quad (27)$$

More recently Barb, Baxendale, George, and Hargrave[16] have published the results of an extensive study of the kinetics of the reaction between hydrogen peroxide and both ferrous and ferric ions. They concluded that H_2O_2 does not react with the perhydroxyl radical HO_2 to produce oxygen, but that oxygen comes from the reaction

$$Fe^{+++}+HO_2\rightarrow Fe^{++}+O_2+H^+. \quad (28)$$

In reaction (28) there is no fractionation of the oxygen isotopes as there is no splitting of the O—O bond and as the perhydroxyl radical probably reacts with the ferric ion with little if any activation energy. In the ferrous-ferric system involving reactions (21), (22), and (28), the observed fractionation probably occurs in reaction (21) because this reaction is the only one in which a splitting of the O—O bond definitely takes place. We have no assurance, however, that the kinetics of the homogeneous decomposition of hydrogen peroxide in acid solutions are actually valid for the heterogeneous decompositions studied by us. Nevertheless, for the purposes of this paper we shall assume that the decomposition is represented by the following equations:

$$\epsilon^-+HO^{16}O^{16}H\xrightarrow{k_1}HO^{16}+O^{16}H^- \quad (29)$$

$$\epsilon^-+HO^{16}O^{18}H\xrightarrow{k_2}HO^{16}+O^{18}H^- \quad (30)$$

$$\xrightarrow{k_3}HO^{18}+O^{16}H^- \quad (31)$$

$$HO^{16}+HO^{16}O^{16}H\xrightarrow{k_4}H_2O^{16}+O^{16}O^{16}H \quad (32)$$

$$HO^{18}+HO^{16}O^{16}H\xrightarrow{k_5}H_2O^{18}+O^{16}O^{16}H \quad (33)$$

$$HO^{16}+HO^{16}O^{18}H\xrightarrow{k_6}H_2O^{16}+O^{16}O^{18}H \quad (34)$$

$$\xrightarrow{k_6'}H_2O^{16}+O^{18}O^{16}H \quad (35)$$

$$HO^{18}+HO^{16}O^{18}H\xrightarrow{k_7}H_2O^{18}+O^{16}O^{18}H \quad (36)$$

$$\xrightarrow{k_7'}H_2O^{18}+O^{18}O^{16}H \quad (37)$$

$$O^{16}O^{16}H\xrightarrow{k_8}O^{16}O^{16}+H^++\epsilon^- \quad (38)$$

$$O^{16}O^{18}H\xrightarrow{k_9}O^{16}O^{18}+H^++\epsilon^- \quad (39)$$

$$O^{18}O^{16}H\xrightarrow{k_9'}O^{16}O^{18}+H^++\epsilon^- \quad (40)$$

$$H^++O^{16}H^-\xrightarrow{k_{10}}H_2O^{16} \quad (41)$$

$$H^++O^{18}H^-\xrightarrow{k_{11}}H_2O^{18}. \quad (42)$$

We shall also assume that reactions (29), (30), and (31), are the slow steps in the process and the ones in which fractionation occurs. If this is true, then the following simplifications become possible:

$$k_4=k_5=2k_6=2k_6'=2k_7=2k_7' \quad (43)$$

$$k_8=k_9=k_9'. \quad (44)$$

Assuming first order kinetics and that

$$\frac{1+2x(k_2+k_3)/k_1}{1+4x}$$

may be set equal to unity (x is of the order 0.002 and $(k_2+k_3)/k_1$, nearly unity), it is possible to derive the expressions

$$(HO^{16}O^{16}H)=(HO^{16}O^{16}H)_0e^{-2k_1t}, \quad (45)$$

$$(HO^{16}O^{18}H)=(HO^{16}O^{18}H)_0e^{-(k_1+k_2+k_3)t}, \quad (46)$$

[13] F. Haber and J. Weiss, Proc. Roy. Soc. (London) **147A**, 332 (1934).

[14] Baxendale, Evans, and Park, Trans. Faraday Soc. **42**, 155 (1946).

[15] V. Sten Andersen, Acta Chem. Scand. **2**, 1 (1948); also discussed by J. A. Christiansen, XII International Congress of Pure and Applied Chemistry, New York, Sept. 10, 1951.

[16] Barb, Baxendale, George, and Hargrave, Trans. Faraday Soc. **47**, 462, 591 (1951).

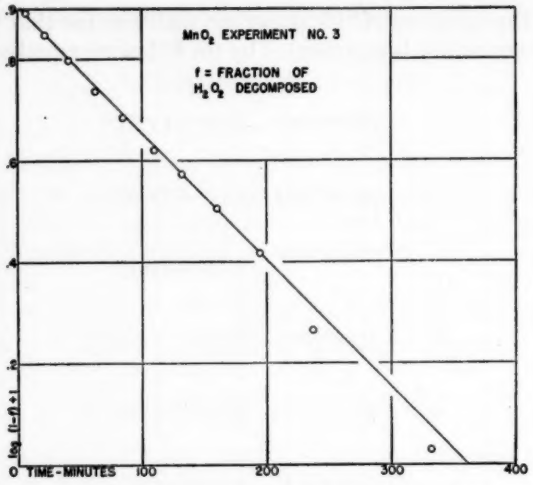

FIG. 1. First-order plot of the hydrogen peroxide decomposition reaction.

$$(O^{16}O^{16})=\frac{(HO^{16}O^{16}H)_0 k_1\cdot k_8}{k_8-2k_1}\times\left[\frac{1}{k_8}(e^{-k_8 t}-1)-\frac{1}{2k_1}(e^{-2k_1 t}-1)\right], \quad (47)$$

$$(O^{16}O^{18})=\frac{(HO^{16}O^{18}H)_0 k_1\cdot k_8}{k_8-k_1-k_2-k_3}\times\left[\frac{1}{k_8}(e^{-k_8 t}-1)-\frac{1}{k_1+k_2+k_3}(e^{-(k_1+k_2+k_3)t}-1)\right], \quad (48)$$

where the subscript zero refers to zero time. Also

$$\frac{(O^{16}O^{18})/(O^{16}O^{16})}{(HO^{16}O^{18}H)/(HO^{16}O^{16}H)}=\frac{y}{x}. \quad (49)$$

At infinite time when the hydrogen peroxide has been completely decomposed, it follows from Eqs. (45), (46), (47), and (48) that

$$\frac{y_\infty}{x_0}=\frac{2k_1}{k_1+k_2+k_3}. \quad (50)$$

Letting

$$\epsilon=\frac{k_1}{k_2+k_3}, \quad (51)$$

then

$$\frac{y_\infty}{x_0}=\frac{2\epsilon}{1+\epsilon}, \quad (52)$$

and

$$\beta=\epsilon. \quad (53)$$

As far as the kinetics adopted by us is concerned, we cannot distinguish between reactions (30) and (31) so that k_2 can be set equal to k_3, and ϵ equal to $k_1/2k_2$.

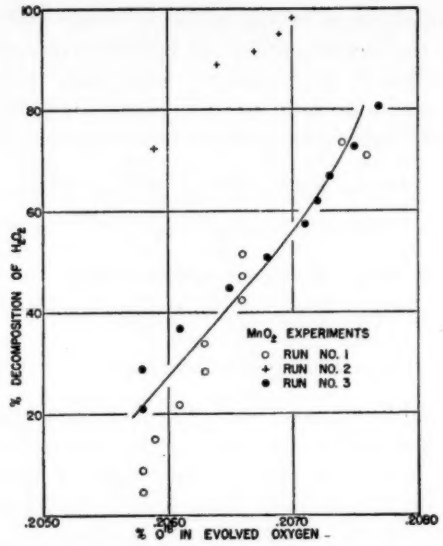

FIG. 2. Isotopic composition of the total oxygen evolved in the catalytic decomposition of hydrogen peroxide, MnO_2 as the catalyst.

Bigeleisen[17] has derived relations based on the absolute reaction rate theory and partition function ratios for molecules differing only in isotopic composition which enable ϵ to be calculated theoretically. The equations are

$$\epsilon=\frac{k_1}{2k_2}=\left\{\frac{m_2^\ddagger}{m_1^\ddagger}\right\}^{\frac{1}{2}}\times\{1+\sum^{3m-6}G(u_i)\Delta u_i-\sum^{3m'-6}G(u_i^\ddagger)\Delta u_i^\ddagger\}, \quad (54)$$

$$\Delta u_i=\frac{hc}{kT}(\omega_{1i}-\omega_{2i}), \quad (55)$$

$$G(u_i)=\frac{1}{2}-\frac{1}{u}+\frac{1}{e^u-1}. \quad (56)$$

The frequencies of vibration of the $HO^{16}O^{16}H$ molecule

TABLE III. Fundamental frequencies of hydrogen peroxide of different isotopic composition.

Molecule		ω in cm^{-1}					
		ω_1	ω_2	ω_3	ω_4	ω_5	ω_6
$HO^{16}O^{16}H$	Calc.	3411	1383	834		3412	1406
	Obs.	3360	1418	878	635	3360	1353
$HO^{16}O^{18}H$	Est.	3405	1378	813		3406	1398
$HO^{18}O^{18}H$	Calc.	3399	1373	793		3400	1391
$\Delta\omega$ $HO^{16}O^{16}H$ $-HO^{16}O^{18}H$		12	10	41		12	15
$\Delta\omega$ $HO^{16}O^{16}H$ $-HO^{18}O^{18}H$		6	5	20		6	7

[17] J. Bigeleisen, J. Chem. Phys. **17**, 344, 675 (1949); J. Bigeleisen and M. G. Mayer, J. Chem. Phys. **15**, 261 (1947).

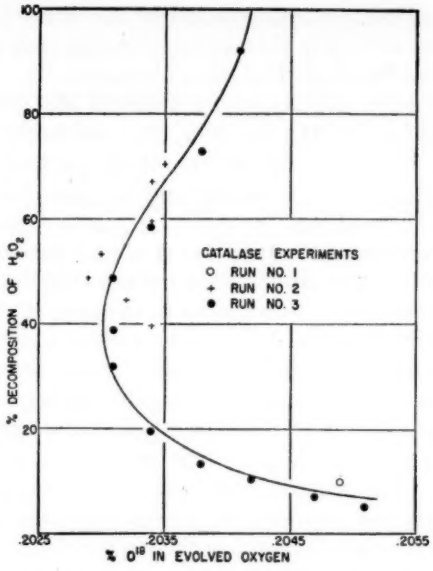

FIG. 3. Isotopic composition of the total oxygen evolved in the catalytic decomposition of hydrogen peroxide, catalase as the catalyst.

have recently been discussed by Giguère.[18] From force constants given by Bailey and Gordon[19] and from the equations of Morino and Mizushima,[20] it is possible to calculate the frequencies of the fundamental modes of vibration of the $HO^{16}O^{16}H$ and $HO^{16}O^{18}H$ molecules.[21] The frequencies of the $HO^{16}O^{18}H$ molecule can then be estimated, and the rate constant ratio, $k_1/2k_2$, calculated. In Table III the frequencies of the various isotopic molecules are collected together. We used 1.48A for the O—O bond distance, 0.98A for the OH distance, 102° for the H—O—O angle, and 6.5×10^5, 3.6×10^5 and

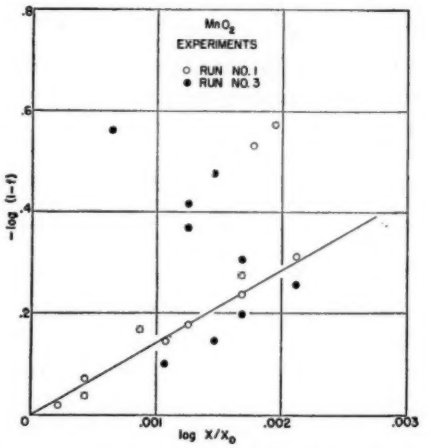

FIG. 4. Test of Eq. (9) for the MnO_2 experiments.

[18] P. A. Giguère, J. Chem. Phys. **18**, 88 (1950); See also R. C. Taylor, J. Chem. Phys. **18**, 898 (1950).
[19] C. R. Bailey and R. R. Gordon, Trans. Faraday Soc. **34**, 1133 (1938).
[20] Y. Morino and S. Mizushima, Sci. Papers Inst. Phys. Chem. Research, (Tokyo) *32*, 220 (1937); quoted by Bailey and Gordon.
[21] We are indebted to Dr. Gordon M. Barrow for aid in these calculations.

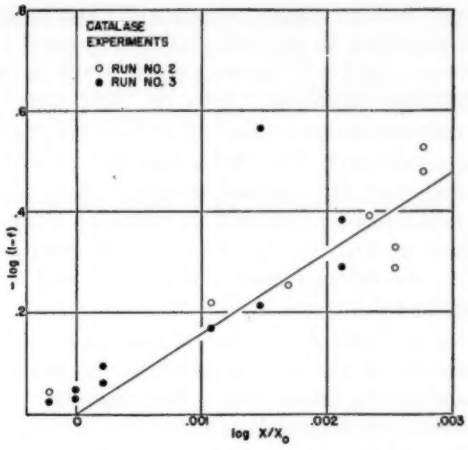

FIG. 5. Test of Eq. (9) for the catalase experiments.

1.0×10^5 dynes/cm for the force constants of the OH vibration, the O—O vibration, and the HOO bending mode, respectively. The observed frequency values of Table III were taken from the paper of Giguère[22] as well as the bond distances and angles mentioned above. Assuming that the frequencies ω_1 and ω_5, the OH stretching frequencies, are the same in the activated complex as they are in the normal molecule, and assuming that ω_4, the frequency of the torsional mode, is unchanged in passing from one isotopic species to the other, it becomes necessary only to calculate $G(u)$ and Δu values for the frequencies, ω_2, ω_3, and ω_6. When this is done, we find 1.078 for the value of $k_1/2k_2$, a value which is significantly higher than the observed (β) of 1.048 (iron catalysis) or 1.035 (manganese catalysis). These calculations suggest that the O—O stretching and bending frequencies are not entirely negligible in the activated complex as we have assumed—provided, of course, that the kinetics adopted by us for the decomposition is correct.

In this connection it might be pointed out that if the hydrogen peroxide or its ion HOO^- forms a tight complex with the catalyst such as $FeOOH^{++}$, in which the FeO bond is strong with a large force constant, then the isotopic fractionation to be expected on splitting the O—O bond would be reduced because of a reduction in the shift of frequencies in passing from one isotopic species to the other.

A few experiments were performed in which the isotopic composition of the liberated oxygen was measured as a function of the extent of the reaction using catalase and MnO_2 as the catalysts. A first-order plot of the data for one of the MnO_2 experiments is shown in Fig. 1 while in Figs. 2 and 3 are illustrated the change in the isotopic composition of the liberated oxygen as a function of the percentage decomposition of hydrogen peroxide for the MnO_2 and catalase experiments, re-

[22] P. A. Giguère, J. Chem. Phys. **18**, 88 (1950); see also R. C. Taylor, J. Chem. Phys. **18**, 898 (1950); L. R. Zumwalt and P. A. Giguère, J. Chem. Phys. **9**, 458 (1941).

spectively. In Figs. 4 and 5 the data of Figs. 2 and 3 are plotted according to the relationship expressed by Eq. (9). When $-\log(1-f)$ becomes equal to 0.3 or greater, the calculated values of x from the data have such a large experimental uncertainty that they are practically without significance. The MnO_2 data seem to fit Eq. (9) fairly well, but the catalase results deviate from the straight line relationship at low values of $-\log(1-f)$. According to Eq. (9), the linear curve should extrapolate to the origin (where both $(1-f)$ and x/x_0 are equal to unity).

From the slopes of the straight lines of Figs. 4 and 5 it is possible to calculate γ which in the two cases is 0.993 and 0.994, respectively. The close agreement of these two values suggest that there may be a diffusional separation of the oxygen isotopes inasmuch as in the catalase experiments there is no net fractionation for complete decomposition. By diffusional separation we mean a more rapid diffusion of the $HO^{16}O^{16}H$ molecule to the catalyst than the $HO^{16}O^{18}H$ molecule resulting in a smaller O^{18}/O^{16} ratio of the evolved oxygen at the start of the decomposition than at the end.

According to the kinetics adopted in this paper, the initial value of y/x_0 should be unity, as computed by approximating the exponential terms by a series expansion and taking only the first term of the expansion. The experimental data do not bear out this prediction, perhaps because the initial mechanism is unknown.

We have carried out a more complete mathematical study of Eqs. (29) through (42) without assuming that reactions (29), (30) and (31) are the slow steps in the process. This work demonstrates that β does not change with time being given at all times by the expression

$$\beta=2k_1\cdot k_6/k_4(k_2+k_3). \qquad (57)$$

It also predicts that the initial O^{18} fraction in the evolved oxygen, y_i, should be *less* than the O^{18} fraction for the undecomposed peroxide, or

$$y_i=2x_0\cdot k_6/k_4, \qquad (58)$$

inasmuch as we would expect k_6 to be smaller than k_4. This is not in agreement with observation and is, in fact, the most perplexing aspect of our work. The new expression for β, Eq. (57), agrees even less well with the predictions based on Bigeleisen's equation.

Incidentally, our values of β, 1.035 for MnO_2 catalysis and 1.048 for $Fe(OH)_3$ catalysis, are considerably higher than the value calculated for isotopic exchange equilibrium between the water and oxygen formed in reaction (1), or 1.006.[23]

An interesting feature of our results is the change in the isotopic composition of the oxygen with fraction of hydrogen peroxide decomposed in the case of the catalase experiments, Fig. 3. From the work of George[24] it is evident that hydrogen peroxide is decomposed by catalase at an initial rapid rate, which declines more or less exponentially to a slower steady rate. George believes that the hydrogen peroxide forms a reversible complex with catalase which has a lower catalytic activity than the original free catalase molecule. The fact that the percentage of O^{18} in the oxygen evolved in the catalase decomposition goes through a minimum bears out the finding of George of two types of catalytic activity. Addition of cyanide or azide suppresses the initial rapid reaction; hence George's observation cannot be due to a diffusion effect—a diffusion layer increasing in width with the time could also explain a decrease in the initial rate. In the case of the MnO_2 experiments a rapid decrease in the initial rate was also observed (note that the straight line of Fig. 1 does not extrapolate to a zero value of $\log(1-f)$ at zero time as it should if the rate followed the first-order kinetics to zero time). It is also interesting to note that the percentage of O^{18} in the initially evolved oxygen in the catalase experiments seems to approach that of the MnO_2 experiments. This fact suggests that the initial reaction of the catalase catalyzed decomposition may involve a splitting of the O—O bond.

The clarification of the effects observed initially must await further experimentation.

---

[23] H. C. Urey, J. Chem. Soc. 562 (1947).
[24] P. George, Nature **160**, 41 (1947); Biochem. J. **44**, 197 (1949).

The Dielectric Properties of Compressed Fluoromethane

H. G. David, S. D. Hamann, and J. F. Pearse
Commonwealth Scientific and Industrial Research Organization, Division of Industrial Chemistry, High Pressure Laboratory, Chemical Engineering Department, University of Sydney, Sydney, Australia

(Received January 22, 1952)

The dielectric constant, dielectric loss, and density of compressed fluoromethane have been measured at 50°C and 75°C in the pressure range 20 to 160 atmospheres. The ratio $(\epsilon-1)/d(\epsilon+2)$ shows a large and regular decrease as the density increases. The theories of Debye, Onsager, and Kirkwood have been applied to the results. Evidence of the restriction of molecular rotation at high densities is adduced.

INTRODUCTION

THERE is considerable information[1] on the dielectric properties of polar liquids and of their vapors at atmospheric pressure. Behavior in the range of densities between these two states is of great interest and can be observed by the study of compressed gases. It appears, however, that the only polar gas for which such measurements have been made is ammonia, as reported by Keyes and Oncley.[2]

This paper reports measurements on fluoromethane, which was chosen for its conveniently low critical temperature, 44.55°C,[3] its high dipole moment, 1.81×10^{-18} esu,[4] and its lack of reactivity.

EXPERIMENTAL

CH_3F was prepared by heating an equimolecular mixture of sodium methyl sulfate and sodium fluoride to 250°C.[5,6]

The gases evolved were passed through two wash bottles containing conc. H_2SO_4 and two containing 40 percent NaOH solution to remove the byproducts of the reaction, $(CH_3)_2O$, HF, SO_2, and SiF_4. The CH_3F was dried by magnesium perchlorate, led at atmospheric pressure through a dry ice and alcohol trap, finally condensed on a liquid air trap and permanent gases were pumped off. It was then fractionally distilled and stored in the manner previously described for ethylene.[7]

The vapor pressure of a sample of the fluoromethane at dry ice temperature agreed with that of a sample prepared by the decomposition of tetramethylammonium fluoride.[8]

Capacity and Density Measurements

Simultaneous measurements of pressure (P) and capacity were made in the manner previously reported for ethylene.[7] Since no P-V-T data were available for fluoromethane, measurements of the density (d) were made by the constant volume method. (Holborn[9] and Bartlett[10]). A 2-cc high pressure gas pipette was connected to the gas condenser and pressure balance through a needle valve. When capacity and pressure measurements were completed the valve was closed, this action causing a negligible pressure change in the system. The quantity of gas thus enclosed in the pipette was later determined by expanding it to atmospheric pressure in a 1-liter gas burette. Pressure in the burette was measured by a mercury manometer. The pipette and burette were mounted in the same thermostat as the condenser.

Dielectric Loss Measurement

During the course of the capacity measurements it was found that the minimum anode current in the Henriquez oscillator[11] increased with increasing density. This implied[12] that a power loss was occurring in the gas condenser. To measure the loss the gas condenser was replaced by an equal low loss capacitor and variable series resistor. The resistor was adjusted until the same minimum anode current was obtained. From the values of resistance and capacitance the power factor could be estimated.

At densities greater than the critical, the power loss in the gas condenser was found to cause an error in the capacity as measured, owing to the change in the characteristics of the measuring circuit. A series of measurements of the magnitude of this error at various densities was made at the same time as the power loss measurements. From a smooth curve drawn through these points a correction was applied to the dielectric constant results. The correction amounted to about $1\frac{1}{2}$ percent in the factor $(\epsilon-1)/d(\epsilon+2)$ at the highest densities.

RESULTS

Dielectric Constant and Density

The results are shown in Tables I and II. In the calculation of densities from the gas burette measure-

[1] A General Discussion on Dipole Moments, Trans. Faraday Soc. **30**, 677 (1934).
[2] F. G. Keyes and J. L. Oncley, Chem. Revs. **19**, 195 (1936).
[3] W. Cawood and H. S. Patterson, J. Chem. Soc. 2180 (1932).
[4] C. P. Smyth and K. B. McAlpine, J. Chem. Phys. **2**, 499 (1934).
[5] J. Dumas and E. Péligot, Ann. chim. et phys. (2) **61**, 193 (1836).
[6] E. Moles and T. Batuecas, J. de Chim. Phys. **17**, 35 (1919).
[7] H. G. David, S. D. Hamann and J. F. Pearse, J. Chem. Phys. **19**, 1491 (1951),
[8] S. D. Hamann and J. F. Pearse, Trans. Faraday Soc. (to be published).
[9] L. Holborn and H. Schultze, Ann. Physik (4) **47**, 1089 (1915).
[10] E. P. Bartlett, J. Am. Chem. Soc. **49**, 687 (1927).
[11] P. Cohen Henriquez, Physica **2**, 429 (1935).
[12] J. Reilly and W. N. Rae, *Physico-Chemical Methods* (D. Van Nostrand Company, Inc., New York, 1939), Vol. II, p. 513.

TABLE I. Dielectric constant and density of fluoromethane at 50.00°C.

P (Int. ats.)	ϵ	d (moles/liter)	$(\epsilon-1)/d(\epsilon+2)$ (cc/mole)	PV/RT[a]
21.706	1.2176	0.960	70.4	0.853
29.919	1.3330	1.433	69.7	0.787
36.512	1.4477	1.879	69.1	0.733
41.373	1.5512	2.265	68.5	0.689
45.463	1.6572	2.646	67.9	0.648
49.400	1.7834	3.084	67.1	0.604
53.068	1.9313	3.570	66.4	0.561
55.683	2.0669	3.997	65.6	0.525
57.970	2.2206	4.474	64.6	0.4887
60.819	2.4956	5.29	62.9	0.4337
63.530	2.979	6.60	60.2	0.3628
63.630	3.001	6.65	60.1	0.3606
64.799	3.420	7.69	58.1	0.3178
64.721	3.414	7.70	57.9	0.3170
65.468	3.811	(8.67)[b]	(55.8)	(0.2849)
65.541	3.828	8.68	55.9	0.2848
65.826	4.019	9.24	54.3	0.2686
65.962	4.123	9.51	53.6	0.2616
66.190	4.210	9.69	53.4	0.2577
66.636	4.496	10.28	52.4	0.2445
67.287	4.726	10.79	51.4	0.2353
68.670	5.143	11.68	49.67	0.2218
69.052	5.214	11.78	49.57	0.2210
70.948	5.541	12.40	48.55	0.2157
71.724	5.659	12.68	47.99	0.2134
73.480	5.843	12.97	47.62	0.2137
74.993	5.992	13.29	47.00	0.2128
77.205	6.163	13.55	46.67	0.2149
79.830	6.340	13.90	46.08	0.2167
81.402	6.422	14.02	45.91	0.2189
118.25[c]		16.05		0.2779
160.42[c]		17.14		0.3531

[a] Calculated as P/dRT using $R=82.053$ cc atmos/mole as given by J. A. Beattie in *Temperature* (Reinhold Publishing Corporation, New York, 1941), p. 87.
[b] This density was found by interpolation in the d/P data.
[c] The capacities here were beyond the range of the apparatus.

ments the variation of PV with P was allowed for. The values of the second virial coefficient $B(T)$ used in doing this were taken from earlier low pressure measurements made in this laboratory.[8] The figures were

$$B(323.16)=-171 \text{ cc/mole},$$
$$B(348.16)=-141 \text{ cc/mole}.$$

TABLE II. Dielectric constant and density of fluoromethane at 75.00°C.

P (Int. ats.)	ϵ	d (moles/liter)	$(\epsilon-1)/d(\epsilon+2)$ (cc/mole)	PV/RT
28.885	1.2552	1.190	65.9	0.850
39.664	1.3902	1.762	65.3	0.788
54.288	1.6359	2.724	64.2	0.698
63.930	1.8611	3.535	63.1	0.633
71.993	2.1143	4.396	61.6	0.573
77.687	2.3463	5.15	60.1	0.528
78.556	2.3865	5.25	60.2	0.524
81.365	2.5289	5.68	59.4	0.501
85.623	2.7732	6.44	57.7	0.4657
90.681	3.1138	7.41	55.8	0.4286
93.086	3.303	7.88	55.1	0.4136
98.526	3.736	8.98	53.1	0.3840
102.92	4.061	9.79	51.6	0.3680
107.80	4.390	10.60	50.0	0.3560
115.10	4.809	11.58	48.32	0.3480
122.68	5.141	12.37	46.88	0.3471
133.63	5.530	13.22	45.51	0.3539
147.73	5.920	14.00	44.38	0.3695

Included in the tables are the values of PV/RT for the various densities. The variation of this factor with pressure is shown in Fig. (1), which illustrates the relation of the region studied to the critical point. For each temperature the values of PV corresponding to the seven lowest densities were fitted to a curve of the form

$$PV=RT+a(T)d+b(T)d^2+c(T)d^3$$

by the method of least squares. The second virial coefficient was calculated from the relationship $B(T)=a(T)/RT$. The following values were obtained:

$$B(323.16)=-168 \text{ cc/mole},$$
$$B(348.16)=-140 \text{ cc/mole}.$$

These are in good agreement with the low pressure values quoted above.

The difference between the density of the gas in the high pressure pipette and that in the gas condenser, due

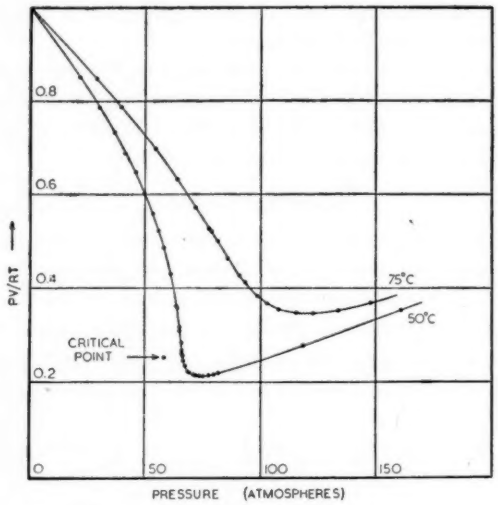

FIG. 1. Isotherms for fluoromethane.

to the head of gas between them, was calculated to be never greater than 0.01 percent and was therefore neglected.

Dielectric Loss

The variation of the tangent of the loss angle δ with density is shown in Table III and in Fig. (2). It must be emphasized that these measurements were made by an extempore method and the results can only be regarded as approximate. They are, however, of considerable interest qualitatively. The power loss is zero until the critical density is approached and then increases rapidly with increasing density, the rate of increase being more pronounced at 50°C than at 75°C ($T_c=44.55$°C).

APPARENT DIPOLE MOMENT

The most extensively applied theories of polarization in dipolar media are those of Debye and Onsager. Both

theories are approximate and a discussion of their relative merits is found in the Faraday Society's "General Discussion on Dielectrics."[13] If the molecular dipole moment were constant, Debye's theory would require that the Clausius-Mosotti function $(\epsilon-1)/d(\epsilon+2)$ be independent of density at a given temperature. Tables I and II show that there is a large decrease in the C–M ratio for CH_3F with increasing density. It is noteworthy that Keyes and Oncley[2] report an *increase* in this ratio for NH_3. Onsager's theory would require the function $(\epsilon-n^2)(2\epsilon+n^2)/\epsilon d(n^2+2)^2$ to be similarly independent of density (here n is the refractive index). For the present case this function increases by 7 percent. These effects might arise either from the inadequacy of the theories or from changes in the dipole moment of CH_3F with density.

There is no reason to suppose that the dipole moment, μ, of a CH_3F molecule in the compressed gas is the same as that of an isolated molecule since a variation of μ with density might easily occur if the molecules were distorted by the intermolecular forces. In this respect the apparent dipole moments calculated from the Debye and Onsager theories and given in Table IV are of interest. The change in the Debye values is larger than would be expected from considerations of the magnitude of the intermolecular forces in the pressure range studied. Onsager's model leads to a smaller apparent change in μ and appears to be the more satisfactory in the present case.

If it were possible to calculate the distribution function for compressed CH_3F, Kirkwood's precise treatment[13,14] of polar fluids could be applied to the experimental data to find the real change in μ. This calculation is unfortunately exceedingly difficult. In the next section the theory is used in the opposite way, assuming μ to be constant, to find the change in Kirkwood's correlation parameter, g.

TABLE III. Dielectric absorption in fluoromethane at 1 megacycle.[a]

50°C		75°C	
Density (moles/l)	tanδ	Density (moles/l)	tanδ
≤6.6	0.00000	≤6.9	0.00000
7.03	0.00022	7.70	0.00009
7.40	0.00046	8.38	0.00030
7.94	0.00128	9.05	0.00072
8.43	0.00176	9.67	0.00164
8.93	0.00227	10.30	0.00312
9.50	0.00330	10.87	0.00504
10.06	0.00444	11.42	0.00787
10.58	0.00518	11.94	0.01022
11.03	0.00669		
11.51	0.00935		

[a] Measurements to 5 megacycles showed an increase in the absorption with frequency in this range.

[13] "General Discussion on Dielectrics," Trans. Faraday Soc. **42A** (1946).

[14] J. G. Kirkwood, J. Chem. Phys. **7**, 911 (1939).

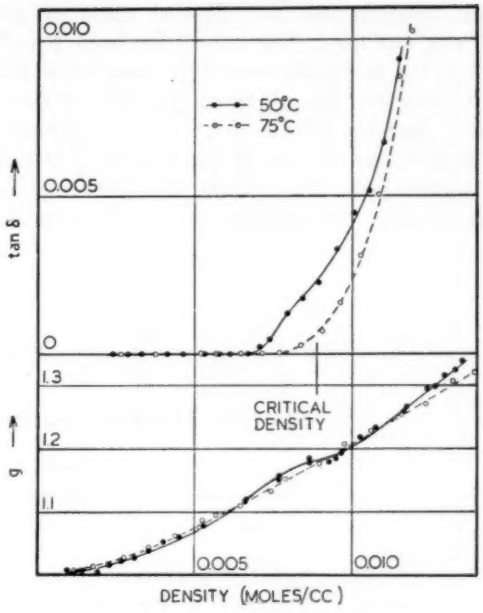

FIG. 2. Dielectric loss and correlation parameter for fluoromethane.

RESTRICTED ROTATION NEAR THE CRITICAL POINT

In an earlier note[15] the sudden development of the dielectric loss near the critical density of CH_3F was taken as evidence of a fairly sharp transition between free and restricted rotation of the dipolar molecules. Some further evidence of this is found in the change of ϵ with density. Kirkwood,[13,14] allowing for the effects of hindered rotation on the dielectric constant, obtained the expression

$$(2\epsilon+1)(\epsilon-1)/9\epsilon d = {}_DP + 4\pi N_0 g\mu^2/9kT,$$

where ${}_DP$ is the molar distortion polarization, N_0 is Avogadro's number, and μ is the dipole moment of an isolated molecule. The correlation parameter g can be related to the forces restricting the rotation of the molecules. Its divergence from unity is a measure of the extent of the restriction.

Figure (2) shows g as a function of density and temperature. It was calculated on the assumption that μ is

TABLE IV. Apparent dipole moment of fluoromethane.

50°C			75°C		
d (moles/l)	μ_{App} (esu $\times 10^{-18}$)[a] Debye	Onsager[b]	d (moles/l)	μ_{App} (esu $\times 10^{-18}$)[a] Debye	Onsager[b]
0.960	1.806	1.813	1.190	1.804	1.813
3.570	1.745	1.819	3.535	1.759	1.825
7.69	1.615	1.857	6.44	1.670	1.838
10.28	1.517	1.859	9.79	1.562	1.863
12.40	1.449	1.876	11.58	1.500	1.865
14.02	1.400	1.889	14.00	1.423	1.869

[a] Smyth and McAlpine's figure (see reference 4) for the distortion polarization ${}_DP = 8.95$ cc/mole was used in calculating μ_{App}.

[b] An "effective" refractive index n was calculated from the relationship $(n^2-1)/d(n^2+2) = {}_DP$.

[15] David, Hamann, and Pearse (to be published).

constant. Smyth and McAlpine's[4] value of $\mu=1.81\times10^{-18}$ esu was used. The curves for both g and $\tan\delta$ show that the molecules lose their freedom of rotation at high densities. In addition, the 50°C curves have shoulders near the critical density, d_c, suggestive of a fairly sudden loss of some of the rotational freedom as d_c is approached. To confirm the existence of the comparatively low shoulder on the g curve some further measurements were made several weeks after the original series. These gave results in complete agreement with the earlier ones.

The authors wish to thank Professor R. J. W. Le Fèvre for suggestions leading to this investigation and for some helpful discussions.

The advice and assistance of Dr. J. S. Dryden in the dielectric absorption measurements were of great value.

THE JOURNAL OF CHEMICAL PHYSICS VOLUME 20, NUMBER 6 JUNE, 1952

Specific Heat of Germanium between 20°K and 200°K*

I. ESTERMANN† AND J. R. WEERTMAN‡
Department of Physics, Carnegie Institute of Technology, Pittsburgh, Pennsylvania
(Received December 26, 1951)

High precision measurements of the specific heat of germanium were carried out in the temperature region between 20°K and 200°K. Three samples of germanium were investigated: an extremely pure sample, one of intermediate purity (10^{18} impurity centers/cm^3), and one with an addition of 0.006 atomic percent aluminum (2×10^{20} impurity centers/cm^3). No anomaly such as reported by Cristescu and Simon was found in any of the samples. However, a small dependence of the specific heat on the concentration of impurity centers was observed.

INTRODUCTION

IN 1934 S. Cristescu and F. Simon[1] reported measurements of the specific heat of germanium as a function of temperature (Fig. 1) which exhibit an extremely anomalous behavior. Between 70 and 90°K there is a high peak in the curve, amounting to an increase in C_p of 1.4 cal/degree-mole above the normal value. Furthermore, the values of the specific heat on the low temperature side of the peak are much higher than would be expected from a continuation of the high temperature side of the curve. If the upper part of the curve is fitted to a Debye curve, using the parameter $\theta=290°$, and this curve is extrapolated down to absolute zero, it is found that the total difference in energy between this curve and the measured curve amounts to 85 calories.

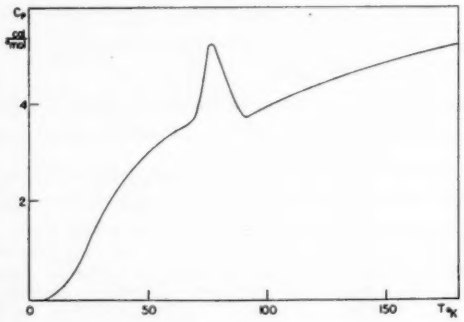

FIG. 1. Specific heat of germanium *versus* temperature after Cristescu and Simon.

A theoretical interpretation of these results as a lattice phenomenon is difficult in view of the fact that germanium is not known to undergo any phase transformation in the temperature range under consideration. Because very pure germanium was not available when the cited work was carried out, and also because the scattering of the points on the graph of specific heat *versus* temperature given by Simon and Cristescu indicated that the precision of their measurements was not very high, it was decided to repeat the measurements. Preliminary measurements on a pure sample of germanium were carried out in 1944 at the Carnegie Institute of Technology, and the anomalous behavior was not observed. Furthermore, at all temperatures, the magnitude of the specific heat per mole that was obtained in these measurements was considerably smaller than that reported by Simon and Cristescu. The theory of semiconductors as developed during the last ten years suggested the possibility that anomalies of the specific heat might be produced by the presence of impurity centers acting as electron donors or acceptors. It was decided, therefore, to undertake a systematic investigation, using high precision methods, of the specific heat of germanium as a function, not only of temperature, but also of impurity concentration. Thus it could be seen if any unusual electronic behavior of the impurity atoms led to the anomalous specific heat behavior.

* Assisted by the ONR. Results were presented at the Washington Meeting of the American Physical Society, April, 1951; Phys. Rev. **83**, 228 (1951).
† Now at the ONR, Navy Department, Washington, D. C.
‡ Abstract of thesis submitted by J. R. Weertman in partial fulfillment of the requirements for the degree of Doctor of Science at the Carnegie Institute of Technology.
[1] S. Cristescu and F. Simon, Z. physik Chem. **B25**, 273 (1934).

THEORETICAL REMARKS

For the general theory of semiconductors we refer to the recent work by W. Shockley.[2] The separation in energy between the filled band and the conduction band in germanium is 0.72 electron-volts. As a result, the number of electrons having sufficient energy to make the transition from the filled band to the conduction band at or below room temperature is so small that contributions to the specific heat from these electrons would be negligible. However, P. Aigrain and C. Dugas[3] have proposed recently that the anomaly in the specific heat of germanium observed by Simon and Cristescu might be caused by the ionization of electrons to or from impurity levels, which requires only an energy of about 0.05 electron-volts. Their calculations indicated that the process of ionization would take place over a rather limited temperature range, thus leading to a pointed maximum in the specific heat curve as reported by Cristescu and Simon.

PROCEDURE

(a) Thermometry

It has been pointed out recently[4] that results on low temperature heat capacity work obtained in different laboratories are not directly comparable, since the temperature scales used are not standardized. As a result of the Conferences on Low Temperature Calorimetry, the National Bureau of Standards has undertaken to calibrate strain-free platinum resistance thermometers made according to specifications laid down by the Bureau. The work described below was carried out with the use of a thermometer calibrated by the National Bureau of Standards from 10°K to the boiling point of sulfur. The temperatures given are therefore those of the International Temperature Scale of 1948 above 90°K, and those of the National Bureau of Standards scale below 90°K.

(b) The Calorimeter

The equipment was patterned after the vacuum calorimeter described first by Nernst and Eucken. Its main parts are a cryostat, a calorimeter capsule, and a thermometer.

A drawing of the cryostat is shown in Fig. 2. The capsule (A) containing the sample was suspended from the lid of the inner can (B) by silk threads. The can was sealed onto the lid with "Cerrobend," and a solution consisting of about one part of concentrated hydrochloric acid to two parts of water was used as flux. Connection to the vacuum system was made through a monel tube (C). The leads entered at the top of the cryostat through a Teflon plug. To prevent heat from leaking into the capsule the leads were wrapped around a copper ring (D) soldered into the lid of the can. Between this ring and the capsule the wires were wound in the form of helices in order to gain additional length. All of the leads were made of 0.008-cm diameter (No. 40) enameled copper wire except the current leads to the heater, which were of 0.01-cm diameter (No. 38) enameled copper wire.

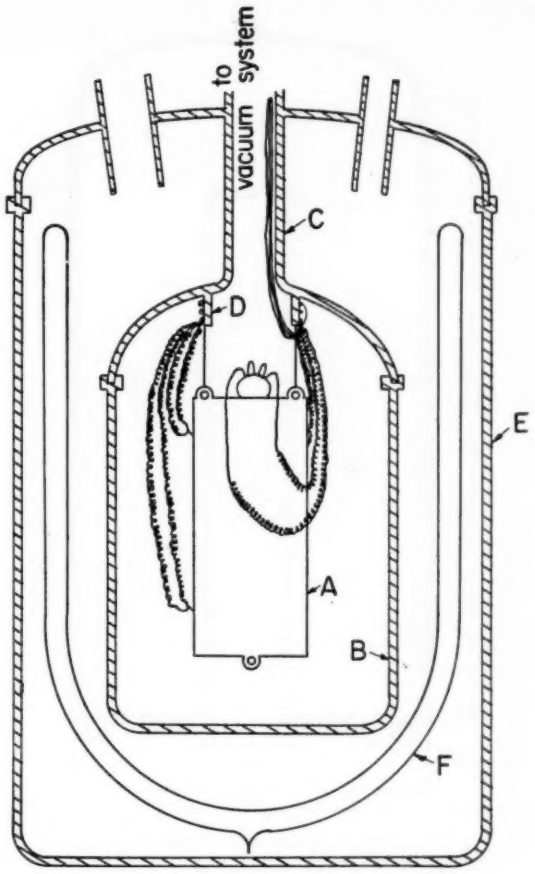

FIG. 2. Cryostat.

The outer can (E) contained a Dewar (F) which was used to hold the temperature bath. The pressure over the bath could be reduced by connecting a pump to the filling tube and plugging the exhaust tube. When liquid hydrogen or solid nitrogen was used for the temperature bath, the outer can was placed in a Dewar containing liquid nitrogen.

In order to minimize the heat exchange between the calorimeter capsule and the surroundings and to eliminate the need for an adiabatic shield, a rather large number of constant temperature baths was used. Thus a fairly complete curve of heat capacity *versus* temperature could be obtained without having to heat the capsule to a temperature very far above that of the bath. This method combines some of the advantages of the isothermal and the adiabatic calorimeter.

The calorimeter capsule is shown in Fig. 3. Temperatures were measured by means of the calibrated ther-

[2] W. Shockley, *Electrons and Holes in Semi-Conductors* (D. Van Nostrand Company, Inc., New York, 1950).
[3] P. Aigrain and C. Dugas, Compt. rend. **13**, 1277 (1950).
[4] Conference on Low Temperature Calorimetry, Chem. Eng. News **24**, 2782 (1946).

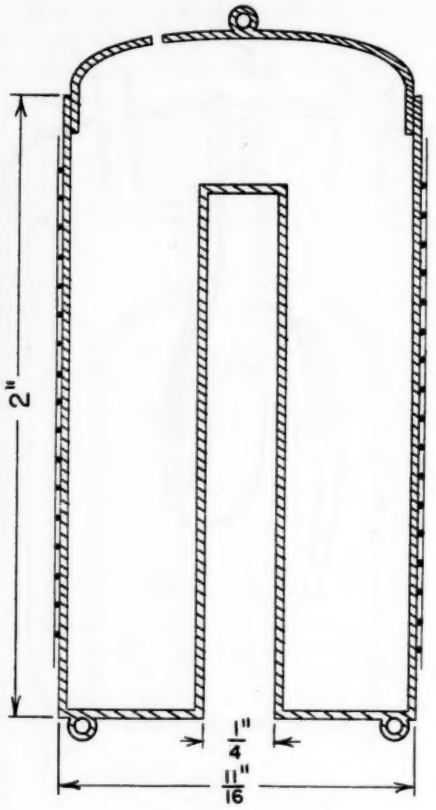

FIG. 3. Calorimeter capsule.

mometer, which was placed in the re-entrant well. The space between the wall of the well and the thermometer was filled with Wood's metal. Bare 0.016-cm diameter (No. 34) constantan wire wound around the outside of the capsule served as a heater. Electrical insulation was effected by a thin piece of lacquered paper placed between the winding and the capsule and another which covered the winding. A piece of shiny aluminum foil was wrapped around the winding to cut down radiation. After placing the sample in the capsule and soldering on the lid, helium gas was introduced through a pin hole in the lid and the hole was then quickly plugged. This helium insured good heat transfer. The same amounts of solder and Wood's metal were always used and thus no correction for their contribution to the heat capacity was necessary for the comparison of the specific heats of the different samples.

The resistance of the thermometer was measured by measuring the emf produced by a known current. The value of the current was determined by measuring the emf across a standard resistor kept in a thermostated oil bath. Potential measurements were made with a Rubicon Double Thermofree potentiometer. An attempt was made to choose a value of the measuring current which would give as large an emf across the thermometer as could be measured by the potentiometer. However, the currents used never exceeded 1 ma. Temperatures could be measured to about 1/1000 of a degree.

The heater circuit was so arranged that the current was always on, going through the heater during the heating periods, and through a dummy resistor of about the same resistance (approximately 18 ohms) during the rest of the time. The current through the heater was measured by measuring the emf across a 10-ohm standard resistor in series with the heater.

An electric stop clock was started and stopped together with the heater current, allowing the total time

TABLE I. Hall constants and impurity concentrations of the germanium samples.

Sample	Temperature (°K)	Hall constant (cm^3/coulomb)	Number of impurity centers/cm^3
Pure	298°	-26×10^3	2.8×10^{14}
	77	-35×10^3	2.1×10^{14}
Intermediate	302	− 7.77	9.5×10^{17}
	77	− 7.4	1.0×10^{18}
	4.2	−14.8	5.0×10^{17}
0.006 at. % Al	297	+ 0.033	2.2×10^{20}
	77	+ 0.066	1.1×10^{20}
	4.2	+ 0.198	$.4\times10^{20}$

TABLE II. Specific heat of the three germanium samples.

T (°K)	Specific heat, C_p (cal/°K mole) Pure sample	Intermediate sample	0.006 at. % Al sample
20	0.224_4	0.224_4	0.224_4
25	0.418_5	0.418_5	0.418_6
30	0.638_5	0.638_5	0.638_7
35	0.858_6	0.858_6	0.858_7
40	1.074	1.074	1.075
45	1.281	1.281	1.282
50	1.497	1.497	1.497
52.5	1.596	1.596	1.597
55	1.678	1.683	1.687
60	1.881	1.885	1.899
65	2.080	2.080	2.097
70	2.278	2.282	2.304
75	2.472	2.477	2.499
80	2.662	2.671	2.684
85	2.839	2.843	2.861
90	2.999	3.012	3.038
95	3.158	3.167	3.193
100	3.309	3.326	3.349
105	3.465	3.473	3.495
110	3.598	3.611	3.633
115	3.732	3.741	3.772
120	3.857	3.870	3.897
125	3.978	3.991	4.005
130	4.086	4.090	4.104
135	4.189	4.194	4.199
140	4.293	4.293	4.294
145	4.375	4.375	4.376
150	4.453	4.453	4.453
155	4.522	4.522	4.522
160	4.578	4.578	4.579
165	4.638	4.638	4.639
170	4.694	4.694	4.695
175	4.746	4.746	4.747
180	4.798	4.798	4.799
185	4.849	4.849	4.850
190	4.893	4.893	4.894
195	4.944	4.944	4.945
200	4.992	4.992	4.993

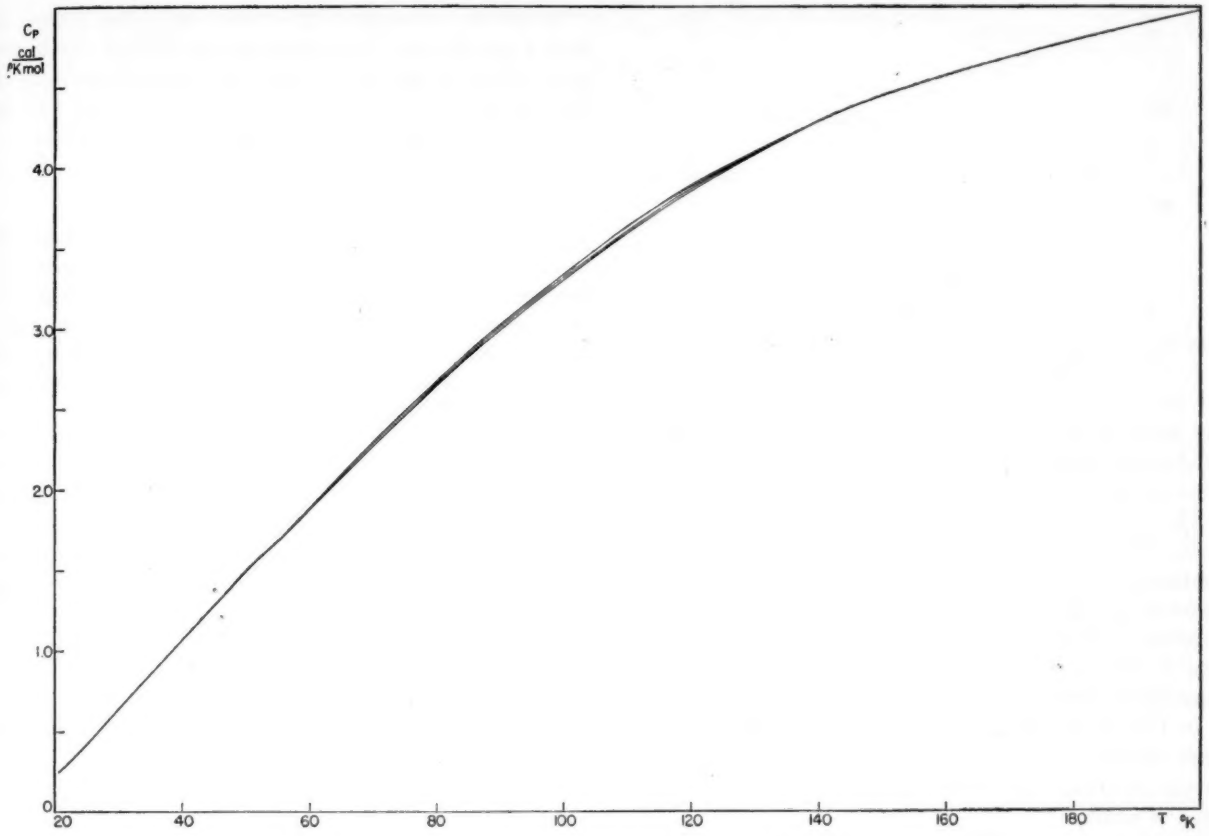

FIG. 4. Specific heats of the three germanium samples *versus* temperature. Upper curve—0.006 atomic % Al sample; middle curve—intermediate sample; lower curve—pure sample.

of the heating period to be measured to approximately 1/100 of a second.

RESULTS

Three samples of germanium were measured. The first is extremely pure germanium. Its Hall constant is -26×10^3 cm³/coulomb at room temperature. Since the Hall constant R is related to the number of conducting particles per unit volume n by the equation[2]

$$R=\frac{7.37\times10^{18}}{n}\ \text{cm}^3/\text{coul},$$

this value of the Hall constant corresponds to an impurity concentration of 2.8×10^{14} impurity centers/cm³. The second sample is N-type of an intermediate purity, having a Hall constant of -7.77 at room temperature (9.5×10^{17} impurity centers/cm³). The third sample, which is P-type, is pure germanium with an addition of 0.006 atomic percent aluminum, giving a Hall constant of 0.033 at room temperature (2.2×10^{20} impurity centers/cm³). Values of the Hall constant and the corresponding number of impurity centers/cm³ of the three samples at various temperatures are given in Table I. About 16.8 grams of each sample were used in the specific heat measurements.

Since the difference in temperature between the sample capsule and the external temperature bath was always quite small, the temperature drifts during the pre- and post-heating periods were so regular that the effective temperature increase during a heating period could be measured to about one part in a thousand (this was checked by using different heating periods and different external bath temperatures in some cases). The amount of heat was known to better than one part in a thousand. The heat capacity of the calorimeter capsule plus sample could thus be measured to a few tenths of one percent. Since the same amounts of material, solder, and Wood's metal were used in each set of measurements, variations in the heat capacities must be attributed to differences in the specific heat of the different samples. Between 20 and 50°K, the values for all three samples lie on the same curve within the accuracy given above. The same situation seems to exist above 140°K, although the increased scattering of the points of these temperatures, because of the lack of suitable temperature baths and greater heat interchange between bath and calorimeter, makes such an accurate comparison impossible. Between 50 and 140°K, however, the heat capacities increase with impurity content.

For the determination of the molal specific heats C_p,

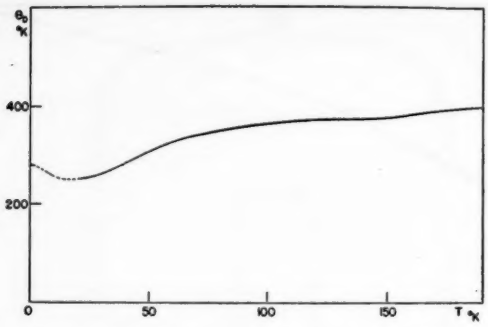

FIG. 5. Debye characteristic temperature θ_D of pure germanium *versus* temperature.

the heat capacity of the empty calorimeter was measured and subtracted from the values obtained with the filled calorimeter.

The results for the three samples are tabulated in Table II and graphically shown in Fig. 4. It will immediately be seen that none of the samples has an anomalous specific heat curve such as reported by Cristescu and Simon. Moreover, at all temperatures the new values of the specific heat are much smaller than those given by Cristescu and Simon.

In the temperature range between 50 and 55°K all three samples have a slight bump in their specific heat curves. Although this effect is small, it is well beyond the limit of error.

The total energy difference between the specific heat curves for the pure and for the 0.006 atomic percent aluminum samples, i.e., the area between the two curves, was calculated and found to be 2.28 calories. The ordinary electronic specific heat is too small to account for this difference. However, using the simple model proposed by Aigrain and Dugas, and assuming an energy gap of 0.05 ev, the number of impurity centers necessary to produce the observed energy difference of 2.28 calories (the energy difference between the specific heat curves for the pure germanium and for the 0.006 atomic percent aluminum germanium) was calculated. This number came out to be $0.9\times10^{20}/\text{cm}^3$, which agrees reasonably well with the value of 1.1×10^{20} as computed at 77°K from Hall effect measurements. However, work done by G. L. Pearson and J. Bardeen[5] on silicon seems to indicate that the energy gap decreases with increasing impurity concentration. Because the energy gap at this high concentration of impurities is not known, it was felt that the effort of making calculations which take into account the degeneracy of the electrons was not justified.

[5] G. L. Pearson, and J. Bardeen, Phys. Rev. **75**, 865 (1949).

In order to compare the results with the theory of lattice specific heat, it is necessary to convert the measured values of the specific heat at constant pressure to the corresponding values at constant volume. There is a thermodynamic relationship between the two:

$$C_p-C_v=(9\alpha^2VT)/k,$$

where α is the linear coefficient of thermal expansion, V the molar volume, and k the compressibility. Grüneisen's law which states that the ratio of the linear coefficient of thermal expansion to the specific heat is a constant independent of temperature, along with the assumption that k and V do not change much with temperature, leads to the simplified equation

$$C_p-C_v=AC_p^2T$$
$$A=9\alpha^2V/(kC_p^2).$$

A further simplification is due to Nernst and Lindemann.[6] They show that A may be related to the melting temperature T_s of the solid as follows:

$$A=0.0214/T_s.$$

The melting temperature of germanium is 1231.7°K. Thus

$$C_p-C_v=1.737\times10^{-5}C_p^2T \text{ cal/degree-mole.}$$

Using this equation, the C_p values for the pure sample were converted to the corresponding values of C_v. The Debye characteristic temperature θ_D was then calculated as a function of temperature (Fig. 5). Down to about 100°K, θ_D decreases rather slowly, but below this temperature it drops rapidly and seems to be leveling off around 20°. However, according to Blackman's theory[7] of specific heat, it is quite likely that the region around 20° is a spurious region of θ_D constancy, and that θ_D will rise at still lower temperatures.§

ACKNOWLEDGMENTS

We are indebted to the Research Corporation for a grant from which part of the equipment used in this work was purchased. We also wish to thank Dr. Shockley of the Bell Telephone Laboratories for the germanium sample No. 1, and Mr. R. B. Scott of the National Bureau of Standards for germanium sample No. 3.

[6] W. Nernst and F. Lindemann, Z. Elektrochem. **17**, 817 (1911).
[7] M. Blackman, Reports on Progress in Physics **8**, 11 (1941).
§ Measurements of the specific heat of germanium at liquid helium temperatures by S. A. Friedberg (thesis, Carnegie Institute of Technology, 1951) give a value of 280° for θ_D between 1.8 and 4°K.

Vibrational Intensities. II. The Use of Isotopes

BRYCE CRAWFORD, JR.
School of Chemistry, University of Minnesota, Minneapolis 14, Minnesota
(Received February 18, 1952)

Two rules are presented which relate the intensities of vibrational fundamentals of different isotopic species. They are thus analogous to the Teller-Redlich product rule which relates frequencies. They apply to either infrared or Raman intensities. One rule permits the calculation of dipole-moment derivatives without the determination of normal coordinates. The application of the rules is illustrated.

IN the study of vibrational intensities, we may expect the comparison of isotopic molecules to be fruitful, as it has been in the study of vibrational frequencies. We have looked into the relations to be expected among fundamental-band intensities, and in this paper we report two sum-rules which should be useful. One supplies an analog of the Teller-Redlich product rule; this should serve as a useful check on assignments and may also aid in estimation of isotopic distributions. The other permits us to calculate dipole-moment derivatives without determining the normal coordinates; this should be a welcome short-cut.

Both rules are based on what we call the double harmonic approximation: i.e., we take the potential energy to be a quadratic function of the displacements, neglecting mechanical anharmonicity, and the dipole moment to be a linear function of the displacements, neglecting electrical anharmonicity.[1] The value of the rules will therefore depend on how well these approximations hold, which can only be found out by experiments. We shall present our discussion in terms of infrared intensities; the same arguments apply, *mutatis mutandis*, to Raman intensities.

PRELIMINARY STATEMENT

The integrated band intensity of the ath fundamental is related to the effect of the ath normal coordinate Q^a on the (molecular) dipole moment $\mathbf{p}$ by the relation[2]

$$A \equiv \int_{\text{band}} \alpha_\nu d\nu = (\pi N/3c)(\partial \mathbf{p}/\partial Q^a)^2, \tag{1}$$

where the symbols have their usual meaning.[2] We may use subscripts 1, 2, $\cdots$ to distinguish isotopic molecules, and write

$$p_{1a}{}^x = (\partial p^x/\partial Q_1{}^a) \tag{2}$$

for the effect of the ath normal coordinate in isotope 1 on the x component of the dipole moment. Then if we conveniently tuck the universal constants in with the integrated band intensity and call the result I_{1a}, we may rewrite (1) as

$$I_{1a} = \sum_x (p_{1a}{}^x)^2. \tag{3}$$

Now in interpreting intensity data, we really seek $\mathbf{p}$ as a function, not of the normal coordinates, but of chemically intelligible coordinates; usually these are chosen to be valence-force coordinates. Let us call these coordinates R^k; then the quantities we are interested in are the derivatives

$$p_{1k}{}^x \equiv [\partial p^x/\partial R^k]_1. \tag{4}$$

(The coordinate R^k is defined without explicit references to atomic masses, and hence carries no isotopic subscript; but its effect on $\mathbf{p}$ may differ in the different isotopes, as we shall presently discuss.) The R^k are related to the normal coordinates by a transformation L_1:

$$R^k = (L_1)_a{}^k Q^a. \tag{5}$$

We shall use the summation convention: summation is understood over an index repeated once in subscript and once in superscript. Our notation and our methods are based on the papers of Wilson.[3] We may therefore write

$$I_{1a} = \sum_x p_{1k}{}^x p_{1j}{}^x (L_1)_a{}^k (L_1)_a{}^j. \tag{6}$$

Now Wilson[3] has shown that

$$\sum_a (L_1)_a{}^k (L_1)_a{}^j = G_1{}^{kj}, \tag{7}$$

where his G matrix may be written down *a priori* from atomic masses and molecular geometry; similarly

$$\sum_a (L_1)_a{}^k \lambda_{1a}{}^{-1} (L_1)_a{}^j = (F^{-1})^{kj}, \tag{8}$$

where the matrix F^{-1} is the reciprocal of Wilson's force-constant matrix F, and is thus the same for all isotopes. (Here $\lambda_{1a} = 4\pi^2 \omega_{1a}{}^2$, ω_{1a} being the frequency of the ath normal vibration in isotope 1.) So we may form two sums over intensities as follows:

$$\sum_1{}^F \equiv \sum_a (I_{1a}/\omega_{1a}{}^2) = 4\pi^2 \sum_x p_{1k}{}^x p_{1j}{}^x (F^{-1})^{kj} \tag{9}$$

$$\sum_1{}^G \equiv \sum_a I_{1a} = \sum_x p_{1k}{}^x p_{1j}{}^x G_1{}^{kj}. \tag{10}$$

The first sum $\sum_1{}^F$ will often be invariant under isotopic substitution and supply us with an intensity sum-rule analogous to the product rule. For, since the matrix (F^{-1}) is the same for all isotopes, the R.H.S. of Eq. (9) will be the same whenever the derivatives $p_{1k}{}^x = p_{2k}{}^x$; we shall presently find the conditions for this. It is clear that symmetry considerations may be

[1] See B. L. Crawford and H. L. Dinsmore, J. Chem. Phys. **18**, 983, 1682 (1950).
[2] Thorndike, Wells, and Wilson, J. Chem. Phys. **15**, 157 (1947).
[3] E. B. Wilson, Jr., J. Chem. Phys. **7**, 1047 (1939); **9**, 76 (1941).

TABLE I.

Band	ω_a (cm^{-1}) HCN	DCN	A (cm^{-1}/cm atmos) HCN	DCN	I_a(D^2/amu A^2) HCN	DCN
ν_1	2089	1921	0.64	12.2	0.0034	0.0648
ν_3	3312	2629	241.0	136.0	1.28	0.723

applied as usual; if the coordinates R^k are chosen to be symmetry coordinates,[3] then the sums over a, k, and j may be restricted to a single symmetry species.

The second sum $\sum_1{}^G$ gives us no invariant; but it does relate the quantities we seek, the p_{1k}, to the quantities we measure, the I_{1a}, in terms of easily calculated coefficients, the $G_1{}^{kj}$, which can be calculated without the trouble of a normal-coordinate determination.

Before extending these sums to the case where $p_{1k}{}^x \neq p_{2k}{}^x$, let us illustrate their application.

A SIMPLE EXAMPLE

We may use some recent data[4] on the parallel vibrations of HCN and DCN; for the two vibrations in the parallel species, $p_{1k}{}^z = p_{2k}{}^z$. The data are given in Table I. For the $\sum^F$ sums we have from (9)

$$(0.64/2089^2)+(241.0/3312^2) = (12.2/1921^2)+(136.0/2629^2)$$
$$(0.0147+2.19)\times 10^{-5} = (0.33+1.97)\times 10^{-5}$$
$$2.20 = 2.30$$

agreeing within 5 percent.

In using the $\sum^G$ rule, we need consider only the z component of $\mathbf{p}$ (the axial component) as affected by the bond coordinates (CH) and (CN): i.e., we seek $p_{\mathrm{CH}}{}^z$ and $p_{\mathrm{CN}}{}^z$. We take as our units: of electric moment, Debyes (D); of mass, the atomic mass unit (amu); of length, the angstrom (A). The conversion factor from band intensities (cm^{-1}/cm atmos N.T.P.) to I_a(D^2/amu A^2) is then $3V_0c^2 10^{20}/\pi N_0{}^2 = 0.00532$. The needed G-matrix elements[5] are

$$G_1{}^{\mathrm{CH,\,CH}} = 1.083,\ G_2{}^{\mathrm{CH,\,CH}} = 0.583;$$
$$G_1{}^{\mathrm{CN,\,CN}} = G_2{}^{\mathrm{CN,\,CN}} = 0.1548;$$
$$G_1{}^{\mathrm{CH,\,CN}} = G_2{}^{\mathrm{CH,\,CN}} = -0.0833.$$

Hence (10) applied in turn to each isotope gives

$$(\mathrm{HCN}):\ 0.0034+1.28 = 1.2834 = 1.083(p_{\mathrm{CH}}{}^z)^2 - 2\times 0.0833(p_{\mathrm{CH}}{}^z)(p_{\mathrm{CN}}{}^z)+0.1548(p_{\mathrm{CN}}{}^z)^2$$
$$(\mathrm{DCN}):\ 0.0648+0.723 = 0.7878 = 0.583(p_{\mathrm{CH}}{}^z)^2 - 2\times 0.0833(p_{\mathrm{CH}}{}^z)(p_{\mathrm{CN}}{}^z)+0.1548(p_{\mathrm{CN}}{}^z)^2.$$

These equations yield $p_{\mathrm{CH}}{}^z = \pm 0.996$, $p_{\mathrm{CN}}{}^z = \pm 1.793$ or ∓ 0.717.

[4] G. E. Hyde and D. F. Hornig, Brown University ONR Report No. 18, NR-019-102.

[5] J. C. Decius, J. Chem. Phys. **16**, 1025 (1951).

EXTENDED STATEMENT

As hinted above, $p_{1k}{}^x = p_{2k}{}^x$ only in special circumstances.[6] The reason this is not true in general stems from the requirement that "internal" coordinates, such as the R^k, conserve linear and angular momenta. A bending motion will therefore usually require some compensating rotation of the molecule as a whole; and this will carry an additional contribution to the dipole-moment change.

To formulate these effects, let us start from a set of Cartesian coordinates $x^s (s = 1, 2, \cdots, 3n$ where n is the number of atoms in the molecule): we may surely take $m_s{}^x = (\partial p^x/\partial x^s)$ the same in all isotopes. Another complete set of coordinates will consist of the $R^k[k = 1, 2, \cdots, (3n-6)]$ plus 6 translations and rotations $\rho_1{}^n$ $(n = 1, 2, \cdots, 6)$. We may transform by the coefficients $B_s{}^k$, $(\beta_1)_s{}^n$, $(A_1)_k{}^s$, $(\alpha_1)_n{}^s$, so defined that

$$x^s = (A_1)_k{}^s R^k + (\alpha_1)_n{}^s(\rho_1)^n;$$
$$R^k = B_s{}^k x^s;\quad (\rho_1)^n = (\beta_1)_s{}^n x^s. \tag{11}$$

The reciprocity conditions on these transformations demand, *inter alia*,

$$(A_1)_k{}^s B_t{}^k + (\alpha_1)_n{}^s(\beta_1)_t{}^n = \delta_t{}^s;$$
$$B_s{}^k(A_1)_j{}^s = \delta_j{}^k;\quad (\beta_1)_s{}^n(A_1)_k{}^s = 0; \tag{12}$$

whence we easily find

$$(A_2)_k{}^s = (A_1)_k{}^s - (\alpha_2)_n{}^s(\beta_2)_t{}^n(A_1)_k{}^t. \tag{13}$$

Now the coefficients we seek, $p_{1k}{}^x$, may be written

$$p_{1k}{}^x = m_s{}^x(A_1)_k{}^s \equiv (mA_1)_k{}^x, \tag{14}$$

and if we define

$$(v_{21})_k{}^x = [m_s{}^x(\alpha_2)_n{}^s][(\beta_2)_t{}^n(A_1)_k{}^t] \equiv (m\alpha_2)_n{}^x(\beta_2 A_1)_k{}^n, \tag{15}$$

then (13) gives us

$$p_{2k}{}^x = p_{1k}{}^x - (v_{21})_k{}^x = p_{1k}{}^x + (v_{12})_k{}^x. \tag{16}$$

Then we get, in place of (9) and (10), the general statements:

$$\sum_2{}^F = \sum_1{}^F + 4\pi^2(F^{-1})^{kj}\{\textstyle\sum_x (v_{12})_k{}^x[(v_{12})_j{}^x + 2p_{1j}{}^x]\} \tag{17}$$

$$\sum_2{}^G = (G_2)^{kj}\textstyle\sum_x\{p_{1k}{}^x p_{1j}{}^x + 2p_{1k}{}^x(v_{12})_j{}^x + (v_{12})_k{}^x(v_{12})_j{}^x\}. \tag{18}$$

Whenever the $(v_{12})_k{}^x$ vanish, these sums reduce to (9) and (10). And in general, since we can calculate $(v_{12})_k{}^x$, the G sum (18) is valuable just as (10) is. The F sum (17) is not as useful: the F matrix will be known all too seldom!

To evaluate the $(v_{12})_k{}^x$, we may look at the groupings in (15), and the definitions in (11). We quickly see that $(m\alpha_2)_n{}^x$ describes the change in the x component of the

[6] For a discussion of the effect of rotation on isotopic intensity shifts in connection with the theory of Raman intensities in light and heavy benzene, see R. D. Lord, Jr., and E. Teller, J. Chem. Soc. 1728 (1937).

moment μ^z per unit translation or rotation ρ_2^n. Translations do not affect $\boldsymbol{\mu}$; so we need consider only rotations. Let ρ_2^X, ρ_2^Y, ρ_2^Z be the x, y, z components of the rotation $\boldsymbol{\varrho}_2$: Then, if $\mathbf{p}_0$ is the permanent moment, the change in moment due to $\mathbf{p}_2$ is

$$\Delta\boldsymbol{\mu}=\boldsymbol{\varrho}_2\times\mathbf{p}_0 \tag{19}$$

so that

$$(m\alpha_2)_Y{}^x=p_0{}^z=-(m\alpha_2)_X{}^y, \tag{20}$$

and so on cyclically. The coefficient $(\beta_2A_1)_k{}^n$ is more subtle; we need consider only the case where n is X, Y, Z, corresponding to a rotation. Then this coefficient describes the rotational component produced in isotope 2 when the displacements appropriate to unit R^k in isotope 1 are employed. (We recall that $\beta_1A_1=0$.) Its evaluation in terms of atomic masses and molecular geometry is described in the Appendix. Here we may note that, where symmetry factoring is helpful, the rotation ρ^n and the coordinate R^k must belong to the same symmetry species, or $(\beta_2A_1)_k{}^n$ vanishes.

As *conditions for the nonvanishing of the* $(v_{12})_k{}^x$, then, we have (1) the molecule must have a nonvanishing permanent moment $\mathbf{p}_0$; (2) the symmetry species considered must include some rotation $\boldsymbol{\varrho}$ such that $\boldsymbol{\varrho}\times\mathbf{p}_0\neq0$. Thus, the simple sums will apply to all vibrations of ethylene and benzene, to the parallel vibrations of linear molecules and of the methyl halides, to the A_1 (but not B_1 or B_2) species of chlorbenzene, etc.

RAMAN INTENSITIES

Raman intensities are, of course, determined by the changes in polarizability rather than in dipole moment. If we define a "change-of-polarizability" tensor $\boldsymbol{\alpha}_{1a}$ by its components

$$\alpha_{1a}{}^{xy}=(\partial\alpha^{xy}/\partial Q_1{}^a) \tag{21}$$

(and similarly for $\alpha_{1k}{}^{xy}$, etc.), then we may define two invariants[7]

$$\bar{\alpha}_{1a}=\tfrac{1}{3}tr(\boldsymbol{\alpha}_{1a})=\tfrac{1}{3}(\alpha_{1a}{}^{xx}+\alpha_{1a}{}^{yy}+\alpha_{1a}{}^{zz}), \tag{22}$$

$$\begin{aligned}\bar{\beta}_{1ab}{}^2&=\tfrac{3}{2}tr[\boldsymbol{\alpha}_{1a}\cdot\boldsymbol{\alpha}_{1b}]-\tfrac{1}{2}[tr\,\boldsymbol{\alpha}_{1a}][tr\,\boldsymbol{\alpha}_{1b}]\\&=\tfrac{1}{2}\{(\alpha_{1a}{}^{xx}-\alpha_{1a}{}^{yy})(\alpha_{1b}{}^{xx}-\alpha_{1b}{}^{yy})\\&\quad+(\alpha_{1a}{}^{xx}-\alpha_{1a}{}^{zz})(\alpha_{1b}{}^{xx}-\alpha_{1b}{}^{zz})\\&\quad+(\alpha_{1a}{}^{yy}-\alpha_{1a}{}^{zz})(\alpha_{1b}{}^{yy}-\alpha_{1b}{}^{zz})\\&\quad+6[\alpha_{1a}{}^{xy}\alpha_{1b}{}^{xy}+\alpha_{1a}{}^{xz}\alpha_{1b}{}^{xz}+\alpha_{1a}{}^{yz}\alpha_{1b}{}^{yz}]\},\end{aligned} \tag{23}$$

and the intensity of the ath fundamental is given by

$$I_{1a}{}^R=(\omega_e-\omega_{1a})^4[P_\alpha(\bar{\alpha}_{1a})^2+P_\beta(\bar{\beta}_{1aa}{}^2)]/\omega_{1a}, \tag{24}$$

where the constants P_α, P_β depend only on the conditions of observation, and ω_e is the frequency of the exciting line. Normally we may neglect ω_{1a} in comparison with ω_e, and absorb the $\omega_e{}^4$ in the constants P_α and P_β.

Then, by arguments strictly analogous to those used above, we may form the sums

$$\begin{aligned}\textstyle\sum_1{}^{RF}&=\textstyle\sum_a(I_{1a}{}^R/\omega_{1a})\\&=(F^{-1})^{kj}[P_\alpha(\bar{\alpha}_{1k})(\bar{\alpha}_{1j})+P_\beta(\bar{\beta}_{1kj}{}^2)],\end{aligned} \tag{25}$$

$$\begin{aligned}\textstyle\sum_1{}^{RG}&=\textstyle\sum_a(I_{1a}{}^R/\omega_{1a})\\&=(G_1)^{kj}[P_\alpha(\bar{\alpha}_{1k})(\bar{\alpha}_{1j})+P_\beta(\bar{\beta}_{1kj}{}^2)],\end{aligned} \tag{26}$$

and, where $\boldsymbol{\alpha}_{1k}=\boldsymbol{\alpha}_{2k}$, these rules may be used in the same way as the simple infrared-sum rules (9) and (10).

In general, we shall have

$$\boldsymbol{\alpha}_{2k}=\boldsymbol{\alpha}_{1k}+(\mathbf{w}_{12})_k, \tag{27}$$

where the $(w_{12})_k{}^{xy}$ play a role analogous to the $(v_{12})_k{}^x$ of Eq. (16). We shall leave the evaluation of the $(\mathbf{w}_{12})_k$, and the formulation of the extended rules, to the Appendix. Here we may summarize the conditions for the *vanishing* of $(\mathbf{w}_{12})_k$: (1) The polarizability tensor of the undistorted molecule $\boldsymbol{\alpha}_0$ may be spherically symmetrical, or (2) the symmetry species considered may not contain any rotation $\boldsymbol{\varrho}$ which will change $\boldsymbol{\alpha}_0$; i.e., for which $\boldsymbol{\varrho}\times\boldsymbol{\alpha}_0\neq\boldsymbol{\alpha}_0\times\boldsymbol{\varrho}$. Thus we may apply the simple rules to Raman studies on CCl_4, on the parallel (but not the perpendicular) vibrations of the methyl halides, or on the A_{1g} or E_{2g} (but not the E_{1g}) vibrations of benzene.

The application of the simple $\sum^{RF}$ rule to the E_{2g} vibrations of benzene is illustrated[8] in Table II; the agreement is within 5 percent.

TABLE II.

	ω, cm^{-1}	I^R	$(I^R/\omega)\times10^3$
C_6H_6	605.6	2.1	3.47
	1178.0	2.2	1.87
	1584.8	1.9	1.20
	1606.4	1.6	1.01
	3046.8	4.8	1.57
			9.12
C_6D_6	576.7	1.2	2.09
	867.2	2.3	2.66
	1558.6	2.0	1.28
	2263.9	6.1	2.69
			8.72

DISCUSSION

The effect of anharmonicity remains to be determined. In principle, the intensities could be corrected for the anharmonic contribution;[1] but in practice one will seldom have the required information. Fortunately, the effects of anharmonicity on the intensities of fundamentals are of second order, although the effects on frequencies are first order;[1] it may be, therefore, that

[7] See, e.g., G. Herzberg, *Infrared and Raman Spectra* (D. Van Nostrand Company, Inc., New York, 1945), pp. 243; or Bhagavantam, *Scattering of Light and the Raman Effect* (Andhra University, 1940), pp. 160 ff.

[8] The data, giving I^R in arbitrary units, are from Angus, Ingold, and Leckie, J. Chem. Soc. 925 (1936). A complete quantitative discussion of the A_{1g} and E_{1g} intensities is given by Lord and Teller (see reference 6).

these intensity rules will be followed *more* closely than is the (frequency) product rule.

Of course, one should use only gas-phase data: a consideration which will no doubt be honored in the breach because of practical experimental difficulties!

The fundamental relationships, we may note, apply to each component-product $(p_{1a}{}^x)^2$ or $(\alpha_{1a}{}^{xz})(\alpha_{1a}{}^{yy})$ *separately*. This means that where the two isotopes have reasonably similar momental ellipsoids, we may compare the intensities of (say) Q-branches rather than integrated intensities. For the partitioning of the total intensity among the branches depends only on the shape of the momental ellipsoid and the relative magnitudes of the components $p_{1a}{}^x$ or $\alpha_{1a}{}^{xy}$,[9] and the latter factor is cared for by the separate applicability of the sum rules.

The application to isotopic analysis, and this without previous calibration, may be useful in certain cases.[10]

ACKNOWLEDGMENTS

It is a pleasure to acknowledge most helpful correspondence with Professor J. C. Decius. I am also indebted to Professor R. C. Lord, Jr., for calling my attention to the work of Lord and Teller, and the incompleteness of (9) and (10). This work is part of a program of research at the University of Minnesota which receives support from the ONR.

APPENDIX

We wish to compute the $(\beta_1 A_2)_k{}^n$; or more exactly, to evaluate the $(v_{12})_k{}^x$ and $(w_{12})_k{}^{xy}$ as painlessly as possible. We shall look to the G sum (18) to see just what is needed. We shall use matrix notation as convenient, writing B' for the transpose of B.

First, we look back to (11) and see that the coefficients $B_s{}^k$ and $(\alpha_1)_n{}^s$ are easily written down.[11] Unfortunately, we need β_1 and A_2. Let us write M_1 for the mass matrix: i.e., $(M_1)_{rs}=M_{1s}\,\delta_{rs}$ where M_{1s} is the mass associated with the Cartesian x^s in the isotope 1; it is a diagonal matrix, and $(M_1{}^{-1})$ is its reciprocal. Then if we write

$$G_1=BM_1{}^{-1}B', \tag{A1}$$

we may easily show that, if $B\alpha_1=0$ as is true for bond coordinates R^k,

$$A_1=M_1{}^{-1}B'G_1{}^{-1}. \tag{A2}$$

Moreover, if α_1 is normalized so that

$$\alpha_1{}'M_1\alpha_1=E \tag{A3}$$

with E the 6×6 unit matrix, then

$$\beta_1=\alpha_1{}'M_1. \tag{A4}$$

So we have, using the fact that $B\alpha_1=0=\alpha_1{}'B'$,

$$\begin{aligned}\beta_1A_2&=\alpha_1{}'M_1M_2{}^{-1}B'G_2{}^{-1}\\&=\alpha_1{}'(M_1M_2{}^{-1}-M_2M_2{}^{-1})B'G_2{}^{-1}\\&=\alpha_1{}'\Delta_{12}B'G_2{}^{-1}\\&=\theta_{12}G_2{}^{-1}.\end{aligned} \tag{A5}$$

Here Δ_{12} is a diagonal matrix whose elements are the fractional mass changes:

$$(\Delta_{12})_r{}^s=\delta_r{}^s(M_{1s}-M_{2s})/M_{2s}. \tag{A6}$$

The matrix θ_{12} has the components

$$(\theta_{12})_n{}^k=(\alpha_1)_n{}^s(\Delta_{12})_s{}^tB_t{}^k. \tag{A7}$$

For a given k, we need consider only three values of n, namely, those corresponding to the three rotations, $n=X,\ Y,\ Z$; we may collect the three components $(\theta_{12})_X{}^k$, $(\theta_{12})_Y{}^k$, $(\theta_{12})_Z{}^k$ into a vector $(\boldsymbol{\theta}_{12})^k$. This vector is, of course, the rotation set up in isotope 1 when its atoms execute the displacements appropriate to $R_k[=(G_2{}^{-1})_{kj}R^j]$ in isotope 2. If we also collect components of $(v_{12})_k{}^x$ into vectors $(\mathbf{v}_{12})_k$, we may write (see Eq. (19))

$$(\mathbf{v}_{12})_k=[(\boldsymbol{\theta}_{12})^j\times\mathbf{p}_0](G_2{}^{-1})_{jk}, \tag{A8}$$

and if we also collect components $p_{1k}{}^x$ into vectors $\mathbf{p}_{1k}$, the rule (18) takes on the pleasing and perspicuous form:

$$\begin{aligned}\textstyle\sum_2{}^G&=\mathbf{p}_{1k}\cdot\mathbf{p}_{1j}(G_2)^{kj}+2\mathbf{p}_{1k}\cdot[(\boldsymbol{\theta}_{12})^k\times\mathbf{p}_0]\\&\quad+[(\boldsymbol{\theta}_{12})^k\times\mathbf{p}_0]\cdot[(\boldsymbol{\theta}_{12})^j\times\mathbf{p}_0](G_2{}^{-1})_{jk}.\end{aligned} \tag{A9}$$

The only displeasing feature is the need to evaluate $G_2{}^{-1}$.

In calculating the Raman-intensity correction terms, it is quite clear from (A8) that

$$(\mathbf{w}_{12})_k=[(\boldsymbol{\theta}_{12})^j\times\boldsymbol{\alpha}_0-\boldsymbol{\alpha}_0\times(\boldsymbol{\theta}_{12})^j](G_2{}^{-1})_{jk}, \tag{A10}$$

where the usual expression for the change of a tensor due to rotation has been used.[12] Since $\boldsymbol{\alpha}_0$ is symmetrical, $(\mathbf{w}_{12})_k$ is traceless; hence we immediately have

$$\bar{\boldsymbol{\alpha}}_{2k}=\bar{\boldsymbol{\alpha}}_{1k}. \tag{A11}$$

For $\bar{\beta}_{2kj}{}^2$, we need $(\mathbf{w}_{12})_k{:}\,\boldsymbol{\alpha}_{1j}$ and $(\mathbf{w}_{12})_k{:}\,(\mathbf{w}_{12})_j$. A straightforward bit of algebra shows that, if we choose the x, y, z axes along principal axes of $\boldsymbol{\alpha}_0$, so that $\alpha_0{}^{xy}=\alpha_0{}^{yz}=\alpha_0{}^{xz}=0$, we may express matters in terms of a "vector" $(\mathbf{g}_{12})^j$ with components

$$(g_{12})_x{}^j=(\theta_{12})_x{}^j(\alpha_0{}^{yy}-\alpha_0{}^{zz}) \tag{A12}$$

and so on cyclically. Then we find

$$\begin{aligned}\bar{\beta}_{2kj}{}^2&=\bar{\beta}_{1kj}{}^2\\&\quad+3\{\textstyle\sum_{\text{cyclic}}(g_{12})_x{}^l[\alpha_{1k}{}^{yz}(G_2{}^{-1})_{lj}+\alpha_{1j}{}^{yz}(G_2{}^{-1})_{lk}]\}\\&\quad+3(\mathbf{g}_{12})^i\cdot(\mathbf{g}_{12})^l(G_2{}^{-1})_{lj}(G_2{}^{-1})_{ik}.\end{aligned} \tag{A13}$$

We may again illustrate using HCN, this time considering the bending vibration in the xz plane (taking z along the axis of the nuclei). Then our only R^k is the

[9] Herzberg, reference 7, pp. 414 ff.

[10] Qualitatively, see R. L. Arnett and B. L. Crawford, Jr., J. Chem. Phys. **18**, 118 (1950).

[11] Wilson, reference 3, gives vector expressions for the $B_s{}^k$. The $(\alpha_1)_n{}^s$ are rotation displacements: the only reasons for isotopic distinction are that the center of mass may be shifted on isotopic substitution and that the normalization will be different.

[12] See, e.g., E. A. Milne, *Vectorial Mechanics* (Methuen and Company, Ltd., London, 1948), Chapter 3.

H−C−N angle φ; the Cartesian x^s are the x displacements of the H, C, N atoms, x^1, x^2, x^3, respectively. We take HCN as isotope 1, DCN isotope 2; a_1, b_1, c_1 and a_2, b_2, c_2 the distance of the H, C, N nuclei from the center of gravity in the two cases; ρ_H and ρ_N the *reciprocals* of the CH and CN bond lengths. The mass matrix M_1 (3×3) has the diagonal elements $\{M_{1H}, M_{1C}, M_{1N}\}$, and similarly for M_2; the matrix Δ_{12} has only the leading element $(M_{1H}-M_{2H})/M_{2H}=(-1/2)$. Then the B matrix is 1×3:

$$B: \rho_H \; -(\rho_H+\rho_N) \; \rho_N.$$

The only components of α_1 in the symmetry species are the $(\alpha_1)_{Y^s}$:

$$(\alpha_1)_Y: N_1a_1 \; N_1b_1 \; N_1c_1,$$

where N_1 is the normalizing factor: $N_1=[M_{1H}a_1^2+M_{1C}b_1^2+M_{1N}c_1^2]^{-\frac{1}{2}}=[I]^{-\frac{1}{2}}$. So we find only one nonvanishing component of $(\theta_{12})^\varphi$; *viz.*,

$$(\theta_{12})_Y{}^\varphi=N_1a_1(\Delta_{12})_1{}^1\rho_H=-a_1\rho_H/2I^{\frac{1}{2}}.$$

Since μ_0 has only the component $\mu_0{}^z$, we find for $(\mathbf{v}_{12})_\varphi$ only the component

$$(v_{12})_\varphi{}^x=-\mu_0{}^z a_1\rho_H/2I^{\frac{1}{2}}(G_2)^{\varphi\varphi}.$$

Turning to the Raman terms, we find from symmetry that $\alpha_0{}^{xz}=\alpha_0{}^{yy}$, and only the component $\alpha_{1\varphi}{}^{zz}$ exists. So we have

$$(g_{12})_Y{}^\varphi=-(a_1\rho_H/2I^{\frac{1}{2}})(\alpha_0{}^{zz}-\alpha_0{}^{xx})$$

and

$$\bar{\beta}_{2\varphi\varphi}{}^2=\bar{\beta}_{1\varphi\varphi}{}^2-6(a_1\rho_H/2I^{\frac{1}{2}})(\alpha_0{}^{zz}-\alpha_0{}^{xx})\alpha_{1\varphi}{}^{zz}/(G_2)^{\varphi\varphi}$$
$$+3(a_1{}^2\rho_H{}^2/4I)(\alpha_0{}^{zz}-\alpha_0{}^{xx})[\alpha_{1\varphi}{}^{zz}/(G_2)^{\varphi\varphi}]^2.$$

THE JOURNAL OF CHEMICAL PHYSICS VOLUME 20, NUMBER 6 JUNE, 1952

Diffusion in the System $C^{14}O_2-CO_2$ to 1000 Atmospheres Pressure*

K. D. TIMMERHAUS AND H. G. DRICKAMER
Department of Chemistry, University of Illinois, Urbana, Illinois

(Received January 25, 1952)

Diffusion coefficients are presented for the system $C^{14}O_2-CO_2$ in the pressure range 100–1000 atmospheres, at temperatures 0°–25°–50°C. In the lower part of the range the results are consistent with those of Robb (see reference 2) and show little temperature coefficient for diffusion at constant density. At higher densities the temperature coefficient increases rapidly. The dense gas theory of Enskog is totally inapplicable, but the results are correlated in the form

$$D=D_0\exp(-E/RT).$$

The activation energy (E) at constant density and D_0 are given as a function of density in a form useful for extrapolation.

IN previous papers[1,2] diffusion measurements have been presented for the system $C^{14}O_2-CO_2$ in the pressure range 0.5–150 atmospheres, and over a temperature range from 0°C–50°C. In this paper the results are extended to 1000 atmospheres, using a technique similar to that employed by Robb and Drickamer.[2]

KINETIC THEORY

Enskog and Chapman[3] have developed a satisfactory kinetic theory for dilute gases. Enskog[4] has extended this result by approximate means to gases of moderate density. Considering a Lennard-Jones model gas, and using the nomenclature of Hirschfelder[5] *et al.*, the result can be written:

$$D_{11}=\left[\frac{16(kT)^{\frac{1}{2}}}{3(2\pi\mu)^{\frac{1}{2}}r_0{}^2nW_1{}^{(1)}(1)\chi}\right], \quad (1)$$

where

$$\chi=1+(5/12)\pi n\sigma^3+0.1275(\pi n\sigma^3)^2+\cdots. \quad (1')$$

This equation is somewhat inconsistent in that the dense gas correction is developed only for the case of solid elastic spheres, but it is the best available to date. It is assumed here that r_0 and σ, the solid elastic sphere diameter, are identical.

Considering the approximations made it would be surprising if Eq. (1) applied to gases in the density range covered by this work.

EQUIPMENT AND PROCEDURE

The diffusion cell used was similar to that employed previously[2] but with numerous minor but significant differences. A general view of the diffusion bomb is shown in Fig. 1. Essentially it consisted of (1) a diffusion bomb and turning mechanism, by means of which

* This work was supported in part by the AEC.

[1] K. D. Timmerhaus and H. G. Drickamer, J. Chem. Phys. **19**, 1242 (1951).

[2] W. L. Robb and H. G. Drickamer, J. Chem. Phys. **19**, 1504 (1951).

[3] S. Chapman and T. G. Cowling, *Mathematical Theory of Non-Uniform Gases* (Cambridge University Press, London, 1939), pp. 134–167.

[4] See reference 3, pp. 273–294.

[5] Hirschfelder, Curtiss, Bird, and Spotz, *Properties of Gases* (John Wiley & Sons, Inc., New York, to be published).

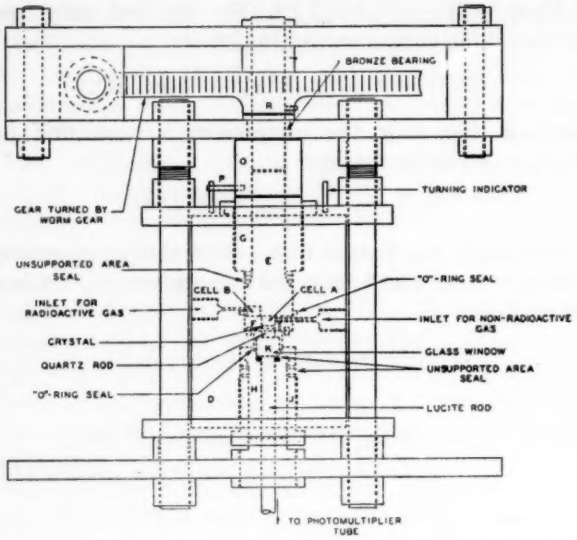

FIG. 1. Schematic diagram of high pressure diffusion apparatus.

two cells, containing different gases, were brought into contact with each other; (2) a scintillation counter, which measured the amount of radioactive gas diffused through one of the cells; and (3) auxiliary equipment for filling the cells, and generating and measuring the pressures. The diffusion bomb consisted of five main pieces: (1) a steel block D with a large hole in the top, (2) a flat metal disk F which was pinned to the bottom of the above hole, (3) a cylinder which fitted into the hole, and rotated on the inserted disk, (4) a nut G to hold the cylinder tightly against the insert, and (5) a cylindrical nut arrangement to hold and support the window and seal. There were two diffusion cells, one in the cylinder (Cell A) and one in the insert (Cell B). In the filling position they were one hundred eighty degrees apart. The insert and cylindrical face were surface ground to maintain a seal between the cells in this position.

Perhaps the most significant difference between this

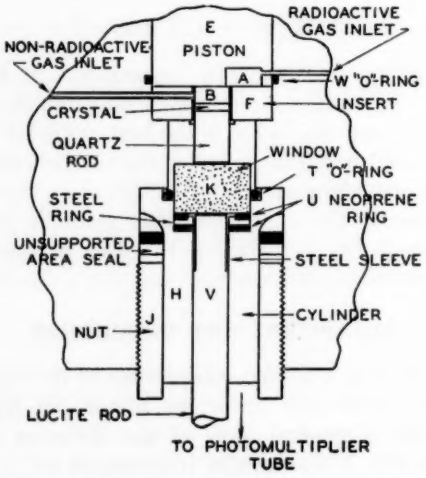

FIG. 2. Cross section view of window seal.

equipment and Robb's is the window seal. This is shown in detail in Fig. 2. It is possible to use a glass metal seal such as is described by Poulter[6] for gases at high pressure, but the window is frequently dislodged in the depressurizing and evacuating step. The window shown, which uses an unsupported area seal with an "O" ring to hold the window in place, was used successfully for several consecutive runs if the depressurizing was done sufficiently slowly.

The cells were filled by simultaneously opening valves leading to two bombs: one containing inert and one containing radioactive CO_2 maintained at identical pressure. The system of generating CO_2 and of pressurizing the system was identical to that employed by Robb.[2] After filling and bringing to pressure, the piston

TABLE I. Measured diffusion coefficients for CO_2 at high pressures.

Run No	Actual[a] length of both cells	Temp K	Pressure[b] atmos	Density g/ml	D_{11} cm²/sec
25	0.214 in.	298.0	113.2	0.862	0.0000905
32	0.145 in.	302.1	103.1	0.782	0.000137
33		300.6	178.9	0.883	0.0000702
34		298.1	103.1	0.822	0.0000934
38		297.9	130.3	0.858	0.0000764
39		298.1	562.0	1.054	0.0000512
42		323.2	232.3	0.824	0.0000916
45		323.2	250.0	0.840	0.0000884
46		323.1	470.5	1.025	0.0000704
53		298.0	402.5	1.003	0.0000409
54		298.2	402.5	1.003	0.0000434
55		298.0	562.0	1.054	0.0000354
56		298.2	752.0	1.106	0.0000318
57		298.2	1023.0	1.159	0.0000253
60		272.9	137.1	0.999	0.0000404
61		273.2	307.1	1.060	0.0000320
62		273.2	512.0	1.103	0.0000246
63		273.1	802.5	1.157	0.0000198
65		323.0	470.5	0.955	0.0000498
66		322.9	596.5	0.993	0.0000453
67		322.9	837.0	1.056	0.0000392
68		322.9	1029.0	1.102	0.0000348
69		298.2	561.0	1.057	0.0000351
70		298.1	1030.5	1.160	0.0000245

[a] Effective length 1.96 times actual length.
[b] The pressure readings up to 340 atmospheres were read to within a tenth of an atmosphere. Above this pressure, readings to within a half of an atmosphere were obtained.

E was rotated until the cells were opposite each other. The concentration of radioactive gas at the surface of the anthracene crystal was measured as a function of time using a photomultiplier tube. The analytical set-up and method of calculating the diffusion coefficient concentrations are described in detail elsewhere.[1,2]

The pressure was measured by a dead weight gauge accurate to 0.1 atmosphere up to 340 atmospheres. Above this point a Bourdon gauge accurate to 0.5 atmosphere was used. The densities were obtained from the p-v-t data of Michels *et al.*[7]

[6] T. C. Poulter, Phys. Rev. **35**, 297 (1930).
[7] A. Michels and C. Michels, Proc. Royal Soc. (London) **A153**, 201 (1936); **A160**, 348 (1937).

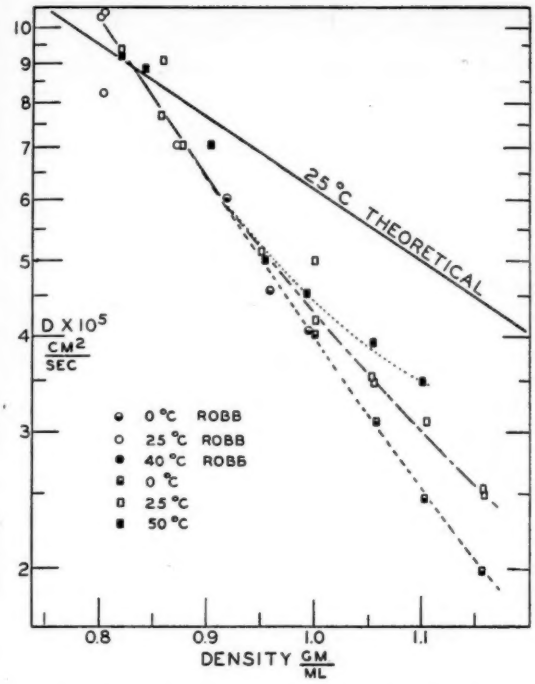

FIG. 3. CO_2 diffusion coefficients at high density.

RESULTS

The results are shown in Table I and in Fig. 3. In the density range 0.7–0.9 there is very little temperature coefficient for diffusion at constant density. This coincides with the results found and discussed by Robb.[2] As the density increases the temperature coefficient of D increases rapidly. The data are not even approximately represented by Eq. (1) as can be seen from the theoretical curve in Fig. 3.

In Table II are shown the values of χ calculated from the experimental data, as compared with the theoretical values. Theoretically, χ should be independent of temperature at constant density. At densities below one g/ml the value of χ decreases with decreasing density corresponding to a lower collision diameter at low temperature near the phase envelope. At higher densities the temperature coefficient of χ reverses.

Rather than calculating χ from Eq. (1′) it is possible to evaluate it from *p-v-t* data[7] as suggested by Enskog. The equation of state derivable from his dense gas

TABLE II. Calculations of χ's from diffusion data and from theory.

Density g/ml	χ0°C	χ25°C	χ50°C	χ_0 3.47A
0.80	2.97	3.21	3.45	1.860
0.85	3.57	3.86	4.12	1.935
0.90	4.27	4.58	4.83	2.010
0.95	5.08	5.32	5.51	2.085
1.00	6.04	5.82	5.73	2.163
1.05	7.25	6.98	6.87	2.243
1.10	8.66	7.91	7.65	2.325
1.15	10.27	8.86		2.409

TABLE III. Calculation of $b\chi$ and of b from *p-v-t* data.

Density g/ml	$(b\chi)$0°C	b0°C	$(b\chi)$25°C	b25°	$(b\chi)$50°C	b50°C
0.80			2.74	0.856	3.45	0.795
0.85			2.98	0.722	4.12	0.724
0.90			3.20	0.70	4.83	0.724
0.95	3.56	0.70	4.00	0.75	5.51	0.804
1.00	3.97	0.658	4.20	0.72	5.73	0.826
1.05	4.11	0.567	4.30	0.616	6.87	0.656
1.10	3.53	0.408	3.98	0.503	7.65	0.578
1.15	2.29	0.223	3.44	0.388		

$b=\frac{2}{3}\pi(\sigma^3/m)=2.87$ if $\sigma=4.63$ (from viscosity data)
$=1.20$ if $\sigma=3.47$ (from diffusion data of Robb)

assumptions is

$$p=nkT(1+b\rho\chi), \tag{2}$$

where

$$b=\tfrac{2}{3}\pi(\sigma^3/m); \tag{2′}$$

then assuming b independent of T,

$$(\partial p/\partial T)=nk(1+b\rho\chi), \tag{3}$$

$$b\chi=\frac{1}{\rho}\left[\frac{1}{nk}\frac{\partial p}{\partial T}-1\right]=\frac{1}{\rho}\left[\frac{M}{RP}\frac{\partial p}{\partial T}-1\right]. \tag{4}$$

In Table III are listed the values of $b\chi$ calculated from the *p-v-t* data of Michels, together with the values of b necessary to give χ's agreeing with the χ's calculated from diffusion data. The values of b vary both with temperature and density; further, they bear no relation to the theoretical values, nor are they consistent with the χ-values.

It is possible that by sufficient adjustment self-consistent values of b and χ might be calculated at each

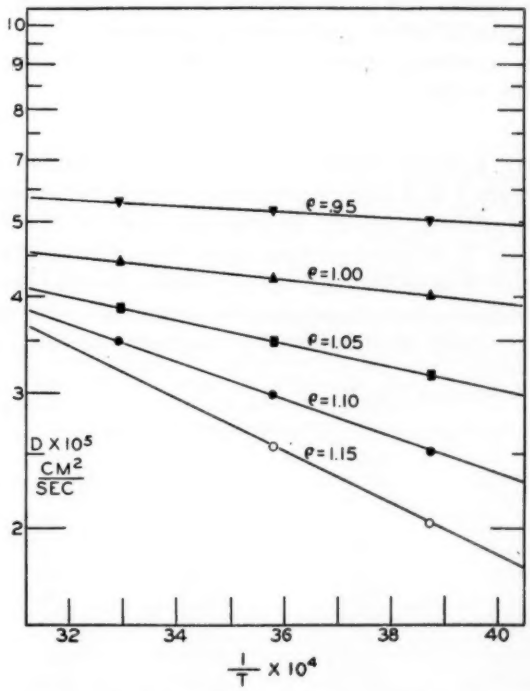

FIG. 4. Plot of ln$D$ *versus* $1/T$ at constant density.

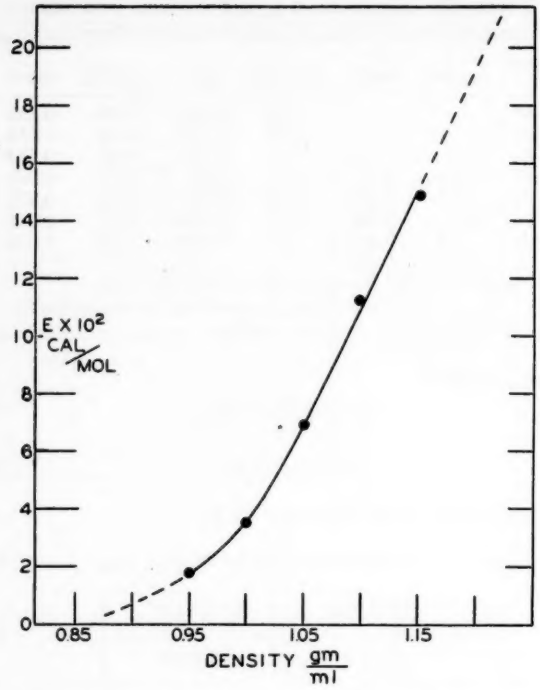

FIG. 5. Activation energy as a function of density.

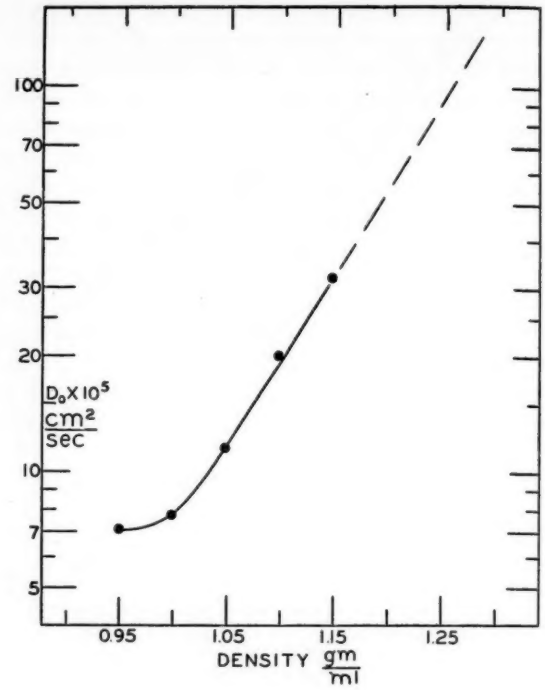

FIG. 6. D_0 as a function of density.

point, but would vary widely with temperature and density. The equations would then be entirely empirical and much of the value would be lost. Chapman and Cowling[8] find very good agreement with theory over the same pressure range for the viscosity of nitrogen. This is probably the result of the greater symmetry of the nitrogen molecule, and to the fact that viscosity of both liquids and gases appears to be less sensitive to molecular structure and easier to correlate.

In condensed systems the diffusion coefficient is usually written

$$D=D_0 \exp(-E/RT). \tag{5}$$

In Fig. 4 $\ln D$ is plotted *versus* $1/T$ at constant density.

Figure 5 is a plot of activation energy (at constant density) *versus* density. Figure 6 is a plot of D_0 *versus* density. It is fortunate that these plots are essentially straight lines in the high density region, as this permits reasonably safe extrapolation to regions where experiment would be difficult. For instance, to obtain a density $\rho=1.25$ g/ml at 50°C would necessitate a pressure of 3610 atmospheres.

The activation energies obtained at the higher densities were of the same order of magnitude as those obtained for most organic liquids, especially when one considers that most data for liquids is at constant (atmospheric) pressure rather than at constant density.

K. D. Timmerhaus would like to thank the Ethyl Corporation and the AEC for financial assistance.

NOMENCLATURE

D_{11} = diffusion coefficient,
E = activation energy, calories/mol,
k = Boltzmann's constant,
m = molecular mass,
n = number of molecules per unit volume,
R = gas constant = $k \times$ Avogadro's number,
r_0 = collision diameter for Lennard-Jones model,
T = absolute temperature,
W_1 = integral depending on E and T only,
μ = reduced mass = $m/2$ for self diffusion,
ρ = density,
σ = collision diameter for solid elastic spheres.

[8] See reference 3, p. 288.

Proton Transfers in Solution

ALFRED NISONOFF AND LESTER P. KUHN, *Ballistic Research Laboratories, Aberdeen Proving Ground*

AND

RONALD W. GURNEY, *Institute for Fluid Dynamics and Applied Mathematics, University of Maryland, College Park, Maryland*

(Received November 29, 1951)

By a spectrophotometric method the acid-base equilibrium between bromcresol green and triethanolamine was measured over the range of temperature from −6°C to +50°C in the three solvents—methanol, ethanol, and *n*-butanol. In each solvent the equilibrium constant was found to vary rapidly with temperature; and in methanol the value of log$K$ was found to change sign near 0°C. This behavior is very different from the well-known results for weak acids in aqueous solution, and in the theoretical part of the paper a unified theory is presented to cover all types of proton transfer. The work required to transfer a proton consists of two parts, a part sensitive to the environment and a part insensitive to the environment; the behavior of the equilibrium constant depends on whether the two parts are of the same sign or of opposite sign. Families of curves are drawn to show the various possible types of behavior.

INTRODUCTION

IN dilute aqueous solutions the dissociation constants of many weak acids are known over a wide range of temperature. In each case we are concerned with the transfer of a proton from solute particle to a solvent molecule. The experiments described in this paper, likewise carried out in solutions of very low ionic strength, differ from the foregoing in two respects: The solvents were pure methanol, ethanol, and *n*-butanol, and in each case the proton transfer was from a solute particle to another species of *solute* particle. The two solute species used in this work were the base, triethanolamine, and the dye bromcresol green, (*tetra*-bromo-*m*-cresolsulfonphthalein). This dye is a dibasic acid whose reactions with triethanolamine can be represented as follows:

$$H_2A+B\rightarrow BH^++HA^-, \quad (1)$$

$$HA^-+B\leftrightarrows BH^++A^=, \quad (2)$$

where B represents triethanolamine and BH^+ is the triethanolammonium ion. Since the first reaction consists in the removal of a proton from the strong sulfonic acid group, it goes essentially to completion. It is, however, possible to determine equilibrium constants for the removal of the second proton, and this paper will be concerned with reaction (2). The analytical technique consisted in the spectrophotometric estimation of equilibrium concentrations of the blue $A^=$ ion.

EXPERIMENTAL

Bromcresol green and triethanolamine were obtained from commercial sources. The former compound was purified by recrystallization from glacial acetic acid and the latter by distillation. Triethanolamine hydrochloride was prepared by passing dry HCl into a solution of triethanolamine in an ethanol-chloroform-ether mixture. The resulting crystals were filtered off, washed with alcohol and ether, and dried in an oven at 50°–60°. Chloride determination gave an equivalent weight of 187.1 (theory, 185.6). Solvents were dried by distillation from sodium with precautions to exclude moisture.

A Beckman spectrophotometer was used for this work. Temperature was controlled to within 0.2° of the desired value by causing a liquid at constant temperature to circulate through a jacket surrounding the absorption cells. Temperatures were referred to a thermometer corrected by the National Bureau of Standards.

RESULTS

It was found that in each of the three solvents investigated—methanol, ethanol, and *n*-butanol—the divalent anionic form of bromcresol green ($A^=$) is blue, and its visible absorption spectrum exhibits maxima at the following wavelengths:

Solvent	λ (mμ)
Methanol	620
Ethanol	625
n-Butanol	630

Extinction coefficients at the above wavelengths were determined by measuring optical densities of solutions containing known concentrations of dye and enough strong alkali to convert the dye quantitatively to the $A^=$ form. The presence of excess alkali was assumed

TABLE I. Cell constants (optical density units per mg/liter of dye). These values can be converted to molar extinction coefficients per centimeter by multiplying by the factor 698,000/3.69, since the molecular weight of bromcresol green is 698 and the length of the absorption cell used is 3.69 cm.

Temperature (deg C)	Solvent: Methanol λ=620 mμ	Ethanol λ=625 mμ	*n*-Butanol λ=630 mμ
60.1		0.235	
50.2	0.228	0.241	0.222
40.1	0.227	0.240	0.230
30.1	0.234	0.248	0.234
20.0	0.234	0.252	0.242
10.0	0.238	0.253	0.252
0.1	0.240	0.256	0.255
−6.2	0.239	0.257	0.256

TABLE II. Composition of solutions investigated.

Solution No.	Solvent	Initial concentrations of components: Triethanolamine (moles/liter)	Triethanolamine hydrochloride (moles/liter)	Bromcresol green (mg/liter)
1	methanol	7.89×10^{-5}	1.00×10^{-4}	10
2	methanol	1.184×10^{-4}	1.00×10^{-4}	10
3	methanol	1.973×10^{-4}	1.00×10^{-4}	10
4	methanol	3.95×10^{-4}	1.00×10^{-4}	10
5	methanol	3.95×10^{-5}	1.00×10^{-4}	10
6	ethanol	7.59×10^{-4}	1.00×10^{-4}	30
7	ethanol	1.519×10^{-3}	1.00×10^{-4}	30
8	ethanol	2.28×10^{-3}	1.00×10^{-4}	30
9	ethanol	3.80×10^{-3}	1.00×10^{-4}	30
10	ethanol	1.90×10^{-4}	1.00×10^{-4}	30
11	ethanol	3.04×10^{-4}	1.00×10^{-4}	30
12	ethanol	3.80×10^{-4}	1.00×10^{-4}	30
13	*n*-butanol	2.46×10^{-4}	...	40
14	*n*-butanol	4.92×10^{-4}	...	40
15	*n*-butanol	9.84×10^{-4}	...	40
16	*n*-butanol	2.05×10^{-3}	...	40

when further addition of alkali caused no increase in optical density. The alkaline material used in each case was the sodium salt of the solvent (sodium methylate, etc.). Values of extinction coefficients are given in Table I.

The equilibrium constant of reaction (2) can be expressed as

$$K=(BH^+)(A^-)/(B)(HA^-).$$

Since A^- is the species whose equilibrium concentration could be measured photometrically, equilibrium concentrations of the other components had to be evaluated in terms of (A^-). It was possible to do this by means of the simple stoichiometric relations since the initial concentrations of BH^+, H_2A, and B were known. The composition of each mixture investigated and experimental values of equilibrium constants are given in Tables II and III.

DISCUSSION

In a process such as (2) above, when the solute particles are in a solvent at temperature T, we are concerned with the amount of work to transfer a proton isothermally from an $(AH)^-$ ion to a distant B particle. The work to carry out such an isothermal process is a change in the free energy, but it is not the total change ΔF in the free energy, which depends on the volume and composition of the solution. In a very dilute solution, when we speak of the work required to transfer a proton from its vibrational level in a particular $(AH)^-$ ion to the vacant level in a particular distant B particle, we speak of a quantity that is obviously independent of the amount of solvent with which the solute particles happen to have been mixed. The first step then is to divide ΔF into parts—a communal part that depends on the composition of the solution and a part which in very dilute solution does not depend on the composition of the solution.

Numbering the four species in (2) from left to right, let n_1, n_2, n_3, and n_4 be the number of particles of each species in the solution, and let x_1, x_2, x_3, and x_4 be their mole fractions. When one additional proton is transferred from an $(AH)^-$ particle to a B particle, the values of n_3 and n_4 are increased by unity, while the values of n_1 and n_2 are diminished by unity. On extrapolating towards infinite dilution, when the activity coefficients no longer differ appreciably from unity, the change from n_1 to (n_1-1) makes to the communal term the contribution $-kT\ln x_1$ and so on for the other particles.[1] Adding together the four contributions, we

TABLE III. Values of equilibrium constant for the reaction of triethanolamine with bromcresol green.

Solution No.	Solvent	−6.2°	0.1°	10.1°	20.0°	30.1°	40.1°	50.2°	60.1°
1	methanol	1.34	9.2×10^{-1}	5.7×10^{-1}	3.4×10^{-1}	...	1.33×10^{-1}	7.1×10^{-2}	
2	methanol	1.31	8.9×10^{-1}	5.6×10^{-1}	3.4×10^{-1}	1.84×10^{-1}	1.11×10^{-1}	7.0×10^{-2}	
3	methanol	...	9.3×10^{-1}	5.3×10^{-1}	3.3×10^{-1}	1.85×10^{-1}	1.17×10^{-1}	6.8×10^{-2}	
4	methanol	...	8.4×10^{-1}	4.9×10^{-1}	3.0×10^{-1}	1.85×10^{-1}	1.15×10^{-1}	7.0×10^{-2}	
5	methanol	1.34	...	...	...	...	...	...	
Mean value		1.33	9.0×10^{-1}	5.4×10^{-1}	3.3×10^{-1}	1.85×10^{-1}	1.19×10^{-1}	7.0×10^{-2}	
6	ethanol	...	6.2×10^{-2}	4.0×10^{-2}	2.5×10^{-2}	1.40×10^{-2}	...	...	...
7	ethanol	...	...	4.0×10^{-2}	2.5×10^{-2}	1.45×10^{-2}	9.5×10^{-3}	6.1×10^{-3}	3.7×10^{-3}
8	ethanol	...	...	3.7×10^{-2}	2.5×10^{-2}	1.48×10^{-2}	9.8×10^{-3}	6.2×10^{-3}	3.6×10^{-3}
9	ethanol	...	...		2.1×10^{-2}	1.46×10^{-2}	10.1×10^{-3}	6.1×10^{-3}	3.8×10^{-3}
10	ethanol	9.4×10^{-2}	6.5×10^{-2}						
11	ethanol	9.4×10^{-2}	5.8×10^{-2}						
12	ethanol	8.9×10^{-2}	5.8×10^{-2}						
Mean value		9.2×10^{-2}	6.1×10^{-2}	3.9×10^{-2}	2.4×10^{-2}	1.45×10^{-2}	9.8×10^{-3}	6.1×10^{-3}	3.7×10^{-3}
13	*n*-butanol	1.42×10^{-2}	9.9×10^{-3}	6.2×10^{-3}	4.7×10^{-3}	3.5×10^{-3}	2.2×10^{-3}	...	
14	*n*-butanol	1.56×10^{-2}	10.0×10^{-3}	6.6×10^{-3}	4.9×10^{-3}	3.4×10^{-3}	2.3×10^{-3}	1.71×10^{-3}	
15	*n*-butanol	1.39×10^{-2}	10.4×10^{-3}	7.0×10^{-3}	4.9×10^{-3}	3.4×10^{-3}	2.3×10^{-3}	1.68×10^{-3}	
16	*n*-butanol	...	9.7×10^{-3}	7.6×10^{-3}	5.2×10^{-3}	3.6×10^{-3}	2.5×10^{-3}	1.74×10^{-3}	
Mean value		1.46×10^{-2}	10.0×10^{-3}	6.9×10^{-3}	4.9×10^{-3}	3.5×10^{-3}	2.3×10^{-3}	1.71×10^{-3}	

[1] Max Planck, *Treatise on Thermodynamics* (Longmans, Green and Company, New York, 1927), Sec. 254. See also R. W. Gurney, *Introduction to Statistical Mechanics* (McGraw-Hill Book Company, Inc., New York, 1949), Chapter 7.

TABLE IV.

	ϵ_0	ϑ	Reference	Freezing point
H_2O	305.7	219	[a]	273.1°K
D_2O	306.7	218	[a]	273.1
methanol	151.1	185	[b]	175.3
ethanol	148.5	164.5	[b]	155.8
n-propanol	150.4	148	[b]	146

[a] J. Wyman and E. N. Ingalls, J. Am. Chem. Soc. **60**, 118 (1938).
[b] G. Akerlof, J. Am. Chem. Soc. **54**, 4125 (1932).

find that the communal term will not differ appreciably from $kT\ln(x_3x_4/x_1x_2)$.

When this communal term is subtracted from ΔF, let the remainder be denoted by NJ, where N is Avogadro's number. Then J denotes the change in free energy per proton transferred, excluding the communal term. When a state of equilibrium prevails, the value of ΔF is of course zero. We may account for this zero value by saying that the two parts of ΔF are equal and opposite; in other words, the communal term is equal to $-J$; after extrapolation to infinite dilution

$$kT\ln x_3x_4/x_1x_2=-J. \tag{3}$$

In a molecule or molecular ion, owing to the small mass of the proton, the energy intervals between successive vibrational levels of a proton are exceptionally wide. At room temperature we are concerned with the lowest vibrational level in each case. In the process (2) above or in any process such as

$$AH+B\rightarrow A^-+(BH)^+,$$

where a proton is transferred to a distant particle, work is done to separate the positive and negative charges against their mutual attraction. But the binding energy of the proton in $(BH)^+$ may be considerably larger than the binding energy of the proton in AH. In this case the energy liberated by quantum-mechanical forces may be more than sufficient to supply the energy required to separate the electrostatic charges against their mutual attraction. In this case there will be a net liberation of energy instead of work to be done.

Depending on the relative binding energies, the value of J may be positive or negative. In a particular case we may find J equal to zero. This condition could only be satisfied at a particular temperature, since the electrostatic energy in the ionic fields varies with temperature. At a higher temperature the thermal agitation opposes more successfully the alignment of the solvent dipoles by the ionic field; the solvent loses less free energy when an ionic field is created, and more work has to be done to create the fields. At a particular temperature the electrostatic work may be exactly equal and opposite to the remaining contributions to J with the result that J is zero. Such a case will be found in the experimental results.

We see the necessity of dividing J into a part that is sensitive to the environment and a part independent

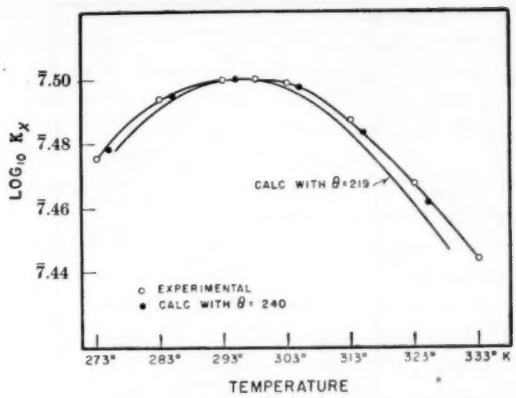

FIG. 1. Logarithms of the dissociation constant of acetic acid in aqueous solution between 273° and 333°K.

of the environment. The former part, which will be denoted by J_{env}, will be sensitive to temperature, while the latter part, denoted by J_{non}, will not vary with temperature. We have then

$$-\ln\frac{x_3x_4}{x_1x_2}=\frac{J_{\text{non}}+J_{\text{env}}}{kT}. \tag{4}$$

Some standard of comparison is now needed with which to compare the experimental results. We obtain such a standard behavior, if we suppose that J_{env} is almost entirely electrostatic in origin and, furthermore, varies with temperature as demanded by the macroscopic dielectric constant ϵ of the medium; that is to say, if we assume that J_{env} as a function of temperature is inversely proportional to ϵ.[2] For this standard electrostatic term we may use the notation J_{el} instead of J_{env}.

Now in the neighborhood of room temperature ϵ for H_2O, D_2O and for several common solvents can be expressed in the form

$$\epsilon=\epsilon_0e^{-T/\vartheta}, \tag{5}$$

where the ϑ is a temperature characteristic of the solvent. Values[3] of ϑ are given in Table IV, together with those of ϵ_0. If in the standard behavior J_{el} is proportional to $1/\epsilon$, it is clear that (3) takes the form

$$\ln K_x=-C(a+e^{T/\vartheta})/T, \tag{6}$$

where $Ca=J_{\text{non}}/k$ and $Ce^{T/\vartheta}=J_{\text{el}}/k$.

The function $-(e^{T/\vartheta})/T$ passes through a maximum at $T=\vartheta$; that is to say, for pure electrostatic forces with J_{non} equal to zero, values of $\ln K$ would be found to lie on a curve passing through a maximum at $T=\vartheta$. Addition of a nonelectrostatic contribution shifts the position of this maximum. With a positive the maximum is shifted to a higher temperature, that is to say, towards room temperature as shown in Fig. 2. In this

[2] L. P. Hammett, *Physical Organic Chemistry* (McGraw-Hill Book Company, Inc., New York, 1940), p. 81; E. C. Baughan, J. Chem. Phys. **7**, 951 (1939).
[3] It will be noticed that, with the exception of water, ϑ lies, in each case, a little above the freezing point of the liquid.

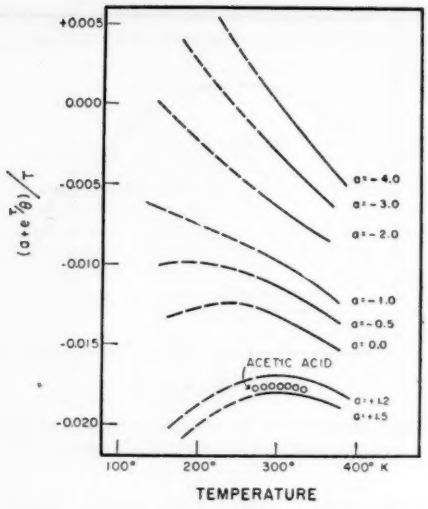

FIG. 2. Theoretical curves in aqueous solution for various values of a.

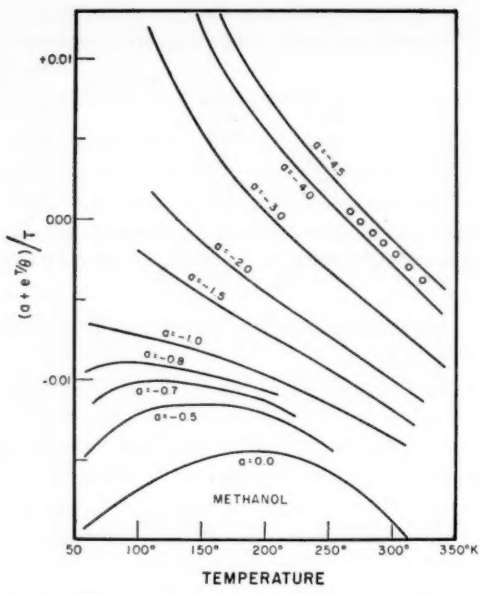

FIG. 3. Theoretical curves in methanol solution for various values of a.

way one accounts for the maximum that has been observed near room temperature for so many weak acids in aqueous solution. The value of (6) passes through a maximum at a temperature T^* given by

$$T^*=\vartheta\left(1+\frac{a}{e^{T^*/\vartheta}}\right)=\vartheta\left(1+\frac{J_{\text{non}}}{J_{\text{el}}^*}\right), \tag{7}$$

where J_{el}^* denotes the value of J_{el} at the temperature T^*. Thus the position of the maximum depends not on the value of J_{non} or of J_{el}^* but only on their ratio.

For negative values of a families of curves are obtained like those shown in Figs. 2 and 3; these are drawn for $\vartheta=219$ (water) and for $\vartheta=185.6$ (methanol).

We have now to ask whether the experimental results agree at all closely with this standard behavior. This would not be expected, since most of the electrostatic energy in an ionic field is contributed by the few solvent molecules in immediate contact with the ion, and there is no reason to suppose that their interaction energy would show the same variation with temperature as does the macroscopic dielectric constant. We know, however, from the analysis of experimental results in aqueous solution made by Baughan,[2] that in this solvent rather good agreement for ΔH can be obtained between experiment and simple electrostatic theory, though with values of atomic radii that are too small. The use of (6) is illustrated in Fig. 1, which shows the well-known experimental results for the ionic dissociation of acetic acid in aqueous solution.[4] The points plotted are values of $\log_{10}K_x$ which, in this case, is obtained from the usual dissociation constant K by the relation[5]

$$\log_{10}K_x=\log_{10}K-\log_{10}55.51. \tag{8}$$

[4] H. S. Harned and N. D. Embree, J. Am. Chem. Soc. **56**, 1050 (1934).

[5] See for example, L. E. Steiner, *Introduction to Chemical Thermodynamics* (McGraw-Hill Book Company, Inc., New York, 1948), p. 260.

The theoretical curve in Fig. 1 is drawn for $\vartheta=219$, $a=1.35$, and $C=850.2$. To obtain still better agreement, a somewhat larger value of ϑ is necessary. With $\vartheta=240$ instead of 219 almost perfect agreement is obtained in Fig. 1.

Turning now to the results in Table III, let us discuss the data obtained in methanol. The results are of a very different character from those depicted in Fig. 1. The values of $\log K$ show no sign of tending towards a maximum, and furthermore, the value of $\log K$ passes through a zero value at a certain temperature and changes sign. The families of theoretical curves plotted in Figs. 2 and 3 show that this difference in behavior is due, not to the change in solvent, but to the difference in J_{non}. In both Fig. 2 and Fig. 3 the curve for $a=0$ shows the behavior to be expected for pure electrostatic forces, while the small circles near the bottom of Fig. 2 give the values of $(\ln K_x)/C$ for acetic acid, taken from Fig. 1. The points lie very nearly on the theoretical curve for $a=+1.35$, as already shown in Fig. 1.

In both Fig. 2 and Fig. 3 the curve for $a=-2$ is almost a straight line, while for larger negative values of a the curves have changed from convex to concave. It is on a curve of the latter type that the experimental values in Table III above are found to lie. The small circles near the top of Fig. 3 give the experimental values of $(\ln K)/645$. The points lie on the theoretical curve for $a=-4.32$.

Before this is accepted as an approximate interpretation, one should ask whether the values of J_{el} that have been used are reasonable values. Although the removal of a proton from the $(AH)^-$ ion leaves a doubly charged ion $A^=$, this is not of importance, since the second charge lies on a different part of the molecu-

lar ion. In the negative ion we have to fix attention on the atom or group of atoms that bears the negative charge when this proton has been removed; in the positive ion we have to fix attention on the atom or group of atoms that bears the positive charge when the proton has been introduced. If R_- and R_+ denote the radii of these two groups of atoms, we can obtain a rough value for the electrostatic energy by using the macroscopic dielectric constant ϵ. The energy associated with the fields of the separate ions obtained in this way would amount to

$$\frac{e^2}{2\epsilon}\left(\frac{1}{R_+}+\frac{1}{R_-}\right)=J_{el}=Cke^{T/\vartheta}=Ck\epsilon_0/\epsilon.$$

To obtain an order of magnitude, we may write $R_+ + R_- = R$ and obtain

$$R=\frac{e^2}{Ck\epsilon_0}.$$

In methanol

$$R=\frac{(4.8\times10^{-10})^2}{645\times1.38\times10^{-16}\times151}$$

$$=1.7\times10^{-8}\text{ cm}.$$

A family of curves with $\vartheta=164.5$ for proton transfers in ethanol is so similar to those in methanol that they are not reproduced here. Values of $(\ln K)/484$ taken from Table III are found to lie on the curve for $a=-3.7$. There do not seem to be accurate data on the temperature variation of the dielectric constant of *n*-butanol.

In all three solvents for the process (2) the magnitude of J_{env} is greater at room temperature than J_{non}. In methanol it is only slightly greater, and on lowering the temperature, J_{env} becomes equal and opposite to J_{non} near 0°C with the result that the value of $\log K$ changes sign, as shown in Table III and in Fig. 3. In ethanol the electrostatic forces are stronger, and on lowering the temperature, we should not expect J_{env} to become equal to J_{non} until a *lower* temperature had been reached. Extrapolation of the experimental results shows that the value of $\log K$ will pass through zero near 220°K and in *n*-butanol at a still lower temperature, as is likewise to be expected.

In conclusion we may point out why the results for weak acids in aqueous solution are so different from the experimental results presented in Table III of this paper. The reason is that in the ionic dissociation of any weak acid the proton transfer is from a solute particle to a solvent molecule. Now the concentration of the solvent molecules is not under our control, and in a very dilute solution the solvent molecules are many thousand times more numerous than the acid solute molecules. Under these circumstances we only obtain a measurable equilibrium when a large amount of work is required to transfer the proton—that is to say, when J_{env} and J_{non} are of the same sign; electrostatic forces alone are insufficient to give a feebly dissociated acid; a positive J_{non} is required in addition.

This must be true, not only in aqueous solution, but also in methanol. There can be no doubt that if the dissociation constants for weak acids in methanol solution were measured over a wide range of temperature, the results would be found to lie on curves like those near the bottom of Figs. 2 and 3. Such curves have, in fact, been obtained in methanol-water mixtures,[6] though results in pure nonaqueous solvents do not seem to be available. On the other hand, when we are dealing with proton transfers of type (1) or type (2), the concentrations of all the relevant species are under our control, and by adjusting the relative concentrations, we can investigate proton transfers where J_{env} and J_{non} are of opposite sign, as in the experiments that have been described in this paper.

[6] H. S. Harned and N. D. Embree, J. Am. Chem. Soc. **57**, 1669 (1935).

NOTICE

The following officers have been elected for the Division of Chemical Physics of the American Physical Society, with terms as indicated, and take office at the May 2, 1952, annual business meeting.

J. E. Mayer	Chairman (1952–3)
J. O. Hirschfelder	Vice-Chairman (1952–3)
B. L. Crawford, Jr.	Secretary (1952–5)
F. G. Brickwedde	Treasurer (1952–5)

Other members of the Executive Committee:

J. G. Kirkwood	(1952–3)
H. H. Nielsen	(1952–3)
R. S. Mulliken	(1952–4)
D. F. Hornig	(1952–5)

The Growing of Single Crystals of Magnetite*

J. SMILTENS
Laboratory for Insulation Research, Massachusetts Institute of Technology, Cambridge, Massachusetts
(Received January 28, 1952)

Large, single crystals of magnetite, 1 cm in diameter and up to 4.3 cm long, of high purity and perfection have been grown from the melt. The density at 20° is 5.185, i.e., 99.58 percent of the x-ray density. The composition corresponds to stoichiometric Fe_3O_4 within analytical error. Phase diagram considerations, growing procedure, methods of chemical analysis, and composition data are discussed.

INTRODUCTION

A FUNDAMENTAL research program on ferromagnetic semiconductors is in progress in the Laboratory for Insulation Research. Magnetite (F_3O_4) plays the role of a key material in these investigations, since the other ferrites can be derived from it by substitution. Unfortunately, the material has thus far been available only as microcrystalline synthetic samples or as natural crystals of varying composition and impurity content. A fundamental study of the magnetic and electric properties of magnetite requires pure and sufficiently large and perfect single crystals. That new information of great interest can be obtained with such material is shown by two recent publications from this laboratory[1,2] and by an investigation using our crystals at the Bell Telephone Laboratories.[3]

Consequently, we embarked on the somewhat formidable task of growing single crystals from the melt at *ca* 1600°C by a modified Bridgman-Stockbarger method. Fortunately, the phase diagram of iron-oxygen was well known. How, on the basis of this information, a satisfactory growing technique was developed for large single crystals of magnetite and how these were studied for composition and density is described in the present report.

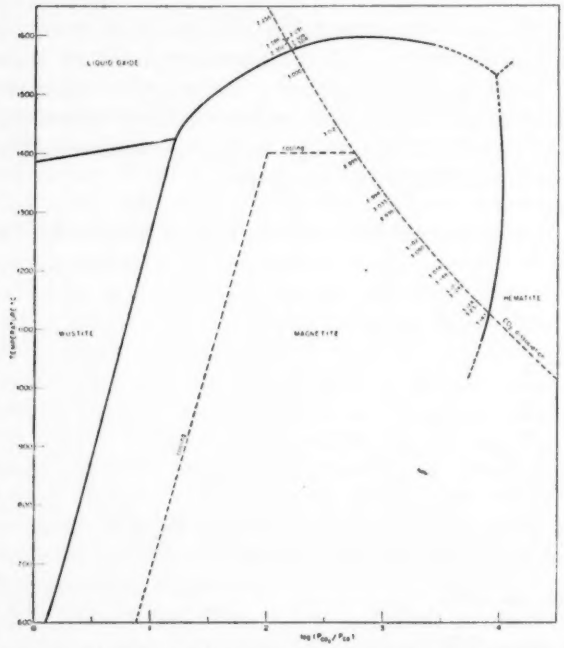

FIG. 1. Magnetite field and adjacent areas, dissociation curve of CO_2, and cooling curve of the crystal.

THE IRON-OXYGEN PHASE DIAGRAM

Figure 1, derived from the data of Darken and Gurry,[4] shows a projection of the three-dimensional phase diagram of iron-oxygen (composition, temperature, oxygen pressure condition) as seen in the direction of the composition axis. The dissociation curve of carbon dioxide is also included, since in the preparation of our magnetite crystals an atmosphere of CO_2 has been maintained above the melt.

The gas in equilibrium with the iron oxide phase in question is actually oxygen, formed according to the reaction

$$2CO_2 \rightleftharpoons 2CO + O_2. \quad (1)$$

If the composition of the initial mixture of CO_2+CO is known, the partial pressure of oxygen at a given temperature may be calculated by making use of the mass action law

$$(P_{CO}^2 \times P_{O_2})/P_{CO_2}^2 = K_P, \quad (2)$$

that is,

$$P_{O_2} = K_P(P_{CO_2}/P_{CO})^2. \quad (3)$$

From Eq. (3) we see that the oxygen pressure can be represented either directly by P_{O_2} or indirectly by P_{CO_2}/P_{CO}. While P_{O_2} is more fundamental, P_{CO_2}/P_{CO} is more convenient in referring to our experimental conditions.

The coordinates for the dissociation curve of carbon dioxide have been computed (Table I) by the formula[5,†]

$$\log(P_{CO_2}/P_{CO}) = -(\log K_P + \log 2)/3. \quad (4)$$

* Sponsored by the ONR, the Army Signal Corps, and the Air Force under ONR Contract N5ori-07801.

[1] L. R. Bickford, Jr., Phys. Rev. **78**, 449 (1950).
[2] C. A. Domenicali, Phys. Rev. **78**, 458 (1950).
[3] J. K. Galt, Phys. Rev. **85**, 664 (1952).
[4] L. S. Darken and R. W. Gurry, J. Am. Chem. Soc. **68**, 798 (1946) (see their Fig. 7A, p. 805); **67**, 1398 (1945).
[5] Values for K_P taken from L. S. Kassel, J. Am. Chem. Soc. **56**, 1838 (1934).

† Derivation: If 1 mole CO_2 is introduced into the furnace and α-mole dissociates into α-mole CO and $\alpha/2$-mole O_2, $(1-\alpha)$ mole CO_2 is left. Since the sum of partial pressures is 1 atmos, the

The numbers marked along the dissociation curve are the values of the ratio r when

$$r=\frac{Fe^{++}+Fe^{+++}}{Fe^{++}}=\frac{Fe_{total}}{Fe^{++}}. \quad (5)$$

This quantity characterizes the composition of the iron-oxygen phase in equilibrium with oxygen at a given pressure (in the present case, with oxygen formed by the dissociation of CO_2). The value of r was obtained analytically by dissolving the sample of iron oxide in the absence of air, titrating with $KMnO_4$, reducing by means of a Jones reductor, again titrating with $KMnO_4$, and dividing the corrected number of milliliters used in the second titration by that of the first. For a composition corresponding to the stoichiometric $Fe_3O_4(FeO \cdot Fe_2O_3)$ the value of r is exactly 3 (one of three iron atoms is divalent).

According to Fig. 1 the experimental values of r within the magnetite field along the CO_2 dissociation curve lie close to the value 3 and show a general rise from 3.000, corresponding to stoichiometric Fe_3O_4, to 3.147, a composition called by earlier chemists a solid solution of oxygen in Fe_3O_4.‡ The fluctuation of the r values is obviously within the limits of the experimental error§ in these phase diagram studies.

Darken and Gurry state that within the magnetite field the r value is never less than 3, but as already shown, it can be greater. The largest value found thus far is 4.232 (at 1457°C in equilibrium with pure O_2 at 1 atmos), but still higher values are possible, corresponding to the upper right-hand corner of the magnetite field in Fig. 1 and indicated by broken lines (area of equilibria with pure O_2 at pressures higher than 1 atmos).

TABLE I. Calculated values of $\log(P_{CO_2}/P_{CO})$ for pure carbon dioxide.

Temperature	$\log K_P$	$\log(P_{CO_2}/P_{CO})$
1027°C	−13.60	4.43
1127	−11.99	3.90
1227	−10.59	3.43
1477	− 7.81	2.50
1575	− 6.93[a]	2.21
1727	− 5.73	1.81

[a] Interpolated from plot.

partial pressures are

$$P_{CO_2}=\frac{1-\alpha}{1-\alpha+\alpha+\alpha/2}=\frac{1-\alpha}{1+\alpha/2};$$

$$P_{CO}=\frac{\alpha}{1+\alpha/2};\quad P_{O_2}=\frac{\alpha/2}{1+\alpha/2}=\frac{\alpha}{2+\alpha}.$$

Hence: $P_{CO_2}/P_{CO}=(1-\alpha)/\alpha$; and the mass action law becomes $[\alpha/(1-\alpha)]^2\cdot\alpha/(2+\alpha)=K_P$. Since α is a very small number for our purposes, we can approximate $P_{CO_2}/P_{CO}=1/\alpha$; $\alpha^2/1\cdot\alpha/2=K_P$. It follows that $\alpha=(2K_P)^{\frac{1}{3}}$ and $P_{CO_2}/P_{CO}=1/(2K_P)^{\frac{1}{3}}$; $\log(P_{CO_2}/P_{CO})=-(\log K_P+\log 2)/3$.

‡ Actually, we have here the Fe_3O_4 structure with some Fe atoms missing.

§ Caused by: possible impurities in the carbon dioxide, change of composition during the quenching of the sample, and the difficulty of obtaining a complete equilibrium. Where the authors (see reference 4) have given two values by approaching the equilibrium from both sides, we have taken the arithmetic mean for the diagram.

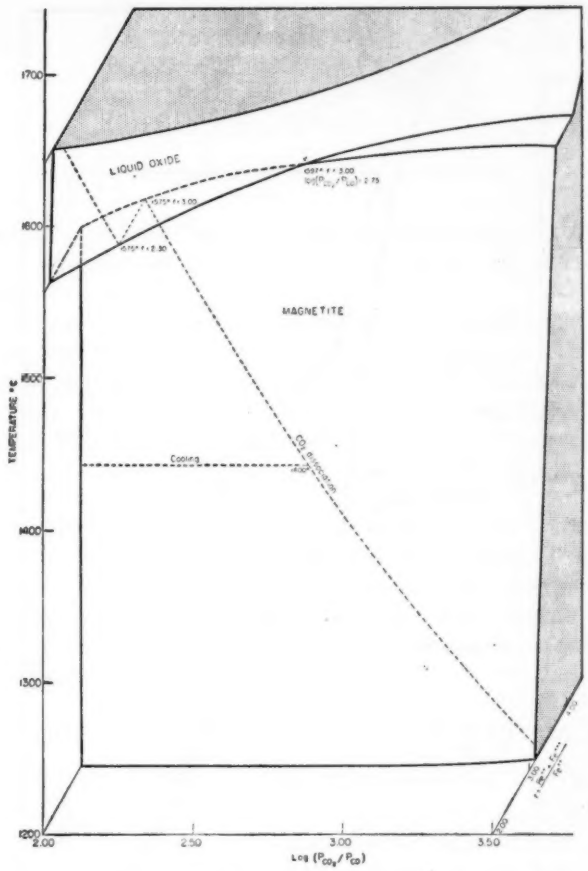

FIG. 2. Relationships of the liquid oxide and magnetite phases near the point V.

The r values of Fig. 1 may be compared with the depths in a nautical map; the magnetite field appears as a wide plateau which becomes depressed as we move within the high temperature range towards the boundary of magnetite-hematite. The hematite phase, for which $r=\infty$ (Fe_2O_3), is the lowest level in the diagram, whereas metallic iron (not shown in Fig. 1), having $r=1$, is the highest. Between the magnetite and the metallic iron phase there lies the triangular, nonhorizontal wüstite (⟨FeO⟩) field‖ in which the r values range from 1.116 to 1.673.

The liquid oxide field is a wide, inclined area which, towards wüstite, lies above the magnetite field ($r<3$), and towards the hematite, below it ($r>3$). There is, consequently, one point at which both surfaces, the magnetite field and the liquid oxide field, intersect. In Fig. 2 this point is designated as V. The coordinates of V are $T=1597\pm2$°C,¶ $r=3.000$, and $\log(P_{CO_2}/P_{CO})$

‖ Horizontal indicates constant r value, that is, constant composition.

¶ According to the phase diagram this must be the highest temperature in the magnetite field.

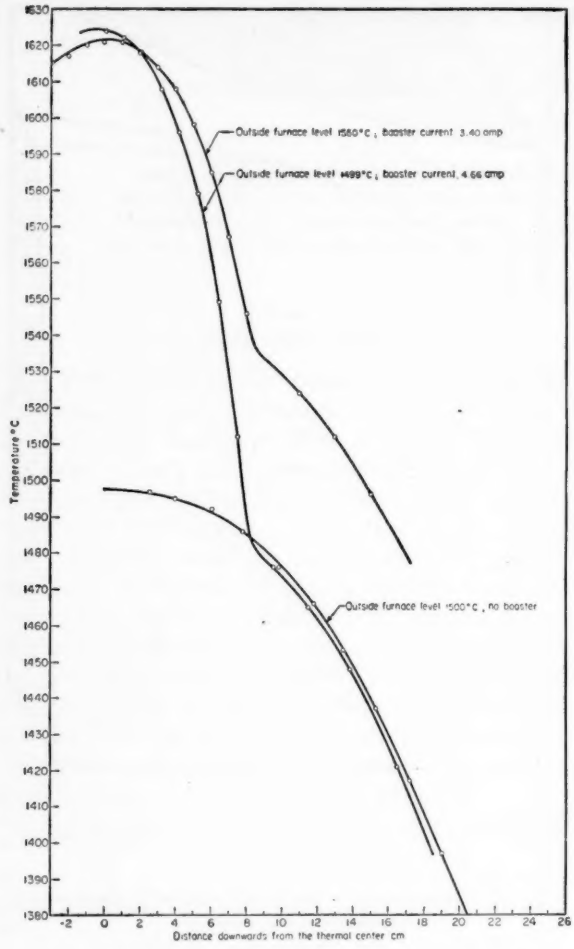
Outside furnace level 1580°C, booster current 3.40 amp
Outside furnace level 1499°C, booster current, 4.66 amp
Outside furnace level 1500°C, no booster
Temperature °C
Distance downwards from the thermal center cm

FIG. 3. Temperature fields of the combined furnace.

$=2.75$ (which corresponds to an input gas mixture of 94.25-vol percent CO_2+5.75-vol percent O_2). This point V might appear as the point at which a crystal of Fe_3O_4 should be grown because the liquid as well as the solid phase have the same desired composition of the stoichiometric Fe_3O_4.

Actually we have not worked at this point V for the following reasons: (1) The magnetite field is bent in the neighborhood of V, hence it would be very difficult to preserve the stoichiometric composition during cooling. (2) Beyond the "stoichiometric point" V the liquid phase has higher r values than the solid phase; this means that upon solidification a certain amount of oxygen will be liberated if we overshoot V by a slight increase in oxygen pressure. This would produce cavities in our samples. (3) Liquid iron oxide reacts with the platinum container in the sense that iron diffuses into the platinum. This increases locally the oxygen content of the melt and thus causes a shift towards a higher r value. For a melt adjusted to $r=3$ this would mean an increase above 3 and again the danger of cavity formation.

We therefore did not grow our crystals at the point V but used instead an atmosphere of pure CO_2. In this case the solidification occurs at 1575°C, forming a stoichiometric Fe_3O_4, whereas the melt at the moment of solidification has an r value of only about 2.304 (see Figs. 1 and 2). The danger that by crystallization the melt would be depleted of oxygen did not materialize. Calculation shows that the solid with $r=3.000$ contains 27.64 percent of oxygen, whereas the melt with $r=2.304$ contains 26.88 percent, the difference being only 0.76. Moreover, the already-discussed interaction of the iron oxide melt with the platinum walls, undesired in other cases, worked in our favor. In cooling, the composition of the CO_2+CO mixtures has to be adjusted according to Table II to maintain the correct magnetite composition. Table II has been obtained from the cooling curve shown in Fig. 1.

The initial temperature of the melt was adjusted to 1605–1615°C. Since the solidification in an atmosphere of CO_2 starts at 1575°C, it was overheated by about 35°C. One reason for this was the necessity of completely destroying all nuclei. Another reason is that because of the interaction of the oxide melt with the platinum walls a thin layer of melt with a high r will form at the boundary of melt and crucible. Consequently, incipient solidification can occur at this place at temperatures higher than 1575°C. Since the highest possible temperature within the magnetite field is 1597°C (point V), the temperature throughout the melt before the slow lowering of the crucible should lie above it.

PREPARATION OF THE IRON OXIDE

A high purity iron** served as the starting material for the preparation of a very pure iron oxide. The major nonvolatile impurities of this iron, according to spectroscopic analysis by the manufacturer, are Ni, *ca* 0.0015 percent; Co, *ca* 0.001 percent; Cu, *ca* 0.0008 percent; P, <0.001 percent; Si, <0.001 percent.[6] It is

TABLE II. The composition of CO_2+CO mixtures used during the cooling of single crystals of Fe_3O_4.

Temperature	Vol % CO in mixture
1400°C	1.0
1300	1.4
1200	2.0
1100	2.4
1000	3.2
900	4.8
800	6.2
700	9.1
600	11.
500	14.
400[a]	20.

[a] Below 400°C the mixture was not further altered; it was assumed that the vertical cooling line, with $P_{CO_2}/P_{CO}=4$ from 400°C down to room temperature, remains within the magnetite field.

** "Puron," Westinghouse Electric Corporation, Pittsburgh, Pennsylvania.

[6] A complete analysis is given in the brochure, "Westinghouse Metals and Alloys," p. 18.

supplied in the form of rods 15-cm long and 5-mm diam, weighing *ca* 23 g each. After washing a rod in 1:1 nitric acid to remove surface impurities, it was dissolved in nitric acid (85-ml conc acid diluted with 5-vol water) overnight, then filtered and diluted to 2 liters. Ammonia†† was distilled into the solution, precipitating iron hydroxide. The end of the precipitation is indicated by a sudden thickening of the whole mass, which again becomes fluid on further stirring. This iron hydroxide does not have the jelly-like consistency of that formed by the addition of ammonium hydroxide solutions and settles readily. After standing *ca* 3 hr, it was filtered on a carefully selected Büchner funnel, pre-dried for 3 days in a vacuum desiccator, and finally heated at 250°C in a Pt crucible to remove the residual ammonium nitrate and moisture. The dry oxide was ground in a steel mortar to a coarse powder, then densely packed into clean platinum crucibles (12 cm long, 10 mm diam). Each crucible contained *ca* 15-g oxide and was covered with a small lid; its edge is serrated to facilitate gas exchange. The crucibles were suspended in the furnace and heated to 1400°C while surrounded by mixtures of CO_2 and CO, varied according to Table II, which produced and maintained the magnetite phase. Above 1400°C the atmosphere was pure CO_2. The gas mixture before entering the furnace was passed through $KMnO_4$ solution acidified with H_2SO_4 and dried over silica gel. The flow velocity and the mixing ratio of the gas mixture was controlled by a capillary flow meter. The gas was introduced through the bottom of the furnace and its linear flow velocity maintained at 1 cm/sec[7] (calculated for room temperature).

The first heating cycle was designed to produce a relatively dense multicrystalline magnetite rod. The material was therefore heated overnight to only 1550°C and then returned to room temperature in the presence of the correct gas mixtures. The very pure oxide prepared in this way sinters much less readily than cp material, as would be expected.

FURNACE ASSEMBLY

To grow single crystals, a tubular globar furnace (5 kw, 50 mm i.d.) was used with the addition of a small platinum-wound internal "booster" furnace. The booster furnace, which establishes the steep temperature gradient required for the growth of single crystals, is placed concentrically in the thermal center of the outside furnace. For lowering the crucible into the furnace a synchronous motor drive and reduction gear system were used. To avoid backlash the gear system was spring-loaded by means of a flat spiral.

The temperature of the outside furnace was controlled by a Leeds and Northrup Speedomax to ±0.6°C and the booster temperature by a special thyratron circuit to ±0.4°C.

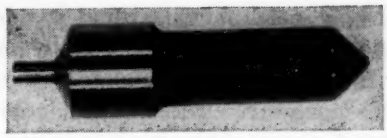

FIG. 4. Single crystal of magnetite (natural size).

Figure 3 shows a diagram of the temperature fields obtained with the combined furnace arrangement. The upper curves can be closely approximated by two intersecting parabolas, the booster parabola superposed above that of the outside furnace. For most of the work the temperature field was that obtained with the outside furnace at 1550°C and a booster current of 3.60 amp. The temperature gradient of this curve below 1575°C (the temperature of beginning solidification) is about 20°C/cm. Our thermocouples were checked against the melting point of palladium wire (1554°C) and the resulting correction applied throughout the working range (1490°–1620°C).

FORMATION OF MAGNETITE SINGLE CRYSTALS

With the furnace at room temperature the Pt crucible, covered by a small, welded-on cap of 1-mil platinum foil, was suspended by a platinum wire (1-mm diam). The length of the wire and the initial position of the drive shaft were so adjusted that the point of the crucible was located at the thermal center of the booster. Then the outside furnace was slowly brought up to temperature while CO_2+CO mixtures, as already explained, were passed through the furnace. With the outer furnace at its fixed temperature the booster current was started and gradually increased. The melting of the crucible charge at 1575°C begins at the conical point of the crucible and proceeds slowly upwards, thus facilitating the escape of the oxygen liberated upon melting. At this stage the final centering of the crucible was done by means of suspension set screws. After allowing an additional ½ hr for complete equilibrium, the slow lowering process was started. The lowering rate was 5.5 mm/hr. After completion of the crystallization the system was cooled down at a rate of *ca* 50°C/hr. Again, the atmosphere was adjusted by proper CO_2+CO mixtures.

Since the magnetite crystal is tightly embedded in the Pt crucible, the Pt sheet was peeled off after sectioning it by a steel disk saw. The crystal was then mounted in a steel holder (Fig. 4). A series of back-reflection Laue photographs taken through the length of the samples demonstrated that most of them were single crystals throughout. Some samples contained several crystals and were used only for specific purposes.

†† The use of gaseous ammonia avoids contamination by the silica and silicates usually present in ammonium hydroxide solutions.

[7] A value recommended by L. S. Darken and R. P. Smith, J. Am. Chem. Soc. **67**, 1399 (1945).

The ratio r of total to divalent iron was determined by manganometric titrations[8] as already mentioned. The value of r was always found correct within the limits of the analytical error. Density measurements, carried through on one of the crystals, gave 5.185 g/ml at 20°C. The x-ray density, taking the edge of the unit cell as 8.39A,[9] is 5.207, thus the volume-mass density is 99.58 percent of the x-ray density.[10] The literature value is 5.16 to 5.18. Spectroscopic analysis indicated practically no platinum in the crystals.‡‡

ACKNOWLEDGMENTS

The author wishes to express his indebtedness to Professor A. von Hippel for suggesting the problem and for many helpful discussions, to D. H. Fryklund for the construction of the thyratron controller for the booster and other valuable help, to H. T. Evans, Jr. and R. D. Burbank for the x-ray analysis of the crystals, and to P. Kelleher and A. W. Hooper for the precision machine work.

[8] See W. F. Hillebrand and G. E. F. Lundell, *Applied Inorganic Analysis* (John Wiley & Sons, Inc., New York, 1946), pp. 781–785.

[9] E. J. W. Verwey and E. L. Heilmann, J. Chem. Phys. **15**, 174 (1947).

[10] The density was calculated according to the Annual Conference of the X-Ray Analysis Group, Institute of Physics (England), July, 1946 [J. Sci. Instr. **24**, 27 (1947)].

‡‡ The analysis was by three independent outside laboratories: "*A*" reported 0.000014 percent Pt (upper limit); "*B*," Pt not detected; and "*C*," Pt not found (sensitivity 0.002 percent).

THE JOURNAL OF CHEMICAL PHYSICS VOLUME 20, NUMBER 6 JUNE, 1952

Gaseous Detonations. V. Nonsteady Waves in $CO-O_2$ Mixtures*

G. B. KISTIAKOWSKY, HERBERT T. KNIGHT,† AND MURRAY E. MALIN†
Gibbs Chemical Laboratory, Harvard University, Cambridge, Massachusetts

(Received January 21, 1952)

The velocity of steady detonation waves in 2.5 $CO-O_2$ mixtures containing hydrogen agrees with the calculations of the Chapman-Jouguet theory. When all sources of hydrogen atoms are eliminated from such mixtures, much hotter shock waves must be used to initiate detonation. The detonation waves in hydrogen-free mixtures are stable but nonsteady. The velocities observed by piezoelectric pressure gauges undergo violent and not very regular fluctuations similar to, but not identical with, spinning detonations. Moving film slit photographs show that these fluctuations are caused by detonation fronts developing behind the forward shock, overtaking it at irregular intervals, and decaying in their stead. Similar detonation fronts are observed in delayed initiations of explosive mixtures capable of stationary detonation, but the waves upon initiation and after a few fluctuations settle into the stationary Chapman-Jouguet regime. Photographic observations show that the detonations developing behind the shock front are initially localized near the opposite walls of the cylindrical tube, while the gauge records demonstrate that the fronts of nonsteady waves are not normal to the tube axis but undergo irregular girations. The significance of these observations in terms of the rates of chemical reactions in shock fronts is discussed.

IT is well known that gaseous detonation waves do not acquire stationary character immediately upon initiation.[1,2] The nonsteadiness in chemically unbalanced explosive mixtures appears to be indefinitely maintained in the form of spinning detonations. These phenomena have been the subject of much speculation, and it has been repeatedly suggested that they are the consequence of delays in chemical reactions following the passage of the primary shock.[2] The observations, while favoring this idea, indicate nonetheless that a theory which does not take into account the effects of the containing walls cannot be correct. Thus, the pitch of spinning detonations[2] and the run-up distance of flames developing into detonations[3] are roughly proportional to the tube diameter.

It seemed to us that additional information on the nature of these phenomena might be gained by observing detonations in wide tubes in order to obtain better resolution of the spatial structure and by choosing the system investigated so that the effects of slow chemical reaction rates are separated from thermodynamic consequences of unbalancing explosive mixtures. A system of this type is available, the studies of flame velocities and of the rates of the thermal reaction in carbon monoxide-oxygen mixtures having shown both to be dependent on the concentration of water vapor and other hydrogen-containing compounds.[1,2] The effect of water vapor on detonation waves in such mixtures is not definitely settled, since Dixon[4] found a large reduction in velocity upon drying, but Bone, Fraser, and Wheeler[5] claim to have found no such effect.

* The research reported in this document was made possible by funds extended Harvard University under ONR Contract N5ori-76 T.O. XIX NR-053-094.

† Present address: Los Alamos Scientific Laboratory.

[1] B. Lewis and G. v. Elbe, *Combustion, Flames and Explosions in Gases* (Academic Press, Inc., New York, 1951).

[2] W. Jost, *Explosion and Combustion Processes in Gases* (McGraw-Hill Book Company, Inc., New York, 1946), translated by H. O. Croft. German edition: Verlag Julius Springer, Berlin, 1939.

[3] K. I. Shchelkin, J. Tech. Phys. USSR **17**, 613 (1947).

[4] H. B. Dixon, Trans. Roy. Soc. (London) **A184**, 97 (1893).

[5] Bone, Fraser, and Wheeler, Trans. Roy. Soc. (London) **A235**, 29 (1935).

EXPERIMENTAL DETAILS

The velocity measurements were carried out with the aid of piezoelectric gauges and associated equipment which has been described in Part III.[6] Four sections of the 10-cm tube were used. A 50-cm length served as the initiator. A 25-cm section filled with nitrogen was used as a buffer. For the experimental mixtures two 100-cm sections could be bolted together to study detonation further away from the 0.003-in. polythene diaphragm separating the experimental mixture from the adjoining one. One of these 100-cm sections was equipped for photographic work.

The photographic camera viewed a slit pressed against round glass windows set in a row into the wall of a section of the 10-cm diameter steel tube. The windows had a clear aperture of 9/16 in. and were spaced $1\frac{1}{8}$ in. on centers. Their location, relative to that of gauge holes in this section of the tube, was accurately measured. The optically flat glass windows were set with the aid of rubber gaskets into brass rings which were threaded into the tube walls. Although care was taken to have the windows flush with the inner wall of the tube, slight edges remained here and there. It was observed in experiments with nondetonating and barely luminous shocks that tiny luminous reflected waves were formed on these edges. This was of considerable advantage in some experiments in which the appearance of the reflections supplied accurate timing for the impact of the nonluminous shock on the edges of the windows. However, the reflections could be the cause of some of the initiation phenomena observed. Therefore, in later work small pieces of Apiezon *Q* putty were pressed by hand around the edge of the windows until no reflections could be further observed. No change in initiation phenomena resulted from this operation.

The luminous phenomena were observed with a moving film camera, designed on the principle of the camera of Payman.[7] It consisted of a 10-in. inside diameter shallow aluminum drum driven by a belt at 7000 rpm. The 35-mm film fitted into a groove on the inner surface of the drum. A 90-mm Elmar *f*:4 lens, parallel to the drum axis, a 90° reflecting prism sending the image on the film, and an ordinary photographic shutter completed the camera. It was built on a dolly and was enclosed in a removable box; for loading and removal of the film it was taken into the photographic dark room. For exposures it was accurately located on a concrete block, such that no weight rested on the dolly wheels.

The radiation from the after-burning was found to fog the film so badly that a faster shutter had to be interposed between the camera and the detonation tube. It consisted of an open 80° sector in an aluminum disk mounted on the shaft of a 1725-rpm motor and located in front of the camera lens. Thus the lens was open for roughly the duration of one revolution of the camera drum and was then closed for approximately 3 revolutions; the after-burning radiation was sufficiently reduced to eliminate objectionable fogging. The shaft of the rotating disk was provided with a commutator which fired the detonating spark in proper phasing upon the closure of the manual firing switch. To establish an accurate correlation between the piezoelectric gauge signals and the photographic record, the time bases of the two were tied together. A part of the amplifier output of each of two gauges, one located at the start of the photographically observed section of the detonation tube, the other at the end, was fed to the grids of 2D21 thyratrons. Each of these discharged a condenser through a Sylvania R1130B crater arc tube. Their light flashes were brought by suitable lenses and right-angle prisms into the field of view of the camera lens, so that each produced a dot on the moving film. The spatial relation of these dots on the film to the image of the slit of the detonation tube was determined from photographs taken on a stationary film. In order to measure the time delays of the crater arc flashes, a portion of a gauge signal was fed through the gauge amplifier to the scope; the other part triggered the thyratron of a crater arc tube which illuminated a photocell. The pulse from the latter triggered a second gauge amplifier. Thus two pips were obtained on the trace of the scope, the delay of the second being due to the crater arc, the photocell, and the amplifier. Allowing 0.6-μsec delay to the gauge amplifier[6] and a negligible delay to the photocell, it was found that out of three tubes tried, two crater arcs gave signals with a reproducible delay of 2.1 ± 0.1 μsec. These tubes were used in all subsequent experiments.

Commercial compressed gases were used as the source of acetylene, oxygen, nitrogen, hydrogen, and carbon monoxide. It was found that no amount of drying caused any change in the detonation patterns, presumably because, as stated by the manufacturer, the carbon monoxide contained 0.97 percent hydrogen, 0.8 percent saturated hydrocarbons, and 1.2 mg/l of iron as the carbonyl. For experiments on dry mixtures, therefore, carbon monoxide was prepared by decomposition of Mallinckrodt Analytical Reagent grade formic acid by cp sulfuric acid. The gas was passed through an alkaline pyrogallol tower, calcium chloride drying tower, and a dry-ice-cooled trap to a Cornelius compressor which collected the gas in a pressure cylinder. The absence of hydrogen and of hydrogen containing compounds was tested by passing the gas over a $CuO-Fe_2O_3$ catalyst at 250–275° and collecting water formed in weighing tubes filled with Anhydrone. The maximum content of hydrogen thus found was 0.03 percent by volume.

After mixing the components in the desired proportions as described in Part III of this series, the gases were led into the tube through six drying towers filled with Anhydrone and one more filled with P_2O_5 distributed on glass wool. The moisture content of the

[6] Kistiakowsky, Knight, and Malin, J. Chem. Phys. **20**, 884 (1952).

[7] Payman, Shepard, and Woodhead, "Safety in mines," Research Board Paper No. 99 (1937).

gases entering the tube was checked by interposing an Anhydrone-filled weighing tube and found to be below 0.01 percent.

THE RESULTS

The runs described in the following were made with mixtures of 2.5 $CO+O_2$, which are close to those for which maximum velocity has been reported.[8] Using commerical carbon monoxide, whether dried or not, completely steady velocities were observed with gauges spaced 8 cm apart, provided that the distance from the diaphragm to the first gauge exceeded 45 cm. At closer distances excess velocity was observed, when using a 50–50 acetylene-oxygen mixture as the initiator. Five runs gave average velocities of 1832, 1805, 1831, 1837, and 1844 m/sec over the 60-cm interval covered by the gauges. Camera records of these detonations showed steady waves with a homogeneous luminous front. The velocity of a steady wave in the 2.5-cm diameter tube was measured to be 1792 m/sec. In the 5-cm tube the velocity was 1812 m/sec, but the wave was not completely steady, probably because the gauges were placed too close to the diaphragm. When these velocities are combined with the average of the runs in the 10-cm tube, one obtains 1844 m/sec by the method discussed in Part III for the velocity of the infinite plane wave with an estimated standard deviation of 15 m/sec.

The thermo-hydrodynamic calculations were carried out as described in Part III and allowed for the dissociation of carbon dioxide and oxygen, but not for that of carbon monoxide or water. They gave 1821 m/sec for the velocity and 3518°K for the temperature of these detonation waves, assuming that the hydrocarbon reported by the manufacturer was methane. To be comparable with this figure, the experimental value must be corrected to the ideal gas state. By a method discussed in Part III, this correction has been estimated as −6 m/sec. The disagreement between the calculation and the corrected experimental average is 17 m/sec, or possibly 23 m/sec, if the second run in the 10-cm tube is omitted in averaging, as probably due to a gross error. It is statistically not significant because of the approximate character of the calculations and some uncertainty about the composition of the carbon monoxide used in these experiments.

With pure carbon monoxide no runs were made in presence of more than 1 percent added hydrogen and even then a slight unsteadiness of the wave remained The two runs with 1 percent hydrogen gave 1800 and 1824 m/sec, which with the corrections described above give 1820±15 m/sec for the ideal wave. For a mixture containing 1 percent hydrogen the calculations predict a velocity of 1813 m/sec. These comparisons with calculated velocities provide further evidence, discussed in more detail in Part III, that the velocity of steady waves is calculable by the Chapman-Jouguet theory.

Bone, Fraser, and Wheeler[5] reported stable but spinning detonations in carbon monoxide-oxygen mixtures containing less than 8 percent hydrogen. In the present experiments the waves were completely steady with commercial carbon monoxide containing only 2.5 percent hydrogen. This must be attributed to the higher stability of detonation waves in the larger tubes used in these experiments.[9]

Systematic studies of the initiation process in carbon monoxide mixtures containing hydrogen showed the same pattern of events as described earlier[10]; increasing the strength of the initiating shock waves entering through the nitrogen-filled buffer section caused the initiation of detonation to occur nearer the diaphragm. Table I shows the distance at which initiation took place and the maximum velocity observed, the gauges being spaced 5.8 cm apart. The initial burst of velocity is seen to be the greater the more delayed the initiation. It was followed by several oscillations of the velocity, which are undoubtedly related to the transient appearance of "spin" observed by Bone, Fraser, and Wheeler[5] on initiation of the hydrogen-containing mixtures.

The data of Table I together with the measurements of shock velocity prior to initiation permit the calculation of the velocity and temperature of a shock wave which is just able to initiate detonation after a long travel through the mixture. The velocity of such waves near the diaphragm is 1320 m/sec, with an uncertainty of about 50 m/sec.

Experiments with pure and carefully dried carbon monoxide-oxygen mixtures revealed that their initiation was far more difficult. In fact, none of the acetylene-oxygen initiators tried, even at 200-mm excess pressure, would initiate these mixtures through the buffer section filled with nitrogen. It became necessary, therefore, to omit the buffer and to separate the initiator compart-

TABLE I. Effect of initiator strength on the initiating delay in carbon monoxide-oxygen mixtures containing 2 percent hydrogen at 76 cm Hg.

Pressure of the 40% C_2H_2+60% O_2 initiator, cm Hg	Distance from the diaphragm to the velocity peak, cm	Maximum velocity observed
70	No detonation	
73	91	These distances are estimated from the appearance of "retonation" waves in the camera records.
76	84	
78	48	
81	29	2500 m/sec
82	10	2250
83	5	2100

[8] Campbell, Whitworth, and Woodhead, J. Chem. Soc. 59, (1933).

[9] In some recent experiments of one of us (Herbert T. Knight) with glass tubes and commercial carbon monoxide of the same origin, spinning detonations were observed in 1/2-in. diameter tubes but not in tubes of 1-in. diameter, using the 2.5 $CO+O_2$ mixture.

[10] Berets, Greene, and Kistiakowsky, J. Am. Chem. Soc. 72, 1086 (1950).

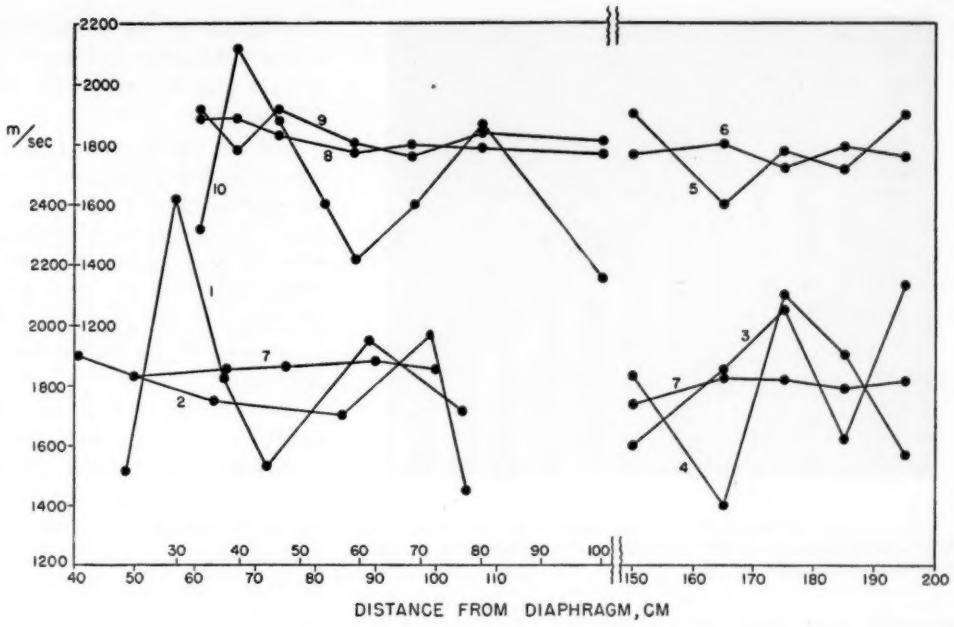

FIG. 1. Gauge measurements of the fluctuations of detonation velocity in mixtures of pure carbon monoxide and oxygen, with and without hydrogen. See text for a detailed explanation of the data.

ment from the experimental mixture by only one polythene diaphragm. As pointed out by Mooradian and Gordon,[11] however, the shock wave next to the diaphragm is weaker than it is further in the experimental section, and therefore the danger of direct initiation by the initiator mixture is slight. Indeed, as in the presence of the buffer section, the weaker initiator mixtures started detonation farther away from the diaphragm. The velocity of a shock wave just strong enough to initiate detonation in carbon monoxide-oxygen mixtures, as free from hydrogen as we were able to make them, was found to be 1500 m/sec. It was produced by an initiator mixture containing 39 percent acetylene and 61 percent oxygen at 760-mm pressure.

Using the accepted heat capacities of oxygen and carbon monoxide and assuming that chemical reactions do not occur in the non-initiating shocks, the Rankine-Hugoniot equations give 1070°K and 1280°K, respectively, for shocks just barely initiating hydrogen-containing and hydrogen-free carbon monoxide-oxygen mixtures. While these exact initiation temperatures are questionable, the fact that absence of hydrogen raises very substantially the initiation temperature is firmly established by the data.

The actual initiation temperatures are in doubt because the assumption of the absence of chemical reactions is definitely incorrect. Non-initiating shock waves in the reactive mixtures were consistently recorded by the camera because of their substantial luminosity. Experiments were made, therefore, in which shocks of similar velocity and temperature passed through nitrogen-carbon monoxide and through nitrogen-oxygen mixtures. In neither case was the faintest record obtained in the camera, which is not surprising, considering the low temperature of these waves. It is of interest to note that, in distinction to steady detonation waves in which the luminosity is at a maximum at the shock front, the luminosity of nondetonating shock waves in the reactive mixtures grows for as long as 20 μsec from a very low level at the shock front. An obvious conclusion is that a "slow" volume reaction does occur in under-strength shock waves while they advance without detonation. Consistent with this finding are those of Mooradian and Gordon[11] who observed gradual pressure rise behind the front of understrength shocks and attributed them also to a "slow" reaction.

It was impossible to produce steady detonation waves in hydrogen-free mixtures regardless of the strength of the initiator. The velocity of the observed waves fluctuated wildly about average values which were not far from that of steady waves. Camera records showed quasi-periodic dying out of the luminosity of the wave front, while new regions of luminosity developed in the rear and overtook the decaying shocks. The wave front of these nonsteady waves was in general not normal to the tube axis and its orientation kept changing with the progress of the wave.

Figure 1 shows gauge records of a few representative detonations with pure carbon monoxide-oxygen mixtures. Each point on this graph is the average velocity between two adjacent gauges, the point being placed on the graph halfway between the positions of the gauges. The lines have no physical significance, being drawn merely to connect the measurements of a single run. The lines numbered 1, 2, 3, and 4 show the range of velocity fluctuations in thoroughly dried mixtures and demonstrate that they persist over a total distance of at least 200 cm. The fluctuations are nearly random, although there is a hint of a periodicity with a "wavelength" of 20 to 40 cm. Lines 5 and 6 represent velocities

[11] A. J. Mooradian and W. E. Gordon, J. Chem. Phys. **19**, 1166 (1951).

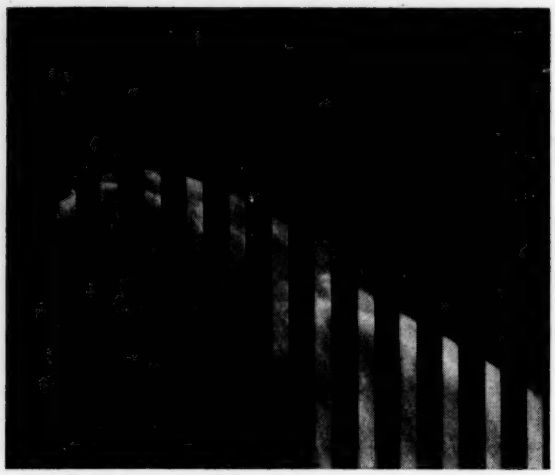

FIG. 2. The development of detonation waves behind the initial shock front in a nonsteady detonation of a mixture of pure carbon monoxide and oxygen.

observed after adding 0.1 percent and 1.0 percent water vapor to the mixture; line 7 after adding 1.0 percent hydrogen. It is evident that increasing quantities of water vapor reduce the fluctuations and that hydrogen is more effective in this respect than water. Record 8 was obtained after freshly mounting the gauges in the tube, during which operation red Glyptal cement was generously used on the threads and gaskets. Record 9 was a repeated detonation in this assembly after about twelve hours of pumping with slight heating of the tube; record 10 was obtained after a second such treatment of the tube. These three records furnish a striking demonstration that Glyptal solvent vapors are an extremely effective agent in restoring steadiness to the wave. All these sources of hydrogen, no doubt, produce hydroxyl free radicals, the accepted chain carrier in the oxidation of carbon monoxide.

The macroscopic cause of the nonsteady behavior in hydrogen-free mixtures is revealed by many camera records, one of which is reproduced in Fig. 2. The first window on the left was 30 cm from the diaphragm. Detonation was initiated closer to the diaphragm, and it passed by this window at a high velocity (2450 m/sec) being accompanied by strong luminosity. The velocity of the wave rapidly decreased so that it passed the fourth and fifth windows at only 1250 m/sec; the luminosity of the shock front decreased so much that the front is invisible in the reproduction. At the time that the shock passed the fifth window, a region of high luminosity had developed between the third and fourth windows, about 40 mm behind the shock front, and was spreading backward and forward with extremely high apparent velocity. This phenomenon, which has all the earmarks of a detonation, overtook the original shock at the sixth window and formed the highly luminous detonation front which passed by the seventh window at about 2500 m/sec and slowed down to about 1500 m/sec by the eleventh window. In the meantime a new detonation developed in the rear, between windows 8 and 9, overtaking the decaying front by the 12th window.

Not all the records taken showed such clear periodicity as Fig. 2 does, and in some the luminous regions developing behind the shock front are not sharply defined. The overwhelming evidence of the records, however, is that sudden bursts of velocity shown by the piezoelectric gauges (Fig. 1) are the result of new detonation waves developing behind the shock front, overtaking it shortly afterwards and then decaying in their turn.

The extremely high transient velocity of these detonations is understandable, considering that they propagate in a medium which has been already compressed, heated, and brought into forward motion by the initial shock. With the high velocity of these waves goes also high pressure. Therefore when the new detonation overtakes the old shock, it is overdriven by the high pressure from behind and so maintains for a while a velocity higher than the Chapman-Jouguet value.

Although the parameters of such waves can be calculated, the results cannot be compared with the camera and the piezoelectric gauge records (Fig. 1) because the phenomena observed do not extend over the entire cross section of the tube as plane fronts normal to the tube axis. This is demonstrated by Fig. 2 which shows that in addition to the detonation front which developed between the third and fourth windows another came into being a little later at the left edge of the third window and moved forward *behind* the other one. A similar situation prevails at the eighth window. Altogether, the "double" detonation fronts appeared to be the rule rather than the exception. The natural explanation of these findings is that the double fronts are not actually behind each other but only appear to

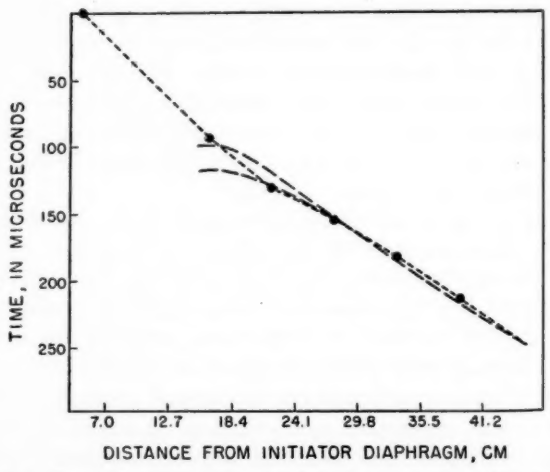

FIG. 3. Simultaneous gauge (dots) and camera (dashed lines) observations of the initiation process in a mixture of carbon monoxide, hydrogen, and oxygen, leading to a stationary detonation.

be so to the camera because they originate at the opposite walls of the tube and initially at least do not extend over the entire cross section of the tube.

The development of detonation fronts behind the front shock was observed also in the initiation process of commercial carbon monoxide-oxygen mixtures. The essential difference between the behavior of these mixtures and of those containing pure dried carbon monoxide is that in the latter the nonsteadiness of the wave persists as far as the range of these measurements, 200 cm, whereas in the former the wave settles soon after initiation into a stationary pattern.

The initiation process in the commercial carbon monoxide-oxygen mixture is illustrated in Fig. 3 which for the sake of clarity has been drawn by hand from the original records. The dotted line connects the time signals from a row of piezoelectric gauges which were located on the vertical diameter of the tube whereas the camera viewed the horizontal diameter. The gauge spacing was 5.8 cm. The faint shock entering the field of view of the camera from the left was recorded simultaneously by the gauges and the camera, so that its front must have been normal to the tube axis. The camera also showed a double detonation head developing about 15 cm from the diaphragm, the forward half of which overtook the shock front about 2 cm further along the tube. The gauges continued to report a slowly moving shock front to a distance of 21 cm, at which point the second of the two detonation heads caught up with the gauge signals. Only then did the gauges register a sudden rise in the velocity of the pressure front. The gauge signals and the luminous fronts reached again complete simultaneity about 40 cm from the diaphragm, or about 20 cm from the point of initiation. Several other experiments showed that at still greater distances from the point of initiation they remained as closely simultaneous as it was possible to measure, namely a few tenths of a μsec. To be interpreted, the phenomena shown in Fig. 3 require the postulate that the luminous zones, in the early stages

TABLE II. The determination of the spacing of gauges in triangular arrangements by three stationary waves in acetylene-oxygen mixtures.

Detonation velocity	Gauge intervals	1_1-2_1;	2_1-3_1	1_2-2_2;	2_2-3_2	1_3-2_3;	2_3-3_3
2915 m/sec	Measured time interval, μsec	3.3	0.7	3.6	1.4	3.0	1.7
	Calc. distance, cm	0.96	0.20	1.05	0.41	0.87	0.50
2915 m/sec	Measured time interval, μsec	3.8	0.8	3.3	1.2	3.1	1.5
	Calc. distance, cm	1.10	0.23	0.96	0.35	0.90	0.44
2840 m/sec	Measured time interval, μsec	4.1	0.4	2.7	1.0	3.3	1.4
	Calc. distance, cm	1.15	0.11	0.76	0.30	0.96	0.41
	Average, cm	1.07	0.18	0.92	0.35	0.91	0.45

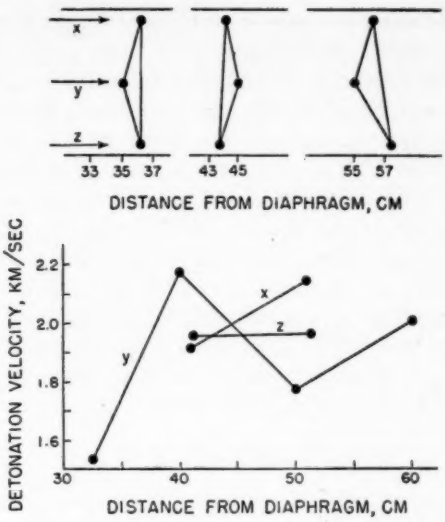

FIG. 4. Orientation of the wave front (upper drawing) and local shock velocity (lower drawing) in a nonsteady detonation of a pure carbon monoxide-oxygen mixture.

of their existence, are not plane fronts extending over the entire cross section of the tube.

Two other sets of experiments provide information on the configuration of the wave front. One arrangement used gauges mounted on the ends of rods projecting into the 10-cm tube from the end plate, as described in Part II.[10] One of the gauges was on the axis of the tube, the other near the wall. The diameter drawn through these gauges was in line with a wall gauge on the opposite wall. The wall gauge was closest to the diaphragm, the axial gauge was 4.8 mm and the other rod gauge 2.9 mm behind it, in order that a signal from a given gauge might be clearly distinguished on the C.R.O. trace. Two runs were made with this arrangement which are shown in Fig. 1. In run No. 8 the instability, as shown by the gauges, was slight. The axial gauge signalled the passage of the wave 3.7 μsec later and the other rod gauge 3.9 μsec later than the wall gauge. If it is assumed that the shape of the wave front and its velocity remain constant over a small distance over which the gauges were distributed, one finds that the wave front was advanced by 2 mm at the wall gauge against the center and by 4.2 mm against the opposite side of the tube. In run No. 9 of Fig. 1 such deviations from normality amounted to 9.3 and 17.3 mm, respectively, as calculated from time delays of 8.6 and 12.6 μsec. These data only suggest that the wave fronts are plane, but they certainly show their lack of normality to the tube axis.

In another arrangement groups of three gauges were mounted in the walls of the tube to form equilateral triangles, slightly inclined to the tube axis. Three such triangles were located approximately 10 cm behind each other. There were present additional wall gauges in line with one corner of the triangles. The axial distances between the three gauges of each triangle were

measured with the help of stationary detonation waves in acetylene-oxygen mixtures. As these measurements show how precisely normal such wave fronts are, they are given in Table II. Since several runs with unsteady waves gave qualitatively the same results, only one is shown in Fig. 4. The upper portion of this figure presents the inclination of the wave front at each of the three gauge triangles, computed under the same assumptions as were stated for the runs with rod gauges. The lower portion shows the shock velocities along the three lines of gauges, no assumptions being necessary for this calculation. The wave front is seen to undergo very violent girations. The results of other such runs indicated no regularity in its motion.

DISCUSSION

Perhaps the most important of the findings of these experiments is that it is possible, by a reduction in chemical reaction rates and without significantly changing the thermodynamics of the explosive mixtures, to suppress steady detonation waves obeying the Chapman-Jouguet theory and to replace them with highly unsteady but self-maintained pulsating waves. Such waves are undoubtedly related to the spinning detonations recorded by others in narrower tubes, but they lack the regularity and some other features of the latter. Perhaps they are the further development of what has been described as multiple spinning heads.[12]

The pulsations are very similar to the "overshoot" on initiation of steady detonations.[10] The camera records show that the cause of both is the formation of detonation fronts close behind the forward shock. The difference is that in mixtures capable of steady detonation the "over-shooting" wave settles to the Chapman-Jouguet regime when the overdriving high pressure region is dissipated. In pulsating waves the chemical reactions are evidently too slow to maintain the Chapman-Jouguet regime, and so the wave decays further. This is not the result of a complete absence of chemical reactions because such reactions do occur even in shocks too weak to initiate detonation. However, chemical conversion must be slight, and so the region behind the shock becomes gradually filled with a reactive gas mixture capable of releasing much additional heat. It is then that a new detonation front develops.

The new detonation fronts arising behind the shocks, as the cause of spinning detonation, have been suggested more than once.[2] However, in so far as the processes occurring were treated as unidimensional phenomenon, it was extremely difficult to explain why the slow reactions behind a decaying shock should suddenly be converted into a new detonation front. The evidence of irregular and changing orientation of the wave front[13] shows that the phenomena observed cannot be treated as unidimensional. The occurrence of double detonations and the approximate planarity of the wave fronts observed with gauges in the interior of the tube suggest that the new detonations develop at the opposite walls of the containing tube. The reason for this becomes apparent from the theory of standing waves which follow the primary shock, as developed by Manson[14] and recently further refined and extended by Fay and Kantrovitz[15] to interpret spinning detonations. An alternative treatment of spinning detonations, which considers oblique shocks and reaction zones behind the primary shock, has been proposed by Shchelkin[16] and developed mathematically by Zeldovitch.[17] Similar ideas are presented qualitatively also by Lewis and v. Elbe.[1] The experiments here described do not permit a decisive choice between these two points of view, but the Manson-Fay treatment could very well be applicable to the present experiments if allowance is made for the fact that the ratio of tube length to tube diameter in the experiments was comparatively small, and therefore the gas oscillations behind the initial shock would not be expected to reach a fully stationary character.

[12] W. A. Bone and R. P. Fraser, Trans. Roy. Soc. (London) **A228**, 223 (1929).

[13] In Part II of this series a few experiments with rod gauges indicated planarity and normality of the front of a newly initiated detonation. The interpretation of the gauge signals was then somewhat uncertain because of the type of the electronic circuits used, and so the reported results might have been in error. On the other hand, in some of our gauge triangle experiments the wave front was normal to the tube axis and it might be that, accidentally, only such configurations were observed in previous work.

[14] N. Manson, *Propagation des Detonations*, etc. (Office Natl. d'Etudes Aer. et des Petroles, Paris, 1947); Compt. rend. **222**, 46 (1946).

[15] J. A. Fay, thesis, Cornell University, 1951.

[16] K. I. Shchelkin, Dokl. Akad. Nauk (USSR) **47**, 501 (1945).

[17] Y. V. Zeldovitch, Dokl. Akad. Nauk (USSR) **52**, 147 (1946).

Equation of State Computations

JOSEPH E. MAYER AND GIORGIO CARERI*
Institute for Nuclear Studies, University of Chicago
(Received January 8, 1952)

A logical computation method is suggested for approximating the thermodynamic properties of a simple molecular system. In this method the thermodynamic functions of a nonequilibrium system are computed exactly. The state of the system is then varied at fixed volume and temperature so as to give a minimum Helmholtz free energy, consistent with such conditions as are imposed to permit the exact computation. The condition under which this method leads to self-consistent equations is discussed. The method is then applied in a way that is very close to the Lennard-Jones and Devonshire cell method, but with cells of variable size. The distribution within a cell is assumed to be Gaussian. The method is numerically far easier than the cell method, and apparently somewhat better.

I. INTRODUCTION

THERE exist at present three general approaches to the calculation of the equation of state of a macroscopic system of molecules, if one assumes that the forces between the individual molecules are known. These three methods may be classified as follows:

(1) The Calculation of the Virial Coefficients[1]

Use is made of the fact that the exponential of the negative potential energy divided by kT is unity when all molecules are far from each other, and this function is expanded as unity plus correction terms which are nonzero only when pairs or subsets of molecules are close together. The integral of the exponential then contains the leading term unity which, integrated over the coordinate space, gives V^N and leads to the perfect gas equation. The remaining correction terms can be shown to give expressions for the virial coefficients, namely the coefficients in an expansion of PV/NkT in a power series of the number density. This method is numerically practical, but the series converges only when the system is in the gaseous state.

(2) The Method of Integral Equations

Yvon[2] in France, Kirkwood[3] and Mayer[4] in America, and Born and Green[5] in Britain have all developed essentially similar methods by which the distribution functions for pairs or small sets of molecules can be determined as the solutions of certain integral equations. The distribution functions then determine the pressure. At best the solutions of the integral equations are numerically difficult. In all cases they must be solved subject to an approximation which is sometimes called the superposition principle and which was first suggested by Kirkwood. This approximation consists of the assumption that the distribution function for triples is at least approximately a product of the functions for the three pairs. Even with this assumption the difficulties of this method are sufficiently great that no numerical equation of state has been obtained by its use as yet.

(3) The Cell Method or Free Volume Method

In its original form this method was intuitive in conception and consisted essentially of the assumption that the integral of the exponent of the negative potential energy over kT was proportional to the Nth power of a representative integral for a single particle moving in the average position of all the others. Probably the best of the earlier attempts along this line was that of Lennard-Jones and Devonshire.[6] The particle over which the integration is made is assumed to lie in a cell surrounded by the other molecules whose positions are at the centers of equivalent cells composing some simple crystalline lattice, usually the face-centered cubic. This method has the advantage of leading to numerical results by a finite amount of calculation, but because of its intuitive basis it is difficult to improve upon it by any successive approximation method of development.

Recently Kirkwood[7] has made this method more respectable by showing that it is, in a certain approximation, the solution of a minimization of the free energy. In this paper we wish to follow a method suggested by Kirkwood's approach and show how more accurate equations of state may be developed by successively improving the solutions of the original cell method.

---

* Present address: Centro di Studi per la Fisica Nucleare del C.N.R. Istituto di Fisica dell'Universita, Roma, Italy.

[1] See for instance: Ursell, Proc. Cambridge Phil. Soc. **23**, 685 (1927); J. E. Mayer, J. Chem. Phys. **5**, 67 (1937); J. E. Mayer and S. F. Harrison, J. Chem. Phys. **6**, 87, (1938); M. Born and K. Fuchs, Proc. Roy. Soc. (London), **A166**, 391 (1938); B. Kahn and G. E. Uhlenbeck, Physica **5**, 237 (1938); J. E. Mayer, J. Chem. Phys. **10**, 629 (1942).

[2] J. Yvon, *La theorie statistique des fluides et l'equation d'etat*, No. 203 of Actualities scientifiques et industrielles (Hermann and Cie, Paris, 1935).

[3] J. G. Kirkwood and E. M. Boggs, J. Chem. Phys. **9**, 514 (1941); **10**, 307 (1942); **10**, 394 (1942).

[4] J. E. Mayer, J. Chem. Phys. **15**, 187 (1947).

[5] M. Born and H. S. Green, Proc. Roy. Soc. (London) **A188**, 10 (1946–47); **A189**, 103 (1947); **A191**, 168 (1947); **A193**, 166 (1947–48); **A194**, 244 (1948); and *A General Kinetic Theory of Liquids* (Cambridge University Press, Cambridge, 1949).

[6] J. E. Lennard-Jones and A. F. Devonshire, Proc. Roy. Soc. (London), **A169**, 317 (1939).

[7] J. G. Kirkwood, J. Chem. Phys. **18**, 380 (1950).

II. STATEMENT OF THE PROBLEM

If the distribution of molecules of a single system in configuration space is specified by some more detailed description than the mere statement that it corresponds to a canonical equilibrium distribution, then the entropy of the system depends upon the detail with which this distribution is specified. However, one may discuss an ensemble of systems for which the distribution in configuration space is specified by a probability density function: $W(x_1y_1\cdots z_N)$, such that $Wdx_1\cdots dz_N$ gives the probability that one member of the ensemble will have molecules at the coordinate position $x_1, \cdots, z_N$ within the volume element $dx_1\cdots dz_N$. The probability density function must necessarily be so normalized that

$$\int\int\cdots\int W dx_1\cdots dz_N = 1. \tag{1}$$

One may similarly specify the distribution in momentum space. We shall here assume that this momentum distribution is canonical so that the average kinetic energy per degree of freedom is $\frac{1}{2}kT$ and the additive contribution to the entropy of a system due to the kinetic energy has the usual classical form $\frac{1}{2}k\ln(2e\pi mkT/h^2)$ per degree of freedom.

For such an ensemble the average potential energy per system is given by:

$$\bar{U} = \int\int\cdots\int WU dx_1\cdots dz_N, \tag{2}$$

where $U=U(x_1, \cdots z_N)$ is the potential as a function of coordinates. The entropy contribution, S_τ, due to the configuration space is:

$$S_\tau = -k\int\int\cdots\int W[\ln WN!]dx_1\cdots dz_N. \tag{3}$$

Since energy and entropy for the ensemble are determined, one may also calculate the Helmholtz free energy:

$$A = E - TS, \tag{4}$$

or more particularly the contribution A_τ to the Helmholtz free energy due to the configuration space:

$$A_\tau = \bar{U} - TS_\tau. \tag{5}$$

In these equations the temperature is that determined by the canonical distribution of the molecules in momentum space.

Now suppose the probability density function W is limited in some arbitrary way to have a particular mathematical form. This limitation may be such as to exclude the known equilibrium probability density

$$W(x_1, \cdots z_N) = \exp(1/kT)[A_\tau - U(x_1, \cdots z_N)]. \tag{6}$$

If, however, we choose the probability density function subject to our arbitrary limitation to be that which minimizes A_τ, we may then see that we have the "best" probability density function subject to our particular arbitrary limitations.

Now the usual problem of determining the equation of state uses Eqs. (6) and (1). In Eq. (6) A_τ is unknown, but the potential energy U as a function of the coordinates of the N molecules is assumed to be known. The normalization condition, Eq. (1), determines the contribution A_τ to the Helmholtz free energy due to the configuration space of the system. However, the integration of Eq. (1) is impractical when the number N of molecules is large enough that in the volume V of the system there are, in the greater range of the configuration space, many molecule pairs whose mutual potentials divided by kT are not small compared to unity.

If, however, we arbitrarily limit our choice of the analytical form of W to be such that the integrals of Eqs. (1), (2), and (3) can actually be performed, we may then calculate the thermodynamic functions of an average member system of the fictitious nonequilibrium ensemble. The cell method accomplishes just this. In its simplest form W is assumed to be product over all molecules, i, of functions $W_1(x_iy_iz_i)$ of the single molecules. The function W_1 is then assumed to be periodic in the three-dimensional space of the coordinates x_i, y_i, z_i of the center-of-mass of the single molecule. The periodicity is arbitrarily assumed to be such that there are exactly N identical, nonoverlapping, contiguous cells, located around the centers of some particular simple crystalline lattice such as the face-centered cubic. The additional restriction, however, is placed on the function that no two molecules can occupy the same cell. This restriction can be expressed in a simple mathematical manner by introducing a factor in W which is a product of functions W_2 of all pairs of molecules. These functions W_2 are zero when two molecules are in the same cell and identically unity otherwise.

Such a probability density function leads to simple integrals of Eqs. (1), (2), and (3). The minimization condition on A_τ leads to a relatively simple integral equation connecting the distribution function for the single molecules within their cells and the potential energy U. This is the method which leads to the same result as Kirkwood's.[7]

Now a considerable numerical improvement over the equations obtained this way can be introduced without appreciable mathematical complication of the problem. Instead of specifying that the periodicity of the functions W_1 of the single molecules shall be such that there are exactly N cells, we may only retain that the periodicity shall be that of a close-packed lattice with an arbitrary number, Ω, of cells, where, however, our restriction that there shall never be more than two particles per cell will necessarily lead to the condition

$$\Omega \geq N. \tag{7}$$

Now Ω can be determined again by the minimization condition, namely, that the cells are of such a size that the free energy is a minimum. In this case it turns out

that even in the limit of zero density, $N/V \to 0$, the cells remain of finite size compared to molecular dimensions.

Essentially this improvement has been discussed by Ono[8] and by Terrell Hill[9] although neither use the complete minimization condition for both the functions W_1 and the number of cells.

As has been said, the introduction of a variable number of cells hardly complicates the calculation at all. However, further improvements are perfectly possible. For instance, it is formally simple to permit the functions W_2 to have a nonzero value when two molecules are in a cell and to determine this function, subject to some arbitrary restriction on its form, in such a way as to further minimize the free energy. One may then introduce as a factor in W a product of functions W_3 of coordinates of triples of molecules which are zero when three are in a cell and unity otherwise. However, with only one molecule per cell, if the size of the cells is left variable, the cells are very small even at low density, and therefore it might appear doubtful whether the added complication of relieving the restriction that there shall never be more than one particle per cell would be the most useful improvement.

It is interesting, however, to note what happens if we successively increase the allowed numbers of particles per cell, introducing increasing numbers of functions $W_2, W_3, W_4, \cdots, W_n, W_{n+1}$ of the coordinates of $2, 3, 4, \cdots, n+1$ molecules in a single cell, respectively, with the last function W_{n+1} arbitrarily restricted to be zero, and all functions restricted to be unity when any of the molecules are in different cells than any others of the subset.

In this case, if the potential energy U is assumed to consist of a sum of pair terms:

$$U(x_1, \cdots, z_N) = \sum_{N \geq i > j \geq 1} \sum u(x_i, y_i, z_i, x_j, y_j, z_j), \quad (8)$$

then the solution for n sufficiently large leads to:

$$\left.\begin{aligned} &W_3 = W_4 = \cdots = W_n = 1 \\ &W_2 = B \exp -u(x_i, \cdots, z_j)/kT \end{aligned}\right\}, \quad (9)$$

the value of B depending on the choice n of the maximum number of molecules per cell. W_1 and the size of the cells depends also on n. In the limit $n = N$ one obtains only one cell, occupying the whole volume, and Eq. (6) is satisfied with W_1 unity and:

$$W = \prod_{N \geq i > j \geq 1} \prod W_2(x_i \cdots z_j). \quad (9')$$

This is again the true equilibrium solution.

Probably a more practical step than that of increasing the allowed numbers per cell would be to permit the functions W_2 to have values other than unity for two molecules in neighboring cells. This immediately introduces considerable complication in the integrals of Eqs. (1)–(3). However, as long as the deviations of W_2 from unity are not too large, the integration can still be performed by a method somewhat analogous to the method used in the virial development.

Before concerning ourselves with such possible improvements in the calculations, we shall return to the original problem of the calculation of the thermodynamic properties of an ensemble specified by an arbitrary probability density function W and show certain theorems regarding these thermodynamic functions. We wish to show that by obeying certain simple rules we can always construct an ensemble which has perfectly definite thermodynamic properties and contains no self-inconsistencies in its calculable thermodynamic functions.

III. SELF-CONSISTENCY

The ensemble of systems which we have conceived is specified by the probability density function W at some arbitrary time, $t = 0$. The equations of motion are such that at a later time the probability density function will change and presumably approach asymptotically the equilibrium function of Eq. (6). However, at time $t = 0$ there will be a definite average force per unit area exerted on the walls of the systems composing the ensemble. This average force can be calculated from the virial expression, which is fully determined by the functions U and W. However, there also exists a thermodynamic relationship:

$$P = -(\partial A_\tau / \partial V)_T. \quad (10)$$

One may well ask whether the thermodynamic pressure given by Eq. (10) will be the same as that given by the virial expression, which latter gives the average force per unit area and therefore the true pressure. One immediately sees that we have not yet sufficiently defined our ensemble to assign a meaning to Eq. (10), since we have arbitrarily specified the function W for a particular number of molecules N and a particular volume V and have not stated how we determine W at another volume. Now what we propose to show is the following: Assume that W is specified by any arbitrary restrictions on its analytical form, but in a coordinate space

$$\left.\begin{aligned} \xi_i &= x_i/R, \\ \eta_i &= y_i/R, \\ \zeta_i &= z_i/R, \end{aligned}\right\}, \quad (11)$$

in which an arbitrary scale parameter R enters. The analytical form of W may involve any number ν of other arbitrary parameters $\beta_1, \beta_2, \cdots, \beta_\nu$. If, however, the one parameter R is determined at each volume V of the system by minimizing A_τ, and the other parameters $\beta_1, \cdots \beta_\nu$ are either individually kept constant as V changes *or* are also allowed to change individually with V in such a way as to minimize A_τ, then the ther-

[8] Syu Ono, Memoirs of the Faculty of Engineering, Kyushu University, X, 195 (1947).

[9] H. M. Peek and T. L. Hill, J. Chem. Phys. 18, 1252 (1950).

modynamic pressure given by Eq. (10) and the virial pressure become identical.

To demonstrate this it is convenient to introduce the scale of volume

$$\omega = R^3, \tag{12}$$

and

$$\Omega = V/\omega, \tag{13}$$

which is the dimensionless volume of a system in the dimensionless coordinate space of the ξ's. We also introduce the number density ρ in the dimensionless volume space,

$$\rho = N/\Omega, \tag{14}$$

and the number density c in the metric space:

$$c = N/V. \tag{15}$$

These two densities are related by the equation:

$$c = \rho/\omega. \tag{16}$$

If now the probability density function W is expressed in the dimensionless coordinates of Eq. (11), we normalize it as

$$\int\int_{\Omega}\cdots\int W(\xi_1, \cdots\zeta_N)d\xi_1\cdots d\zeta_N = 1. \tag{17}$$

The quantity

$$s(\rho, \beta) = -(1/N)\int\int_{\Omega}\cdots\int W \ln(WN!)d\xi_1\cdots d\zeta_N, \tag{18}$$

is now related to the configuration entropy contribution of Eq. (3) by

$$S_\tau/Nk = s + \ln\omega. \tag{19}$$

It is to be particularly noted that s depends on ρ and the β's alone, and does not explicitly depend on R or ω. Now define

$$\bar{u}(\rho, \beta, T, \omega) = \bar{U}/NkT$$

$$= (1/NkT)\int\int\cdots\int U(R\xi_1, \cdots, R\zeta_N)$$

$$\times W(\xi_1, \cdots, \zeta_N)d\xi_1\cdots d\zeta_N, \tag{20}$$

$$\bar{u}' = \omega(\partial\bar{u}/\partial\omega)_{\rho,\beta,T} = (R/3)(\partial\bar{u}/\partial R)_{\rho,\beta,T}$$

$$= (\tfrac{1}{3}NkT)\int\int\cdots\int W[\textstyle\sum_i R\xi_i(\partial U/\partial R\xi_i)$$

$$+ R\eta_i(\partial U/\partial R\eta_i) + R\zeta_i(\partial U/\partial R\zeta_i)]d\xi_1\cdots d\zeta_N$$

$$= (\tfrac{1}{3}NkT)\int\int\cdots\int W(x)[\textstyle\sum_i x_i(\partial U/\partial x_i)$$

$$+ y_i(\partial U/\partial y_i) + z_i(\partial U/\partial z_i)]dx_1\cdots dz_N. \tag{21}$$

The virial expression for the pressure is:

$$p = PV/NkT = 1 - \bar{u}'. \tag{22}$$

Define

$$a(\rho, \beta, T, \omega) = A_\tau/NkT$$

$$= \bar{u}(\rho, \beta, T, \omega) - s(\rho, \beta) - \ln\omega. \tag{23}$$

For any single one of the parameters β_μ the minimization of A_τ at constant value of c and T leads to an equation of the type,

$$\partial a/\partial\beta_\mu = 0 = \partial\bar{u}/\partial\beta_\mu - \partial s/\partial\beta_\mu, \tag{24}$$

for each β_μ which may vary. However, the two explicit parameters ρ and ω are related to c by Eq. (16) so that

$$(d\ln\rho/d\ln\omega)_c = 1. \tag{25}$$

There is, therefore, just one minimization condition for ρ and ω, namely:

$$\omega(\partial a/\partial\omega)_{c,\beta,T} = -1 - \rho(\partial s/\partial\rho) + \rho(\partial\bar{u}/\partial\rho) + \bar{u}' = 0, \tag{26}$$

$$\rho(\partial\bar{u}/\partial\rho) - \rho(\partial s/\partial\rho) = 1 - \bar{u}' = p. \tag{26'}$$

The thermodynamic pressure is given by

$$c(\partial a/\partial c)_T = PV/NkT. \tag{27}$$

However, from the rules of differentiation we have

$$c(\partial a/\partial c)_T = \omega(\partial a/\partial\omega)(d\ln\omega/d\ln c)$$
$$+ \rho(da/d\rho)(d\ln\rho/d\ln c) + \textstyle\sum_\mu(\partial a/\partial\beta_\mu)(d\beta_\mu/dc)$$
$$= -(1-\bar{u}')(d\ln\omega/d\ln c) + [\rho(\partial\bar{u}/\partial\rho)$$
$$- \rho(\partial s/\partial\rho)][d\ln\rho/d\ln c], \tag{28}$$

where the last line follows from Eqs. (24) and (21). In view of Eqs. (16) and (26') we have:

$$c(\partial a/\partial c)_T = (1-\bar{u}')[-(d\ln\omega/d\ln c) + d\ln\rho/d\ln c]$$
$$= p[d\ln(\rho/\omega)/d\ln c] = p = PV/NkT. \tag{29}$$

Thus, the thermodynamic pressure determined by Eq. (27) is the same as the virial pressure determined by Eq. (22).

In a completely similar manner we notice that $Ta = A_\tau/Nk$ contains the temperature only as a factor multiplying $s + \ln\omega$. In view of the minimization conditions, we, therefore, have

$$[\partial(T\alpha)/\partial T] = (-s - \ln\omega) = -S_\tau/Nk, \tag{30}$$

which is the correct thermodynamic expression for the entropy as the negative derivative of the Helmholtz free energy with respect to the temperature. Thus our nonequilibrium ensemble of systems has all the properties of a thermodynamic ensemble. Any thermodynamic relationship will be obeyed by it, and the thermodynamic pressure is actually the average force per unit area normal to the walls of the systems. We are in no danger of finding two inconsistent equations for the same thermodynamic quantity even though our ensemble is not one at true equilibrium and is a wholly fictitious figment of the imagination. The general proposal of this paper is that by a suitable choice of the probability density function W one is enabled actually

to calculate the properties of the ensemble and to approach reasonably closely to those of a real equilibrium system.

IV. THE OPEN SYSTEM

Although we have previously discussed an ensemble consisting of "closed systems" all having the same number N of particles in the same volume V and at the same temperature, it is sometimes more convenient for purely mathematically reasons to calculate using an "open system." By an open system we mean one which corresponds to the Gibbs grand canonical ensemble. For such a system we define a set of functions $W_{N,\Omega}(\xi_1, \cdots \zeta_N)$ in the dimensionless space of Eq. (11) which have the following significance: the open system is of infinite extent and $W_{N,\Omega}d\xi_1\cdots d\zeta_N$ is the probability that in a finite volume Ω there will be exactly N molecules, no more and no less, and that these will be located at the coordinate positions $\xi_1, \cdots, \zeta_N$ within $d\xi_1\cdots d\zeta_N$ (we count different permutations of the identical particles as different positions). We then have

$$\int\int\cdots\int W_{N,\Omega}d\xi_1\cdots d\zeta_N = w_{N,\Omega}, \tag{31}$$

which is the probability that there are exactly N molecules in the volume Ω. Then necessarily the normalization is that

$$\sum_{N\geq 0} w_{N,\Omega} = 1, \tag{32}$$

and

$$\sum_{N\geq 0} N w_{N,\Omega} = \bar{N}(\Omega), \tag{33}$$

for the average number, $\bar{N}$, of molecules in the dimensionless volume, Ω.

The distribution functions $F_n(\xi_1, \cdots, \zeta_n)$ are defined as being proportional to the probability that there will be n particles at the coordinate positions $\xi_1, \cdots, \zeta_n$ independently of where other particles may be in the system. It is convenient to choose the proportionality constant in such a way that

$$\lim_{\Omega\to\infty}\left[1/\Omega^n\int\int\cdots\int F_n d\xi_1\cdots d\zeta_n\right] = 1. \tag{34}$$

These function are determined from the functions $W_{N,\Omega}$ by the equation

$$\rho^n F_n(\xi_1, \cdots \zeta_n) = \sum_{N\geq 0}\frac{(N+n)!}{N!}\int\int_\Omega\cdots\int \times W_{n+N,\Omega}d\xi_{n+1}\cdots d\zeta_{n+N}. \tag{35}$$

It is clear from the logical definition of F_n that the functions defined by Eq. (35) are proportional to those defined by the logical statement. That the normalization, Eq. (34), follows from Eq. (35) is obtained by integrating Eq. (35) over the coordinates of the n molecules within the volume Ω so that one finds:

$$\rho^n\int\int_\Omega\cdots\int F_n d\xi_1\cdots d\zeta_N = \left\langle\frac{N!}{(N-n)!}\right\rangle_{Av}. \tag{36}$$

Since

$$\rho = \bar{N}/\Omega, \tag{37}$$

one has

$$\frac{1}{\Omega^n}\int\int_\Omega\cdots\int F_n d\xi_1\cdots d\zeta_n = \left(\frac{1}{\bar{N}}\right)^n\left\langle\frac{N!}{(N-n)!}\right\rangle_{Av} = \frac{1}{(\bar{N})^n}\left[\bar{N}^n - \frac{n(n-1)}{2}\langle N^{n-1}\rangle_{Av} + \cdots\right]. \tag{38}$$

In the limit that Ω goes to infinity, the right-hand side of Eq. (38) is unity if the fluctuations in the open system remain finite. For a normal thermodynamic system this is always the case, except at a phase transition.

We now use the notation:

$$\left.\begin{aligned}(i) &= \xi_i, \eta_i, \xi_i,\\ d(i) &= d\xi_i d\eta_i d\zeta_i,\end{aligned}\right\} \tag{39}$$

for the coordinates, and express $W_{N,\Omega}$ in the form

$$W_{N,\Omega} = (1/N!)\exp -\Psi_N(\xi_1, \cdots \zeta_N), \tag{40}$$

where

$$\Psi_N = \psi_0 + \sum_i\psi_1(i) + \sum_{N\geq i>j\geq 1}\sum\psi_2(i,j) + \sum_{N\geq i>j>k\geq 1}\sum\sum\psi_3(i,j,k) + \cdots. \tag{41}$$

The normalization conditions, Eqs. (31) and (32), will determine ψ_0 if the functions ψ_1, ψ_2, etc., are given. Thus ψ_0 is not an arbitrary parameter and is not at our disposal to be varied.

If now the potential energy of the molecules is written as a sum of the potentials between pairs,

$$U = \sum_{N\geq i>j\geq 1}\sum u(Rr_{ij}), \tag{42}$$

where

$$r_{ij} = [(\xi_i-\xi_j)^2 + (\eta_i-\eta_j)^2 + (\zeta_i-\zeta_j)^2]. \tag{43}$$

If we define

$$\varphi = 1/kT\Omega\int\int_\Omega\cdots\int F_2 u(Rr_{ij})d(i)d(j), \tag{44}$$

we find

$$\bar{u} = \tfrac{1}{2}\rho\varphi. \tag{45}$$

If one similarly defines

$$\varphi' = 1/3kT\Omega\int\int\cdots\int F_2 Rr_{ij} \times[du(Rr_{ij})/d(Rr_{ij})]d(i)d(j) = \omega(\partial\varphi/\partial\omega), \tag{46}$$

one has

$$\bar{u}' = \tfrac{1}{2}\rho\varphi'. \tag{47}$$

Now define

$$\sigma_\nu = 1/\Omega \int\int \cdots \int \psi_\nu F_\nu d(1) \cdots d(\nu). \tag{48}$$

The thermodynamic functions s defined by Eq. (19), p defined by Eq. (22), and a defined by Eq. (23) now become:

$$s = \psi_0/\bar{N} + \sigma_1 + \tfrac{1}{2}\rho\sigma_2 + \cdots + (1/\nu!)\rho^{\nu-1}\sigma_\nu, \tag{49}$$

$$p = 1 - \tfrac{1}{2}\rho\varphi', \tag{50}$$

$$a = -(\psi_0/\bar{N}) - \sigma_1 + \tfrac{1}{2}\rho(\varphi - \sigma_2) - \cdots - (1/\nu!)\rho^{\nu-1}\sigma_\nu - \ln\omega. \tag{51}$$

The chemical potential μ is given by

$$\mu/kT = a + p = 1 - (\psi_0/\bar{N}) - \sigma_1 + \tfrac{1}{2}\rho(\varphi - \sigma_2) - \cdots - (1/\nu!)\rho^{\nu-1}\sigma_\nu - \ln\omega. \tag{52}$$

In the open system the proper treatment of the minimization condition would be to maximize the pressure P subject to a fixed value of the chemical potential μ and a fixed temperature T. The operations can be carried out quite readily, but the result is exactly the same as the result of the previous section, namely, one obtains Eqs. (24) and (26′). The main object of introducing the open system in this section is merely that the evaluation of the functions F_n and the σ_ν's are sometimes much easier using Eq. (35) than with the equivalent expression for the closed system.

V. ONE OR LESS MOLECULES PER CELL

If no limitations are placed on the functions ψ_ν of the previous section, the minimization conditions result that $\psi_2 = u(Rr_{ij})/kT$ and that ψ_1 is a constant which can be shown to be the logarithm of the activity. One thus obtains the equilibrium distribution as a formal result, but the parameter ψ_0 cannot be evaluated when the temperature is low and the chemical potential μ is high, nor can the distribution functions be determined in any simple way from Eq. (35). By an artificial division of the coordinate space into cells and the imposition of arbitrary conditions on the functions ψ_ν such that they behave differently when coordinates of the molecules that enter these functions are in the same cell, in neighboring cells, or in distant cells, one makes it possible to evaluate ψ_0 from the normalization conditions, Eqs. (31) and (32), and to evaluate the distribution functions F_n from Eq. (35). The simplest assumption is that only the ψ_1's are permitted to vary in any significant way and the ψ_2's are arbitrarily assigned to have such values that no two molecules can be in the same cell, but that molecules in different cells are independent of each other. This can be expressed mathematically by writing

$$\left.\begin{aligned} &\psi_1(i) = -\ln(\rho/1-\rho) + \sum_{\alpha=1}^{\alpha=\Omega} \psi_{1\alpha}(i), \\ &\psi_{1\alpha}(i) = 0 \text{ if } (i) \text{ is not in cell } \alpha, \end{aligned}\right\} \tag{53}$$

where the space is divided into Ω contiguous nonoverlapping cells labeled by the running index α, each of unit volume in the dimensionless coordinate space. The constant, ρ, Eq. (53) is determined by an arbitrary normalization condition on $\psi_{1\alpha}$:

$$\int\int\int_{(i)\subset\alpha} [\exp -\psi_{1\alpha}(i)] d(i) = 1, \tag{54}$$

where the symbol $(i)\subset\alpha$ means that the integration is carried out over the unit volume of cell α. The numerical evaluation of Eq. (33) for the average number of molecules N in the system will show that ρ has the meaning of Eq. (37), namely, that it is the average number of molecules per cell.

The condition that no two molecules can be in the same cell is imposed by a condition on ψ_2, namely:

$$\left.\begin{aligned} &\psi_2(i,j) = \infty \text{ if } (i), (j) \text{ are in same cell,} \\ &\quad = 0 \text{ if } (i), (j) \text{ are not in same cell.} \end{aligned}\right\} \tag{55}$$

Using Eq. (31) with (53) and (54) in Eq. (40), one finds $w_{N,\Omega} = e^{-\psi_0}[\Omega!/(\Omega-N)!N!][\rho/(1-\rho)]^N$ for $N \leq \Omega$, and $w_{N,\Omega} = 0$ for $N > \Omega$. Put this in Eq. (32) that says the sum must be unity and one finds:

$$1 = e^{-\psi_0}[1/(1-\rho)]^\Omega.$$

This leads to

$$\psi_0/\bar{N} = -(1/\rho)\ln(1-\rho). \tag{56}$$

In a similar manner one finds from Eq. (33) that ρ has the meaning of the number density in the dimensionless space given by Eq. (37). Using Eq. (35) for the distribution functions, one finds

$$F_1(i) = \exp -\textstyle\sum_\alpha \psi_{1\alpha}(i), \tag{57}$$

$$F_2(i,j) = F_1(i)F_1(j)\exp -\psi_2(i,j). \tag{58}$$

Now ψ_2 is zero when molecules i and j are not in the same cell but infinity if they are. Equation (58) shows that F_2 goes to zero as the exponent of minus ψ_2 when the molecules are in the same cell. The integral of Eq. (48), which gives σ_2, is, therefore, zero. Since ψ_ν is zero for $\nu \geq 3$ one has $\sigma_\nu = 0$ for $\nu \geq 2$. The expression for the terms occurring in the entropy is then given by:

$$\sigma_2 = \sigma_3 = \sigma_\nu = 0, \quad \nu \geq 2, \tag{59}$$

$$\left.\begin{aligned} &\sigma_1 = -\ln[\rho/(1-\rho)] + \sigma, \\ &\sigma = \int\int\int_\alpha \psi_{1\alpha}(i)[\exp -\psi_{1\alpha}(i)] d(i), \end{aligned}\right\} \tag{60}$$

where again the integration is to be carried out only over the unit volume of a single cell.

The expressions for φ and φ' are

$$\varphi=\frac{1}{kT}\sum_{\beta\neq\alpha}\int\int\cdots\int_{(i)\subset\alpha,(j)\subset\beta}F_1(i)F_1(j)u(Rr_{i,j})d(i)d(j), \quad (61)$$

$$\varphi'=\frac{1}{3kT}\sum_{\beta\neq\alpha}\int\int\cdots\int_{(i)\subset\alpha,(j)\subset\beta}F_1(i)F_1(j)Rr_{ij}\frac{du(Rr_{ij})}{d(Rr_{ij})}\times d(i)d(j). \quad (62)$$

The expressions for the thermodynamic functions are then

$$\bar{u}=\bar{U}/\bar{N}kT=\tfrac{1}{2}\rho\varphi, \quad (63)$$

$$(S_\tau/\bar{N}k)=S+\ln\omega=-[(1-\rho)/\rho]\ln(1-\rho)-\ln\rho+\sigma+\ln\omega, \quad (64)$$

$$a=A_\tau/NkT=u-s-\ln\omega=[(1-\rho)/\rho]\ln(1-\rho)+\ln\rho-\ln\omega+\tfrac{1}{2}\rho\varphi-\sigma, \quad (65)$$

$$p=PV/NkT=1-\tfrac{1}{2}\rho\varphi', \quad (66)$$

$$\mu/kT=a+p=1+[(1-\rho)/\rho]\ln(1-\rho)+\ln\rho-\ln\omega+\tfrac{1}{2}\rho(\varphi-\varphi')-\sigma, \quad (67)$$

where

$$\left.\begin{aligned}\varphi&=\varphi(\omega,\beta),\\ \varphi'&=\omega(\delta\varphi/\delta\omega)_\beta,\\ \sigma&=\sigma(\beta),\end{aligned}\right\} \quad (68)$$

and β is used to symbolize any parameter which occurs in $\psi_{1\alpha}$. From Eq. (26′) one obtains

$$-(2/\rho)[1+(1/\rho)\ln(1-\rho)]=-(\varphi+\varphi')\cong 1+\tfrac{2}{3}\rho+\cdots, \quad (69)$$

where the last expression indicates the form for small values of ρ. Equation (69) is an implicit equation determining the size of the cells in the ordinary metric coordinate system. For a given value of R where the cell volume is $\omega=R^3$ one may compute φ and φ'. The value of ρ, the number of particles per unit cell, is then determined by Eq. (69). In practice not all values of R lead to physically significant (i.e., positive real) values of ρ. This will be discussed in more detail later.

If β_μ is used to indicate any parameter which occurs in $\psi_{1\alpha}$, the minimization condition Eq. (24) leads to

$$\delta\sigma/\delta\beta_\mu=\tfrac{1}{2}\rho\delta\varphi/\delta\beta_\mu, \quad (70)$$

which is an implicit equation for determining the parameter β_μ.

VI. THE LIMIT OF ZERO DENSITY

At high values of the concentration c of molecules in the system, these equations lead to values of ρ which are practically unity. In this case the equations do not result in values of the thermodynamic functions which are significantly different from those obtained by the limitation that the number of cells of the system shall be equal to the number of molecules. However, the usual cell method in which the number of cells equals the number of molecules does not lead to good results at the critical density and leads to a completely wrong deviation from the perfect gas law in the limit of zero density. With these equations, however, the deviation from the perfect gas law is found to be proportional to the density, as it should be, and the coefficient obtained is a reasonable approximation to the second virial coefficient. In Eq. (69) the quantity $\varphi+\varphi'$ is $(\partial/\partial\omega)_\beta(\omega\varphi)$. The quantity φ as a function of $R=\omega^{\frac{1}{3}}$ is essentially proportional to the interaction potential of two molecules at a distance apart of about R. It is, of course, exactly an average potential on a single molecule in one cell of volume ω due to the other molecules in the surrounding cells. It therefore has a sharp minimum at about the equilibrium distance, and $\omega\varphi$ also has a minimum at a slightly greater distance. The derivative $(\partial/\partial\omega)(\omega\varphi)$ is negative for values of ω smaller than the minimum and decreases to zero at the minimum. Equation (69) does not have a positive solution for ρ unless the value of the negative derivative exceeds unity. The largest cell size which one obtains is therefore smaller than that for which there is a minimum in $\omega\varphi$, and remains finite even in the limit of zero density. The value of $-\frac{1}{2}\varphi'$ at this limiting cell size is seen, from Eq. (66), to be the coefficient of ρ in the first deviation from the perfect gas law. This quantity, $-\frac{1}{2}\varphi'$, given by Eq. (62) has the correct form for the second virial coefficient except that the distribution function F_2 which enters Eq. (62) as the product of the functions in different cells is not the correct form of the limiting distribution function. It is, however, not an impossibly bad approximation to it. The fact that the cell method as employed here leads to a reasonably good expression for the first deviation from the perfect gas law encourages one to believe that it should offer a considerable improvement in the neighborhood of the critical point over methods leading one to a single molecule per cell.

VII. THE DETERMINATION OF THE CELL SIZE

It was remarked earlier in the paper that the introduction of a variable cell size hardly complicates the mathematics of the problem. It will be shown in this section that if complete calculations have been performed using one molecule per cell in a consistent manner, transition to a smaller number of molecules per cell can be made without any actual recomputation but only by a reinterpretation of the values of temperatures and concentration c to which the calculations apply. The equations of Section V apply to one molecule per cell if Eq. (69) is omitted and ρ is set arbitrarily equal to unity in all the other equations. Now suppose we have tabulated values of

$$\bar{u}^*=\bar{U}/\bar{N}kT^*,$$
$$s^*=S_\tau/\bar{N}k-\ln\omega,$$
$$p^*=(PV/\bar{N}kT^*),$$

calculated with $\rho \equiv 1$ for which case the concentration, $c^* = 1/\omega$. The parameters β that determine $\psi_{1\alpha}$ are assumed to have been determined by Eq. (70), with ρ set equal to unity. Since φ is explicitly proportional to $1/T^*$ the same Eq. (70) would have lead to exactly the same solutions for β if used with $\rho \neq 1$ but with $\rho/T = 1/T^*$,

$$T = \rho T^*. \tag{71}$$

So had we been following the Section V with a variable ρ and computing at the temperature T given by Eq. (71) we would have computed the same values of the parameters, and hence of $\varphi = 2u^*$, $\varphi' = 2(1-p^*)$ at this value of ω. We would then use Eq. (69), which we can now write as

$$-[1+(1/\rho)\ln(1-\rho)] = -[\bar{u}^* + 1 - p^*] \tag{72}$$

to determine ρ. The concentration c to which this computation applies is then

$$c = \rho/\omega = \rho c^*. \tag{73}$$

We would then have computed

$$\bar{u} = \bar{u}^*, \tag{74}$$

$$p = p^*, \tag{75}$$

but would have interpreted them to have applied at temperature T and concentration c given by Eqs. (71) and (73), respectively.

The value of σ, Eq. (60), will be the same as the values computed with one molecule per cell. We must, however, correct the equation for the entropy S_r^* obtained in the calculation with exactly one molecule per cell by adding the terms due to ρ,

$$s = s^* - [(1-\rho)/\rho]\ln(1-\rho) - \ln\rho, \tag{76}$$

which occur in Eq. (64).

Thus if we have computed the thermodynamic functions marked with asterisks on the assumption that there is exactly one cell for every molecule, we can improve the calculations by using Eq. (72) to determine a value of ρ, $\rho < 1$, and using Eqs. (71) and (72) to compute new temperatures and concentrations to which the tabulated values apply, retaining the tabled values for $\bar{u}^*$ and p^*, and correcting the entropy by Eq. (76). Since the new values necessarily decrease the Helmholtz free energy at any given temperature and concentration, they represent an improvement over the old values.

VIII. THE KIRKWOOD INTEGRAL EQUATION

We have spoken as though the function $\psi_{1\alpha}(i)$ were determined by a number of parameters, the β's, whose numerical values are determined by Eq. (70). If the function $\psi_{1\alpha}$ is left entirely arbitrary, one obtains an integral equation for this function. An arbitrary $\psi_{1\alpha}$ amounts to leaving an infinite continuum of parameters β which are the values of the function at all values of the coordinate (i). The integral equation which one obtains is essentially that given by Kirkwood[7] and differs from it only in that ρ/kT replaces $1/kT$. The equation is

$$\ln\psi_{1\alpha}(\mathbf{r}_{\alpha i}) = \psi + (\rho/kT)\sum_{\beta}{}' \int\int\int_{\beta} u(Rr_{ij}) \times \exp -\psi_{1\beta}(\mathbf{r}_{\beta j})\, d(j). \tag{77}$$

In this equation the prime on the summation indicates that the sum goes over all cells β except $\beta = \alpha$. The coordinate $\mathbf{r}_{\alpha i}$ is the vector position of particle i measured from the center of cell α, and $\mathbf{r}_{\beta j}$ is the vector position j measured from the center of cell β. The coordinate r_{ij} is the magnitude of the dimensionless distance from particle i to particle j. The constant ψ in Eq. (77) must be determined by the normalization condition, Eq. (54).

Although the exact solution of Eq. (77) would give the best function $\psi_{1\alpha}$ and, therefore, the lowest possible free energy consistent with the assumption of cells containing no more than one particle, and with no correlation between the occupancy of the different cells, it is still doubtful whether a simple assumption of a specified analytical form for $\psi_{1\alpha}$ might not be a more economical method of obtaining a solution to the problem. An approximate solution to Eq. (77) is easy to find. The simplest approximate solution is obtained by putting a δ-function for $\psi_{1\beta}$ under the integral, the δ-function corresponding to the assumption that the particles in the cells surrounding α are all at the cell centers. This approximation leads to the Lennard-Jones and Devonshire equation, as remarked by Kirkwood.[7] However, an exact solution of Eq. (77) would be tedious to obtain, especially so since one must obtain solutions for all values of ρ/kT and for all values of the distance between cell centers. By using a limited analytical form for $\psi_{1\alpha}$ one may obtained the best solution consistent with this analytical form with a more reasonable amount of computation. Such a best solution for a simple analytical form may be better than the first approximation to Eq. (77). It at least has the advantages over an only approximate solution of Eq. (77) that the thermodynamic pressure and mechanical pressure preserve their equality.

IX. GAUSSIAN DISTRIBUTION

The simplest assumption one could make regarding $\psi_{1\alpha}$ would be to assume it to be absolutely constant within the cell volume and therefore equal to unity, in view of the normalization of Eq. (54) and the fact that the cell volume has been chosen to be unity. This assumption does not lead to particularly simple equations since the energy integral is still reasonably complicated. In addition, the assumption is very poor since it permits zero distance approach with high probability density between two molecules.

Another obvious assumption to use for $\psi_{1\alpha}$ would be that it is constant in a spherical volume less than the

volume of the cell around the cell center. The edges of the cell would thus always be empty, and the closest approach between two molecules would be greater than zero. This assumption does not appear to lead to any simpler equations than the assumption of a Gaussian distribution within the cell.

A Gaussian distribution is obtained by writing

$$F_{1c}(r)=(\beta/2^{1/6}\pi^{\frac{1}{2}})^3\exp-(\beta/2^{1/6})^2r^2, \tag{78}$$

where $F_{1c}(r)$ is the part of F_1 defined within one cell, and r is the radial distance of the particle position from the cell center.

The cell volume has been chosen to be unity so that if the cell is assumed to be spherical the maximum value r_m of r, is given by $r_m=(3/4\pi)^{\frac{1}{3}}$. If the value of β is such that $(\beta 2^{-1/6}r_m)^2=\beta^2 2^{-5/3}(3/\pi)^{\frac{2}{3}}$ is considerably greater than unity, then F_{1c} will be essentially zero at the edges of the cell and we can safely integrate the value of r to infinity instead of limiting ourselves to the exact value of the cell volume. If $\beta^2=20$ then $(\beta 2^{-1/6}r_m)^2=5$ and $F_{1c}\cong 10^{-2}$ at the cell edges. We shall carry out the subsequent algebra under the assumption that our result gives $\beta^2\geq 20$, and reject the answer if β^2 is less than 20. The factor in front of the exponential of (78) has been so chosen that,

$$\int_0^\infty 4\pi r^2 F_{1c}(r)dr=1. \tag{79}$$

In order to compute the energy integral φ it is convenient to introduce a function $P(r)$,

$$P(r)=(\beta/2^{\frac{1}{2}}\pi^{\frac{1}{2}})^3\exp-(\beta/2^{\frac{1}{2}})^2r^2, \tag{80}$$

such that $4\pi r^2P(r)dr$ is the probability that for two molecules (in different cells) the magnitude of the vector sum of their displacements from the cell center lies between r and $r+dr$. The function $P(r)$ is also normalized so that

$$\int_0^\infty 4\pi r^2P(r)dr=1. \tag{81}$$

We neglect the interactions of molecule pairs in cells more distant than nearest neighbors. The energy integral φ is then given by

$$\varphi=\frac{12}{kT}\int\int\int_{r_{ij}=2^{1/6}} P(r_{ik})u(Rr_{kj})d(k)$$

$$=\frac{24\pi}{kT2^{1/6}}\int_0^\infty yP(y)\left[\int_{|2^{1/6}-y|}^{|2^{1/6}+y|} zu(Rz)dz\right]dy. \tag{82}$$

The parameter R is the scale parameter of dimensions of length, Eq. (11), so chosen that the cell volume shall be unity in the dimensionless coordinate system. For a close-packed lattice having one particle per unit volume the distance between neighboring lattice points is $2^{1/6}$. The potential function $u(Rr)$ will have minimum at some value, $Rr=R_e$, so that R_e is the equilibrium distance between a pair of molecules. We introduce as a parameter,

$$x=2^{1/6}R/R_e, \tag{83}$$

so that x is the ratio of the distance between neighboring lattice points to the equilibrium distance between a molecule pair. When $x=1$ and $\beta\to\infty$, the lattice is at the position of minimum energy.

The most obvious potential energy function to choose would be the Lennard-Jones function with a R^{-6} attractive part and a R^{-12} repulsive term. This function introduces difficulties in the integration of Eq. (82) because we have not chosen a distribution function that goes identically to zero at the cell boundary. Since the repulsion of the Lennard-Jones potential equation is violently infinite at zero distance, the integral diverges. For this reason it is more convenient to use, in these calculations, a Morse-type potential function which does not become infinite at zero approach. The Morse function probably represents the repulsive part of the potential near equilibrium rather better than the Lennard-Jones function and does not deviate from the latter very much in the attractive region. If one choses

$$u(Rr)=u_0[\{\exp-12[r(x/2^{1/6})-1]\}$$
$$-2\{\exp-6[r(x/2^{1/6})-1]\}], \tag{84}$$

one has a potential function given by a Morse equation having a minimum $-u_0$ at the distance R_e and having the same curvature at the bottom as a Lennard-Jones function. With this function the integration of Eq. (82) can be performed. The result contains terms which can be expressed analytically and terms which can be expressed in terms of the Gaussian integral from some value of the parameter to infinity. These latter terms are small when β is sufficiently large. The error made in omitting them is of the same order as the error made in choosing the normalization condition of Eq. (79) instead of the integral over the cell volume only. If these small terms are omitted one finds:

$$\varphi=(12u_0/kT)\{[1-(12x/\beta^2)]\exp[72(x/\beta)^2-12x+12]$$
$$-2[1-(6x/\beta^2)]\exp[18(x/\beta)^2-6x+6]\}. \tag{85}$$

Introduce a reduced temperature,

$$\tau=kT/u_0, \tag{86}$$

and the volume v_0, when $\rho=1$, $x=1$, which is the volume per molecule of the (classical) crystal at absolute zero,

$$v_0\equiv 2^{-\frac{1}{2}}R_e^3. \tag{87}$$

Our volume, $\omega=R^3$, of the cells is then, from (83),

$$\omega=x^3v_0, \tag{88}$$

and the volume per molecule, v, is

$$v=\omega/\rho=x^3v_0/\rho. \tag{89}$$

We also simplify the equations somewhat by introducing

$$y=6/\beta^2, \tag{90}$$

$$d\ \ln y/d\ \ln\beta=-2. \tag{91}$$

The quantity σ, defined by Eq. (60), is obtained by using $F_{1c}(r)$ of (78) as $\exp-\psi_{1\alpha}(i)$ in (60), and is found to be

$$\begin{aligned}\sigma&=(3/2)+2\ \ln 2+(3/2)\ln\pi-3\ \ln\beta\\&=(3/2)+(1/2)\ln 2+(3/2)\ln(\pi/3)+(3/2)\ln y\\&=\tfrac{1}{2}\ \ln 2(\pi e y/3)^3=1\cdot 915\ 75+(3/2)\ln y.\end{aligned} \tag{92}$$

The equations for determining x and y are to be taken from (69) and (70) with $(\partial/\partial\ \ln v)=(1/3)(\partial/\partial\ \ln x)$, becoming

$$-[\varphi+(1/3)(\partial\varphi/\partial\ \ln x)_\beta]=-(2/\rho)[1+(1/\rho)\ln(1-\rho)], \tag{93}$$

$$(\partial\varphi/\partial\ \ln y)_x=(2/\rho)(d\sigma/d\ \ln y)=3/\rho. \tag{94}$$

If one writes:

$$\begin{aligned}\psi&=x^3\tau\varphi,\\\psi_x&=-(\partial x^3\tau\varphi/\partial\ \ln x)_y,\\\psi_y&=(\partial x^3\tau\varphi/\partial\ \ln y)_x,\end{aligned} \tag{95}$$

then

$$\psi_x=-(6x^3\tau/\rho)[1+(1/\rho)\ln(1-\rho)], \tag{96}$$

$$\psi_y=3x^3\tau/\rho=3(v/v_0)\tau. \tag{97}$$

If

$$\begin{aligned}F(x,y)&=x^3(1-xy)\exp 3(x^2y-2x),\\f_x(x,y)&=-(\partial\ \ln F/\partial\ \ln x)_y\\&=6x(1-xy)-3+[xy/(1-xy)],\\f_y(xy)&=(\partial\ \ln F/\partial\ \ln y)_x\\&=3x^2y-xy/(1-xy),\end{aligned} \tag{98}$$

then from Eq. (85) for φ with the substitution of y in place of β given by (90) one has

$$\begin{aligned}\psi&=(3e^{12}/2)F(2x,y)-24e^6F(x,y),\\\psi_x&=(3e^{12}/2)f_x(2x,y)F(2x,y)-24e^6f_x(x,y)F(x,y),\\\psi_y&=(3e^{12}/2)f_y(2x,y)F(2x,y)-24e^6f_y(x,y)F(x,y).\end{aligned} \tag{99}$$

At any value of the variables x, y, and in terms of the minimum $-u_0$ of the potential energy between a pair of molecules, and the volume v_0 per molecule of the crystal at absolute zero, (which occurs at $v_0=2^{-\frac{1}{2}}R_e^3$ with R_e the equilibrium distance between pairs) one may compute the thermodynamic functions of the system with the use of the quantities defined by Eqs. (98) and (99). The subsidiary parameter ρ is the average number of particles per unit cell of volume $\omega=2^{-\frac{1}{2}}(xR_e)^3$ which occurs in the theory. The equations are:

$$-(1/\rho)\ln(1-\rho)=1+(\psi_x/2\psi_y), \tag{100}$$

$$V/\bar{N}v_0=v/v_0=x^3/\rho, \tag{101}$$

$$kT/u_0=\tau=\rho\psi_y/3x^3, \tag{102}$$

$$\bar{U}/\bar{N}kT=\bar{u}=3\psi/2\psi_y, \tag{103}$$

$$\bar{U}/\bar{N}u_0=\bar{u}\tau=\rho\psi/2x^3 \tag{104}$$

$$S_\tau/\bar{N}k=[1-\rho][1+(\psi_x/2\psi_y)]+\tfrac{1}{2}\ \ln 2(\pi e y/3)^3+\ln v, \tag{105}$$

$$A_\tau/\bar{N}kT=a=(3\psi/2\psi_y)-[1-\rho][1+(\psi_x/2\psi_y)]-\tfrac{1}{2}\ \ln 2(\pi e y/3)^3-\ln v, \tag{106}$$

$$Pv/kT=p=1+(3\psi/2\psi_y)+(\psi_x/2\psi_y), \tag{107}$$

$$Pv_0/u_0=\tfrac{1}{2}(\rho/x^3)^2[\psi+\tfrac{2}{3}\psi_y+\tfrac{1}{3}\psi_x], \tag{108}$$

$$\mu_\tau/kT=a+p=(3\psi/\psi_y)+\rho[1+(\psi_x/2\psi_y)]-\tfrac{1}{2}\ \ln 2(\pi e y/3)^3-\ln v. \tag{109}$$

These follow from the use of Eqs. (63) to (70) inclusive, with (25), (46), (88), and (95).

For a perfect gas the quantity $S_\tau/\bar{N}k$, which is defined by Eq. (3) as the integral of $-N^{-1}W\ \ln WN!$ over the configuration space of volume V^N, is obtained by setting the probability density function W equal to the constant V^{-N}, and therefore is:

$$(S_\tau/\bar{N}k)_{\text{perfect gas}}=1+\ln v. \tag{110}$$

The negative quantity:

$$\Delta S/\bar{N}k=(1/\bar{N}k)[S_\tau-S_\tau\ (\text{perfect gas, same } v)], \tag{111}$$

is the amount by which the entropy of the system differs from that of a perfect gas at the same density.

One sometimes defines a free volume v_f per molecule, by the equation:

$$S_\tau/\bar{N}k=1+\ln v_f. \tag{112}$$

From (110), (111), and (112), one finds,

$$\ln(v_f/v)=\Delta S/\bar{N}k, \tag{113}$$

so that one may describe $\Delta S/\bar{N}k$ as giving the natural logarithm of the ratio of free volume to volume per molecule. From (105), (110), and (111),

$$\begin{aligned}-\Delta S/\bar{N}k&=1-\tfrac{1}{2}\ \ln 2(\pi e y/3)^3-(1-\rho)[1+(\psi_x/2\psi_y)]\\&=-0\cdot 915\ 75-(1-\rho)[1+(\psi_x/2\psi_y)+\tfrac{3}{2}\ \ln y].\end{aligned} \tag{114}$$

The value of μ_τ/kT for a perfect gas is

$$(\mu_\tau/kT)_{\text{perfect gas}}=-\ln v_g. \tag{115}$$

The fugacity f of a system is kT/v_g with v_g the volume per molecule of the perfect gas given by (115), and μ_τ the chemical potential contribution from configuration space for the system, so that

$$fv_0/kT=\exp[(\mu_\tau/kT)+\ln v_0]. \tag{116}$$

One may use,

$$(\mu_\tau/kT)+\ln v_0=(\bar{U}/NkT)-(\Delta S/\bar{N}k)-[1-(Pv/kT)]-\ln(v/v_0), \tag{117}$$

as an easy means of computation.

At low temperatures, for which the vapor in equilibrium with the condensed phase is at low pressure,

and hence is nearly a perfect gas, f is the vapor pressure. The pressure of the condensed phase which is in equilibrium with its own vapor will be given when fv_0/kT given by (110) and Pv_0/kT given by $(v_0/v)p$ from (107) are equal. At higher temperatures and vapor pressures, for which the vapor is far from perfect, two phases will be in equilibrium at two different values of (v/v_0) but the same T when both (108) and (110) lead to identical values of P and f for the two different volumes.

X. NUMERICAL RESULTS

Choosing values of x and y one may readily use Eqs. (98) to (102) to find $\tau=kT/u_0$ and v/v_0. The range of these variables which is experimentally interesting occurs with $1.04\leq x\leq 1.28$ and $0.03\leq xy=z\leq 0.19$, the larger values of z occurring only at the larger values of x, and the smaller z values at the smaller x's. The more important thermodynamic functions are tabulated in Table I for x and $z=xy$ in intervals of 0.01 unit in this range.

The largest value of y that occurs is at $x=1.28$, $z=0.19$, or $y=z/x=0.1485$, so that $\beta^2=6/y=40.4$. The Gaussian distribution function, $F_{1c}(r)$, of Eq. (78) has then been reduced at the cell boundary, $r=r_m=(3/4\pi)^{\frac{1}{3}}$, by the factor $\exp-12.3=0.5\times10^{-5}$ times the value at the center. This is adequate *a posteriori* justification for carrying out the integrations to infinity instead of strictly to the cell boundaries.

The various thermodynamic quantities computed at the x and z values listed in Table I have been plotted on large scale graphs so that values of any of them at prescribed values of one of them may be read. The graphical interpolations are over rather large intervals, but when a few points were checked by using two alternative sets of three points to make quadratic analytical interpolations it was always found that the graphical values, and both analytical values, checked within better than two percent. By such graphical means the values for the subsequent tables were obtained.

Argon was chosen for most of the experimental comparisons. Hirschfelder[10] and co-workers have used gaseous viscosity data to obtain:

$$u_0/k=124.0^\circ\text{K},$$
$$v_0N_0=24.05\ \text{cm}^3/\text{mole},$$
$$P=423\ \text{atmos}\times(Pv_0/u_0),$$

for argon.

Table II gives the experimental and computed liquid volumes for the liquid in equilibrium with its own vapor. Table III gives critical data, and Table IV the vapor pressures. Actually the recorded "theoretical" values of Table IV are the fugacities, which are higher than the vapor pressures when the temperature and pressures are high. The experimental values of Table IV are true vapor pressures.

[10] Hirschfelder, Curtiss, Bird, and Spotz, University of Wisconsin Naval Research Laboratory and Department of Chemistry Report CF-1505, 13 March 1951.

TABLE I. Volume, temperature, pressure, and entropy, calculated at various x and $z=xy$ values. v_0 is volume of crystal at 0°K, u_0 is minimum of the pair potential. ρ is the average number of molecules per cell.

x	z	ρ	v/v_0	kT/u_0	Pv/kT	$-\Delta S/Nk$
1.22	0.13	0.5397	3.365	0.659	−0.49605	1.78097
1.23	0.14	0.5756	3.233	0.799	−0.09202	1.71251
1.24	0.15	0.5972	3.192	0.936	+0.2298	1.63949
1.25	0.16	0.6098	3.203	1.074	+0.4880	1.56562
1.26	0.17	0.6169	3.242	1.215	+0.6954	1.49300
1.27	0.18	0.6195	3.307	1.360	+0.8630	1.42144
1.28	0.19	0.6191	3.388	1.509	+0.99910	1.35171
1.19	0.11	0.6186	2.724	0.662	−1.0152	2.06162
1.20	0.12	0.6439	2.683	0.790	−0.4911	1.96690
1.21	0.13	0.6589	2.689	0.919	−0.07932	1.87374
1.22	0.14	0.6670	2.722	1.052	+0.24852	1.78282
1.23	0.15	0.6703	2.776	1.189	+0.51028	1.69486
1.24	0.16	0.6701	2.845	1.330	+0.7204	1.61005
1.25	0.17	0.6670	2.928	1.476	+0.8893	1.52802
1.26	0.18	0.6621	3.021	1.626	+1.0260	1.44942
1.17	0.10	0.7341	2.181	0.786	−0.9895	2.29376
1.18	0.11	0.7372	2.229	0.907	−0.4568	2.16701
1.19	0.12	0.7369	2.287	1.033	−0.0389	2.04890
1.20	0.13	0.7339	2.354	1.166	+0.29087	1.94014
1.21	0.14	0.7287	2.431	1.303	+0.55313	1.83361
1.22	0.15	0.7216	2.516	1.445	+0.76206	1.73472
1.23	0.16	0.7142	2.605	1.594	+0.93042	1.64243
1.24	0.17	0.7058	2.701	1.750	+1.0666	1.55509
1.25	0.18	0.6959	2.806	1.909	+1.1753	1.47112
1.16	0.10	0.8230	1.896	1.017	−0.3155	2.38838
1.17	0.11	0.8060	1.987	1.135	+0.0356	2.23585
1.18	0.12	0.7953	2.066	1.271	+0.3630	2.10463
1.19	0.13	0.7840	2.150	1.413	+0.6204	1.98333
1.20	0.14	0.7722	2.238	1.561	+0.82751	1.87013
1.21	0.15	0.7609	2.328	1.717	+0.99203	1.76630
1.22	0.16	0.7486	2.425	1.877	+1.12360	1.66775
1.13	0.08	0.8963	1.610	0.944	−0.8005	2.79415
1.14	0.09	0.8804	1.683	1.079	−0.2600	2.60436
1.15	0.10	0.8646	1.759	1.218	+0.1512	2.43457
1.16	0.11	0.8497	1.837	1.364	+0.4715	2.28257
1.17	0.12	0.8349	1.918	1.516	+0.7216	2.14408
1.18	0.13	0.8200	2.004	1.673	+0.9191	2.01649
1.19	0.14	0.8050	2.093	1.835	+1.0758	2.00926
1.20	0.15	0.7905	2.186	2.005	+1.2003	1.78936
1.21	0.16	0.7750	2.286	2.177	+1.2995	1.68571
1.10	0.06	0.96000	1.387	0.825	−1.3396	3.31316
1.11	0.07	0.94160	1.452	0.970	−0.6064	3.06088
1.12	0.08	0.9283	1.513	1.125	−0.0745	2.83915
1.13	0.09	0.9122	1.582	1.281	+0.3229	2.64551
1.14	0.10	0.8957	1.654	1.441	+0.6260	2.46959
1.15	0.11	0.8789	1.730	1.605	+0.8604	2.31380
1.08	0.05	0.98588	1.277	0.799	−1.0392	3.63226
1.09	0.06	0.97480	1.328	0.968	−0.3106	3.33825
1.10	0.07	0.96200	1.383	1.141	+0.1969	3.09684
1.06	0.04	0.99684	1.195	0.734	−0.5489	3.98171
1.07	0.05	0.99148	1.236	0.927	+0.1396	3.63839
1.08	0.06	0.98308	1.281	1.100	+0.5908	3.34943
1.04	0.03	0.99973	1.125	0.630	+0.3058	4.40071
1.05	0.04	0.99817	1.160	0.848	+0.8499	3.97415

The columns headed "experimental" are computed from the values in the *Handbook of Chemistry and Physics*.[11] The columns headed "computed, this paper"

[11] *Handbook of Chemistry and Physics* (Chemical Rubber Publishing Company), thirtieth edition.

TABLE II. Experimental and computed volumes of the liquid which is in equilibrium with its own vapor. The experimental values are for argon. The symbol v_0 is for the volume of the crystal at 0°K, and u_0 is for the minimum of the pair potential.

Temperature		Volume, v/v_0			
		Experimental	Computed		
T°K	kT/u_0		This paper	$\rho\equiv1$	Hirschfelder
90	0.7260	1.209	1.159	1.159	1.05
111	0.9026	1.357	1.224	1.213	1.11
122	0.9871	1.459	1.259	1.235	1.17

refer to computations made from Eqs. (98) to (109). The column heading "$\rho\equiv1$" refers to computations made by assuming strictly one molecule per cell, and minimizing the free energy only with respect to the parameter β (or $y=6/\beta^2$). The values in this column, $\rho\equiv1$, of Table III for the critical data, required extrapolation beyond the computed points and are given to correspondingly fewer significant figures. The values in the columns headed "Hirschfelder" are from the Wisconsin laboratory report[10] which will appear shortly in book form. These values have been computed using the Lennard-Jones and Devonshire type of computation, with one molecule per cell, and with a Lennard-Jones potential, $-A/R^6+B/R^{12}$.

Table V summarizes the results of the calculations for intervals of 0.05 of kT/u_0 in the range of temperatures for which the liquid exists.

XI. DISCUSSION

The comparison of the numerical results obtained here with those of a typical Lennard-Jones and Devonshire type of computation, such as that of Hirschfelder and co-workers, is made difficult by the several differences between the methods. The characteristics of our computations may be listed by five items: (1) A Morse function, Eq. (84), was used for the interaction between molecule pairs. (2) The distribution of molecules within cells was assumed to be Gaussian, Eq. (78), described by one parameter β (or $y=6/\beta^2$), which was determined by minimizing the free energy. (3) The potential of interaction of the system was computed by assuming that pairs of molecules in cells more distant than nearest neighbors did not contribute. (4) The potential energy of the system was computed by using the correct distribution of the distances between two neighboring molecules, and not by assuming that only one of the molecules, and not its neighbor, was displaced from the cell center. (5) The number of cells, and hence the distance apart of their centers, was variable and determined by minimizing the free energy.

It is our opinion that the Morse curve does not differ enough from the $(A/R^{12})-(B/R^6)$ potential used by Hirschfelder to account for significant differences in the results. Similarly, we believe that the Gaussian distribution is adequately close to that given by a solution of the Kirkwood integral equation, and that this is not responsible for significant numerical differences. This point will be further discussed in a succeeding paper by one of us.

The inclusion of the interactions between molecules in cells more distant than neighbors could have been included in the present computations at the cost of some additional labor. The effect of the inclusion would be to lower the internal energy, particularly at low temperatures and volumes, without greatly affecting the other quantities. This would have improved the results. The change would be significant, but in no way adequate to make the agreement with experiment good. Item 3 above is then a logical neglect in our computations, owing to laziness, which leaves the results poorer by a significant, but probably not very appreciable, amount.

The main difference between our method and that used by Hirschfelder then lies in items 4 and 5, namely, the difference in the method of computation of the average potential energy and the use of adjustable cell size. In order to get some indication of the relative numerical importance of these two items, the computations listed under $\rho\equiv1$ have been carried out using exactly one cell per molecule.

TABLE III. Experimental and computed critical data; v_0 = volume of crystal at 0°K, and u_0 = minimum of pair potential.

Gas	Force constants from viscosity data		$\frac{kT_c}{u_0}$	$\frac{v_c}{v_0}$	$\frac{pv_0}{u_0}$	$\frac{pv_c}{kT}$
	u_0/k	v_0 Å				
N_2	91.46	3.680	1.38	3.00	0.134	0.292
A	124.0	3.418	1.22	3.13	0.133	0.291
Ne	35.7	2.80	1.24	3.15	0.117	0.296
Computed, this paper			1.42	2.320	0.414	0.676
Computed, $\rho\equiv1$			2.0	2.1	1.4	0.7
Computed, Hirschfelder			1.30	1.768	0.434	0.591

The energy in the usual cell method is computed by placing all molecules but one at the lattice sites of the cell centers and computing first a distribution and then an energy with this distribution of the one molecule. The distribution of a single molecule is given by the Gaussian of Eq. (78), whereas that of the vector sum of the displacements of two molecules is given by (80). The Gaussian of Eq. (80) differs from that of (78) only by the replacement of β in (80) by $2^{\frac{1}{2}}\beta$ in (78) or by $y=6/\beta^2$ in (80) by $y/2$ in (78). The equivalent of the usual method would be for us to use (78) to replace (80) in computing φ of Eq. (82), which would mean the replacement of y by $y/2$ in the energy expression. The change due to this is not inconsiderable.

The value of $\bar{U}/\bar{N}u_0$ is -6 at $T=0$, which corresponds to $x=1$, $y=0$. At the boiling point, $kT/u_0=0.7056$, the value we compute for $\bar{U}/\bar{N}u_0$ is -4.8. The potential energy per molecule has risen $1.2u_0$ above the value at 0°K. If computed with $\frac{1}{2}y$ one finds this value approximately halved, or the potential energy $0.6u_0=0.9kT$ lower than our computations. This leads to a corresponding reduction in free energy.

In terms of the method proposed here, namely the self-consistent computation of the thermodynamic properties of a fictitious nonequilibrium ensemble, the usual cell method computation is incorrect. However, since it leads to lower energy and higher entropy than the self-consistent computation it leads to a better result. The difference is obvious in the comparison of the columns marked "$\rho\equiv 1$" and "Hirschfelder" in Table III, which difference is primarily due to the difference in computing potential energies.

The difference between the values headed "this paper" and those headed "$\rho\equiv 1$" is purely the difference of item 5, the introduction of a variable cell volume determined by minimizing the free energy.

The computations made with $\rho\equiv 1$ have, for given x and $z=xy$, the same value of Pv/kT and $\bar{U}/\bar{N}kT$, as those made with Eqs. (98) to (109). For given x, y, however, we now find $v/v_0=x^3$ instead of $v/v_0=x^3/\rho$, and $kT/u_0=\psi_y/3x^3$ instead of $\rho\psi_y/3x^3$. The value of $S_\tau/\bar{N}k$ is now $(S_\tau/\bar{N}k)_{\rho=1}=\frac{1}{2}\ln 2(\pi ey/3)^3+\ln v$, and this is less than the result with adjusted ρ, Eq. (105), by the omission of

$$-[(1-\rho)/\rho]\ln(1-\rho)=(1-\rho)[1+(\psi_x/2\psi_y)],$$

and by the change in $\ln v$. The negative quantity $\Delta S/\bar{N}k$, the amount by which the entropy of the system differs from that of a perfect gas of the same volume as the system, Eqs. (111) and (114), is now, with $\rho\equiv 1$, more negative by the omission of the positive term $-[(1-\rho)/\rho]\ln(1-\rho)$ only.

This term, $-[(1-\rho)/\rho]\ln(1-\rho)$, may be identified with the much discussed communal entropy of the cell theory. It varies from zero in value, at low temperature and high density, when $\rho\to 1$, to unity for low densities when $\rho\to 0$. It arises from the number of ways in which the N molecules can be distributed among the $\Omega=N/\rho$ cells. It enters, however, in a physiological manner in the derivation, and not as an *ad hoc* quantity. It should be noted, however, that the entropies with ρ adjusted, and $\rho\equiv 1$, at given volume and temperature, do not differ by only this term, since for given volume and temperature both x and y will be different if ρ is adjusted than if ρ is held fixed at unity.

TABLE IV. Experimental (argon) and computed vapor pressure of liquid; v_0 is volume of crystal at 0°K, and u_0 is minimum of pair potential.

Temperature		Vapor pressure Experimental		Computed[a] Pv_0/u_0	
T°K	kT/u_0	Atmos	Pv_0/u_0	This paper	$\rho\equiv 1$
87.50	0.7056	1.000	0.00236	0.017	0.017
111.93	0.9027	7.433	0.01757	0.096	0.097
122.59	0.9886	13.707	0.03239	0.180	0.19
132.36	1.0674	22.185	0.05243	0.317	0.33
143.33	1.1559	35.846	0.08472		

[a] Computed values are fugacities.

TABLE V. Computed quantities. Values of Pv_0/u_0, v/v_0, $-\Delta S/\bar{N}k$, $-U/\bar{N}u_0$, at various values of kT/u_0 along line for which $Pv_0/u_0=fv_0/u_0$ (approximately the vapor pressure curve) and values of v/v_0 at various Pv_0/u_0 values: v_0 = volume of crystal at 0°K, u_0 = minimum of pair potential.

On line $Pv_0/u_0=fv_0/u_0$					v/v_0				
$\frac{kT}{u_0}$	$\frac{Pv_0}{u_0}$	$\frac{v}{v_0}$	$-\frac{\Delta S}{\bar{N}k}$	$-\frac{U}{\bar{N}u_0}$	$\frac{Pv_0}{u_0}$ =0.0	$\frac{Pv_0}{u_0}$ =0.1	$\frac{Pv_0}{u_0}$ =0.2	$\frac{Pv_0}{u_0}$ =0.3	$\frac{Pv_0}{u_0}$ =0.4
0.65	0.010	1.140	4.288	4.900	1.140	1.133	1.128	1.123	1.118
0.70	0.017	1.152	4.163	4.802	1.153	1.146	1.140	1.134	1.129
0.75	0.028	1.167	4.031	4.703	1.169	1.162	1.155	1.148	1.141
0.80	0.044	1.184	3.922	4.603	1.188	1.180	1.171	1.163	1.156
0.85	0.065	1.203	3.807	4.499	1.210	1.199	1.189	1.181	1.174
0.90	0.095	1.224	3.697	4.390	1.236	1.223	1.211	1.202	1.104
0.95	0.137	1.244	3.594	4.273	1.265	1.249	1.236	1.226	1.217
1.00	0.195	1.264	3.498	4.148	1.296	1.279	1.263	1.251	1.240
1.05	0.278	1.282	3.408	4.021	1.337	1.315	1.295	1.279	1.267
1.10	0.420	1.295	3.321	3.902	1.386	1.359	1.334	1.313	1.297

With $\rho\equiv 1$ the quantity $(\mu_\tau/kT)=(\bar{U}/\bar{N}kT)+(Pv/kT)-(S_\tau/\bar{N}k)$ at given x, y is now greater than that obtained with the adjusted ρ by the addition of $-[(1-\rho)/\rho]\ln(1-\rho)-\ln\rho$, the first being the "communal entropy" term, and the second, $-\ln\rho$, arising from the different volume of the system.

These changes have been made, and by graphical interpolation as before, the values listed in Tables II, III, and IV under $\rho\equiv 1$ have been obtained. These represent the results of a computation adhering to items 1 to 4, in our characteristics, but replacing 5 with a cell lattice containing exactly as many cells as there are molecules.

The computed values for $\rho\equiv 1$ are seen to give essentially the same values as those listed under "this paper" at the lower temperatures. At higher temperatures, Tables II and IV show that the values with adjusted ρ are superior both for the volume of the system and for the vapor pressures. Table III shows how poorly the computations with $\rho\equiv 1$ fit the critical point.

Hirschfelder's computations of the condensed phase volume seem to be surprisingly poor compared to ours, even with $\rho\equiv 1$, Table II. It is not quite clear to us why this is so marked, although qualitatively the same features that lead to a fictitiously low energy computation will lead to a low pressure, and hence a lower volume at a fixed pressure. Presumably the marked difference between the values at the critical point obtained by Hirschfelder and by the computation with $\rho\equiv 1$ are due to the difference in computing the potential energy, which difference becomes quite great at the higher temperature and volume. Hirschfelder's computation of the vapor pressures were not available to us for comparison in Table IV. However, as discussed previously his internal energy will be lower than that computed here with $\rho\equiv 1$, and hence μ_τ/kT should also be lower.

The volumes of the condensed phase, Table II, do not at first appear to be too bad, with $v/v_0=1.209$ experimental *vs* 1.162 computed at a temperature somewhat above the normal boiling point. If, however, one considers that the significant calculation is the relative

volume increase above 0°K, 0.209 experimental *vs* 0.162 computed, the result looks poorer, as only 80 percent of the true expansion has been computed.

Table IV, giving the vapor pressures, shows most dramatically how poor the equations really are. The computed value of Pv/u_0 in Table IV is sevenfold too high at $kT/u_0=0.7$, showing that the Gibbs free energy is too high by $RT\ln 7$ per mole, or μ_τ/kT too high by $\ln 7=2$. The quantity $(\mu_\tau/kT)-\ln v$ is the difference between μ/kT for the system and that of a perfect gas at the same volume as the system. This is the configurational free energy per molecule, divided by kT. At $kT/u_0=0.7056$ the experimental value is -6.2 whereas our computed value is only -4.2. This means that our restrictions on the form of the distribution function permit the nonequilibrium ensemble to utilize only 68 percent of the reduction in free energy which is available to an equilibrium configuration.

The main advantage which we may claim for the method used here is that of logic and self-consistency. We have defined a nonequilibrium ensemble with definite prescribed characteristics, and, except for the one remedial error of neglecting interactions between more distant than neighboring cells, we have computed its thermodynamic characteristics correctly. These are necessarily such that at fixed V and T the Helmholtz free energy is too large, at fixed P and T the Gibbs free energy is too large, and at fixed μ and T the PV product is too small.

Since the prescription of the distribution is exact, one may proceed to investigate improvements. The most obvious one, and the one which appears to offer the greatest hope of improvement, is the introduction of a correlation function between the positions of two molecules in neighboring cells. It would not appear to be impossible to handle such a distribution.

THE JOURNAL OF CHEMICAL PHYSICS VOLUME 20, NUMBER 6 JUNE, 1952

The Infrared Absorption Spectra of *Cis*- and *Trans*-1,2-Dichlorohexafluorocyclobutane*

JOHN R. LACHER, ALFRED BÜCHLER, AND J. D. PARK
University of Colorado, Boulder, Colorado

(Received February 20, 1952)

The thermal dimerization of chlorotrifluoroethylene leads to 1,2-dichlorohexafluorocyclobutane consisting mainly of the high boiling isomer. On the other hand, the photochemical or catalytic chlorination of hexafluorocyclobutene yields a dichloride consisting mainly of the low boiling isomer. These isomers may be readily separated by fractional distillation. Dielectric constant measurements permit one to indicate that the high boiling one is *cis* and the low boiling is the *trans*. The infrared spectra in the sodium chloride region were measured and compared with the existing data on the Raman spectra.

HENNE and Ruh[1] first prepared 1,2-dichlorohexafluorocyclobutane. They showed that the thermal dimer of monochlorotrifluoroethylene consisted entirely of the "head-to-head" compound.[2] However, no attempt was made to separate the *cis*- and *trans*-isomers. The Raman spectrum of the unresolved mixture of the two isomers has been reported by Edgell and Kite.[3]

PREPARATION OF THE ISOMERS

The high boiling isomer of 1,2-dichlorohexafluorocyclobutane was obtained by the dimerization of monochlorotrifluoroethylene[4] under autogenous pressure at 200° in the presence of du Pont Terpene *B* inhibitor.[1] The dimer was distilled on a Podbielniak column having 100 theoretical plates. The last cut and pot residue were identified as the pure high boiling isomer by an inspection of their freezing point curve. The estimated purity was 99 percent. It is believed that the thermal dimer produced in this way consisted of at least 80 percent of the high boiling isomer.

TABLE I. *Cis* and *trans* isomers of 1,2-dichlorohexafluorocyclobutane.

	cis	*trans*
B.P.	54°/630 mm	51.3°/630 mm
F.P.	−14.2°	−24.2°
n_D^{20}	1.3340	1.3340

The low boiling isomer was produced by either photochemical or catalytic chlorination of hexafluorocyclobutene. 1,2-dichlorohexafluorocyclobutane (thermal dimer) was dechlorinated with zinc in boiling *n*-butanol to give hexafluorocyclobutene. The photochemical chlorination was carried out batchwise using a 5-l glass bulb in the usual fashion. The thermal chlorination was carried out over a ferric chloride-activated charcoal catalyst using methods previously described.[5] The dichloride produced by either of these

* This research was supported by the ONR Contract N6-onr-231, Task Order VI, United States Navy.

[1] A. L. Henne and R. P. Ruh, J. Am. Chem. Soc. **69**, 279 (1947).

[2] A. L. Henne and W. J. Zimmerschied, J. Am. Chem. Soc. **69**, 281 (1947).

[3] W. F. Edgell and F. E. Kite, J. Chem. Phys. **15**, 882 (1947).

[4] A sample of monochlorotrifluoroethylene was kindly furnished us by Dr. E. G. Young of the Kinetic Chemicals Division of the du Pont Company.

[5] Lacher, McKinley, Walden, Lea, and Park, J. Am. Chem. Soc. **71**, 1334 (1949).

methods was found on distillation to consist of at least 80 percent of the low boiling isomer. The purity of the final product was checked spectroscopically by the disappearance of the high boiling isomer's absorption band at 9.56μ and was judged to be 99 percent.

In order to identify the nature of each isomer, an attempt was made to measure their dipole moments. Theoretically, the *trans*-compound should have a zero moment, while the *cis*-compound should have a moment of the order of 0.1 Debye unit using the group moment values recently given by Myers and DeVries.[6] In practice it was found that in a 4 mole percent solution of 1,2-dichlorohexafluorocyclobutane in benzene, the dielectric constant of the low boiling isomer was the same as that of pure benzene, while the solution containing the high boiling isomer was 1 percent higher. While the instrument did not permit measurements which could be extrapolated to zero concentration, the difference of 1 percent is larger than the experimental error and permits the deduction that the low boiling isomer is *trans* and that the high boiling one is the *cis* isomer. A summary of some of their physical properties is given in Table I.

TABLE II. Infrared and Raman bands for 1,2-dichlorohexafluorocyclobutane.

Infrared		Raman[a]
cis	*trans*	mixture
7.25μ	7.27μ	7.18μ
	7.46	
7.80	7.81	7.77
8.07	8.09	8.04
8.18[b]		
8.45	8.47	8.40
	(8.88)[c]	
		9.00
9.18	9.22	
		9.31
9.56		
9.78	9.80	
10.40	10.27	10.35
11.24		
11.61	11.58	11.59
12.40	12.49	12.35
(14.49)[c]		
	(13.25)[b,c]	
	(14.54)[c]	

[a] See reference 3.
[b] Shoulder.
[c] Not a fundamental band.

[6] A. L. Myers and T. DeVries, J. Am. Chem. Soc. **73**, 1813 (1951).

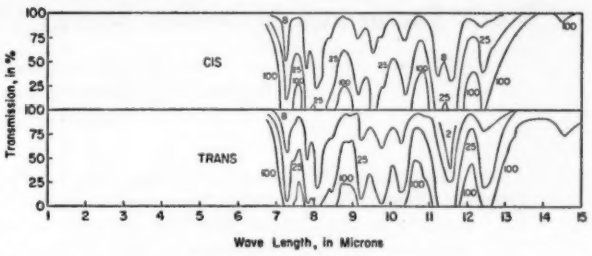

FIG. 1. Infrared absorption spectra of *cis*- and *trans*-1,2-dichlorohexafluorocyclobutane. 10-cm cell and pressures as indicated in mm.

INFRARED ABSORPTION SPECTRA

A Perkin-Elmer mode 12B infrared spectrometer with NaCl optics was used in the region 2.15 to 15μ. Using gaseous samples, the spectra were obtained in the usual way and are shown for the 2 isomers in Fig. 1. The wavelength of the absorption bands are given in Table II. If we assume a planar ring, the *cis* isomer will belong to the symmetry group C_s (one plane of symmetry) and the *trans*-isomer to the symmetry group C_2 (one twofold axis of symmetry). The distribution of fundamentals will be: for the *cis*-isomer, $15A'+15A''$; and for the *trans*-isomer, $16A+14B$. All of these fundamentals should be both infrared and Raman active, with the A' and A vibrations polarized and the A'' and B vibrations depolarized in the Raman spectrum. The probable fundamentals in this region, together with the Raman shifts reported by Edgell and Kite[3] on what was possibly a *cis-trans* mixture, are listed in Table II. The agreement is good, the Raman bands not occurring in the infrared probably involve very small changes in the dipole moment as compared to the polarizability, and vice versa. It is seen that most bands in the *trans*-spectrum are shifted slightly towards the red. The *cis*-bands at 8.18 and 9.56μ disappear in the *trans*-spectrum, while the band at 11.24μ either disappears or is shifted and masked completely by the *trans*-band at 11.58μ. On the other hand, the band at 10.40μ in the *cis*-spectrum is shifted to 10.27μ in case of the *trans*.

The bands at 7.25, 7.80, 8.07, and 8.18μ for the *cis*-isomer, and at 7.27, 7.81, and 8.09μ for the *trans*-isomer probably involve C—F stretching vibrations. Of the other bands, those at 9.56, 10.40, and 11.24μ for the *cis*-isomer obviously involve the —CFCl—CFCl— part of the ring as a whole and therefore are shifted or disappear altogether in the *trans*-spectrum; while the bands whose location changes only very slightly apparently involve CF, CF_2 and perhaps CFCl and CCl group motions unaffected by the structure of the ring.

Steric Factor and Activation Energy of the Reaction $Na+C_2H_5Cl=NaCl+C_2H_5$

R. J. CVETANOVIĆ* AND D. J. LE ROY
Department of Chemistry, University of Toronto, Toronto, Canada
(Received November 23, 1951)

The reaction between atomic sodium and ethyl chloride has been studied over the range 260° to 380°C by the diffusion flame method. From the temperature coefficient of the rate constant the activation energy was found to be 10.2 kcal per mole. The maximum uncertainty in this quantity from all causes, is estimated to be ±0.5 kcal per mole. The steric factor was 1.0±0.3, based on the customary value assigned to the collision diameter.

INTRODUCTION

SINCE the development of the "diffusion flame" technique by Hartel and Polanyi[1] a great fund of information has accumulated about the relative rates of reaction of atomic sodium with organic and inorganic compounds and, in particular, with organic halides. Polyanyi has shown[2] that the magnitudes of the rate constants follow definite patterns, in relation to the various homologous series studied, and it is generally agreed that the diffusion flame technique, as well as the related "life period" method,[3] has added greatly to our knowledge of the mechanism of chemical reaction. The results have formed the basis of a number of theoretical papers.[4–6]

The extent to which the results have been utilized has undoubtedly exceeded the expectations of the original authors. In 1932 Hartel, Meer, and Polanyi[7] rejected the quantitative use of the method and proposed that it be applied to comparative studies of reaction rates only. Somewhat later Heller[8] published the results of a critical survey of the method in which he suggested a number of experimental conditions under which the simplifying assumptions implicit in the original theoretical treatment[1] might be expected to be approached. According to Heller, the method could be used for the determination of absolute values of rate constants with an uncertainty not exceeding a factor of two under the best conditions.

The quantities of theoretical interest to the chemist are, of course, not rate constants, but steric factors and activation energies or the corresponding quantities in transition state theory. Although it was not the intention of the authors of the method, the practice has grown up of calculating "activation energies" from data accumulated at a single temperature. This was done by the simple expedient of *assuming* that the steric factor p was equal to unity, assigning a constant mean collision diameter σ for all reactions, and calculating the activation energy E from the expression

$$k=p\sigma^2\left(8\pi RT\frac{M_1+M_2}{M_1M_2}\right)^{\frac{1}{2}}e^{-E/RT}. \qquad (1)$$

A value of 3.5×10^{-15} cm^2 for σ^2 was suggested originally by Hartel and Polanyi[1] and has been used quite generally in the literature, although Warhurst[9] has suggested that 5.1×10^{-16} would be more suitable for sodium and monohalogenated compounds.

Only a very few experiments have been performed to confirm the validity of these assumptions. Hartel and Polanyi[1] investigated the reaction of sodium with methyl chloride and methyl bromide over a range of temperature and found activation energies, from the temperature coefficients, of 7.5 and 3.0 kcal per mole, in comparison with "single temperature" values of 8.8 and 3.2, respectively. However, the values used for the diffusion coefficient of sodium in the carrier gas were greater than those found experimentally somewhat later;[7] also their experimental conditions deviated considerably from those laid down by Heller.[8] Frommer and Polanyi,[3] using the life period method, found a distinct increase in the rate constant for the reaction with methyl bromide for a temperature increase of 40° but did not feel justified in calculating an activation energy from the temperature coefficient. Warhurst[9] determined the rate constants for the reaction with phenyl bromide at 225° and 330°C and obtained a value of 3.8 kcal per mole, in comparison with the "single temperature" value of 4.6 found previously by Tuck and Warhurst.[10]

On the basis of this evidence it seemed desirable to make a careful study of the factors which might influence the magnitudes of the various kinetic quantities derived from diffusion flame experiments. The authors have recently[11] re-examined and extended the original theory of the method,[1] which has been used exclusively

* Present address: Division of Chemistry, National Research Council, Ottawa, Canada.

[1] H. v. Hartel and M. Polanyi, Z. physik. Chem. **B11**, 97 (1930).
[2] M. Polanyi, *Atomic Reactions* (Williams and Norgate, London, England, 1932).
[3] L. Frommer and M. Polanyi, Trans. Faraday Soc. **30**, 519 (1934).
[4] A. G. Evans and H. Walker, Trans. Faraday Soc. **40**, 384 (1944).
[5] E. Warhurst, Quarterly Rev. Chem. Soc. V, 44 (1951).
[6] R. P. Smith and H. Eyring, J. Am. Chem. Soc. **74**, 229 (1952).
[7] H. v. Hartel, N. Meer, and M. Polanyi, Z. physik. Chem. **B19**, 139 (1932).
[8] W. Heller, Trans. Faraday Soc. **33**, 1556 (1937).
[9] E. Warhurst, Trans. Faraday Soc. **35**, 674 (1939).
[10] J. L. Tuck and E. Warhurst, Trans. Faraday Soc. **32**, 1501 (1936).
[11] R. J. Cvetanović and D. J. Le Roy, Can. J. Chem. **29**, 597 (1951).

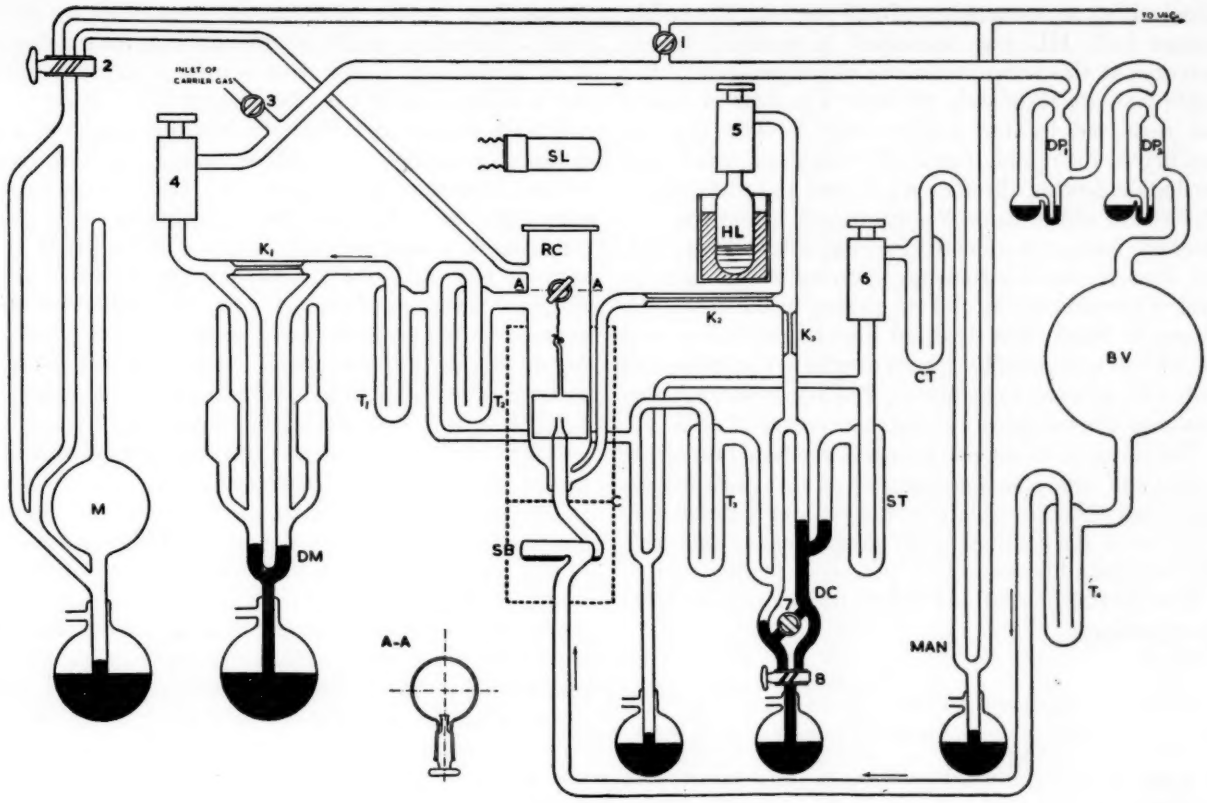

FIG. 1. Diffusion flame apparatus.

up to this time. In the present paper we report the results of an investigation of the effect of temperature on the rate constant for the reaction of atomic sodium with ethyl chloride and interpret the results in the light of the extended theory.

EXPERIMENTAL

The arrangement of the apparatus is illustrated in Fig. 1. The reaction cell *RC* was a cylindrical glass tube 6 cm in diameter and 35 cm long. The sodium and the nitrogen carrier gas entered at the bottom through a jet 0.25 cm in diameter. While making the preliminary adjustments, the walls of the reaction vessel were protected from the deposition of sodium chloride by a cylindrical glass tube which could be raised and lowered by means of the windlass *A*. Light from the sodium lamp *SL* entered the vessel through a Pyrex window at the top. The inside of the furnace was blackened and the "flame" was viewed from a direction at right angles to the incident beam. The maximum diameter of the visible flame was measured by means of an external horizontal scale; any distortion resulting from the curvature of the cell was checked beforehand by viewing a scale placed inside the tube.

The sodium saturator *SB* was placed in a separate furnace and consisted of a tube bent in the form of a horizontal circle in order to expose a large area of molten sodium to the carrier gas. The sodium was distilled into the saturator after being subjected to a number of distillations under high vacuum conditions to remove dissolved hydrogen.

The nitrogen used as the carrier gas had to be free from traces of oxygen. This was done by passage through alkaline pyrogallol solution, Fieser's solution, lead acetate solution, concentrated sulfuric acid, Drierite, hot copper turnings, and finally through a trap containing silic gel cooled with liquid air. The ethyl chloride was purified by distillation; dissolved air was removed in the usual way.

Fluctuations in the flame diameter were avoided by using the large buffer volume *BV* and two multiple stage mercury diffusion pumps *DP* in series. The flow rate of the carrier gas was calculated from the pressure drop across the precision bore capillary K_1, measured by the double McLeod gauge *DM*. A value of 176.5 $\times 10^{-6}$ poise was taken for the viscosity of nitrogen at 23°C.

A common source of difficulty in measurements of this kind is the accurate determination of the relatively small flow rate of the halide. In the present system the flow into the cell through the capillary K_2 was not measured directly but was calculated from the larger amount of halide passing through the parallel capillary K_3 and into a sampling trap cooled with liquid air. The ratio of the flow rates through the two capillaries was measured in calibration experiments and was deter-

mined with a reproducibility of 0.25 percent. The halide storage bulb HL was immersed in partially frozen mercury; at this temperature the vapor pressure of the halide was approximately 64 mm. The flow of halide was regulated by the needle valve 5. The level of mercury in the double cutoff *DC* was so adjusted that the halide flowing through K_3 during the preliminary adjustment of the flame was frozen out in the trap T_3. After the flame was adjusted the stopcock 7 was opened, and through the simultaneous lowering of the mercury level in one arm of *DC* and the raising in the other, the stream of halide was diverted into the sampling trap *ST*. It was subsequently frozen over into the calibrated bulb *CB*, allowed to vaporize, and its pressure determined on the constant volume manometer *MAN*.

The pressure in the reaction cell, the flow rate of the carrier gas, and the temperatures of the two furnaces were measured immediately before and immediately after taking the halide sample; no appreciable difference was ever found between the two sets of readings.

The partial pressure of halide was calculated from the expression,

$$p_{\text{halide}}=p_{\text{cell}}\frac{F_{\text{halide}}}{F_{\text{halide}}+F_{\text{nitrogen}}}, \tag{2}$$

in which p_{cell} is the total pressure in the reaction cell, measured by the McLeod gauge *M*, and the *F*'s are flow rates.

EVALUATION OF THE RATE CONSTANTS

The quantities required for the calculation of rate constants to the Hartel-Polanyi approximation[1] may be seen from their equation

$$k_p=\frac{(\ln c_1^i/c_1^0-\ln R/r)^2 D_1}{(R-r)^2 c_2}. \tag{3}$$

The quantities c_1^i and c_1^0 represent, respectively, the concentration of sodium atoms at the surface of a sphere of radius *r*, taken as the radius of the jet, and at the edge of the visible flame, a distance *R* from the center. D_1 is the diffusion coefficient of sodium in the reaction mixture; c_2 is the concentration of halide, assumed in their treatment to be uniform throughout the reaction zone.

The value of c_1^i was calculated from the data of Rodebush *et al.*[12] and Gordon,[13] on the assumption that the partial pressure of sodium in the carrier gas was equal to the vapor pressure of sodium at the temperature of the saturator. The partial pressure of sodium at the visibility limit, corresponding to c_1^0, was taken to be 7×10^{-6} mm, because most of the glare from the central part of the flame was eliminated by our sighting device. The smaller value has also been used by Warhurst.[9] The effect on the results of the arbitrary choice of c_1^0 is discussed below. In the present experiments *r* was 0.125 cm and *R* was of the order of 1.5 cm.

Hartel, Meer, and Polanyi[7] made a study of the diffusion coefficient of sodium vapor in hydrogen, helium, nitrogen, and argon, the four carrier gases commonly used. In their two experiments with pure nitrogen they obtained the values 0.88 and 0.94 cm^2 sec^{-1} at 655° and 654°K, respectively, corrected to a standard total pressure of one atmosphere. Their average value, 0.91 cm^2 sec^{-1} at 655°K, has been accepted for all diffusion flame work. The preliminary value of 0.68 obtained by Cvetanović and Le Roy[14] for 526.7°K agrees with this within 3 percent, if it can be assumed that the diffusion coefficient varies as the 3/2 power of the absolute temperature.

The presence of halide in the flame will, of course, have an influence on the value of D_1. However, because of the impossibility of using halides in their diffusion work, Hartel, Meer, and Polanyi used pentane as a model substance and assumed that on a molar basis it would have the same effect. We have followed the practice of previous workers in this regard and used their values for pentane-nitrogen mixtures at 655°K and one atmosphere. The concentration of halide does not remain constant throughout the flame, and the present calculations were carried out using a value of D_1 for a mean halide concentration of $0.77c_2^i$, in which c_2^i is the initial concentration of halide, calculated from Eq. (2). The estimated impoverishment of 23 percent is necessarily somewhat arbitrary, but it is in line with the predictions of the extended theory[11] and the experimental measurements of Heller.[8] As a result of the relatively low concentration of halide used the correction is small, and the error arising from this source will not affect the value of *E* obtained from the temperature coefficient of *k* to any appreciable extent. The values of D_1 for any particular temperature and total pressure were calculated from the expression

$$(D_1)_{T_1,P_1}/(D_1)_{T_2,P_2}=(P_2/P_1)(T_1/T_2)^{\frac{3}{2}}. \tag{4}$$

The rate constants calculated from Eq. (3) were corrected on the basis of the extended theory by applying Eq. (18) of reference (11). A value of 0.9 was taken for the quantity α in that equation. The concentration of halide at *r* was assumed to be zero. The values of the rate constants calculated in this way are of the same magnitude as those obtained by correcting for the influence of halide impoverishment using Heller's experimental measurements.[8] This agreement was not unexpected, since in the present experiments c_2^i was much greater than c_1^i, and consequently the diffusion term in the extended equation was very small.

[12] W. H. Rodebush and W. F. Henry, J. Am. Chem. Soc. **52**, 3159 (1930); W. H. Rodebush and E. G. Walters, J. Am. Chem. Soc. **52**, 2654 (1930).

[13] A. R. Gordon, J. Chem. Phys. **4**, 100 (1936).

[14] R. J. Cvetanović and D. J. Le Roy, J. Chem. Phys. **20**, 343 (1952).

TABLE I.

Expt.	Temp. °K	p_{cell} mm	p_i mm×10³	R cm	p_{halide} mm	655°K D_{11} atmos. cm² sec⁻¹	k_p cm³ molec⁻¹ sec⁻¹	k cm³ molec⁻¹ sec⁻¹	E "single temp." kcal/mole	ΔF kcal/mole
1	532.7	4.04	0.83	1.55	0.250	0.72	0.55	0.667	10.06	63.88
2	532.7	3.96	0.90	1.55	0.290	0.71	0.51	0.621	10.13	63.95
3	534.2	4.06	0.93	1.50	0.348	0.68	0.46	0.554	10.28	64.26
4	532.7	3.81	0.77	1.60	0.242	0.72	0.51	0.618	10.14	63.96
5	532.9	3.79	0.80	1.50	0.344	0.67	0.43	0.517	10.33	64.17
6	533.2	3.79	0.80	1.50	0.362	0.65	0.39	0.477	10.42	64.29
Mean	533.1							0.572	10.23	64.09
7	575.2	3.34	1.38	1.60	0.251	0.70	1.07	1.292	10.15	68.31
8	574.7	3.29	1.38	1.60	0.276	0.68	0.96	1.157	10.27	68.37
9	572.5	3.76	1.30	1.50	0.265	0.71	1.04	1.266	10.12	68.00
10	575.5	4.02	1.30	1.65	0.172	0.77	1.25	1.518	9.97	68.16
Mean	574.5							1.302	10.13	68.21
11	612.4	4.04	1.32	1.70	0.126	0.79	1.89	2.267	10.16	72.11
12	612.0	3.89	0.75	1.50	0.119	0.79	1.89	2.289	10.14	72.06
13	613.4	3.94	1.10	1.60	0.114	0.83	2.34	2.826	9.91	71.97
14	613.2	3.96	0.90	1.45	0.152	0.78	1.87	2.279	10.17	72.20
Mean	612.8							2.405	10.09	72.09
15	653.0	3.76	0.85	1.50	0.084	0.82	3.77	4.584	9.96	76.07
16	653.0	3.86	0.85	1.50	0.099	0.81	3.08	3.743	10.22	76.33
17	653.0	3.87	0.85	1.50	0.104	0.80	2.88	3.501	10.31	76.42
18	651.5	3.77	0.90	1.50	0.103	0.80	3.12	3.789	10.18	76.13
Mean	652.6							3.883	10.17	76.23
[a]	548	(3.22)	2.6	1.25	(0.66)	(0.42)	1.02		9.90	64.68
[a]	548	(3.24)	2.6	1.00	(0.97)	(0.33)	1.07		9.85	64.54
[b]	543	2.0	1.0	1.00	0.95	0.56	1.76		9.22	63.20

[a] Hartel, Meer and Polanyi's data (see reference 7), recalculated. The bracketed values are arithmetic means for eight determinations. The k_p values were calculated from mean values of $\log k_p$. Nitrogen used as carrier gas.
[b] Recalculation of Hartel and Polanyi's data (see reference 1) for a single determination. Hydrogen used as carrier gas.

RESULTS AND DISCUSSION

In Table I are shown the results of experiments at four temperatures in the range 260° to 380°C, together with values calculated from the data obtained by Hartel and Polanyi[1] and Hartel, Meer, and Polanyi.[7] The values of D_1 given in column seven were obtained as described above. The rate constants in column eight are to the Hartel-Polanyi approximation; those in column nine have been calculated on the basis of the extended theory. Neither this theory nor the correction for the influence of halide impoverishment on the value of D_1 has been applied to the data of the earlier authors. Heller[8] has pointed out that one of the conditions necessary for an accurate determination of the rate constant is that the ratio, v/D_1, of the linear velocity of the carrier gas in the nozzle in meters per second to the diffusion coefficient of sodium, should be in the range 5×10^{-2} to 12×10^{-2}. In our experiments this ratio was kept essentially constant at 10×10^{-2}, but in their experiments with ethyl chloride the other authors exceeded the limit by a considerable amount. As a result, it was felt that there was little justification in the application of these corrections to their data. In column ten are given values of the "single-temperature" activation energies, calculated on the assumption that $p=1.0$ and that $\sigma^2=3.5\times10^{-15}$ cm². Free energies of activation for a standard state of one molecule per cm³ are given in the last column.

In Fig. 2 is shown a plot of the mean values of $\log(Z/k)$ *vs* $1/T$. The straight line corresponds to an activation energy of 10.2 kcal per mole; as mentioned below, the uncertainty in this value should not exceed ±0.5 kcal per mole. The corresponding steric factor, based on the value of σ^2 chosen, is 1.0±0.3; this is in agreement with the constancy of the values in column ten of Table I. On the assumption that $\Delta S^{\ddagger}$ and $\Delta H^{\ddagger}$ are independent of temperature within the range considered, the corresponding values of these quantities, obtained from a plot of $\log(\mathbf{k}T/h)/k$ *vs* $1/T$, are -0.1012 ±0.0008 kcal mole⁻¹ deg⁻¹ and 10.0±0.5 kcal per mole, respectively.

The present work appears to confirm the common assumption that for reactions of this type $p=1.0$ and $\sigma^2=3.5\times10^{-15}$ cm², or at least that $p\sigma^2$ is close to 3.5×10^{-15}. However, the importance of an accurate knowledge of the activation energy is sufficient to justify some consideration of the errors inherent in its evaluation. One of the most serious experimental errors in the determination of the rate constant is in the measurement of the radius of the flame. In most cases

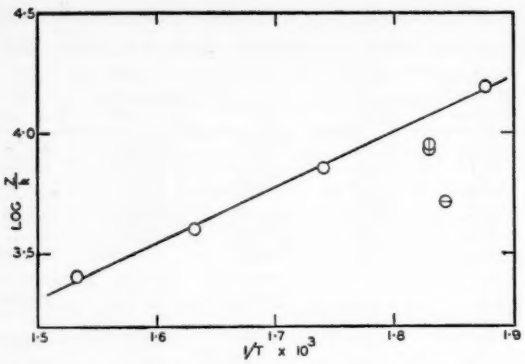

FIG. 2. Plot of log (Z/k) *vs* $1/T$. ○ present work; ⊖ Hartel and Polanyi; ⊕ Hartel, Meer, and Polanyi.

this will not exceed 10 percent, although occasional errors as large as 20 percent may occur. In the present work errors in the flow rates of the halide and the carrier gas would probably contribute less than 3 or 4 percent. An error of the order of 1°C in the temperature of the saturator would influence the rate constant by about 5 or 6 percent. It is believed, therefore, that the total experimental error would be between 10 and 20 percent. Actually, the precision of the measurements was of the order of 8 to 10 percent.

In addition to experimental errors in the determination of R, c_1^i and c_2, the values of the rate constants will be influenced by (a) back diffusion of the halide into the nozzle, (b) axial distortion of the flame, (c) whorl formation in the reaction zone, (d) nonuniformity of the halide concentration, (e) arbitrariness in the value of c_1^0, (f) arbitrariness in the value of r, (g) uncertainty in the value of D_1 in the reaction mixture.

Back diffusion into the nozzle is suppressed by having a sufficiently large linear flow rate of carrier gas at that point. The second and third sources of error become important when this flow rate becomes large. In the absence of a satisfactory solution to this problem of fluid dynamics, it would seem to be necessary to accept Heller's experimentally determined criterion[8] that the three effects can be neglected provided v/D_1 lies within the limits specified. Allowance for the nonuniformity of the halide concentration can be made by applying the extended theory;[11] the correction will be quite important for fast reactions. The effect of the choice of the visibility limit for sodium fluorescence is seen in the fact that for c_1^0 equal to 7×10^{-6} mm the calculated rate constants were 40 percent larger than for $c_1^0=10^{-5}$ mm. However, the value of E calculated from the temperature coefficient of k was unchanged. If the differential coefficient of E, in Eq. (3), is taken with respect to c_1^i, c_1^0, r, and R, it will be seen that the value of E obtained from the temperature coefficient of k will not be affected by the arbitrary choice of these quantities as long as the actual values remain constant throughout the experimental temperature range. Thus, even incomplete saturation of the carrier gas will, under these conditions, have no effect. The value of E calculated from measurements at a single temperature will, of course, be strongly affected.

In the evaluation of the rate constants it has been assumed that the effect of temperature on the diffusion coefficient of sodium is given by Eq. (4). This assumption is based on a simple theory of gaseous diffusion. Sutherland[15] has suggested a more complex relation. Chapman and Cowling[16] have related the temperature dependence to the nature of the forces acting during molecular collisions. Unfortunately, few experimental measurements of the diffusion coefficients of gases have been made with sufficient accuracy to confirm any of the theories. However, the magnitude of the error in E arising from the uncertainty in the temperature exponent of the diffusion constant is probably not large. If the exponent were 7/4, corresponding to a repulsion varying inversely as the ninth power of the distance,[16] E would be increased to 10.5 kcal per mole. The method of correcting D_1 for the halide content will also cause some uncertainty in E. In the extreme case, if no correction were made, the value would be reduced to 9.5 kcal per mole. In the light of these considerations and in view of the precision of the measurements, it is believed that the uncertainty in E probably does not exceed ±0.5 kcal per mole. Relative values of E for different halides, based on temperature coefficients of k, might be expected to have somewhat smaller probable errors.

The authors are indebted to the Associate Committee on Scientific Research of the University of Toronto for financial assistance. One of the authors (R.J.C.) expresses his appreciation to the Senate of the University for the award of a Nadine Phillips Scholarship.

[15] W. Sutherland, Phil. Mag. **36**, 507 (1893).
[16] S. Chapman and T. G. Cowling, *The Mathematical Theory of Non-Uniform Gases* (Macmillan Company, New York, 1939).

Studies of Ionization Efficiency. Part II. The Ionization Potentials of Some Organic Molecules

J. D. Morrison and A. J. C. Nicholson
Chemical Physics Section, Division of Industrial Chemistry, Commonwealth Scientific and Industrial Research Organization, Melbourne, Australia

(Received November 23, 1951)

The ionization potentials of some 83 organic molecules have been measured with the mass spectrometer, using the critical slope method to interpret the ionization efficiency curves for the molecular ions. A self-consistent group of values has been obtained in which the main relationships between ionization potential and molecular structure can be clearly distinguished. The results are compared with those obtained by spectroscopic and other methods, and some regularities in the discrepancies are pointed out.

INTRODUCTION

THE ionization potential of a polyatomic molecule can be used to determine (1), which electron in the molecule is the most loosely bound;[1] (2), to give information about bond strengths, bond lengths, bond order, and the distribution of electric charge in the molecule;[2] and (3), to provide data for the calculation of electronic wave functions.[3] It is generally recognized, moreover, that there is a relationship between ionization potential and chemical reactivity.

In view of these facts, it is surprising that reliable data are available for so few molecules. Vacuum ultraviolet absorption spectra lead to the most accurate values of ionization potential if the observed bands can be fitted to Rydberg series which have unequivocal convergence limits.[4] Electron impact data, obtained from measurements of total ion current or by use of the mass spectrometer, have not been considered as reliable in view of the difficulties of interpretation. However, it appears that improvements in the methods of measurement of ionization efficiency curves by the mass spectrometer provide data on molecules not accessible to the vacuum ultraviolet method which form at least a self-consistent set, and only from such data can there be discovered the exact correlation between ionization potential and molecular structure.

METHOD OF MEASUREMENT

The various methods of determining ionization potentials from molecular ionization efficiency curves have been discussed in an earlier paper,[5] and it was concluded that the critical slope method of Honig[6] gave results which were in best accord with the spectroscopic values.

The vapor of the substance to be measured and either argon or krypton were admitted to the mass spectrometer together and three separate measurements of the ionization potential made, using the methods described in Part I[5] and elsewhere.[7] When the ionization efficiency curves for both calibrating and measured ions were plotted on a semilogarithmic scale, the slopes of the straight-line portions rarely differed by more than 5 percent, corresponding to 0.04 ev in the ionization potential. In one case, marked with an asterisk in the tables, the slopes differed by a greater amount, and here the point at which each curve attained two-thirds of its initial gradient was taken as its critical value. It was noted that slight drifts of the conditions in the ion chamber between successive pairs of measurements caused the slopes of the straight-line regions, which are related to the filament temperature, to vary within narrow limits. The ionization potentials found in separate determinations, however, did not differ by more than about 0.05 ev, and the results given in the tables, the means of three determinations, are reproducible to within 0.04 ev.

The substances used for measurement were checked for purity by recording their mass spectra and comparing these, where possible, with those published in the literature for the pure compounds. Except for one substance, bracketed in the tables, no impurities were present of higher mass than that of the compound studied.

RESULTS

The measured ionization potentials may be listed most conveniently in a set of tables. In Table I the variation in ionization potential with substituent groups in some hydrocarbon derivatives is shown. The group within the dotted lines consists of molecules in which the electron ionized is almost certainly of nonbonding character. Table II illustrates the effect of chain-branching for a few substances, and values for certain miscellaneous compounds are cited in Table III.

AGREEMENT OF RESULTS WITH SPECTROSCOPIC VALUES

In Table IV the substances are classified into groups corresponding to the difference, (ΔI), between the

[1] R. S. Mulliken, Phys. Rev. **46**, 549 (1934); J. Chem. Phys. **3**, 514 (1935).
[2] A. D. Walsh, Trans. Faraday Soc. **42**, 779 (1946).
[3] G. G. Hall and J. E. Lennard-Jones, Proc. Roy. Soc. (London) **A202**, 155 (1950); **A205**, 541 (1951).
[4] W. C. Price, Phys. Rev. **45**, 843 (1934); **46**, 529 (1934).
[5] J. D. Morrison, J. Chem. Phys. **19**, 1305 (1951).
[6] R. E. Honig, J. Chem. Phys. **16**, 105 (1948).
[7] G. R. Hercus and J. D. Morrison, Rev. Sci. Instr. (to be published).

TABLE I. The ionization potentials of some hydrocarbon derivatives.

	H	CH_3	C_2H_5	nC_3H_7	nC_4H_9	$CH_2=CH$	C_6H_5
−CN	13.91	12.39	11.85	[a]	[a]	10.75	9.95
−Cl	12.78	11.46	11.18	10.96			9.42
−OH	12.76	10.95	10.60	10.46	[a]		9.03
−Br	11.69	10.73	10.49	10.29	10.12		9.41
−COOH	11.51	10.70	10.47	10.22	[a]	10.90	[a]
−CHO		10.28	10.06	10.01		10.34	9.82
−C*Me*O	10.28	9.92	9.76	9.59	9.58	[9.91]	9.77*
−I	10.48	9.67	9.47	9.41	9.32		9.10
$-NH_2$	10.52	9.41	9.32	9.17	9.19		[a]
$-C_6H_5$	9.52	9.23	9.12	9.14	9.14	8.86	[a]

[a] Molecular ion not abundant enough for its appearance potential to be measured.

present electron impact values and the spectroscopic ionization potentials for the molecules where these are known. It is significant that in the only three cases where the electron impact value is less than the spectroscopic some doubt exists as to the correct interpretation of the spectroscopic data. The value for acetone of 10.26 ev[8] is from a "probable Rydberg series" of only three bands, and an early electron impact value is 0.1 ev less.[9] The value obtained in this work is more consistent with the general trend in the ionization potential when a hydrogen atom is replaced by a methyl group. The spectroscopic figures for HCl and HBr are mean values for the two π-states of the molecular ion and are obtained by comparison with the spectra of HI and the alkyl halides.[10] It is possible that the agreement could be improved by a different interpretation of the spectroscopic data. An exceptionally large difference with the previously reported figure occurs for trichlorethylene[11] but here again the new value is more consistent with the figures for the other chlorine-substituted ethylenes[12] than is the earlier value.

Apart from these discrepancies, a number of distinct trends can be discerned in Table IV. The agreement between the electron impact and spectroscopic figures for the rare gases is excellent. Diatomic and triatomic molecules also are in nearly all cases in close agreement. The electron impact figures for the majority of simple organic molecules are slightly higher than the corresponding spectroscopic values, and the figures for aromatic molecules are greater by from 0.3 to 0.5 ev.

When the ionization is that of an electron localized on a particular atom in a molecule, the replacement of that element by a heavier one from the same column of the periodic table causes the discrepancy between the electron impact and spectroscopic values to decrease, as for example, in the cases of CO_2 and CS_2; H_2O and H_2S; and the methyl- and ethyl-chlorides, bromides, and iodides.

Ionization potentials measured by electron impact are usually assumed to be "vertical" ones,[13] corresponding to the transition to the ionic state without much change of internuclear distance, while spectroscopic ionization potentials have been taken to be "adiabatic" values, i.e., corresponding to the energy difference between $v''=0$ and $v'=0$. It appears to the authors that this second assumption need not necessarily be correct. The position of maximum absorption in each band in the Rydberg series will correspond to vertical transitions through the Franck-Condon region, and only in those cases where vibration lines are observed and the (0, 0) transition can be identified positively by analysis of the vibrational structure or by comparison of the spectra of isotopic molecules, can the ionization limit found be labelled adiabatic with certainty.

Even if ΔI is accepted as this difference, its magnitude, especially in the case of the aromatic compounds, seems rather large.

TABLE II. The effect of chain-branching on ionization potential.

	n-Pr	*i-Pr*	*n-Bu*	*i-Bu*	*sec-Bu*	*t-Bu*
−Br	10.29	10.11	10.12	10.24	10.15	[a]
$-NH_2$	9.17		9.19	9.00	8.98	[a]
$-C_6H_5$	9.14	9.13	9.14		9.19	9.35

[a] Molecular ion not abundant enough for its appearance potential to be measured.

AGREEMENT OF RESULTS WITH OTHER ELECTRON IMPACT VALUES

The values found for methane, *n*-hexane, and benzene (13.16, 10.54, 9.52) are in fair agreement with the results obtained by Honig[6] (13.04, 10.48, 9.45).* The agreement with the values obtained by other workers using the mass spectrometer is not usually worse than 0.5 ev, but this is understandable in view of the variety of methods used to interpret the ionization efficiency curves. Earlier values obtained using apparatus of ionization gauge type, including those listed in the International Critical Tables, are in most cases unreliable sometimes being in error by as much as 3.0 ev. This is probably a result of the fact that the calibrating gas, if any, was measured separately from the sample, and it has been noted in this work[14] that the effect of halogen-containing compounds in particular on the mass spectrometer filament is such as to raise the apparent ionization potential by one or two volts.

[8] A. B. F. Duncan, J. Chem. Phys. **3**, 131 (1935); **8**, 444 (1940).
[9] W. A. Noyes, Jr., J. Chem. Phys. **3**, 430 (1935).
[10] W. C. Price, Proc. Roy. Soc. (London) **A167**, 216 (1938).
[11] A. D. Walsh, Trans. Faraday Soc. **41**, 35 (1945).
[12] H. E. Mahncke and W. A. Noyes, Jr., J. Chem. Phys. **3**, 536 (1935). J. P. Teegan and A. D. Walsh, Trans. Faraday Soc. **47**, 1 (1951).
[13] Bleakney, Condon, and Smith, J. Phys. Chem. **41**, 197 (1937).
* From the values given, it might appear that a systematic error of 0.7 percent is present. The potentiometer used in this work was checked and found to be not greater in error than 0.01 percent.
[14] See D. P. Stevenson and J. A. Hipple, J. Am. Chem. Soc. **64**, 2766 (1942).

DISCUSSION

The successive replacement of hydrogen in a molecule by methyl, ethyl, *n*-propyl, etc., groups causes a reduction in the ionization potential, large for the first few, and progressively less as the number of carbon atoms increases. Branching of the hydrocarbon chain causes only slight variations, which are of the order of the experimental error. It is perhaps significant that molecules containing the tert-butyl radical seldom produce a stable molecular ion at all. In molecules containing a hydrocarbon radical, the presence of a double bond causes the ionization potential to be less than that for the saturated structure by from 0.5 to 1 ev, while that of a triple bond leaves the ionization potential almost unchanged. When two heavy atoms such as bromine, which is less strongly electronegative, are present in a molecule, the ionization potential is very little affected by the number of carbon atoms present, e.g., in the polymethylene dibromides.

To a first approximation various structural radicals

TABLE III.

Cl_2	11.80	methane	13.16
Br_2	10.92	*n*-hexane	10.54
I_2	9.41	cyclohexene	9.24
$COCl_2$	11.77	butadiene	9.24
$CCl_2=CHCl$	9.94	diacetyl	9.54
$(CH_2)_2Br_2$	10.30	isoprene	9.08
$(CH_2)_3Br_2$	10.28	diethyl ether	9.72
$(CH_2)_4Br_2$	10.28	dioxane	9.52
C_6H_5F	9.67	ethyl acetate	9.97
$C_6H_5-C\equiv CH$	9.15	*i*-valeraldehyde	9.92

can be placed in a sequence: $-CH>H>CH_3>Cl>OH>Et>Br>COOH>n\text{-}Pr>n\text{-}Bu>$vinyl$>CHO>CMeO>I>NH_2>$phenyl, such that the ionization potential of a molecule made by combining any pair is higher than for any other combination between groups farther to the right in the series. Exceptions occur only for molecules containing the carbonyl group, e.g., when formic and acetic acids are considered as $-OH$ derivatives and when $CH_2=CH$- and phenyl- are combined with CHO, C*Me*O, and COOH, the ionization potentials are higher than would be expected by about one volt. The values for the paraffin molecules also do not fit in very closely with this series, being all slightly higher. From inspection of Table I and a knowledge of the ionization potential of a molecule it is generally possible to decide which electron is ionized.

TABLE IV. The difference (ΔI) between the present electron impact and the spectroscopic ionization potentials for those molecules where the latter is known.[a]

Less than spectroscopic >-0.05 ev	HCl -0.12	HBr -0.40	Acetone -0.34		
Within exptl. error -0.05 to 0.05	H_2S 0.02	Ne -0.05	Acetaldehyde 0.05		
	CS_2 0.03	Furane 0.0	Cyclohexene 0.04		
Above spectroscopic $>0.05<0.30$	HI 0.09	*Me*I 0.13	*Et*I 0.13	N_2 0.08	Butadiene 0.18
	H_2O 0.14	*Me*Br 0.19	*Et*Br 0.20	HCOOH 0.18	Isoprene 0.24
	CO_2 0.09	*Me*Cl 0.24	*Et*Cl 0.36	Benzene 0.28	Acrolein 0.24
Considerably above spectroscopic >0.30	φMe 0.41	φEt 0.35	φF 0.41	Trichlorethylene 1.15	

[a] The spectroscopic ionization potentials were taken mostly from the papers of W. C. Price and A. D. Walsh and their co-workers. For a summary of values see W. C. Price, Chem. Revs. **41**, 257 (1947); Hammond, Price, Teegan, and Walsh, Disc. Faraday Soc. **9**, 53 (1950). Values recalculated using the conversion factor 1 ev = 8067.5 wave numbers.

For example, the ionization potentials of the alkyl halides and chlorine lie in the range 12.8–10.9 ev, while those of the olefins range from 10.6–9.6 ev. The ionization potentials of the chloro-olefins lie around 10.0 ev, and it seems reasonable to assume, therefore, that the electron ionized from these molecules comes from the double bond.

Further discussion of the factors affecting the ease of removal of electrons in ionization, *viz.*, the electronegativity of the atoms present, the extent of the delocalization of the valence electrons, charge transfer, and the stability of the molecular ion, will be reserved for a later paper in this series.

ACKNOWLEDGMENT

The authors are indebted to Miss J. McKay for her assistance in the measurement of the data.

THE JOURNAL OF CHEMICAL PHYSICS VOLUME 20, NUMBER 6 JUNE, 1952

The Spatial Correlation of Electrons in Molecules

J. E. LENNARD-JONES
Department of Theoretical Chemistry, Cambridge, England
(Received February 12, 1952)

The wave functions of molecules in their ground states can be expressed to a good approximation as single determinants made up of terms orthogonal to each other. The probability distribution for such systems can then also be expressed as a determinant. By integrating this quantity over all the spatial and spin coordinates except those of two electrons, a function is obtained which gives in effect the probability of finding a pair of electrons in assigned places with assigned spins. The properties of this function, called for short the correlation function, are examined in some particular cases. It is shown that the electrons of an inert gas atom, like neon, tend to dispose themselves so that those of the same spin subtend tetrahedral angles at the nucleus. The six outer electrons of the nitrogen molecule and acetylene tend to the same approximation to arrange themselves so that those of the same spin are in three planes through the nuclear axis inclined at 120° to each other. Similarly the eight outer electrons of the same spin in carbon dioxide tend to be correlated with each other in such a way that there are four between the carbon and the oxygen nuclei and four at the extremities of the molecule, there being two on each oxygen atom like "lone electrons." In general the "bonds" of a molecule, when interpreted in terms of molecular orbitals, may be regarded as providing the appropriate correlation of electrons of the same spin.

1. INTRODUCTION

THE method of superposition of s and p atomic wave functions to give new wave functions with directed properties, due in the first place to Pauling[1] and Slater,[2] has proved to be of the greatest value in the theory of molecular structure. As first introduced by them, the method was valid only for one electron problems and, indeed, strictly only for the hydrogen atom, where s, p, and d wave functions have the same energy. The essential feature of the method was the construction of linear combinations of sets of wave functions of the same energy so as to produce new sets which were orthogonal to each other. It was then found that these new wave forms had localized properties which rendered them suitable for use in the theory of two interacting atoms by the Heitler-London method. It was assumed that similar hybridized functions could be used for atoms other than hydrogen, although the method was not strictly valid, on the grounds that the energy differences between s, p, and d functions were small compared with the energy changes occurring in the formation of chemical bonds. The relation of one bond to another terminating on the same atom was then tacitly assumed to be the same as that of the directed atomic wave functions constructed for that atom. It was thus the orthogonal property of these wave functions which provided the basis for the theory of directed valency.

A more general method of arriving at the concept of the directed properties of an atom is to represent its wave function as that of a many electron system. An atom such as carbon in its ^5S state, for example, is represented by a determinantal wave function, in which the component parts are s and p functions. It can be shown, as Artmann,[3] and Zimmerman and Van Rysselberghe[4] have done, that in the multi-dimensional space used to describe the coordinates of all the electrons there is a point at which the wave function has a maximum value. The position of the maximum corresponds to that configuration of the electrons for which the vectors joining the electrons to the nucleus in ordinary space are inclined to each other in a particular way. For carbon these vectors are along tetrahedral directions. This, in effect, provides a spatial correlation of electrons in an atom as a result of the exclusion principle, for the wave function is antisymmetric in the spatial coordinates, all the electrons being assumed to have the same spin. The method does not lend itself conveniently to systems containing electrons of opposite spin.

Another method of discussing the electron distribution in many electron systems has been given by the author,[5] and this is applicable to molecules as well as atoms. This method attempts not to give the relative positions of all the electrons simultaneously but rather to find the probability of finding two electrons (no matter which) in any prescribed configuration. This probability function was expressed in the first place in terms of molecular orbitals, but it was shown that its significance was more easily understood when the molecular orbitals were transformed to other orbitals with more localized properties, called equivalent orbitals. If each of these equivalent orbitals were strictly localized so that within a region ω its value were finite and outside it its value were zero, and if the ω regions of the different equivalent orbitals did not overlap, then the interpretation was simple. The arrangement of greatest probability is one in which the electrons so dispose themselves that when an electron is in one ω region, an electron of the same spin will only be found in one of the other ω regions. The properties of this correlation function are considered further in this paper and some examples are given of its interpretations in atoms and molecules.

For a complete electron shell, such as exists in neon, it becomes clear that electrons of the same spin tend to

[1] L. Pauling, J. Am. Chem. Soc. **53**, 1367 (1931).
[2] J. C. Slater, Phys. Rev. **37**, 481 (1931).
[3] K. Artmann, Z. Naturwiss. **1**, 426 (1946).
[4] H. K. Zimmerman and P. Van Rysselberghe, J. Chem. Phys. **17**, 598 (1949).
[5] J. E. Lennard-Jones, Proc. Roy. Soc. (London) **A198**, 14 (1949), paragraph 5.

dispose themselves in tetrahedral directions and in this respect behave like the electrons of methane. Of the six outer electrons of the nitrogen molecule and acetylene (the valency electrons) each set of three of the same spin tends to take up a relative configuration so that there is one in each of three planes through the nuclear axis inclined at 120° to each other. In general the "bonds" of a molecule may be regarded as providing the approximate correlation of electrons of the same spin. The method is illustrated by considering the structure of carbon dioxide, the wave functions of which have recently been worked out by Mulligan.[6]

2. THE CORRELATION FUNCTION

The wave equation for a molecule containing many electrons cannot be solved in explicit terms, but it has been found that for molecules, just as for atoms, a good approximation can be obtained by expressing the wave function in terms of functions of the coordinates of individual electrons. This means that the relative coordinates of the electrons are not introduced and, as the electrostatic interaction involves these coordinates, the assumed form of wave function can never be exact. But in practice it is found to be the best and simplest form of approximation. For molecules in their ground states the electron configuration usually corresponds to a set of complete electron shells (the oxygen molecule being one of the few exceptions), and the wave function can be expressed as a sum of products of functions each containing the coordinates of only one electron, in such a way that it takes the form of a determinant. This conforms to the exclusion principle, as is well known. When the spin factors are included, the wave function takes the form,

$$\psi=\det\{\psi_1(1)\alpha(\sigma_1)\psi_1(2)\beta(\sigma_2)\cdots\psi_p(N)\beta(\sigma_N)\}, \quad (2.01)$$

each function of the space coordinates ψ_p, usually now called an orbital, being multiplied once with an α-spin and once with a β-spin. Moreover, the orbitals can be taken to be orthogonal without loss of generality. The orbitals are then found so as to make the energy a minimum. Equations for the individual orbitals can be found by a variation method, as Fock did for atoms,[7] and the solution of these represents the optimum that can be achieved for the particular form of function (2.01).[8]

When $\bar{\psi}$ has been determined, the probability distribution of the electrons is given by

$$\bar{\psi}\psi d\tau_1\cdots d\tau_N=\det\{\sigma(i,j)\}d\tau_1\cdots d\tau_N, \quad (2.02)$$

where

$$\sigma(i,j)=\sum_{l=1}^{N}\bar{\phi}_l(i)\phi_l(j), \quad (2.03)$$

the functions ϕ_l consisting of one of the orbitals ψ_p and one of the spin factors. Since the forces operative in molecules involve only the relative coordinates of the electrons in pairs, it is sufficient for calculations of the average electrostatic energy to know the probability of finding simultaneously one electron in an element of volume $d\tau_1$ and another in an element of volume $d\tau_2$, the spin coordinate being included in each. This means that the other $(N-2)$ electrons may be anywhere, and so the required probability function is obtained by integrating (2.02) over the space and spin coordinates of all the electrons except two. This two-electron distribution function is found to be proportional to

$$\begin{vmatrix}\sigma(1,1) & \sigma(1,2)\\ \sigma(2,1) & \sigma(2,2)\end{vmatrix}d\tau_1 d\tau_2, \quad (2.04)$$

where

$$\sigma(j,k)=\rho^{\alpha}(j,k)\bar{\alpha}_j\alpha_k+\rho^{\beta}(j,k)\bar{\beta}_j\beta_k, \quad (2.05)$$

and the ρ^{α} is a summation similar to (2.03) over the occupied orbitals which have α-spin and ρ^{β} a similar summation over those with a β-spin. It is to be noted that the ρ functions contain only spatial coordinates.

If as usual the spin-orbit coupling is neglected, the spin coordinates can be varied independently of the space coordinates and for the same elements of space there are four possibilities concerning spin. The element of volume $d\tau_1$ may imply either a spin α or a spin β for electron 1, and independently $d\tau_2$ may imply either a spin α or a spin β for electron 2. When both electrons have a spin α the probability distribution (2.04) becomes

$$\{\rho^{\alpha}(1,1)\rho^{\alpha}(2,2)-\rho^{\alpha}(1,2)\rho^{\alpha}(2,1)\}dv_1dv_2, \quad (2.06)$$

the elements of volume now referring only to space. This result follows from the fact that $\alpha_1=1$, $\beta_1=0$, $\alpha_2=1$, $\beta_2=0$.

Similarly when the electrons have opposite spins, the distributions have one of the two forms,

$$\rho^{\alpha}(1,1)\rho^{\beta}(2,2)dv_1dv_2; \quad \rho^{\beta}(1,1)\rho^{\alpha}(2,2)dv_1dv_2. \quad (2.07)$$

When the two electrons each have β spin, the corresponding result is

$$\{\rho^{\beta}(1,1)\rho^{\beta}(2,2)-\rho^{\beta}(1,2)\rho^{\beta}(2,1)\}dv_1dv_2. \quad (2.08)$$

It is convenient to consider separately the cases of the singly and doubly occupied orbitals.

Case (A). Singly Occupied Orbitals

For a molecule (or atom) in which the outer orbitals are only singly occupied, each having the same spin, the probability distribution for these outer electrons is given by (2.06). If the occupied orbitals are expressed in real form, as they usually can in molecules, the distribution function can be written

$$P(1,2)=\rho^{\alpha}(1,1)\rho^{\alpha}(2,2)-\{\rho^{\alpha}(1,2)\}^2. \quad (2.09)$$

Now it is known from group theory that when the electrons of a molecule fill sets of complete shells (that

[6] J. S. Mulligan, J. Chem. Phys. **19**, 347 (1951).
[7] V. Fock, Z. Physik. **61**, 126 (1930).
[8] J. E. Lennard-Jones, Proc. Roy. Soc. (London) **A198**, 1 (1949).

is, when the orbitals which are occupied span complete sets of irreducible representations), the density-functions $\rho^\alpha(1, 1)$ and $\rho^\alpha(2, 2)$ have the complete symmetry of the molecule. Thus for atoms the completed shells have spherical symmetry and for diatomic molecules the completed shells have symmetry $D_{\infty h}$ or $C_{\infty v}$ according as the nuclei are similar or dissimilar.

Let us suppose that the density function $\rho^\alpha(1, 1)$ is plotted as a set of contours, on each of which it has a constant value. Then these contours will have the complete symmetry of the molecule. Let dv_1 be an element of volume bounded on two sides by two neighboring contours and dv_2 another element of volume bounded by two other neighboring contours. As these elements of volume are moved between their respective contours, the value of

$$\rho^\alpha(1, 1)\rho^\alpha(2, 2)$$

remains constant, and the variation in the probability function is caused by the second term

$$\{\rho^\alpha(1, 2)\}^2.$$

As this is always a positive quantity, the two-electron probability configuration is greatest when the latter quantity is least.

Now

$$\rho^\alpha(1, 2)=\sum_\iota \psi_\iota(1)\psi_\iota(2) \qquad (2.10)$$

and is a summation over all the occupied orbitals. Since the complete wave function has the form of a determinant (2.01), the individual orbitals of which it is composed can be changed by any *ortho*-norm transformation without altering the value of the determinant. Also, any such *ortho*-norm transformation leaves the value of $\rho(1, 2)$ unchanged. It is, therefore, a matter of convenience which set of orbitals are used in examining the properties of $\rho(1, 2)$. One possible set consists of molecular orbitals. These belong to the different irreducible representations appropriate to the symmetry type to which the molecule belongs. They spread throughout the molecule and are distinguished from one another by the nodal surfaces they possess. Consequently, it is not very easy to see from them what value $\rho(1, 2)$ takes for differing coordinates of electrons 1 and 2, since it consists of a summation over orbitals which may have finite values, either positive or negative, in any part of the molecule.

On the other hand, it is possible to derive from the molecular orbitals a set of functions with more localized properties. Examples of these have been given by the author[5,8] for molecules of particular types of symmetry. When they fall into sets such that within each the members are geometrically the same and differ only in orientation, they are called equivalent orbitals. In methane, for example, the eight electrons outside the K shell of the carbon atom can be regarded as in four molecular orbitals, one having the full tetrahedral symmetry, the other three each having a node between pairs of hydrogen nuclei and each having the same energy. Alternatively, they can be regarded as in four equivalent orbitals, each of which embraces one hydrogen nucleus and the carbon nucleus, and corresponds to what is ordinarily described as a chemical bond. The latter orbitals are more localized then the molecular orbitals from which they are derived.

We suppose, then, that a set of orbitals has been obtained with the maximum properties of localization and yet still expressible as an orthonorm transformation of molecular orbitals. If these be labeled $\chi_1, \chi_2, \cdots \chi_\lambda$, the value of $\rho^\alpha(1, 2)$ is given by

$$\rho^\alpha(1, 2)=\sum_\lambda \chi_\lambda(1)\chi_\lambda(2). \qquad (2.11)$$

This implies that, if dv_1 be in a region where χ_λ has a large value, then $\chi_\mu(1)$ is small for every other orbital and the contribution to $\rho^\alpha(1, 2)$ comes mainly from one term $\chi_\lambda(1)\chi_\lambda(2)$. (This can be seen most easily by considering the ideal case in which each orbital χ_λ is confined to a finite region ω_λ and does not overlap any other. Then if dv_1 lies in ω_λ, the value of $\chi_\lambda(1)$ is finite and $\chi_u(1)$ is zero for every other orbital.)

If the location of dv_2 be then varied, as above described, along a contour of constant density, the factor $\chi_\lambda(2)$ will change and will become smallest when dv_2 is in a region where another orbital, say χ_μ, is strong. This suggests that $\rho^\alpha(1, 2)$ will be smallest when electrons 1 and 2 are so disposed that each is in the dense region of a different orbital. The probability function $P(1, 2)$ is then largest when two electrons are in different localized orbitals and this indicates the degree of spatial correlation between any pair of electrons. For this reason this function may conveniently be referred to as the space-correlation function.

Case (B). Doubly Occupied Orbitals

When the orbitals of a molecule are doubly occupied, as is usually the case for molecules in their ground states, it is necessary to consider separately the functions (2.06), (2.07), and (2.08). It appears that the electrons with α-spin are correlated among themselves by (2.06) just like electrons in singly occupied orbitals. The electrons with β-spin are similarly correlated among themselves by (2.08), which has properties similar to (2.06). The electrons with α spin are related to those with β-spin by (2.07). Now the latter function contains only $\rho(1, 1)$ and $\rho(2, 2)$, each of which has the complete symmetry of the molecule. There is thus no correlation between electrons of different spin for a wave function of type (2.01); for the elements of volume dv_1 and dv_2 may be anywhere on the density contour $\rho(1, 1)$ and $\rho(2, 2)$ without altering the value of the correlation function.

The probability of finding an electron in a volume element dv_1 and another in a volume element dv_2, irrespective of their spins, is the sum of (2.06), (2.07), and (2.08), *viz.*,

$$\mathbf{P}(1, 2)=\{\rho^\alpha(1, 1)+\rho^\beta(1, 1)\}\{\rho^\alpha(2, 2)+\rho^\beta(2, 2)\} -\{\rho^\alpha(1, 2)\}^2-\{\rho^\beta(1, 2)\}^2. \qquad (2.12)$$

3. EXAMPLES OF SPATIAL CORRELATION

(A) Carbon in the ^5S State

Carbon in the ^5S state is usually represented by a configuration in which the $2s$ orbital and each of the three $2p$ orbitals are occupied by electrons of the same spin. These orbitals, when written in the approximate Slater form, have a dependence on space coordinates given by

$$f(r),\quad f(r)\sqrt{3}\cos\theta,\quad f(r)\sqrt{3}\sin\theta\sin\phi,\quad f(r)\sqrt{3}\sin\theta\cos\phi,\qquad(3.01)$$

where $f(r)$ is written for

$$f(r)=N_r r\exp(-Zr),\qquad(3.02)$$

N_r being a normalization factor. The numerical factor $\sqrt{3}$ in the p functions is introduced to secure normalization of the angular parts. The correlation function is then given by (2.09) and for the s, p functions it becomes

$$P(1,2)=\{f(r_1)f(r_2)\}^2\{16-(1+3\cos\theta_{12})^2\},\qquad(3.03)$$

where θ_{12} is the angle between r_1 and r_2. It is to be noted that this vanishes when $\theta_{12}=0$, implying that electrons of the same spin do not occupy the same space at the same time. This is the form the exclusion principle takes for electrons of the same spin. The function $P(1,2)$ has its minimum value when $\cos\theta_{12}=-1/3$, that is when r_1 and r_2 are inclined at the tetrahedral angle. There is thus a maximum probability that the electrons so dispose themselves that they subtend tetrahedral angles at the nucleus.

It happens that in the above simple examples the correlation of the electrons can be derived directly from the use of s and p functions, these corresponding to the molecular orbitals in more general systems. It is instructive to transform to equivalent orbitals and to derive similar results from them because this procedure illustrates the method described above for more complex systems. The equivalent orbitals to be used in

$$\rho^\alpha(1,2)=\sum_\lambda\chi_\lambda(1)\chi_\lambda(2)$$

are now the familiar tetrahedral hybridized orbitals of the form

$$\chi_\lambda=\tfrac{1}{2}(s+\sqrt{3}p_\lambda)=\tfrac{1}{2}f(r)(1+3\cos\theta_\lambda),$$

where p_λ has its axis along one of the tetrahedral directions, and θ_λ is measured from that axis. The orbital χ_λ has a node in the cone given by $\cos\theta_\lambda=-1/3$ and this cone contains the axes of the other three equivalent orbitals. It follows at once that $\rho^\alpha(1,2)$ is zero whenever dv_1 is on the axis of one equivalent orbital and dv_2 is on the axis of another. This illustrates the statement made above for the general case that when dv_1 is near the maximum of an equivalent-orbital χ_λ and dv_2 is near the maximum of another one χ_μ, then $\chi_\lambda(1)\chi_\lambda(2)$ and $\chi_\mu(1)\chi_\mu(2)$ will both be small.

The use of Slater functions, as in (3.01), does not give the spatial correlation correctly because the same radial factor $f(r)$, as given in (3.02), is used for both s and p functions. A more general representation of the functions would lead to the result that the value of θ_{12}, for which the correlation function has its maximum value, depends on r_1 and r_2. The radial and angular distributions are then correlated.

(B) Inert Gas Like Atoms (Ne, Na^+, Cl^- ⋯)

In an inert gas atom there is a closed shell of electrons of the type $(ns)^2$, $(np)^6$. The correlation of the α-spins among themselves is given (for Slater functions) by

$$P^\alpha(1,2)=\{f(r_1)f(r_2)\}^2\{16-(1+3\cos\theta_{12}{}^\alpha)^2\},\qquad(3.06)$$

and there is a similar correlation function $P^\beta(1,2)$ containing an angle $\theta_{12}{}^\beta$ for the electrons of β-spins. There is no correlation between the electrons of α-spin and those of β-spin, since the probability function has the form

$$P^{\alpha\beta}(1,2)=16\{f(r_1)f(r_2)\}^2=P^{\beta\alpha}(1,2).\qquad(3.07)$$

The electrons of each kind of spin tend to take up a tetrahedral configuration among themselves but there is no correlation between the two tetrahedra to the approximation implied by the form of (2.01).

(C) Molecules with Triple Bonds (N_2, C_2H_2)

A molecule such as acetylene has six electrons associated with the carbon-carbon bond, usually assigned to orbitals $\sigma_g{}^2$, $\pi_{xu}{}^2$, $\pi_{yu}{}^2$. These orbitals may be represented approximately by functions

$$f(\rho),\quad f(\rho)\sqrt{2}\cos\phi,\quad f(\rho)\sqrt{2}\sin\phi,\qquad(3.08)$$

where $f(\rho)$ is some function of position relative to the nuclei. The same factor is assigned to each by analogy with the Slater atomic functions, used in (3.07). Then,

$$P^\alpha(1,2)=\{f(\rho_1)f(\rho_2)\}^2\{9-(1+2\cos\phi_{12})^2\},\qquad(3.09)$$

where ϕ_{12} is the angle between the azimuthal planes containing the two electrons. This function has a maximum when $\phi_{12}=120°$. The electrons with β-spin are correlated in a similar way. As in the previous example the members of the α-set are not correlated with the members of the β-set (to the same approximation as before).

Thus we have a picture of a triple bond in which the electron density in three-dimensional space has axial symmetry, but the electrons participating in the bond tend to arrange themselves so that those of the same spin are in azimuthal planes making an angle of 120° with each other. This concept gives some point to the picture adopted by chemists of three equivalent bent-springs to represent the triple bonds of acetylene and nitrogen, but it should be generalized to allow for two sets of bent-springs, one for each set of electrons of the same spin.

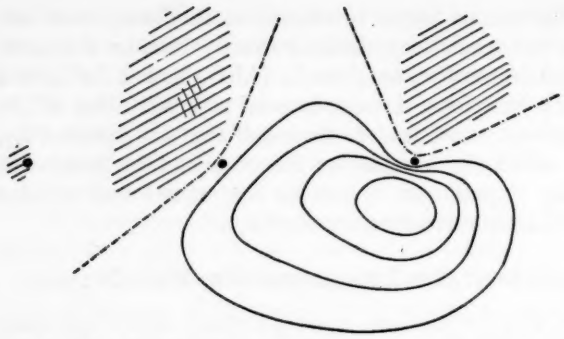

FIG. 1. An equivalent "bond" orbital of carbon dioxide.

(D) Symmetrical Triatomic Molecule (Carbon Dioxide)

An instructive example of the value of equivalent orbitals is provided by carbon dioxide. Recently the structure of this molecule has been calculated by Mulligan[6] by the use of molecular orbitals. These are represented as linear combinations of atomic orbitals in the usual way, the coefficients being determined so as to make the energy a minimum. At the same time the equations which the orbitals must satisfy are rendered as self consistent as possible. The outer sixteen electrons are assigned in pairs to four orbitals of the σ-type and four of the π-type, the former being labeled as $1\sigma_g$, $2\sigma_g$, $1\sigma_u$, $2\sigma_u$, and the latter as $1\pi_u$, $1\pi_g$, $1\pi_u^*$, $1\pi_g^*$. The π-orbitals are degenerate in pairs, π_u and π_u^* for example being equivalent but having their planes of symmetry at right angles to each other. The wave function of the electrons is expressed as a determinant containing these eight functions, each being associated with an α-spin and a β-spin.

Mulligan's results can be used to construct equivalent orbitals for the eight occupied orbitals, but there is a certain flexibility in doing this because there are two orbitals of the same symmetry type σ_g and two of σ_u. Thus we can use any unitary transform of these functions

$$(\sigma_g)_a = \cos\epsilon_a(1\sigma_g)+\sin\epsilon_a(2\sigma_g),$$
$$(\sigma_g)_a' = -\sin\epsilon_a(1\sigma_g)+\cos\epsilon_a(2\sigma_g),$$
$$(\sigma_u)_b = \cos\epsilon_b(1\sigma_u)+\sin\epsilon_b(2\sigma_u),$$
$$(\sigma_u)_b' = -\sin\epsilon_b(1\sigma_u)+\cos\epsilon_b(2\sigma_u),$$

and then construct two sets of equivalent orbitals in the form

$$\chi_1 = 1/\sqrt{2}\{(\sigma_g)_a+(\sigma_u)_b\}, \quad \chi_1' = 1/\sqrt{2}\{(\sigma_g)_a-(\sigma_u)_b\},$$
$$\chi_2 = 1/\sqrt{2}\{(\sigma_g)_a'+(\sigma_u)_b'\}, \quad \chi_2' = 1/\sqrt{2}\{(\sigma_g)_a'-(\sigma_u)_b'\}.$$

There are thus two degrees of freedom, the values of ϵ_a and ϵ_b being arbitrary, and these can be determined to produce the greatest degree of localization. For this purpose the values were found which gave the best lone pair orbital, one at each end of the molecule, in the sense that the sum of the coefficients of the s and p atomic orbitals of one of the oxygen atoms was as large as possible. This was found to be given very nearly by $\epsilon_a=\epsilon_b=\pi/2$, so that the lone pairs are given approximately by $\sigma_l=1/\sqrt{2}(2\sigma_g+2\sigma_u)$, $\sigma_l'=1/\sqrt{2}(2\sigma_g-2\sigma_u)$. The other equivalent pair are then obtained by a similar combination of $(1\sigma_g)$ and $(1\sigma_u)$ as

$$\sigma = 1/\sqrt{2}(1\sigma_g-1\sigma_u),$$
$$\sigma' = 1/\sqrt{2}(1\sigma_g+1\sigma_u).$$

These sets of σ-orbitals can next be combined with the π-orbitals to four equivalent 'bond' orbitals and four equivalent 'lone pair' orbitals. Thus the former can be written as

$$\tau_x = 1/\sqrt{2}(\sigma+\pi_{ux}), \quad \tau_x' = 1/\sqrt{2}(\sigma-\pi_{ux}),$$
$$\tau_y = 1/\sqrt{2}(\sigma'+\pi_{uy}), \quad \tau_y' = 1/\sqrt{2}(\sigma'-\pi_{uy}).$$

These τ-functions have the same distribution in space and can be obtained from one another by rotation and displacement. A typical member of the set is shown in Fig. 1. This shows the contours of equal values of the wave function, the outer one having a value 0.1 and the inner one a value of 0.4. The contours are, of course, sections of closed surfaces. The dotted lines correspond to the nodal surfaces and beyond them the value of the wave function has the opposite sign. The absolute value of the wave functions in these regions does not reach the value 0.1 and for this reason the regions of low negative values are shown by hatching.

τ_x and τ_x' have their maxima in the same plane and are closely associated with the carbon and one of the oxygens; τ_y and τ_y' are similar distributions but have their maxima in a plane at right angles to that of the other two. They are associated with the carbon and the other oxygen. It is to be understood, of course, that the x and y planes represent relative directions within the molecule and not absolute directions. Interaction of the system with another molecule might, however, localize these planes.

Similarly, the lone pair sets of σ-orbitals can be combined with the π_g-orbitals to give

$$\lambda_x = 1/\sqrt{2}(\sigma_l+\pi_{xg}), \quad \lambda_x' = 1/\sqrt{2}(\sigma_l-\pi_{xg}),$$
$$\lambda_y = 1/\sqrt{2}(\sigma_l'+\pi_{yg}), \quad \lambda_y' = 1/\sqrt{2}(\sigma_l'-\pi_{yg}).$$

The members of this set are related to each other like those of the τ-set, but the two orbitals associated with any one oxygen atom have their maxima in a plane at right angles to the two τ-orbitals associated with that oxygen.

A typical λ-orbital is shown in Fig. 2. The continuous lines give the contours where the wave function has the values 0.1 to 0.5 and the broken line shows a nodal surface. Within the nodal surface the wave function does not reach the value 0.1. On the remote side of the carbon nucleus there is a small region where the wave function has a finite but small value. The main concentration of the wave function is seen to be beyond the nuclear axis. The τ- and λ-orbitals may now be used in the correlation function, defined above, to obtain some idea of the dis-

tribution of the electrons relative to each other in CO_2. The orbitals are seen to be quite well localized and not to overlap each other seriously. This means that when an electron of specified spin is in the region where one of these orbitals has large values, there is a strong probability that another electron of the same spin will be found in the region of one of the other orbitals. On this view the CO_2 molecule may be pictured as having two electrons of one kind of spin in λ-orbitals at each end of the molecule, the plane of the orbitals at one end being perpendicular to those at the other. There are also two electrons of the same spin in equivalent τ-orbitals between the carbon and each oxygen atom. The correlation of electrons of the same spin thus gives to the molecule a skew structure, two electrons being alternatively in planes at right angles to each other. Since the molecule has an axis of symmetry, these planes are not defined uniquely and the electron configuration in ordinary space is axially symmetric. It is only the relative distributions of the electrons that have the skew arrangement described.

The set of electrons of the other kind of spin have a similar skew structure but owing to the axial symmetry of the nuclear field there is no correlation between the two sets of electrons (this again being a result of (2.07) and (2.01)).

There are some features of this picture of carbon dioxide of particular interest. One is that each atom is surrounded by eight electrons in accord with the concept of completed octets, used originally by Lewis and Langmuir.[9] The eight electrons surrounding the carbon each participate in a "bond." In the language of paired electrons this means that there are four "bonds" terminating on the carbon. The picture obtained in this paper is a little different, because the eight electrons should be regarded as forming eight "one-electron-bonds" (or half-bonds). These fall into two sets of four which are not correlated to one another because of their opposite spins. The electron distribution, as given by τ- and λ-orbitals, thus gives some support for the usual structural formula O=C=O.

Further it is to be noted that the regions of greatest concentration of the electrons are nearer to the oxygen than to the carbon. This corresponds to the property of the oxygen usually described as its electron affinity, this being greater than that of the carbon. The region of the oxygen is electron rich, that of the carbon is electron deficient. An oversimplified version of the distribution would be to say that the structure of CO_2 is $O^{--}C^{+4}O^{--}$.

Another point of interest is that there are four electrons at each end of the molecule, projecting away from the nuclear axis. These correspond to what are usually called "lone pairs."

From the distribution of charges given by the τ- and λ-orbitals a rough electrostatic model of the molecule could be constructed by placing electrons at certain average positions and this might be useful in calculating the interaction of one CO_2 molecule with another, or with a different molecule which was electrophilic or protophilic.

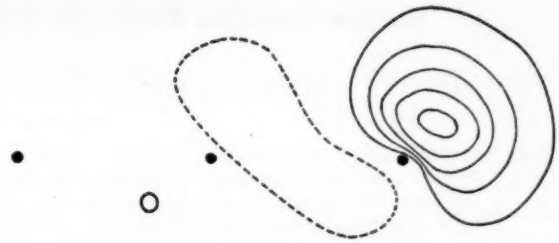

FIG. 2. An equivalent "lone pair" orbital for carbon dioxide.

(E) Asymmetric Molecules

The examples so far discussed have one feature in common in that the electron density functions denoted by $\rho(1, 1)$ all have axial symmetry about one or more axes. This led to the result that the density function of the electrons of α-spin could be rotated relative to that of the electrons of β-spin without observable change. But this only occurs for atoms with complete shells or for linear molecules. In a triangular molecule such as water the density function ρ^α is the same as ρ^β and the location of each is fixed by the nuclear field. This implies that the same set of equivalent orbitals must be used for the two kinds of spins. Whereas in carbon dioxide, for example, the nonbonding electrons assigned to λ-orbitals were correlated if they had the same spin, but were otherwise uncorrelated, the electrons of water have to be assigned in pairs to the same set of orbitals, whether these are the bonding or nonbonding types. In water two of the equivalent orbitals correspond to the OH chemical bonds and the other two to the lone pairs of electrons. The distribution of the latter has been discussed by Lennard-Jones and Pople.[10] The lone pairs of electrons in carbon dioxide may be regarded as distributed with axial symmetry at the end of the molecule, but those of water appear to be concentrated in a plane at right angles to the plane of the OH bonds.

The author is indebted to the members of the Conference on Molecular Structure at Shelter Island (September, 1952), particularly to Professor Joseph E. Mayer, for remarks which helped to clarify the ideas presented in this paper. He also is indebted to Mr. P. P. Manning, Department of Theoretical Chemistry, Cambridge, for drawing the figures illustrating the equivalent orbitals of carbon dioxide and for making the necessary calculations.

[9] G. N. Lewis, J. Am. Chem. Soc. **38**, 762 (1916). J. Langmuir, J. Am. Chem. Soc. **54**, 3876 (1919).

[10] J. E. Lennard-Jones and J. A. Pople, Proc. Roy. Soc. (London) **205**, 155 (1951).

On the Reaction Field and Dielectric Constant of Polar Liquids

D. G. Frood and A. J. Dekker
*Department of Physics, University of British Columbia, Vancouver, Canada**

(Received October 29, 1951)

It is shown that Onsager's formula for the dielectric constant of liquids, derived on the assumption of spherical molecules and a central mathematical dipole, still holds for extended dipoles of arbitrary position and direction as long as the molecules are spherical in shape.

I. INTRODUCTION

A THEORY of the dielectric constant of polar liquids has been developed by Onsager[1] on the basis of a simple molecular model. In this model the molecules are assumed to be spheres filled with a homogeneous substance representing the polarizability and bearing a mathematical dipole at the center. The substance outside a particular sphere under consideration is assumed to be homogeneous and characterized by the macroscopic dielectric constant of the sample. The essential point of Onsager's theory is the introduction of the reaction field of a dipole. The theory has been extended by Böttcher,[2] who also applied the resulting expression for the dielectric constant in terms of the polarizability and dipole moment of the molecules to a large number of experimental data on pure liquids and mixtures. The results are remarkably satisfactory in that the calculated dipole moments are sufficiently independent of temperature and concentration and in good agreement with values determined from measurements on gases.

It therefore seems interesting to investigate the possible influence of changes in the model on the final Onsager-Böttcher formula. As has been shown by one of us[3] before, no change results from assuming an excentric mathematical dipole of radial direction rather than one in the center of the spherical molecule. In the present paper it will be shown that even for an extended dipole of arbitrary position and direction the Onsager-Böttcher formula still holds, assuming the molecules are spherical in shape.

It may be interesting to note that ellipsoidal shapes have been investigated by Scholte.[4] The more general theory of the dielectric constant of liquids developed by Kirkwood[5] should also be mentioned. It allows the introduction of short-range forces, which are completely neglected in the other papers referred to and in the present one. However, if one wants to derive from Kirkwood's formula a relation between the dielectric constant of the liquid and the dipole moments of the composing molecules in the gaseous state, the problem discussed here cannot be left aside.

In view of the proof given below it is necessary to review briefly the work of Onsager and Böttcher. For the present purpose it seems most convenient to follow closely the presentation of the latter author.

II. THE ONSAGER-BÖTTCHER THEORY

Consider a spherical cavity of radius R inside a homogeneous substance with dielectric constant ϵ_0. When a rigid mathematical dipole $\mathfrak{y}$ is located at the center of the sphere, the field inside the cavity consists of the dipole field and a superimposed homogeneous field, the "reaction field." According to Onsager, the reaction field is given by

$$\mathbf{E}_r=\frac{1}{R^3}\cdot\frac{2(\epsilon_0-1)}{2\epsilon_0+1}\mathfrak{y}\equiv f\cdot\mathfrak{y}. \tag{1}$$

The dipole polarizes the substance ϵ_0 outside the cavity and this in turn produces the reaction field inside the sphere. If the dipole is not located at the center, the reaction field is of course inhomogeneous and (1) has no immediate relevance to that case.

Consider now a "molecule" represented by a sphere of a homogeneous substance ϵ_i bearing a dipole $\mathfrak{y}$ at its center. The dipole moment of such a molecule may easily be shown to be equal to[6]

$$\mathfrak{y}_0=3\mathfrak{y}/(\epsilon_i+2). \tag{2}$$

When this molecule is embedded in a homogeneous dielectric ϵ_0, the reaction field is evidently given by

$$\mathbf{E}_r=f(\mathfrak{y}_0+\alpha\mathbf{E}_r)=\frac{f}{1-\alpha f}\mathfrak{y}_0, \tag{3}$$

where the polarizability α is determined by ϵ_i, according to the relation of Clausius-Mosotti,

$$\frac{\alpha}{R^3}=\frac{\epsilon_i-1}{\epsilon_i+2}. \tag{4}$$

The dipole moment is thus increased by an amount $\alpha\mathbf{E}_r$ leading to the factor $f/(1-\alpha f)$, which accounts

* The authors are indebted to the Defence Research Board of Canada, Ottawa, for a grant in aid and permission to publish the results obtained.

[1] L. Onsager, J. Am. Chem. Soc. **58**, 1486 (1936).
[2] C. J. F. Böttcher, thesis (Leiden, 1940); Physica **5**, 635 (1938); **6**, 59 (1939); **9**, 937 (1942).
[3] A. J. Dekker, Physica **12**, 209 (1946).
[4] T. G. Scholte, Physica **15**, 437 (1949).
[5] J. G. Kirkwood, J. Chem. Phys. **4**, 592 (1936); **7**, 911 (1939); **8**, 205 (1940).
[6] H. Frölich, *Theory of Dielectrics* (Oxford University Press, London, 1949), p. 166.

for the fact that the dipole moment of a molecule in the liquid is actually larger than that in the gaseous state.

Coming now to the actual problem, let us consider a mixture of liquids containing N_k molecules of component k and subject to a homogeneous external field $\mathbf{E}$. The polarizability of the molecules is denoted by α_k, the electric dipole moment in the gaseous state by $\mathfrak{y}_{gk}$. The problem then is to calculate the electric moment per unit volume P in the direction of the external field $\mathbf{E}$. Let us focus attention on a particular molecule of type k on the basis of the Onsager model. Part of the contribution of this molecule to P is a consequence of the moment induced in it by the presence of the external field. To calculate this contribution, one would have to know the field in which it finds itself, i.e., the "local field." Let us therefore remove the molecule from the liquid, *leaving the state of the surrounding dielectric unchanged*. The field in the spherical cavity thus created is the the local field. Obviously, part of the local field is due to the reaction field of the dipole $\mathfrak{y}_{gk}$. This part then will have the direction of $\mathfrak{y}_{gk}$ before removal and thus a component in the direction $\mathbf{E}$ equal to $E_{rk}\cos\phi_k$, where E_{rk} is given by (3) and ϕ_k is the angle between $\mathfrak{y}_{g\kappa}$ and $\mathbf{E}$. The time-average of this component is thus $E_{rk}\langle\cos\phi_k\rangle$. The remaining part of the local field is clearly determined by the molecule without dipole, i.e., by the polarizability alone. It may be calculated as follows.

Suppose the molecule k is removed from the liquid *allowing the surrounding dielectric* ϵ_0 *to adapt itself to the new situation*. The field inside the cavity is then, according to simple electrostatics,

$$\mathbf{E}_c=3\epsilon_0\cdot\mathbf{E}/(2\epsilon_0+1), \tag{5}$$

where $\mathbf{E}_c$ is independent of the radius of the sphere and known as the "cavity field." Filling the cavity with a homogeneous substance, such that the polarizability of the sphere is α_k, will change the polarized state of the dielectric ϵ_0. Fixing the new charge distribution and removing the substance from within the sphere again then leads to a field which is different from the cavity field, say $\mathbf{E}_{dk}$. It is obvious that $\mathbf{E}_{dk}$ is larger than $\mathbf{E}_c$ by an amount equal to the reaction field of a dipole of magnitude $\alpha_k\mathbf{E}_{dk}$. Hence

$$\mathbf{E}_{dk}=\mathbf{E}_c+f_k\alpha_k\mathbf{E}_{dk}. \tag{6}$$

It should be noted that $\mathbf{E}_{dk}$ is a homogeneous field in the direction $\mathbf{E}$. From (1) and (4) follows

$$E_{dk}=\frac{(\epsilon_{ik}+2)\epsilon_0}{\epsilon_{ik}+2\epsilon_0}\cdot E. \tag{7}$$

We have thus considered two contributions to the component of the local field in the direction of the external field; the first one depended on the polarizable dipole $\mathfrak{y}_{gk}$, the second one on the polarizability alone. As there are no other contributions in the present model, it follows that the component of the local field in the direction of $\mathbf{E}$ is given by

$$E_{lk}=E_{dk}+E_{rk}\cdot\langle\cos\phi_k\rangle=E_{dk}+\frac{f_k}{1-\alpha_k f_k}\cdot\mu_{gk}\langle\cos\phi_k\rangle, \tag{8}$$

and thus the average moment induced in the molecule in the direction of the external field is equal to $\alpha_k E_{lk}$.

The orientation of the dipole $\mathfrak{y}_{gk}$ under influence of the external field is the next contribution to P to be considered. To calculate this, it is necessary to know the field that tends to orientate the dipole. This field is obviously not equal to the local field component, because that part of the local field which is due to the reaction field of the dipole, does not produce any orientation (it has the same direction as the dipole $\mathfrak{y}_{gk}$!). From the considerations given above it is immediately clear that the field tending to orientate the dipole in the direction of $\mathbf{E}$ may be identified with E_{dk}. This field has been named the "directing field" by Böttcher. Now, as long as $\mu_{gk}\cdot E_{dk}\ll kT$, Langevin's theory gives

$$\langle\cos\phi_k\rangle=\mu_{gk}E_{dk}/3kT, \tag{9}$$

so that the moment per unit volume may finally be written as

$$P=\frac{\epsilon-1}{4\pi}E=\sum_k N_k\left(\alpha_k E_{lk}+\frac{\mu_{gk}^2}{3kT}E_{dk}\right), \tag{10}$$

which, upon substitution of (7) and (8), leads to the Onsager-Böttcher formula for a mixture of liquids.

III. THE PRESENT PROBLEM

From the presentation given above, it follows that the directing field E_{dk}, determined by (7), is completely independent of the nature of the dipole. In other words, for spherical molecules containing two separate charges $+q$ and $-q$ of arbitrary position rather than a mathematical dipole in the center, the directing field is still given by (7). Also, the second terms in the sum (10) will remain unchanged under these circumstances. However, the reaction field of such a system, and therefore the local field, is no longer homogeneous. Hence, the moment induced in the molecules should be obtained by taking the average of the local field over the volume of the spherical molecule, multiplied by the polarizability. Thus, if the reaction field averaged over the volume of the sphere is still given by (3), formulas (8) and (10) will still be valid. This is shown below.

IV. THE ELECTROSTATIC PROBLEM

Consider a dipole $\mathfrak{y}$ formed by two charges $+q$ and $-q$, a distance d apart, with arbitrary position inside a sphere of radius R as shown in Fig. 1. The coordinate system is chosen in such a manner that the line joining the center of the sphere and the midpoint of d is taken as z axis. The dipole lies in the xz plane. The dielectric constants of the homogeneous substances inside and

outside the sphere are ϵ_i and ϵ_0, respectively. As spherical coordinates we shall introduce r, θ, and ϕ. The potential V_0 outside the sphere may then be written as

$$V_0=\sum_{n=0}^{\infty}\sum_{m=0}^{n}\frac{B_{mn}}{r^{n+1}}P_n^m(\cos\theta)\cos m\phi, \tag{11}$$

where

$$P_n^m(\cos\theta)\equiv\sin^m\theta\frac{d^m}{d(\cos\theta)^m}\{P_n(\cos\theta)\}.$$

The potential V_i inside becomes

$$V_i=V_{\text{dipole}}+\sum_{n=0}^{\infty}\sum_{m=0}^{n}A_{mn}r^nP_n^m(\cos\theta)\cos m\phi, \tag{12}$$

where

$$V_{\text{dipole}}=\frac{q}{\epsilon_i}\left(\frac{1}{\rho_2}-\frac{1}{\rho_1}\right). \tag{13}$$

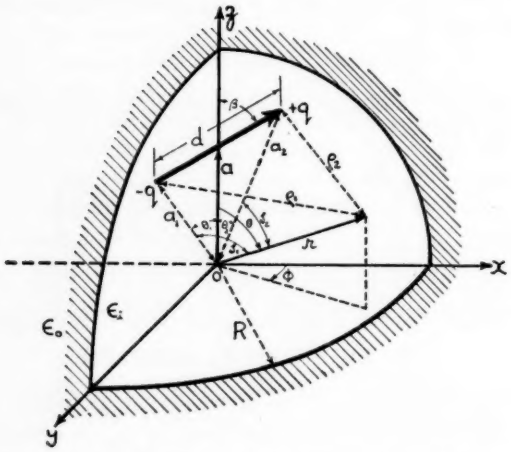

FIG. 1. The geometry of the electrostatic problem.

The first problem is to express the dipole potential in Legendre polynomials, which may be achieved in the following way:

$$\rho_1^{-1}=(a_1^2+r^2-2a_1r\cos\zeta_1)^{-\frac{1}{2}}=\sum_0^{\infty}\frac{a_1^n}{r^{n+1}}P_n(\cos\zeta_1) \tag{14a}$$

$$\rho_2^{-1}=(a_2^2+r^2-2a_2r\cos\zeta_2)^{-\frac{1}{2}}=\sum_0^{\infty}\frac{a_2^n}{r^{n+1}}P_n(\cos\zeta_2). \tag{14b}$$

According to the addition formula for Legendre polynomials we have for two lines passing through the origin with polar and azimuthal angles θ_1, ϕ_1 and θ_2, ϕ_2, respectively.

$$P_n(\cos\zeta)=\sum_{m=0}^{n}(2-\delta_{m0})\frac{(n-m)!}{(n+m)!}\times P_n^m(\cos\theta_1)\cdot P_n^m(\cos\theta_2)\cos m(\phi_1-\phi_2),$$

where ζ is the angle between the lines and $\delta_{m0}=1$ for $m=0$ and zero for $m\neq0$. Applying this to a_1,r and a_2,r we obtain

$$P_n(\cos\zeta_1)=\sum_{m=0}^{n}(2-\delta_{m0})\frac{(n-m)!}{(n+m)!}P_n^m(\cos\theta_1)P_n^m(\cos\theta)\cos m(\pi-\phi)$$

$$P_n(\cos\zeta_2)=\sum_{m=0}^{n}(2-\delta_{m0})\frac{(n-m)!}{(n+m)!}\times P_n^m(\cos\theta_2)P_n^m(\cos\theta)\cos m\phi.$$

Substitution into (14a) and (14b) then leads to

$$V_{\text{dipole}}=\frac{q}{\epsilon_i}\sum_{n=0}^{\infty}\sum_{m=0}^{n}\frac{C_{mn}}{r^{n+1}}P_n^m(\cos\theta)\cos m\phi \tag{15}$$

with

$$C_{mn}=(2-\delta_{m0})\frac{(n-m)!}{(n+m)!}\times[a_2^nP_n^m(\cos\theta_2)-(-1)^ma_1^nP_n^m(\cos\theta_1)]. \tag{16}$$

One finds, for example: $C_{00}=0$, $C_{01}=d\cdot\cos\beta$, $C_{11}=d\cdot\sin\beta$, $C_{02}=2ad\cdot\cos\beta$, $C_{22}=0$, etc.

The boundary conditions to be satisfied by V_0 and V_i are

$$V_0=V_i \quad \text{for} \quad r=R \tag{17}$$

$$\epsilon_i\frac{\partial V_i}{\partial r}=\epsilon_0\frac{\partial V_0}{\partial r} \quad \text{for} \quad r=R. \tag{18}$$

Substitution of (11), (12), and (15) into these expressions leads for the coefficients A_{mn} and B_{mn} to

$$A_{mn}=\frac{C_{mn}}{R^{2n+1}}\cdot\frac{q(n+1)(1-\epsilon_0/\epsilon_i)}{n\epsilon_i+(n+1)\epsilon_0} \tag{19}$$

$$B_{mn}=C_{mn}\cdot\frac{q(2n+1)}{n\epsilon_i+(n+1)\epsilon_0}. \tag{20}$$

V. THE DIPOLE MOMENT IN THE GASEOUS STATE

To find the dipole moment of the "molecule" in the gaseous state, we put $\epsilon_0=1$ in the electrostatic problem solved in the previous section. The potential outisde the sphere is then equal to

$$(V_0)_{\epsilon_0=1}=\frac{3\mu}{(2+\epsilon_i)r^2}[\cos\beta\cos\theta+\sin\beta\sin\theta\cos\phi]+\frac{5\mu a}{(3+2\epsilon_i)r^3}[\cos(3\cos^2\theta-1)+\sin\beta(3\sin\theta\cos\theta)\cos\phi]+\cdots. \tag{21}$$

The first term of this series is a dipole potential and the distance a does not occur in this term. From the ge-

ometry of the system it is easy to see that this term corresponds to a dipole moment in the gaseous phase $\mathfrak{y}_g$ equal to

$$\mathfrak{y}_g=\frac{3}{2+\epsilon_i}\mathfrak{y}, \tag{22}$$

an expression identical with (2). We may note that ϵ_i is equal to the square of the index of refraction of the molecule.

VI. THE REACTION FIELD

In the electrostatic problem dealt with in Sec. IV, the polarized state of the substance outside the sphere, due to the presence of $\mathfrak{y}$ and ϵ_i, is determined by the coefficients B_{mn} in (11). Suppose the charge distribution outside is fixed, i.e., the coefficients B_{mn} are kept constant. The reaction field is then defined as the field existing in the cavity after removal of $\mathfrak{y}$ and ϵ_i. Writing, as a consequence of (19) and (20),

$$A_{mn}=\left(1-\frac{\epsilon_0}{\epsilon_i}\right)\left(\frac{n+1}{2n+1}\right)\cdot\frac{1}{R^{2n+1}}B_{mn}, \tag{23}$$

we obtain for the potential of the reaction field V_r

$$V_r=\sum_{n=0}^{\infty}\sum_{m=0}^{n}(1-\epsilon_0)\left(\frac{n+1}{2n+1}\right)\frac{B_{mn}}{R^{2n+1}} \times r^n P_n^m(\cos\theta)\cos m\phi \tag{24}$$

($\epsilon_i=1$ in the first term of (23) because we are interested in the field in a cavity). It is convenient to introduce a coefficient A' given by

$$A_{mn}'=(\epsilon_0-1)\left(\frac{n+1}{2n+1}\right)\frac{B_{mn}}{R^{2n+1}}, \tag{25}$$

so that (24) may be written as

$$V_r=-\sum_{n=0}^{\infty}\sum_{m=0}^{n}A_{mn}'r^n P_n^m(\cos\theta)\cos m\phi. \tag{26}$$

The reaction field in any point r, θ, ϕ has three components defined by

$$(E_r)_r=-\frac{\partial V_r}{\partial r};\quad (E_r)_\theta=-\frac{1}{r}\frac{\partial V_r}{\partial\theta};\quad (E_r)_\phi=-\frac{1}{r\sin\theta}\frac{\partial V_r}{\partial\phi}. \tag{27}$$

Because the dipole is in the xz plane, the volume average of the y component of $\mathbf{E}_r(x, y, z)$ will vanish. For the x and z components the volume averages are determined by

$$\langle(E_r)_x\rangle=\frac{\int(E_r)_x d\tau}{\int d\tau}\quad\text{and}\quad\langle(E_r)_z\rangle=\frac{\int(E_r)_z d\tau}{\int d\tau}, \tag{28}$$

where $d\tau=r^2\cdot\sin\theta\cdot d\theta\cdot dr\cdot d\phi$, the integration being carried out over the volume of the sphere of radius R. From Fig. 1 it is easily shown that

$$(E_r)_x=[(E_r)_r\sin\theta+(E_r)_\theta\cos\theta]\cos\phi-(E_r)_\phi\sin\phi, \tag{29}$$

$$(E_r)_z=(E_r)_r\cos\theta-(E_r)_\theta\sin\theta. \tag{30}$$

Substituting (26) into (27) and making use of (29) and (30), we finally obtain

$$\langle(E_r)_z\rangle=A_{01}'=\frac{2(\epsilon_0-1)}{R^3(2\epsilon_0+\epsilon_i)}\mu\cos\beta, \tag{31}$$

$$\langle(E_r)_x\rangle=A_{11}'=\frac{2(\epsilon_0-1)}{R^3(2\epsilon_0+\epsilon_i)}\mu\sin\beta. \tag{32}$$

It follows immediately that the vector $\mathbf{E}_r$, of which the components are given by these two expressions, has the same direction as $\mathfrak{y}$. The magnitude of the average reaction field is equal to

$$\langle E_r\rangle\equiv[\langle(E_r)_x\rangle^2+\langle(E_r)_z\rangle^2]^{\frac{1}{2}}=\frac{2(\epsilon_0-1)}{R^3(2\epsilon_0+\epsilon_i)}\mu. \tag{33}$$

Now, from (1), (2), (3), and (4) it follows for the Onsager-Böttcher model with a central mathematical dipole

$$E_r=\frac{2(\epsilon_0-1)}{R^3(2\epsilon_0+\epsilon_i)}\mu.$$

This expression is identical with the volume average of the reaction field for an arbitrary extended dipole as given by (33). From what has been said in Sec. III, it has thus been shown that the expression for the moment P per unit volume is the same for both cases.

A Study of Iodide-Iodine Solutions with the emf Centrifuge

D. A. MacInnes and Margaret Oakley Dayhoff
Laboratories of the Rockefeller Institute for Medical Research, New York, New York
(Received February 8, 1952)

The potentials, observed with a galvanic cell with two iodide-iodine electrodes, at two different radii in a centrifugal field, have been studied with solutions of potassium and sodium iodides, to which were added varying concentrations of iodine. Using a short extrapolation the transference numbers of sodium iodide have been obtained. The earlier results using potassium iodide have been confirmed. These results, when interpreted with the aid of conductance measurements, indicated the presence of the ionic complex I_3^-. A small deviation from the theory has been found with the results for sodium iodide-iodine solutions. The emf centrifuge used in our earlier work has been simplified, and a galvanic cell has been utilized which avoids the collection of suspended particles on the electrodes.

ALREADY understanding of the effect of a gravitational or centrifugal field on the potential of a simple galvanic cell can be gained with the aid of a mechanical analogy. Consider the system shown in Fig. 1, consisting of the masses W_1 and W_2 on a cord passing over a pulley P. If W_1 is greater than W_2 and the system is allowed to operate, then the energy, Z, available is

$$Z=gh(W_1-W_2), \tag{1}$$

in which g is the gravitational constant and h is the distance through which the weights move. If, however, the masses have the volumes V_1 and V_2 and are immersed in a vessel containing a medium of density ρ, Eq. (1) must be modified to give

$$Z=gh[(W_1-V_1\rho)-(W_2-V_2\rho)] \tag{2}$$

in order to allow for the buoyancy of the medium. Considerably greater energy may be obtained if the force of gravity is replaced by a centrifugal field. This can be done by mounting the system of weights, pulley, and vessel so that it can be swung n revolutions per second about a center such as 0, which is distant r_1 and r_2 from masses W_1 and W_2. Under these conditions the energy obtainable from the mechanism is

$$Z=2\pi^2n^2(r_2^2-r_1^2)[(W_1-V_1\rho)-(W_2-V_2\rho)]. \tag{3}$$

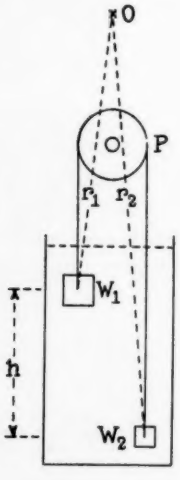

FIG. 1. The mechanical analogy to the galvanic cell process.

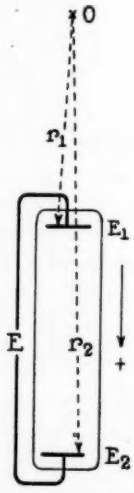

FIG. 2. Diagram of galvanic cell in centrifugal field.

In the emf centrifuge a simple galvanic cell, shown diagrammatically in Fig. 2, may be represented by

$$\underset{r_1}{(\mathrm{Pt})}\ ;\ \mathrm{I_2},\ BI,\ \underset{r_2}{\mathrm{I_2}}\ ;\ (\mathrm{Pt}), \tag{A}$$

in which B is a positive ion constituent. In this cell two otherwise identical iodide-iodine electrodes E_1 and E_2 are situated at distances r_1 and r_2 from a center 0, about which rotation takes place. Under these conditions a potential E will develop. If the cell operates with current passing in the direction indicated, the effect will be (a) the removal of a portion of the salt BI from the region of the anode (the inner electrode) and its reappearance at the cathode, and (b) the reaction of uncharged iodine I^0 to form iodide ion at the cathode, i.e.: $I^0+e^-=I^-$ and the reverse reaction at the anode. For the passage of one faraday equivalent, F, of current the amounts of material thus transported will be t_B mole of BI from the anode to the cathode region (t_B is the transference number of the positive ion), and one mole of iodine in the reverse direction. Thus, we are dealing with a coupled process in which t_BM_{BI} (M_{BI} is the gram-molecular weight of BI) corresponds to mass W_1, and A_I, the gram-atomic weight of iodine, to W_2. Placing these values in Eq. (3) we obtain

$$-EF=Z=2\pi^2n^2(r_2^2-r_1^2)[t_B(M_{BI}-\bar{V}_{BI}\rho)-(A_I-\bar{V}_I\rho)]. \tag{4}$$

In this equation volumes V_1 and V_2 have been replaced by the molal and atomic volumes $\bar{V}_{BI}$ and $\bar{V}_I$. The fact that the mechanical energy Z may be reversibly transformed into the electrical energy, $-EF$, in which E is the measured potential of the cell A at the speed of rotation n, is also indicated in Eq. (4). This equation was first obtained by Tolman,[1] for cells of the type A, though earlier experimental and theoretical work on the

[1] R. C. Tolman, Proc. Am. Acad. Arts Sci **46**, 109 (1910); J. Am. Chem. Soc. **33**, 121 (1911).

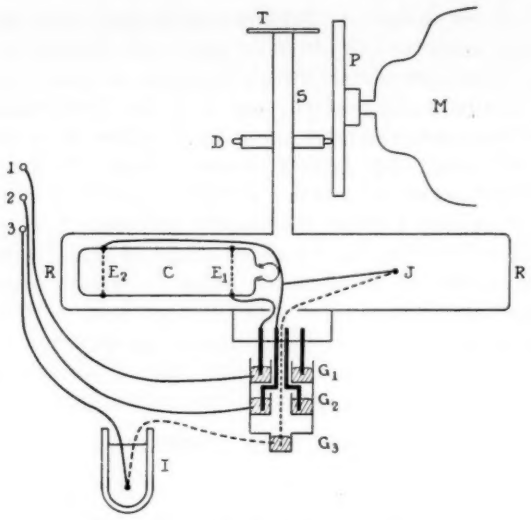

FIG. 3. Diagram of apparatus.

effects of gravitational and centrifugal fields on the potentials of galvanic cells was carried out by Des Condres.[2] A rigorous derivation of Eq. (4) is given in an earlier paper,[3] in which it is shown that the terms $\bar{V}_{BI}$ and $\bar{V}_I$ are *partial* molal and *partial* atomic volumes, respectively. In that paper it is also shown that Eq. (4) must be modified to include the effect of the complex resulting from the combination of the iodide ion and iodine which will be further discussed below. This contribution is concerned with modifications of the apparatus used in the earlier work, and with new data on measurements of potassium iodide-iodine and sodium iodide-iodine solutions.

THE APPARATUS

The apparatus as used in the earlier research has been described in detail elsewhere.[3,4] Some modifications have, however, been found desirable in obtaining the results to be described below. The apparatus now in operation is shown schematically in Fig. 3. The rotor $R-R$, a disk of magnesium 23 cm in diameter and 5 cm thick, is turned in a horizontal plane by means of the pressure of the disk D on the plate P, which is rotated by the synchronous motor M. The rotor speed can be varied by changing the position of the disk D with relation to the plate P. The potential between the electrodes E_1 and E_2 of the galvanic cell C can be measured, during the rotation, by electrical contacts through the mercury commutators G_1 and G_2. The temperature of the rotor is found by using a copper-constantan junction J, the commutators G_2 and G_3, and the reference junction in the external ice-bath I. Thus, by shifting the leads of the potentiometer to the appropriate pairs of the contacts 1, 2, and 3, the emf of the cell or the temperature of the rotor may be measured. The cell potentials have been found to be considerably affected by radial temperature gradients. Such gradients are minimized by surrounding the rotor with a chamber in which a vacuum of 10μ or better is maintained. This prevents the production of appreciable heat through gas friction. The heat generated at the vacuum bearing is controlled by the circulation of cooling water. The apparatus previously had a set of 22 thermojunctions arranged around the cell so that differences of temperature at radii corresponding to the positions of the electrodes E_1 and E_2 could be measured. It has been observed, however, that operating in vacuum this difference of temperature disappears, to 0.001°, if the temperature of a fixed point on the rotor remains constant. The three commutators G_1, G_2, and G_3 are mounted under the rotor, and operate in the vacuum. The temperature of the rotor may be maintained constant by choosing the temperature of the water passing around the rotor bearing, or by keeping the room temperature somewhat lower than that desired for the rotor.

An important change from our earlier practice has been in the design of the galvanic cell. For the previous work, this consisted of a cylindrical glass vessel with platinum disks sealed into each end and about 8 cm apart. However, it was found that one of the chief difficulties in getting accurate measurements was the presence of minute suspended particles in the solutions, which persisted, as shown by a Tyndall beam, even after extraordinary efforts were made to eliminate them. In a centrifugal field such particles tended to collect on the electrodes and seriously affected the accuracy of the measurements. The difficulty has been largely,

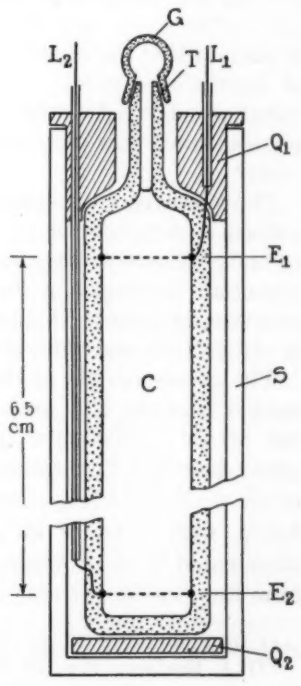

FIG. 4. The galvanic cell.

[2] Th. Des Condres, Ann. Physik u. Chemie **49**, 284 (1892); **57**, 232 (1896).
[3] D. A. MacInnes and B. R. Ray, J. Am. Chem. Soc. **71**, 2987 (1949).
[4] B. R. Ray and D. A. MacInnes, Rev. Sci. Instr. **20**, 52 (1949).

TABLE I. Typical data from measurements of potential, E, *vs* speeds of revolution, n. (Cell I).

Moles NaI / 10^3 g soln	$R=C_{I_2}/C_{NaI}$		n = rev/sec		
			40	80	110
0.19112	0.003146	$E\mu v$	138.8	557.5	1056.1
0.19112	0.003146	$E\mu v$	139.3	557.3	1054.3
		$(E/n^2K)\times10^3$	1.0830	1.0856	1.0871
0.19103	0.021830	$E\mu v$	139.6	562.9	1062.3
0.19103	0.021830	$E\mu v$	140.5	562.2	1063.8
		$(E/n^2K)\times10^3$	1.0907	1.0956	1.0951
0.18885	0.48092	$E\mu v$	173.8	689.0	1304.9
0.18885	0.48092	$E\mu v$	172.4	690.0	1304.4
		$(E/n^2K)\times10^3$	1.3487	1.3430	1.3441

if not entirely, removed by the design of cell shown in Fig. 4. Here the electrodes, in the glass cell C, are the platinum rings E_1 and E_2 sealed into the glass wall several mms from the ends of the cell. With this arrangement the particles, under the influence of the centrifugal force, tend to collect harmlessly at these ends, and out of contact with the electrodes. The platinum leads, L_1 and L_2, are enclosed in flexible plastic tubing. Filling and removal of the solution are carried out through the tube T which is closed with a ground-glass cap G. The cell is held in the brass shell S, the space between the shell and the cell being filled with vaseline. This semifluid material helps to equalize the pressure on the cell when in a centrifugal field. The Lucite spacers Q_1 and Q_2 keep the glass cell in a fixed position in the shell S. Since the cell C cannot be made with the electrode rings, E_1 and E_2, with definite values for the radii r_1 and r_2, the cell constant, K, which is the effective value of the term $(r_2^2-r_1^2)$ in Eq. (4), has been obtained by calibrating with $KI-I_2$ solutions, the transference numbers of which are known from the moving boundary measurements of Longsworth,[5] and our earlier work with the emf centrifuge. It is quite important that the counterpoise have the same moment of inertia as the cell, i.e., imitate it closely in distribution of weight, since otherwise, the rotor may precess, and thus not rotate about its geometrical center.

The mercury commutators G_1, G_2, and G_3 are described in detail elsewhere.[4] With them it was possible to make measurements, to one microvolt or better, of potentials developed in the rotor, this precision being necessary because the highest potentials determined are of the order of one millivolt.

The measurements of the speeds of rotation, which ranged between 2400 and 7200 rpm, were made with the aid of stroboscopic patterns, as described in a paper from this Laboratory.[6] The rotating top surface of the shaft S of Fig. 3 carries a disk T which is painted black, with a white radial streak. This surface is illuminated by a stroboscopic lamp, which is operated from the local ac current, and yields flashes at the rate of 60 per second. At definite speeds stationary stroboscopic patterns are observed which are related by the formula: rpm $=(3600\times m)/n$ in which n is the number of bands in the pattern, and m is the "multiplicity." Patterns are observed for integral values of m and n except when they have a common factor. As the same pattern occurs at a series of related speeds it is necessary to have a rough preliminary estimate of its value. This is furnished by a scale attached to the adjustment mechanism of the disk D. Since stationary patterns could be obtained for indefinite periods, with occasional slight manual adjustments, the accuracy of the speed measurement was nearly that of the ac source, and was more than necessary for our purpose.

RESULTS AND DISCUSSION

The measurements described in this paper were made with potassium and sodium iodides to which varying amounts of iodine were added. In preparing these solutions the best commercial salt was recrystallized several times, and dried in an electric oven, followed by heating to 500° in a platinum boat in a current of dried nitrogen. The material was then weighed with the aid of the Richards bottling apparatus,[7] after which the salt was dissolved in a weighted amount of conductivity water. Iodine, several times sublimed, was then added by weight to the salt solutions. The stronger iodine solutions were sometimes diluted quantitatively with the appropriate salt solution.

Typical results of measurements in sodium iodide-iodine solutions are shown in Table I, which is largely self-explanatory. The potentials, E, are in microvolts, and the two values for each solution and for each speed of revolution, n, are from separate runs of the centrifuge. It will be observed that the agreements are of the order of 1 microvolt. The potentials remained substantially constant, following an initial rise,[8] for periods of one half hour. According to Eq. (4), and the modified expression, Eq. (5), to be given below, values of E/n^2K (in which K is the effective value of $(r_2^2-r_1^2)$) should be independent of the speed of rotation n for the measurements on each solution. This is seen to be the case in Table I to high precision though the variations are smaller for the two higher speeds, the data for which were used in the computations to be outlined below.

In Table II new data are given for values of E/n^2K on potassium iodide-iodine solutions which are essentially in accord with those given in the previous paper,[3] but have been obtained with the modified technique described in this communication. The results for sodium iodide-iodine solutions, also obtained with the newer technique, appear in Table III. It will be seen from

[5] L. G. Longsworth, J. Am. Chem. Soc. **57**, 1185 (1935).
[6] D. A. MacInnes, Rev. Sci. Instr. **14**, 14 (1943).
[7] T. W. Richards and A. G. Parker, Proc. Am. Acad. Arts. Sci. **33**, 69 (1906).
[8] As shown by J. Beams, J. Appl. Phys. **8**, 795 (1927) this rise is due to adiabatic compression. A computation indicates that a difference of temperature of 0.04°, or a potential of about 20 microvolts, between the electrodes would be developed if the speed were increased rapidly from zero to 7200 rpm.

the data in Tables II and III that the value of the quantity E/n^2K increases quite rapidly as the proportion of iodine in solution ascends. In the following discussion it is shown that this is due to the effect of an iodide-iodine complex on the mechanism of the cell.

During the passage of current through the cell

$$(Pt);\quad I_2, BI, I_2;\quad (Pt)$$

the electrochemical reaction

$$I^- = I^0 + e^-$$

occurs at the anode and

$$e^- + I^0 = I^-$$

at the cathode. Here, I^0 represents iodine in an uncharged condition. It may be in the form of I_2 or as I^-_{j+1}, in which j is the number of equivalents of uncharged iodine in an equivalent of the complex. During the passage of one faraday F through the cell, t_B equivalent of the positive ion constituent, B, will migrate from the region of the anode and appear at the cathode, t_B representing a Hittorf transference number. The remainder of the current is transported in the reverse direction by t_I equivalent of I^- and t_c equivalent of the complex ion. The net loss around the anode is t_B equivalent of the positive ion and $(1-t_I-t_c)=t_B$ equivalents of negatively charged ions. Thus, there is a net loss of t_B equivalent of potassium iodide from the region of the anode. Since reverse phenomena occur at the cathode, a transport of t_B equivalent of salt from one electrode to the other takes place. This is accompanied by the appearance of one equivalent of I^0 at the anode by the electrochemical reaction, and jt_c equivalent of that material by transference.

The transport process per faraday for the galvanic cell A is, therefore, t_B equivalent of BI from the anode to the cathode and $(1+jt_c)$ equivalents of I^0 in the reverse direction, and Eq. (4) must obviously be modified to give

$$-EF = 2\pi^2 n^2 K[t_B(M_B - \bar{V}_{BI}\rho) - (1+jt_c)(A_I - \bar{V}_I\rho)]. \quad (5)$$

It will be observed that this equation reduces to Eq. (4), as the proportion of iodine, and thus the transference number t_c decreases. Thus, using that equation and the limiting value of E/n^2K obtained by a short linear extrapolation from the data in Table III, the transference number of the sodium ion in 0.19112 normal sodium iodide is found to be $t_{Na}=0.3827$. An extrapolation of the E/n^2K values for potassium iodide in Table II, and Longsworth's[9] moving boundary figure, 0.4887, for the cation transference number at $0.2N$ for that salt were used in obtaining the values of the cell constants, $K=(r_2^2-r_1^2)$, for Eqs. (4) and (5). These constants were found to be 80.22 and 82.20 cms^2, for cells I and II, respectively.

TABLE II. The results of emf centrifuge measurements on potassium iodide-iodine solutions at 25°.

Moles KI / 10^3 g soln	$R=C_{I^0}/C_{KI}$	$E/n^2K\times10^3$ obs	calc	Cell
0.17147	0.005248	0.783_7	0.783_7	*II*
0.18988	0.04225	0.797_9	0.797_9	*I*
0.18566	0.06206	0.804_4	0.805_3	*I*
0.19140	0.11675	0.828_6	0.826_8	*II*
0.18903	0.31970	0.905_5	0.908_8	*II*
0.18821	0.52272	0.993_3	0.995_5	*II*
0.18697	0.6519	1.051_1	1.055_2	*I*

TABLE III. The results of emf centrifuge measurements on sodium iodide-iodine solutions at 25°.

Moles NaI / 10^3 g soln	$R=C_{I^0}/C_{NaI}$	$E/n^2K\times10^3$ obs	calc	Cell
		1.084_3	1.084_3	*I*
0.19112	0.003146	1.086_3	1.085_9	*I*
0.19103	0.021830	1.095_0	1.095_5	*I*
0.19082	0.06388	1.115_1	1.117_3	*I*
0.19043	0.14829	1.157_0	1.162_2	*I*
0.18944	0.35654	1.270_3	1.278_8	*I*
0.18885	0.48092	1.344_1	1.352_7	*I*
0.18737	0.79898	1.539_3	1.557_3	*I*

To make these computations and those which follow, it was necessary to use values of the partial molal and atomic volumes, $\bar{V}$, and of the solution densities, ρ. The determination of these constants, by the magnetic float method, is the subject of a recent contribution from this laboratory.[10] In that paper it is shown that $\bar{V}_{KI}=46.12$ at the concentration used in these experiments. The effect of the presence of iodine on this constant was investigated and found to be small. For $\bar{V}_{NaI}$ the value 35.92 was obtained. The partial atomic volume, $\bar{V}_I$ of iodine was found to be constant at 29.96 for sodium iodide solutions, but for potassium iodide solutions to vary slightly according to the relation

$$\bar{V}_I = 29.98 + 1.46m,$$

in which m is the number of equivalents of iodine in 1000 grams of solution. These values, based on our most recent data, replace those given in the earlier paper.[3]

With the aid of conductance measurements on potassium and sodium iodide solutions with varying proportions of added iodine, a test of the validity of Eq. (5) may be made. The data are given in Table IV, which is self-explanatory. The conductances were measured using a bridge of the type described by Shedlovsky[11] with conductance cells of the form employed in other work from this laboratory.[12] The measured equivalent conductances Λ_m, (based on the salt concentration) may be expressed by the formula

$$(\Lambda_{KI}-\Lambda_m)/R = 15.20 - 3.2R$$

[9] J. Am. Chem. Soc. **57**, 1185 (1951).
[10] D. A. MacInnes and M. O. Dayhoff, J. Am. Chem. Soc., **74**, 1017 (1952).
[11] T. Shedlovsky, J. Am. Chem. Soc. **52**, 1793 (1930).
[12] Longsworth, Shedlovsky, and MacInnes, J. Expt. Med. **70**, 399 (1939).

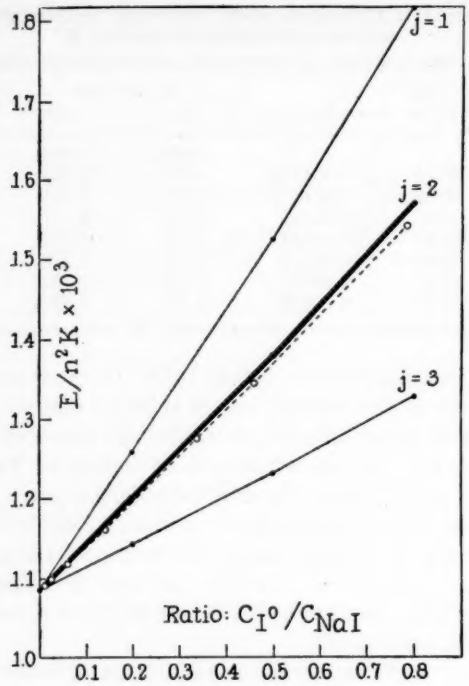

FIG. 5. The variation of E/n^2K values with the ratio C_{I^0}/C_{NaI}.

for potassium iodide and

$$(\Lambda_{NaI}-\Lambda_m)/R=15.10-0.51R$$

for sodium iodide, in which $R=C_{I^0}/C_{BI}$. Assuming Kohlrausch's law of independent ion mobilities, the measured equivalent conductance A_m is given by

$$\Lambda_m=\lambda_B+(1-R/j)\lambda_I+(R/j)\lambda_c,$$

in which the λ-values are equivalent conductances of ion constituents; and j is, once more, the number of equivalents of uncharged iodine carried by the complex, C. From this equation

$$\Lambda_C=\lambda_I-(j/R)(\Lambda_{KI}-\Lambda_m) \quad (6)$$

and also

$$t_B=\lambda_B/\Lambda_m \quad \text{and} \quad t_c=R\lambda_c/j\Lambda_m, \quad (7)$$

since transference numbers are, in this case, the proportion of the total current carried by a given ion constituent. Substituting these values in Eq. (5) we have

$$-EF=2\pi^2n^2K\left[\frac{\lambda_B}{\Lambda_m}(M_{BI}-\bar{V}_{BI}\rho)-\left(1+\frac{R\lambda_I-j(\Lambda_{BI}-\Lambda_m)}{\Lambda_m}\right)(A_I-\bar{V}_I\rho)\right]. \quad (8)$$

The values of λ_K, λ_{Na}, and λ_I used with Eqs. (6), (7), and (8) were obtained from the Λ_m figures given in Table IV for the solutions containing no free iodine, together with the transference number 0.4887 for potassium iodide from Longsworth's work[9] and 0.3827 for sodium iodide, as given above.

Assuming that j in Eq. (8) is an integer, values of E/n^2K have been computed for $j=1$, 2 and 3. The results of this computation for the data for the sodium iodide-iodine solutions have been plotted against $R=C_{I^0}/C_{NaI}$ in Fig. 5 on which the observed data for E/n^2K are also shown as small circles which are connected by a dotted line. It will be seen that the values follow closely the curve based on the assumption of $j=2$, which corresponds to the presence of the complex ion I_3^- in the solutions. There is, however, a small but progressively increasing deviation of the observed from the computed values as the proportion of free iodine is raised. This type of deviation is not found for the potassium iodide solutions, as is shown in Table II, the fourth and fifth columns of which contain observed and computed values, with $j=2$, in which there is close agreement, as was also found in our earlier work.[3] In these computations the values of R have been corrected for the small concentration of I_2 from the equilibrium

$$I^-+I_2=I_3^-,$$

the mass law constant used[13] being 1.40×10^{-3}. Table III contains corresponding observed and computed figures for the sodium iodide-iodine solution. The variation of 1.3 percent in the E/n^2K value at the highest iodine concentration is probably connected with the assumption of the validity of Kohlrausch's additivity law for ion mobilities for solutions as concentrated as 0.2 molal, though the matter will be investigated further. This deviation does not affect the method for the purpose of obtaining transference numbers of the pure iodides, since that requires only a short extrapolation from the data for the solutions containing the smaller proportions of iodine.

TABLE IV. Equivalent conductances, Λ_m, of potassium and sodium iodide-iodine mixtures at 25°.

Salt	Equivalents per liter salt	Equivalents per liter I^0	Λ_m	R
KI	0.18846	0	127.38	
KI	0.18758	0.15398	115.23	0.82086
KI	0.18967	0	127.30	
KI	0.18921	0.080881	120.92	0.42746
KI	0.19377	0	127.15	
KI	0.19304	0.12585	117.45	0.65194
NaI	0.19277	0	104.87	
NaI	0.19262	0.02752	102.73	0.14287
NaI	0.19246	0.05361	100.75	0.27854
NaI	0.19206	0.12227	95.56	0.63663
NaI	0.19184	0.16062	92.72	0.83729
NaI	0.19484	0	104.77	
NaI	0.19432	0.08702	98.17	0.44784
NaI	0.19391	0.15662	93.03	0.80770

[13] G. Jones and B. B. Kaplan, J. Am. Chem. Soc. **50**, 1845 (1928).

Letters to the Editor

THIS section will accept reports of new work, provided these are terse and contain few figures, and especially few half-tone cuts. The Editorial Board will not hold itself responsible for opinions expressed by the correspondents. Contributions to this section should not exceed 600 words in length and must reach the office of the Editor not later than the 15th of the second month preceding that of the issue in which the Letter is to appear. No proof will be sent to the authors. A publication charge of $10.00 per Letter is made which, when honored, will entitle the Institution to 100 free reprints.

Additional Intensity Rules for Isotopic Molecules

J. C. DECIUS
Department of Chemistry, Oregon State College, Corvallis, Oregon
(Received February 25, 1952)

IN a communication appearing in this issue, Crawford[1] has developed some relations between the intensities of the fundamental vibrations of isotopic molecules which are elegant in their simplicity. It is the purpose of this letter to point out the existence of a further type of relation.

Consider Eq. (10) of Crawford's paper:[1]

$$\Sigma_a I_{ia} = \Sigma_x p_{ik}{}^x p_{ij}{}^x G_i{}^{kj}, \tag{1}$$

where the I_{ia} is the intensity of the ath fundamental of a given symmetry species for the ith isotopic molecule. In case this species does not include a rotation and/or the molecule is nonpolar, the dipole derivative $p_{ik}{}^x$ is the same for all isotopic molecules:

$$p_{ik}{}^x = p_k{}^x. \tag{2}$$

Under these circumstances, exactly the same type of relationship will exist between the intensity sums (1) for a series of isotopic molecules as was shown to hold between certain frequency sums by Decius and Wilson.[2] This follows from the fact that the G matrix elements $G_i{}^{kj}$ appearing in (1) are linear functions of the reciprocal masses of the atoms

$$G_i{}^{kj} = \Sigma_\alpha I_\alpha{}^{kj} \mu_{\alpha i}, \tag{3}$$

and the fact that the combination of isotopic molecules involved in such a relation involves such coefficients n_i that cancellation of the $\mu_{\alpha i}$ occurs at every atomic position α:

$$\Sigma_i n_i \mu_{\alpha i} = 0 \quad \text{(for all } \alpha\text{)}. \tag{4}$$

Therefore,

$$\Sigma_i n_i (\Sigma_a I_{ia}) = 0. \tag{5}$$

Unfortunately, no numerical data are yet available to test this rule, and perhaps not much will be forthcoming, but it seems worthwhile to mention several possible applications. The deuterated acetylenes fulfill the condition of nonpolarity, and since the n_i are determined by the reaction equation

$$C_2H_2 + C_2D_2 = 2C_2HD, \tag{6}$$

the rules assume the form,

$$\sum_{a=1}^{3} I_a(C_2H_2) + \sum_{a=1}^{3} I_a(C_2D_2) = 2 \sum_{a=1}^{3} I_a(C_2HD), \tag{7}$$

$$\sum_{a=4}^{5} I_a(C_2H_2) + \sum_{a=4}^{5} I_a(C_2D_2) = 2 \sum_{a=4}^{5} I_a(C_2HD), \tag{8}$$

where the symmetry species of the fundamental modes are identified in Table I.

Note that I_1, I_2, and I_4 actually vanish on the left-hand sides of (7) and (8) in the infrared case.

In the analogous Raman rule, it is the Raman intensity I_3 which vanishes on the left-hand side of (7); the rule cannot be applied to the species II of C_2HD, inasmuch as this species contains

TABLE I. Symmetry species of fundamentals in the acetylenes.

	C_2H_2, C_2D_2	C_2HD
1.	Σ_g^+	Σ^+
2.	Σ_g^+	Σ^+
3.	Σ_u^+	Σ^+
4.	Π_g	Π
5.	Π_u	Π

rotations about the x and y axes which change the equilibrium polarizability.

Modified rules could be formulated taking into account the cases in which the dipole derivatives $p_{ik}{}^x$ or polarizability derivatives are not isotopic invariants. Owing to the paucity of data, however, the time does not yet seem ripe for this undertaking.

The author is indebted to Professor B. L. Crawford, Jr., for a stimulating correspondence on these problems and for the opportunity to study his manuscript prior to publication.

[1] B. L. Crawford, Jr., J. Chem. Phys. **20**, 977 (1952).
[2] J. C. Decius and E. Bright Wilson, Jr., J. Chem. Phys. **19**, 1409 (1951).

Overlap Integrals and the Linkage in Complex Ions

W. S. FYFE
University of Otago, New Zealand
(Received March 24, 1952)

IN a previous discussion of the stability of complex ions formed between cations and either anions or neutral molecules it was suggested that the free energy of formation appeared to be a function of the ionization potential of the metal and the electron affinity of the ligand.[1] A similar conclusion has been reached by Mulliken[2] with all molecular complexes. If the above concept is correct, then a measure of the stability should be given by the overlap integrals involved in these linkages. It must be emphasized that free energy data can only be considered an index of bond strength if entropy values are similar. As in most of the cases to be compared entropy data are not available, or demonstrate that entropies of formation may differ very widely, it is to be expected that correlations will not be exact.

The problem of the stability of complex ions separates itself into two major parts: the order of stability of a series of complexes formed by cations with one ligand and the order of stability of complexes from a single cation and a series of ligands. The present discussion is restricted to the latter problem. In the former the most critical series occur in the transition metal series, and hybrids such as d^2sp^3 have not received adequate treatment as yet. However, Mulliken's results[3] for overlap in binary compounds demonstrate that overlap integrals do, in general, agree with polarity of bond type as indicated by electronegativity difference, and as in the transition metal ion complexes we have an almost linear variation in stability with ionization potential of the metal there is little doubt that such correlation will exist.

Table I contains a series of Slater AO overlap integrals for bonds between Li^+ and various ligand types. These were calculated by means of the formulas and tables of Mulliken.[4] The effective nuclear charges $(Z-s)$ were calculated according to the recipe of Slater.[5] The scanty data on bond lengths in these compounds suggest that a good approximation to the actual internuclear distance in the sum of the radius of the cation plus the van der Waals radius of the ligand atom. These were used in all cases.

If we use these integrals as an index of stability, then the order of stability of ligands from these data would be predicted to be

$$C^- > S^- > C > N^- > Cl^- > O^- > N > O > F^-.$$

This series agrees very well with known data and is certainly in general correct (see J. Bjerrum[6] for a review of data). A feature

TABLE I. Slater AO overlap integrals for Li^+-X bonds.

X	p	t	S_{ss}	S_{ps}	S_{pp}	$S_{\pi\pi}$	S_{sp}
O	6.85	0.25	0.14	0.12	0.17	0.05	0.20
O^-	6.52	0.22	0.16	0.15	0.20	0.06	0.23
N	6.55	0.18	0.15	0.15	0.21	0.06	0.21
N^-	6.20	0.14	0.18	0.19	0.23	0.08	0.24
F^-	8.21	0.23	0.06	0.06	0.10	0.03	0.10
Cl^-	7.28	−0.16	0.17	0.19	0.24	0.04	0.20
C	6.19	0.09	0.18	0.19	0.23	0.09	0.24
C^-	5.82	0.04	0.21	0.23	0.27	0.09	0.25
S	7.33	−0.15	0.16	0.18	0.24	0.03	0.19
S^-	6.95	−0.26	0.19	0.22	0.26	0.05	0.20

of particular interest is the effect of formal charge on the ligand. Thus, although N^- gives greater overlap than O or O^-, N is approximately equal to O^- but greater than O. These effects demonstrate how electron distribution in a system may effect orders of stability which is in agreement with experiment.[7] It must be remembered that in the water molecule the oxygen atom probably carries a formal charge of approximately −0.6. The figures also demonstrate that in fluoride complexes overlap is not very important but stability must largely be due to electrostatic interactions. This is in agreement with the fact that the stable fluoride complexes occur only with cations with a high ionic potential.

Calculations have also been made of the overlap integrals occurring in H, Li, and Mg complexes, and these arrange the complexes in the correct order of stability. It is hoped in the near future to carry out these calculations for a wider range of metals including transition metals.

The writer wishes to gratefully acknowledge helpful communication with Professor C. A. Coulson F.R.S., who suggested this approach to the problem.

[1] W. S. Fyfe, J. Chem. Soc. (to be published).
[2] R. S. Mulliken, J. Chem. Phys. **19**, 514 (1951).
[3] R. S. Mulliken, J. Am. Chem. Soc. **72**, 4493 (1950).
[4] Mulliken, Reike, Orloff and Orloff, J. Chem. Phys. **17**, 1248 (1949).
[5] J. C. Slater, Phys. Rev. **36**, 57 (1930).
[6] J. Bjerrum, Chem. Revs. **46**, 381 (1950).
[7] W. S. Fyfe, Nature **169**, 69 (1952).

A Mechanism for Active Nitrogen*

R. W. NICHOLLS
Department of Physics, University of Western Ontario, London, Ontario, Canada
(Received March 24, 1952)

ACTIVE nitrogen is the somewhat loosely applied name given to the yellow afterglow phenomenon (the Lewis-Rayleigh afterglow), occurring after the main discharge has been switched off in discharge tubes previously running in nitrogen. It may also be observed in side-arms of a running discharge tube, provided that the main discharge is not being maintained in the side-arm. The afterglow exhibits many physical and chemical properties[1] for the complete or partial explanation of which many mechanisms have been suggested. It seems unlikely that any one mechanism could reasonably be expected to explain all the properties of active nitrogen. The concurrent operation of a number of mechanisms with different degrees of relative effectiveness in different experimental arrangements seems to be a more reasonable over-all explanation of the phenomenon.

It is the purpose of this note to suggest a further specific mechanism, which on the basis of our knowledge of the energy level systems of nitrogen and other physical conditions existing in the afterglow, may play an important part in populating the $B^3\Pi g$ levels of N_2 in such a way as to give rise to the subsequent radiation of the first positive bands of N_2 with the intensity distribution characteristic of active nitrogen.

Extensive experimental observations[2,3] and theoretical reasoning[4,5] have indicated that the operation of a metastable state with levels of comparable energies to those of the $B^3\Pi g$ state should be taken into account in any complete explanation of active nitrogen.

The mechanism proposed in this note involves molecules in vibrational levels of the metastable state of $a^1\Pi g$ of N_2.

The excitation processes in the main discharge prior to the afterglow, whether they be direct or indirect excitations by electron collision,[6] will certainly set up populations of molecules in vibrational levels of all electronic states of N_2, including the $a^1\Pi g$ state which is metastable.[7] Upon switching the main discharge off, molecules in excited levels will depopulate them by radiation provided the transition probabilities involved are high. Thus in a very short time after the cessation of the main discharge molecules of nitrogen will be populating only the metastable states $a^1\Pi_g$ and $A^3\Sigma_u$ together with the ground state $X^1\Sigma_g$.

Because of their metastability toward transition to $X^1\Sigma_g$, there will only be a small radiative drain in the populations of levels of the $a^1\Pi_g$ and $A^3\Sigma_u$ states. All other depopulation of these levels must come about by nonradiative collision processes between the metastable molecules and other molecules or electrons. It is known that there is a high concentration ($\sim 10^9$/cc) of slow electrons in the active nitrogen afterglow.[2] Thus, of the nonradiative collision processes mentioned above, those with slow electrons will be appreciable. A simple calculation shows that about 1000 collisions per sec may be expected between an excited molecule and slow electrons. While other molecular processes may be even more numerous, those with slow electrons will be particularly effective in depopulating the metastable $a^1\Pi_g$ levels as follows:

$$N_2(a^1\Pi_g)+e(\text{slow})\rightarrow N_2(B^3\Pi_g)+e.$$

The energy resonance between specific vibrational levels of $a^1\Pi_g$ and $B^3\Pi_g$ is high, in which case the electron exchange processes required to change the multiplicity will have a high expectation per collision.[8,9] Radiation of the first positive system from the $B^3\Pi_g$ levels so populated will then result, and the characteristic intensity distribution will depend upon the respective expectations of the specific $N_2(a^1\Pi_g)\rightarrow N_2(B^3\Pi_g)$ transfers.

A quantitative study involving the excitation kinetics of this and other mechanisms which have been suggested as operative in active nitrogen will be published shortly.

* This work is assisted by Contract AF 19(122)-470 with the Geophysics Research Division, Air Force Cambridge Research Center.
[1] S. K. Mitra, *Active Nitrogen—A New Theory*, Calcutta, 1945.
[2] J. M. Benson, N.A.C.A. Technical Note 2293 (Feb. 1951).
[3] L. M. Branscomb, Phys. Rev. **82**, 83 (1951).
[4] A. G. Gaydon, Proc. Roy. Soc. (London) **A182**, 286 (1944).
[5] A. G. Gaydon, *Dissociation Energies*, p. 159.
[6] R. W. Nicholls, Nature **162**, 231 (1948).
[7] G. Herzberg, Phys. Rev. **69**, 632 (1946).
[8] N. Mott and H. S. W. Massey, *The Theory of Atomic Collisions*, second edition, Chapter 11.
[9] O. Klein and S. Rosseland, Z. Phys. **4**, 46 (1921).

Gold Radioactivity in Neutron Irradiated Diamond

MELVIN S. FREEDMAN
Argonne National Laboratory, Chicago 80, Illinois
(Received March 25, 1952)

SUBSEQUENT to an irradiation of a light yellow colored gem diamond with pile neutrons for 8 hours, low intensity radioactivity was observed. The decay of the activity was followed on a proportional counter for about 25 days, and a single 2.7 day half-life was found with no tailing out over this period. An aluminum absorption curve showed the characteristic shape of a beta-activity, with an initial half-thickness of 44 mg/cm² of aluminum, corresponding to an energy of 1 Mev. Additional longer irradiations of the same diamond exhibited the saturation activity expected.

The only activity fitting these data is that of Au^{198}. About one to two micrograms of gold in the one-tenth gram diamond would account for the observed intensity, and probably also for the initial yellow coloration. Gold as a surface contaminant of this magnitude is not likely since the diamond had never been mounted.

Resonance in the Hydrogen Molecule

LINUS PAULING
*Gates and Crellin Laboratories of Chemistry, California Institute of Technology, Pasadena 4, California**
(Received March 21, 1952)

IN a recent paper[1] Mueller and Eyring have discussed the normal state of the hydrogen molecule with use of a variation function constructed in the usual Heitler-London manner, except with replacement, for each electron, of the hydrogen-atom function about atom a, $\exp(-Z'r_a/a_0)$, by the more complex function $\phi_a=\exp(-Z'r_a/a_0)\exp(-Z''r_b/a_0)$. The authors call one-electron functions of this sort semilocalized orbitals. They have compared the value of the bond energy calculated for the wave function $\psi=\psi_1(1)\psi_2(2)+\psi_1(2)\psi_2(1)$, where $\psi_1=\phi_a+\lambda\phi_b$ and $\psi_2=\phi_b+\lambda\phi_a$, with those given by the simple atomic orbital method and the molecular orbital method, and have pointed out that there is an improvement to 4.20 ev, from the values 3.76 ev and 3.60 ev, respectively.

However, the improvement over earlier calculations that are comparable in complexity with the calculation of Mueller and Eyring is in fact not great. The Mueller-Eyring variation function that leads to the bond energy 4.20 ev contains three parameters, λ, Z', and Z'', which have been varied to minimize the energy. Nearly twenty years ago Weinbaum[2] carried out a calculation with use of a variation function of the Heitler-London type, plus ionic terms, and plus terms involving a polarizing factor $\cos\vartheta$ (see the discussion given by Pauling and Wilson[3]). In this treatment, also with a variation function containing three parameters, the bond energy was found to be 4.10 ev, only slightly inferior to the value obtained by Mueller and Eyring.

The closeness of the results obtained by Weinbaum and by Mueller and Eyring is not surprising. Two simple ways of introducing polarization of the hydrogen atom orbitals in the discussion of the hydrogen molecule-ion have been used: One of these, by Dickinson,[4] involves the addition of a polarization term containing the factor $\cos\vartheta$, and the other, by Guillemin and Zener,[5] the use of a function like that used by Mueller and Eyring; it was pointed out by Pauling and Wilson[3] (page 333) that the introduction of the factor $\exp(-Z''r_b/a_0)$, with Z'' small (equal to 0.23 in the Guillemin-Zener function) is equivalent to a polarization of the atomic orbital $\exp(-Z'r_a/a_0)$. There is, moreover, a similarity between the parameters found by Weinbaum to minimize the energy for his ionic-polarization function and those reported by Mueller and Eyring. The Weinbaum parameters are $Z'=1.19$, $\sigma=0.07$ (the coefficient of the polarization term), and $c=0.176$ (the coefficient of the ionic terms). The values of the parameters found by Mueller and Eyring (converted into values of Z' and Z'') are $Z'=1.15$, $Z''=0.043$, and λ (the coefficient of the ionic terms) $=0.137$.

Accordingly, Mueller and Eyring have discussed a wave function for the hydrogen molecule closely similar to that discussed by Weinbaum in 1933, in that it contains three parameters, which are a scale parameter, a parameter essentially determining polarization of a hydrogen-atom orbital, and a parameter determining the contribution of ionic structures. Their treatment represents the extension to the hydrogen molecule of the treatment used by Guillemin and Zener in 1929 for the hydrogen molecule-ion, plus the inclusion of ionic terms.

Mueller and Eyring end their paper with a surprising statement about resonance, which reads as follows: "Both atomic and semilocalized orbitals can be interpreted as postulating two resonance states. In the first resonance state, the state of electron one is represented by the one-electron eigenfunction on the left and the state of electron two is represented by the one-electron eigenfunction on the right. In the second resonance state, the positions of the electrons are reversed. On the other [hand?] the 'Heitler-London plus ionic terms' eigenfunction has been interpreted as implying resonance between covalent and ionic states. Using the hydrogen 1s atomic orbitals ($Z=1$), the calculated energy difference between the covalent state $(\phi_a(1)\phi_b(2))$ and the ionic state $(\phi_a(1)\phi_a(2))$ is 67.28 kcal. Using the Maxwell-Boltzmann distribution law, the ratio of the number of ionic systems to the number of covalent systems is $e^{-112.13}$ or approximately 10^{-49}. While physical interpretations involving resonance states of equal energy may be naive, those involving resonance between states of widely different energies are likely to be ridiculous."

This statement by Mueller and Eyring has, of course, no meaning whatever. The nature of the wave function for a hydrogen molecule in its normal state, or in any definitely specified quantum state, is independent of the temperature of the system in which the hydrogen molecule is present, and the Maxwell-Boltzmann distribution law relates only to the distribution of molecules among states in a system at equilibrium at a specified temperature. The numbers given in the above quotation indicate that the authors have made the Maxwell-Boltzmann calculation for the temperature 300°K; neither this temperature nor any other temperature bears in any way on the question of the electronic structure of the normal hydrogen molecule, and the statement made above by Mueller and Eyring about resonance has no validity.[6] In fact, if the Mueller-Eyring wave function for the hydrogen molecule is expanded into a sum of terms, and these terms are investigated individually with respect to their distribution in configuration space for the two-electron system, it is seen that their function may be conveniently described as involving a combination (which may just as well be called resonance as anything else) of a Heitler-London structure of polarized atomic orbitals and ionic structures, the latter being structures which place both electrons in the neighborhood of one of the two nuclei.

* Contribution No. 1664.
[1] C. R. Mueller and H. Eyring, J. Chem. Phys. **19**, 1495 (1951).
[2] S. Weinbaum, J. Chem. Phys. **1**, 593 (1933).
[3] L. Pauling and E. B. Wilson, Jr., *Introduction to Quantum Mechanics* (McGraw-Hill Book Company, Inc., 1935).
[4] B. N. Dickinson, J. Chem. Phys. **1**, 317 (1933).
[5] V. Guillemin, Jr. and C. Zener, Proc. Natl. Acad. Sci. **15**, 314 (1929).
[6] It may be mentioned that this misapplication of the Boltzmann distribution law is not made in the excellent discussion of resonance in the book *Quantum Chemistry*, by Eyring, Walter, and Kimball (John Wiley and Sons, Inc., New York, 1944).

The Photochemical Decomposition of Methylamine*

J. S. WATSON† AND B. DEB. DARWENT
National Research Laboratories, Ottawa, Canada
(Received March 20, 1952)

THE results of previous investigations of the photochemical decomposition (direct and photosensitized by mercury) of methylamine[1] have shown that hydrogen, ammonia, and a heavy liquid are the most abundant products. The heavy liquid product is of somewhat uncertain composition and may have the formula $CH_2=N-CH_3$[2] or C_2H_3N[3] or it may be a polymer[3] of either of those substances.

The following reactions:

$$CH_3NH_2+h\nu \text{ (or } Hg(^3P_1))\rightarrow CH_3NH+H(+Hg(^1S_0)) \quad (1)$$
$$H+CH_3NH_2\rightarrow CH_3NH+H_2 \quad (2)$$
$$2\,CH_3NH\rightarrow CH_3N{:}CH_2+NH_3 \quad (3)$$

appear to be generally accepted as representing the initial steps, but Wetmore and Taylor assumed that other reactions such as

$$H+CH_3NH\rightarrow CH_2NH_2 \quad (4)$$
$$CH_3NH\rightarrow CH_2=NH+H \quad (5)$$
$$CH_2=NH+CH_3NH_2\rightarrow CH_2{:}N.CH_3+NH_3 \quad (6)$$
$$CH_2{:}N.CH_3\rightarrow C_2H_3N+H_2 \quad (7)$$

occur in addition to (1) and (2) and instead of (3).

Reactions (3) and (6) are very complicated for elementary reactions and are therefore rather unlikely processes. Reaction (5), if it occurred at low temperatures, implies that the methyl-

amine radical is very unstable. In view of the data of Phibbs and Darwent[4] on the stability of the rather similar radical CH_2OH, this suggestion appears improbable. The mercury photosensitized reaction of methylamine has been investigated in the hope of obtaining additional information about some of the uncertain points in the above mechanisms.

A heavy liquid was obtained and found to consist largely (about 75 percent) of the compound

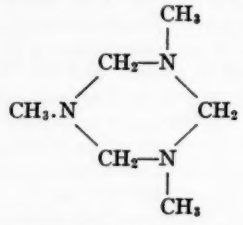

i.e., the trimer of $CH_3N{:}CH_2$. This substance was identified by comparison of the physical properties with those of an authentic sample and by the behavior and properties of the derivatives of the known and unknown samples. The other 25 percent of the liquid was composed of a much heavier liquid and unchanged methylamine which had dissolved in the product.

Examination of the uncondensable products showed that (1) hydrogen was the only important lighter product, (2) the rate of production of hydrogen was, initially, independent of time, (3) the initial rate was independent of methylamine pressure between 16 and 398 mm, and (4) the initial rate was only slightly affected by temperature between 20°C and 200°C. These experiments were repeated with CH_3ND_2, and the following additional points were established: (5) the composition of the hydrogen was about 66 percent HD, 33 percent H_2, and 2 percent D_2, (6) the composition of the hydrogen did not change with the duration of the experiment or with temperature between 25° and 200°C. Some experiments with CD_3NH_2 of uncertain purity gave 70 percent HD, 30 percent H_2, and very small amounts of D_2.

The foregoing results (iii and iv) indicate that the hydrogen atoms, produced in reaction (1) disappear by reaction (2) so that reaction (5) is probably of very minor importance. The structure of the liquid product suggests that reaction (7), as written, does not occur and that subsequent dehydrogenation of the product, if this does occur, is probably due to secondary reactions of the product. Points (v) and (vi) show that both of the radicals CH_3NH and CH_2NH_2 are formed, but we are unable to say whether both are formed in reactions (1) and (2), or whether only one is formed in (1) and the other in (2). Some experiments, now in progress, on the reactions of methyl radicals with the deuterated methylamines should give more information about these reactions.

If our conclusions are correct, then the formation of the substance $CH_3N{:}CH_2$ may be explained logically without the necessity of postulating reactions of the type of (3) or (6), since the recombination of those radicals would be expected to yield

$$CH_3.NH.NH.CH_3 \quad (I), \qquad CH_3NH.CH_2.NH_2 \quad (II),$$

and

$$NH_2.CH_2.CH_2.NH_2 \quad (III).$$

Compound II contains one amino group and one substituted amino group attached to the same carbon atom and may be expected to be unstable and to decompose readily into $CH_3N{:}CH_2$ and ammonia

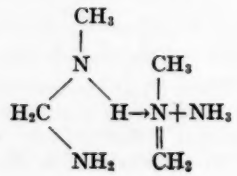

The methyl methyleneimine polymerizes to give the liquid product. It is not surprising that both radical should be produced in these reactions (contrast methyl alcohol)[4] since the C—H and N—H bonds are probably very similar, whereas the O—H bond in methyl alcohol is significantly stronger than the C—H bonds.

Repeated efforts to detect compounds (I) and (III) have proved negative. It must be then concluded that the unlike radicals tend to recombine more readily than do the like radicals, although the reason for this is not clear.

* Contribution No. 2686 from the National Research Laboratories, Ottawa, Canada.
† N.R.C. Postdoctoral Fellow (1950–52).
[1] W. A. Noyes and P. A. Leighton, *The Photochemistry of Gases*, (Reinhold Publishing Company, New York, 1941), p. 382.
[2] H. J. Emeleus and L. J. Jolley, J. Chem. Soc. 1612 (1935).
[3] O. C. Wetmore and H. A. Taylor, J. Chem. Phys. **12**, 61 (1944).
[4] M. K. Phibbs and B. deB. Darwent, J. Chem. Phys. **18**, 495 (1950).

Polyhedral Flames with Hydrogen and Hydrocarbons

HERBERT BROIDA AND WALTER KANE
National Bureau of Standards, Washington, D. C.
(Received March 24, 1952)

MANTON, von Elbe, and Lewis[1] have discussed the formation of cellular flames on the basis of two approximate theories, namely (1) hydrodynamic instability of the combustion front and (2) change of the mixture composition due to differential diffusion. They also present experimental evidence from explosions in bombs to support the latter theory.

During some studies concerning the effects of diluents upon temperatures and flame speeds of premixed combustible mixtures, we have found several mixtures that produce polyhedral flames.[2] These results tend to agree with the diffusion theory. Gaseous fuels and oxygen premixed with helium, argon, and nitrogen were burned above a constant velocity nozzle of one-half inch diameter.[3]

In hydrogen flames with argon or nitrogen making up 60 to 80 percent of the mixture, the usual symmetrical cone of the reaction zone was absent, and the flame consisted of several luminous zones separated by dark regions. The luminous zones were convex

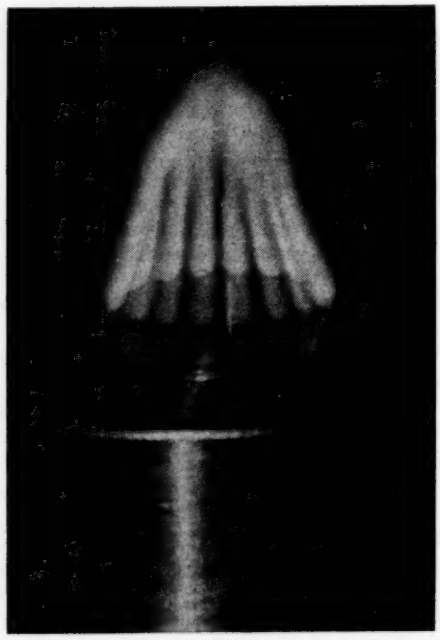

FIG. 1. Flame photograph.

toward the unburned gas. These flames are somewhat similar in appearance to those described recently by Garside and Jackson[4] as occurring in diffusion flames of hydrogen and nitrogen or carbon dioxide mixtures. There was so little luminosity that the structure could best be observed by the refraction of light through the hot gases. The structure was brought out more clearly by the introduction of vaporized sodium chloride into the unburned mixture, giving the characteristic yellow color to the hot regions. The photograph is of one such flame with a lean mixture of hydrogen and oxygen diluted with 75 percent nitrogen. Sixteen bright regions were counted in this particular flame. This was the largest number of regions observed, but the number decreased to as few as four with changes of concentration and velocity.

Similar flames were obtained for hydrogen-oxygen ratios of from 140 to 25 percent of stoichiometric. The polyhedral flames were obtained more readily under conditions near blow-off or flash-back. The width of the dark regions relative to that of the luminous zones increased with decreasing hydrogen concentration. In flames diluted with helium the polyhedral flames were much more difficult to obtain, i.e., greater diluent and leaner mixtures were necessary. This effect of helium is a striking confirmation of the diffusion hypothesis. Both hydrogen and oxygen diffuse more rapidly through helium than through nitrogen or argon, but the ratio of their diffusivities is nearer unity and thus the effect of preferential diffusion of hydrogen from the unburned gas is less pronounced.

In propane flames the same effects were observed except that polyhedral structures appeared in mixtures rich rather than lean in propane. It was only for very rich flames that the wide non-luminous regions as shown in the photograph were found. For mixtures nearer stoichiometric the dark regions were reduced to very thin lines at the edges between the convex surfaces. We were not able to obtain polyhedral structure in the propane-oxygen flame diluted with large amounts of helium.

No polyhedral structure was observed in acetylene flames. This is consistent with the diffusion hypothesis since the diffusion rates of oxygen and acetylene are approximately equal.

[1] Manton, von Elbe, and Lewis, J. Chem. Phys. **20**, 153 (1952).
[2] Similar unusual structures of flames obtained under different conditions have been described in detail by F. A. Smith, and S. F. Pickering, J. Research Natl. Bur. Standards **3**, 65 (1929).
[3] Caldwell, Broida, and Dover, Ind. Eng. Chem., **43**, 2731 (1951).
[4] J. E. Garside and B. Jackson, Nature **168**, 1085 (1951).

On the Complexity of the N—H Stretching Vibration Band in Pyrrole and Indole

NELSON FUSON AND MARIE-LOUISE JOSIEN
Fisk University, Nashville, Tennessee
(Received March 21, 1952)

AT one point in a recent paper published in this journal[1] a comparison was made between the results obtained for the infrared absorption band of the N—H valence vibration frequency fundamental in pyrrole and indole and the results previously observed for the harmonics of this vibration.[2,3,4] Dr. R. M. Badger[5] has kindly called our attention to a paper which we missed in our survey of the literature. This paper[6] is a detailed study of the third harmonic of pyrrole which shows that the secondary bands observed on the low frequency side of the 2nd and 3rd harmonics cannot be either associated bands or bands produced by different species of pyrrole molecules. The 70 cm^{-1} spacing between the main band and the stronger subsidiary in the 3rd harmonic region suggests that for the fundamental one should observe a shoulder separated from the main peak by 20 to 30 cm^{-1}. However, in all our solution spectra[1] the nonassociated band for both pyrrole and indole appears very sharp and without a shoulder. Also a recent trial run over the fundamental band of pyrrole in the vapor state (at room temperature, 7 mm Hg pressure and in a cell 100 mm long) reveals that the "free" N—H valence vibration band lies at 3535 cm^{-1} and is without noticeable structure. There is, of course, the possibility that two or more band systems are so close together in the spectrum of the fundamental that they cannot be even partially resolved. In the light of the above comments, we believe that while our results[1] are not in themselves sufficient to remove the basis for the hypothesis of two types of molecules, they do add weight to the hypothesis of the existence of but one kind of pyrrole (and indole) molecule.

[1] Fuson, Josien, Powell, and Utterback, J. Chem. Phys. **20**, 145 (1952).
[2] O. R. Wulf and U. Liddell, J. Am. Chem. Soc. **57**, 1464 (1935).
[3] M. Freymann, Ann. chim. (11) **11**, 11 (1939).
[4] L. Pauling, J. Am. Chem. Soc. **58**, 94 (1936).
[5] Private communication of February 27, 1952.
[6] L. R. Zumwalt and R. M. Badger, J. Chem. Phys. **7**, 629 (1939).

Catalysis of *Cis-Trans* Isomerization by Paramagnetic Substances

HARDEN MCCONNELL*
Department of Physics, The University of Chicago, Chicago 37, Illinois
(Received March 25, 1952)

CIS-TRANS isomerizations about carbon-carbon double bonds are frequently catalyzed by paramagnetic molecules or atoms such as O_2, NO, NO_2, I, Br, Na, K, Rb, Cs.[1] Magee, Shand, and Eyring[2] suggested that the combination of low frequency factors[3] ($A \sim 10^5$ or less) and low activation energies ($E \sim 10-30$ kcal/mole) found for some noncatalyzed isomerizations (e.g., maleic seter→fumaric ester) indicate that such isomeric molecules pass through a triplet state when twisting from the *cis* to the *trans* form. This idea is illustrated in Fig. 1(a), which gives a schematic representation of the potential energy curves ($V(\theta)$) for the lowest energy singlet (S) and triplet (T) electronic states of an ethylene-type isomer as a function of the angle (θ) of rotation about a carbon-carbon double bond.[4] Isomerizations via T and S electronic states are indicated by horizontal arrows (1) and (2), respectively, in Fig. 1(a).

The frequency factor for isomerization via path (1) can be related to the energy gap (ϵ in Fig. 1(a))[5] which results from a mixing of the S and T states by spin-orbit interaction.[2] For small ϵ's the frequency factor is approximately proportional to ϵ^2.[6] For hydrocarbons,[2,7] $\epsilon \approx 0.3-10$ cm^{-1}.

Eyring and Harman[8] suggested that paramagnetic substances catalyze isomerization through path (1) by providing "a non-homogeneous magnetic field which will act differently on the two magnetic dipoles arising from the spin of the two electrons in the double bond." Since magnetic spin-spin and (spin of one electron)-(orbit of another) interactions are weaker than the here already small (spin of one electron)-(orbit of the same electron) interactions, it is doubtful that magnetic interactions are responsible for the catalysis of isomerization. The following is a qualitative alternative explanation for the catalytic activity of paramagnetic substances.

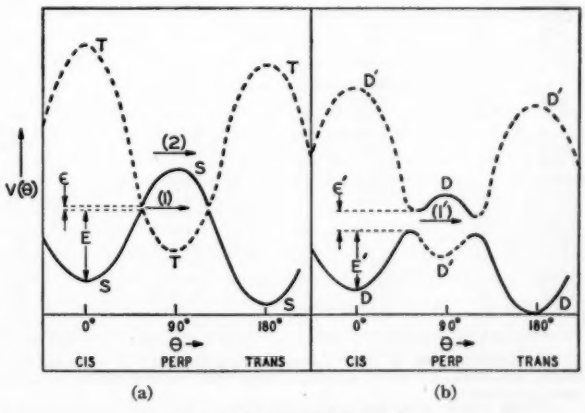

(a) (b)

FIG. 1. Diagram of energies.

If, for example, a doublet electronic state of a catalyst atom interacts with the S and T states of the isomer, two doublet states are formed (D and D' in Fig. 1(b)) together with a quartet state. The minimum separation of these doublet states, ϵ' in Fig. 1(b), will in general be determined by the strength of the chemical binding between catalyst and isomer molecule. Since ϵ' need only be of the order of kT to make isomerization by path (1′) about 10^4-10^7 times more probable than by path (1),[6] it appears that even weak catalyst-isomer chemical interactions can account for the catalytic effect of paramagnetic molecules. Analogous considerations apply for catalysts in triplet states. No corresponding mechanism exists for catalysis of isomerization by substances in singlet states. These conclusions may represent an improvement over the well-known chemical arguments that some atoms (e.g., iodine) catalyze isomerization by binding to an olefinic molecule and "breaking" the carbon-carbon double bond.

* National Research Council Postdoctoral Fellow, 1950–52.
[1] For key references see P. W. Selwood, Chem. Rev. **38**, 41 (1946); B. Tamamushi, Bull. Chem. Soc. Japan **19**, 148 (1944); Dickinson, Wallis, and Wood, J. Am. Chem. Soc. **71**, 1238 (1949).
[2] Magee, Shand, and Eyring, J. Am. Chem. Soc. **63**, 677 (1941).
[3] Specific isomerization rate $(\text{sec}^{-1}) = A \exp(-E/RT)$.
[4] Compare $V(\theta)$ for ethylene given by R. S. Mulliken and C. C. J. Roothaan, Chem. Rev. **41**, 219 (1947).
[5] The energies ϵ and ϵ' are exaggerated in Fig. 1 for clarity.
[6] Glasstone, Laidler, and Eyring, *The Theory of Rate Processes* (McGraw-Hill Book Company, Inc., New York, 1941), pp. 148–150, 323–328.
[7] D. S. McClure, J. Chem. Phys. **17**, 905 (1949).
[8] R. A. Harman and H. Eyring, J. Chem. Phys. **10**, 557 (1942).

Infrared Spectral Data and Tentative Assignments for CF_3Br and CF_3I

PAUL R. MCGEE AND FORREST F. CLEVELAND
Spectroscopy Laboratory, Department of Physics,
AND
SIDNEY I. MILLER
Department of Chemistry, Illinois Institute of Technology, Chicago 16, Illinois
(Received March 20, 1952)

THE recent publication[1] of infrared spectrograms of CF_3Br and CF_3I, together with the absence of any quantitative infrared spectral data in the literature, prompts us to report our results for these compounds. We have obtained wave numbers and estimated relative intensities of gaseous CF_3Br and CF_3I in the region 400–2200 cm^{-1} with a Beckman *IR*-2 spectrophotometer having KBr optics. The CF_3Br (or CF_3I) was prepared by thermal bromination (or iodination) of CF_3COOAg.[2,3]

TABLE I. Infrared spectral data and tentative assignments for gaseous CF_3Br and CF_3I.[a]

CF_3Br		CF_3I		Tentative assignment	Type
ν	I_e	ν	I_e		
300[b]	···	260[b]	···	ν_6	E
405[b]	···	390[b]	···	ν_3	A_1
···	···	(501)	*vw*	···	···
···	···	518	*vw*	$2\nu_6$	A_1+E
···	···	(529)	*vw*	···	···
547	*m*	537	*m*	ν_5	E
···	···	559	*m*	$\nu_1-2\nu_6$	A_1+E
693	*s*	···	···	$\nu_1-\nu_3$	A_1
754	*vs*				
760	*vs*	747	*vs*	ν_2	A_1
768	*vs*	737	*vs*		
···	···	777	*m*	$2\nu_3$	A_1
···	···	811	*m*	$\nu_1-\nu_6$	E
848	*m*	···	···	$\nu_5+\nu_6$	A_1+A_2+E
951	*w*	924	*w*	$\nu_3+\nu_5$	E
···	···	1030	*vs*	$2\nu_5$	A_1+E
1089	*vs*	1080	*vs*	ν_1	A_1
1210	*vs*	1187	*vs*	ν_4	E
1308	*s*	1274	*vs*	$\nu_2+\nu_5$	E
1379	*w*	1334	*w*	$\nu_1+\nu_6$	E
1424	*w*	···	···	$\nu_2+\nu_4-\nu_5$	A_1+A_2+E
1501	*w*	1441	*w*	$\nu_4+\nu_6$	A_1+A_2+E
1622	*w*	1611	*w*	$\nu_1+\nu_5$	E
1747	*w*	1714	*w*	$\nu_4+\nu_5$	A_1+A_2+E
1839	*w*	1814	*w*	$\nu_1+\nu_2$	A_1
1961	*w*	1910	*w*	$\nu_3+\nu_4$	E
···	···	2132	*vw*	$2\nu_1$	A_1

[a] ν = wave number in cm^{-1}; I_e = estimated intensity (*s* = strong, *m* = medium, *w* = weak, *v* = very); and the parentheses enclose bands whose existence is uncertain.
[b] These bands were not measured directly but were determined from overtone and combination frequencies.

The observed wave numbers, estimated relative intensities, and tentative assignments are given in Table I. For both compounds ν_3 and ν_6 had to be determined indirectly from combinations and overtones since they did not fall within the range of the instrument. The present results seem to be in general agreement with the published spectrograms[1] in the region common to the two investigations.

A normal coordinate treatment and a calculation of thermodynamic properties are in progress. Further details and results will be reported later.

[1] Hauptschein, Nodiff, and Grosse, J. Am. Chem. Soc. **74**, 1347 (1952).
[2] A. L. Henne and W. A. Finnegan, J. Am. Chem. Soc. **72**, 3806 (1950).
[3] R. N. Haszeldine, J. Chem. Soc. 584 (1951).

Rotation of the Ammonium Ion in the High Temperature Phase of Ammonium Iodide

C. C. STEPHENSON, L. A. LANDERS, AND A. G. COLE
Department of Chemistry, M.I.T., Cambridge, Massachusetts
(Received March 27, 1952)

THE heat capacity of NH_4I, which we have measured from 14° to 300°K, resembles that of NH_4Cl in many respects. At low temperatures there is an ordered arrangement of the ammonium ions, and the interpretation of the measurements yields a value of 279 cm^{-1} for the frequency of torsional oscillation of the ammonium ion. The gradual transition is somewhat broader than in NH_4Cl and the maximum in the heat capacity occurs at 231.0°K. The entropy change associated with this transition is in agreement with the theoretical value of $R \ln 2$ for an order-disorder transformation similar to that in NH_4Cl.

At about 257°K, ammonium iodide undergoes a first-order transformation from the CsCl structure to a high temperature phase with the NaCl structure. The heat capacity of this high-temperature phase is unusual in that it is 3.8 cal mole^{-1} lower than that of the low temperature phase. This decrease in heat capacity, the small slope of the heat capacity of the phase with the NaCl structure, and the difficulty in placing the ammonium ion in an environment of six rather than eight iodide ions suggest that the ammonium ion is rotating.

Three of the eighteen degrees of freedom for NH_4I may be assigned to a torsional oscillation or a rotation of the ammonium ion, and these three degrees of freedom were clearly identified with torsional oscillation for the phase with the CsCl structure. Each degree of freedom of torsional oscillation contributes R cal mole^{-1} to the heat capacity if fully excited, whereas one degree of freedom of rotation contributes $R/2$ cal mole^{-1}. A change from torsional oscillation to free rotation, both fully excited, would take place with a decrease of 2.98 cal mole^{-1} in the heat capacity for three degrees of freedom. The observed decrease is in agreement with this picture although it is necessary to assume that the other factors contributing to the heat capacities of the two phases are essentially the same. The difference between torsional oscillation and rotation should be more easily recognized, and the interpretation more convincing, from measurements of the heat capacity at much lower temperatures. The heat capacity associated with torsional oscillation obeys an Einstein function at low temperatures, whereas the rotation of the ammonium ion will remain classical down to about 30°K. Hence, a study of the high temperature phase at low temperatures becomes important.

The high temperature phase of NH_4I can be supercooled at least 80°, but the sample in the calorimeter converted to the stable phase at approximately 200°K, and we were unable to supercool

any pure sample below this temperature. However, the transformation is hindered by replacing the ammonium ion with potassium ion and by thorough drying, and the transformation to the stable CsCl structure did not occur in a thoroughly dried sample of a solid solution of NH_4I and KI which contained 45.8 mol percent NH_4I. At temperatures between 14° and 100°K, the heat capacity of this solid solution is higher than the heat capacity of either potassium iodide or the stable phase of ammonium iodide.

The only reasonable interpretation of this excess heat capacity at low temperatures, which is associated with the type of motion of the ammonium ion, is that one or more of the three degrees of freedom is rotational in nature.

Effect of a Liquid Phase Velocity on the Growth and Collapse of Gas Bubbles

V. J. Berry
Stanolind Oil and Gas Company, Tulsa, Oklahoma
(Received March 27, 1952)

THE rates of growth and of collapse of gas bubbles in static, heterogeneous systems have recently been calculated.[1] Although the effect of translational motion in the liquid phase was not considered quantitatively, it was emphasized that in most situations of physical interest such motion does occur. For example, the unbalanced system of forces on a free gas bubble causes it to accelerate upward until a terminal velocity is reached. For very small bubbles in water at atmospheric conditions this terminal velocity may be approximated by the expression[1]

$$V=3\times10^4R^2 \text{ cm/sec}, \tag{1}$$

where R is the bubble radius in cm. Another situation of interest is that of growth and collapse of interstitial gas bubbles in oil reservoirs. The rates of flow of oil and water in reservoirs are generally quite small so that the liquid surrounding a bubble possesses only laminar motion.

In a recent letter to this Journal, Roesler[2] has evaluated the effect of gross liquid movement upon growth times. The effects of both laminar and turbulent regimes were investigated using the quasi-static approximation of Epstein and Plesset. This latter contribution, however, is restricted to a consideration of those situations in which the relative velocity is large.

The time required for a particle to diffuse a distance equal to the bubble radius R may be approximated by Einstein's relation, $t\approx R^2/2K$. If this time is small in relation to the time R/V for convective transport through the same distance, the following condition is derived:

$$RV/K\ll1. \tag{2}$$

It is the purpose of the present discussion to consider the rates of collapse and of growth of bubbles for those situations in which the net translatory motion of the liquid phase is such that Eq. (2) is satisfied. Throughout the following treatment we shall adhere to the notation established by Epstein and Plesset. The effect of surface tension is neglected as in the first-order calculations of Epstein and Plesset.

The differential equation describing concentration of dissolved gas in the liquid phase is

$$K\nabla^2C=(\partial C/\partial t)+\mathbf{V}\cdot\nabla C, \tag{3}$$

in which K is assumed constant. For the velocity term the approximate expressions due to Stokes[3] are valid, since for all conditions of physical interest the inequality of (2) generally insures that the Reynolds number of the flow is also small. The nonlinear velocity term due to the radial motion of the liquid phase during the process of bubble growth or collapse will be neglected. This effect has been computed numerically by the writer and has been found to exert only a small influence for values of $|(C_s-C_i)/\rho|<0.1$.

The quasi-static method of solution which neglects the term $\partial C/\partial t$ was shown by Epstein and Plesset to be reasonably accurate for $|(C_s-C_i)/\rho|\ll1$, which is the usual condition encountered for systems in which chemical reaction does not occur. In any event, the effect of liquid phase motion on the quasi-static calculation will be indicative of the effect to be expected in actual physical situations.

If Stokes' expression for the velocity is introduced and if the partial time derivative is suppressed, the radial component of the concentration gradient, averaged over the entire spherical contour, is given[4] by the following power series in the parameter β, where $\beta=RV/K$.

$$\left.\frac{\partial C}{\partial r}\right|_{r=R}=-\frac{(C_s-C_i)}{R}\left\{1+\tfrac{1}{2}\beta+\frac{581}{960}\beta^2+\cdots\right\}. \tag{4}$$

Following the method of Epstein, the differential equation for β is, neglecting terms of higher order than β^2 (the constant α has the value $|(C_s-C_i)/\rho|K$)

$$\beta(d\beta/dt)=\mp(\alpha\beta_0^2/R_0^2)\left\{1+\tfrac{1}{2}\beta+\frac{581}{960}\beta^2\right\}. \tag{5}$$

For dissolving bubbles the negative sign applies, whereas the positive sign applies to growing bubbles. If Eq. (5) is integrated, the collapse time t_c to terms including β_0^2 is found to be

$$(2\alpha/R_0^2)t_c=1-\tfrac{1}{2}\beta_0-\frac{341}{1920}\beta_0^2. \tag{6}$$

The time t_g required for a bubble to grow to a size $R=10R_0$ is similarly

$$(2\alpha/R_0^2)t_g=99\left\{1-\frac{111}{33}\beta_0-\frac{34441}{1920}\beta_0^2\right\}. \tag{7}$$

The quasi-static solutions due to Epstein yield the results $(2\alpha/R_0^2)t_c=1$ and $(2\alpha/R_0^2)t_g=99$, respectively.

[1] P. S. Epstein and M. S. Plesset, J. Chem. Phys. **18**, 1505 (1950).
[2] F. C. Roesler, J. Chem. Phys. **19**, 512 (1951).
[3] H. Lamb, *Hydrodynamics* (Cambridge University Press, London, 1932), pp. 597–8.
[4] R. Kronig and J. Bruijsten, Appl. Sci. Research **A2**, 439 (1950).

X-Ray Investigation of $Co(NH_3)_6PbCl_6$ and $Co(NH_3)_6BiCl_6$

Masao Atoji[1] and Tokunosuke Watanabe
Faculty of Science, Osaka University, Nakanoshima, Osaka, Japan
(Received March 24, 1951)

TWO cobaltic hexammine complex salts having the compositions $Co(NH_3)_6PbCl_6$ and $Co(NH_3)_6BiCl_6$ were prepared by Mr. M. Mori[2] at Tokyo University. In these compounds Pb and Bi seem to be in the tervalent state, though this is open to some doubt. By Gouy's cylinder method it was found that $Co(NH_3)_6PbCl_6$ is diamagnetic with a mass susceptibility of -0.3×10^{-6} cgs units[2] so that the lead atoms in this compound should be in two valency states, di- and tetravalent. It occurred to the present authors that the structures of these two compounds might be closely related to that of the analogous complex, $Co(NH_3)_6TlCl_6$, whose structure was recently determined by us.[3]

Powder photographs of these three compounds were prepared using Co K_α radiation filtered through Fe_2O_3 and aluminium foil to eliminate general and secondary x-rays. The general features of the photometer curves are quite similar, though they give a small number of additional lines at small diffraction angles not observed in the photographs of $Co(NH_3)_6BiCl_6$ and $Co(NH_3)_6TlCl_6$ (Fig. 1). It was found that the crystal structure of $Co(NH_3)_6BiCl_6$ is completely isomorphous with that of $Co(NH_3)_6TlCl_6$. The crystallographic data and atomic positions of $Co(NH_3)_6BiCl_6$ are as follows: $a=11.54\pm0.01$ A; $z=4$; $d_{calc}=2.515$ g cm^{-3}, $d_{obs}=2.4$ g cm^{-3}; space group is Pa3-T_h^6; atomic coordinates,[4] 4 Bi (a) 0, 0, 0, $+\mathcal{D}$,[5] 4 Co (b) $\frac{1}{2}$, $\frac{1}{2}$, $\frac{1}{2}$, $+\mathcal{D}$, 24 Cl and 24 NH_3 (d) x_i, y_i, z_i, $+\mathcal{D}$, where $x_{Cl}=0.139$, $y_{Cl}=0.150$, $z_{Cl}=-0.075$, $x_{NH_3}=0.09$, $y_{NH_3}=0.09$, $z_{NH_3}=0.04$; interatomic distance, Bi-Cl=2.52 A, Co-NH_3=1.97 A (assumed).

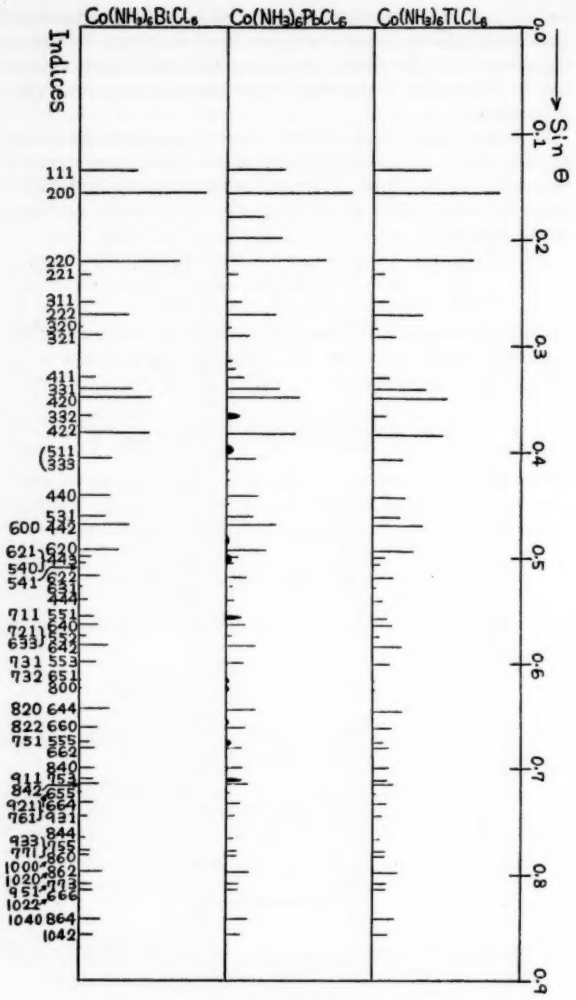

FIG. 1. Intensities deduced from photometer curves.

Most of the diffraction lines of $Co(NH_3)_6PbCl_6$ can be explained in the same manner as those of $Co(NH_3)_6BiCl_6$, where $a=11.52\pm0.01$ A, $z=4$, $d_{calc}=2.520$ g cm^{-3} and space group Pa3-T_h^6 (except for faint additional lines). All the additional lines observed in the photograph of $Co(NH_3)_6PbCl_6$ can be accounted for by slight adjustment of chlorine atom positions and by orientation of the complex radical. Thus the conclusion derived from the magnetic measurements has been confirmed by x-ray analysis. Further work is now in progress using all (*hkl*) reflections obtained from single crystal photographs from which it is hoped to determine accurately the configuration and orientation of the complex radicals.

The color of $Co(NH_3)_6TlCl_6$ is orange. It seems to be somewhat deeper than that expected from $Co(NH_3)_6^{3+}$ and $TlCl_6^{3-}$, which constitute the crystal. We have postulated that $TlCl_6^{3-}$ in this crystal might impart coloration due to the covalent character of the Tl—Cl bonds, as revealed by the short interatomic distances.[3,6] The dark brownish-violet color of $Co(NH_3)_6PbCl_6$, however, may not be interpreted in the same way. We have already shown that Pauling's rule holds exactly in the structure of $Co(NH_3)_6TlCl_6$.[3] However, it should be emphasized that this is not the case for $Co(NH_3)_6PbCl_6$, unless some of the chlorine atoms attached to Pb^{2+} are neutral and some attached to Pb^{4+} carry double negative charges. The color of this crystal may depend upon whether resonance occurs or possibly upon an irregular electrostatic field. These circumstances may give some information on the general problem of the colors of compounds containing the same atom in different valence states.[7,8]

The authors wish to express their best thanks to Professor I. Nitta for his continued interest during the work. One of us (M.A.) wishes to express his gratitude to Professor W. N. Lipscomb of the University of Minnesota for his kindest advice.

[1] Now at School of Chemistry, University of Minnesota, Minneapolis, Minnesota.
[2] M. Mori (to be published).
[3] Watanabe, Atoji, and Okazaki, Acta Cryst. **3**, 405 (1950).
[4] *International Tables for the Determination of Crystal Structures* (1935). Berlin: Borntraeger.
[5] The symbol ↄ represents the face-centered permutation.
[6] K. S. Pitzer and J. H. Hildebrand, J. Am. Chem. Soc. **63**, 2472 (1941).
[7] L. Pauling, Chem. Eng. News **25**, 2970 (1947).
[8] As a possible contribution to this problem, the crystal structures of $(NH_4)_2SbCl_6$ and K_2SbCl_6, in which the antimony atoms show two valency states, are being studied in detail using single crystals (Sasada, Atoji, and Watanabe).

The Dissociation Energies of HS and S_2

HAROLD L. FRIEDMAN
Department of Chemistry, University of Southern California, Los Angeles 7, California
(Received April 7, 1952)

FRANKLIN and Lumpkin[1] have recently determined the ΔH^0_f of the HS radical by an electron impact method. They note that their value is not in accord with Porter's[2] spectroscopic determination of the dissociation energy of this radical. However, this conclusion derives from a calculation using a ΔH^0_f of S atoms[3] which is based on a dissociation energy of S_2 of 76.6 kcal. A value of $D(S_2)=101$ kcal is generally favored,[4,5] and Franklin and Lumpkin themselves offer independent evidence for the higher value. Using $D(S_2)=101$ kcal, we may calculate from their ΔH^0_f of HS that D(HS) = 79.2 kcal, which agrees with Porter's value D(HS) = 84.9 kcal within experimental error.

This is additional evidence for the higher dissociation energy of S_2.

[1] J. L. Franklin and H. E. Lumpkin, J. Am. Chem. Soc. **74**, 1023 (1952).
[2] G. Porter, Disc. Faraday Soc. **9**, 60 (1950).
[3] F. D. Rossini *et al.*, "Selected Values of Chemical Thermodynamic Properties," Natl. Bur. Standards, Washington, D. C., June 30, 1949.
[4] P. Goldfinger, Disc. Faraday Soc. **9**, 81 (1950).
[5] A. G. Gaydon, *Dissociation Energies and Spectra of Diatomic Molecules* (John Wiley & Sons, Inc., New York, 1947), pp. 212, 219.

The Nature of the Gradual Transition in NH_4Cl and ND_4Cl

C. C. STEPHENSON, R. W. BLUE, AND J. W. STOUT
Department of Chemistry, M.I.T., Cambridge, Massachusetts
(Received March 27, 1952)

THE gradual transition in ammonium chloride, characterized by an anomalous heat capacity with a maximum at 242.4°K, has been interpreted as the onset of rotation by Pauling,[1] and as an order-disorder effect by Frenkel.[2] Spectroscopic evidence[3] supports the latter view, in that the frequency of torsional oscillation of the ammonium ion has been observed both above and below the transition region. The recent results of Goldschmidt and Hurst[4] by neutron diffraction support neither hypothesis, and are unsatisfactory in that the ammonium ions seemed to be ordered both above and below the transition region. A more attractive picture is that the room temperature phase of NH_4Cl is similar to that of NH_4Br.[5]

The entropy change associated with the transition affords a test of the two hypotheses, and this entropy change can be estimated from heat capacity measurements. The order-disorder nature of the transitions in potassium and ammonium dihydrogen phosphates and arsentates was established in this manner.[6] If the transition in NH_4Cl is from an ordered state at low temperatures to a state in which the ammonium ion may occupy two positions

of nearly equal energy at high temperatures, the entropy change will be simply $R\ln 2 = 1.36$ cal deg^{-1} mole^{-1}. Furthermore, the same entropy change will be associated with the transition in ND_4Cl, in spite of the fact that the moment of inertia has been doubled.

The heat capacities of NH_4Cl and ND_4Cl were measured in this laboratory some time ago from 20° to 300°K. The entropy change associated with the gradual transition lies between 1.2 and 1.5 cal deg^{-1} mole^{-1} for both compounds. The agreement with the value $R\ln 2$ is convincing evidence for the order-disorder nature of the transition.

[1] L. Pauling, Phys. Rev. **36**, 430 (1930).
[2] J. Frenkel, Acta Physicochim. U.R.S.S. **3**, 23 (1935).
[3] E. L. Wagner and D. F. Hornig, J. Chem. Phys. **18**, 296, 305 (1950).
[4] G. H. Goldschmidt and D. G. Hurst, Phys. Rev. **83**, 88 (1951).
[5] H. A. Levy and S. W. Peterson, Phys. Rev. **83**, 1270 (1951).
[6] C. C. Stephenson and H. E. Adams, J. Am. Chem. Soc. **66**, 1405, 1409 (1944).

The Appearance Potential of C^+ in the Mass Spectra of Some Substituted Methanes and the Heat of Sublimation of Carbon*

HERMAN BRANSON AND CARTER SMITH
Department of Physics, Howard University, Washington 1, D. C.
(Received April 7, 1952)

OF the several values which have been proposed for the heat of sublimation of carbon,[1] the direct and indirect evidence now seems to have narrowed the possibilities to either 7.36 ev (169.7 kcal) or 5.885 ev (135.7 kcal). Glockler[2] states that the higher value 7.36 ev concurred in by three recent experimental determinations[3-5] is more consistent with other informationon CC, CN, CO, NO, OO, and NN bonds. Hagstrum[6] and McDowell and Warren[7] report electron impact data and present arguments in support of the smaller value 5.885 ev. This laboratory has begun a study of the mass spectra of series of carbon compounds. The initial results on C^+ in the mass spectra of CH_4, CH_3Cl, CH_3Br, and CH_3I strongly favor 5.885 ev as the heat of sublimation of carbon.

The Nier type mass spectrometer was constructed in this laboratory. The ion beam current was measured with an *FP*-54 in a Penick type circuit.[8] The instrument was calibrated with argon and neon following the technique described by Stevenson.[9] The potentials were measured with a high resistance voltmeter recalibrated regularly against a potentiometer. The method of vanishing current[10] was used to determine the appearance potentials of Table I.

In interpreting these data the following equations are used:

$$\begin{aligned} CH_3X = C\ (\text{gas}) + 3H + X \quad & D(C-3H-X) \\ \tfrac{3}{2}H_2 = 3H \quad & \tfrac{3}{2}D(H_2) \\ \tfrac{1}{2}X_2 = X \quad & \tfrac{1}{2}D(X_2) \\ C\ (\text{graphite}) = C\ (\text{gas}) \quad & L(C) \\ C\ (\text{graphite}) + \tfrac{3}{2}H_2 + \tfrac{1}{2}X_2 = CH_3X \quad & \Delta Hf^0, \end{aligned}$$

where D is the dissociation energy and ΔHf^0 is the standard heat of formation. These equations yield

$$D(C-3H-X) = \tfrac{3}{2}D(H_2) + \tfrac{1}{2}D(X_2) + L(C) - \Delta Hf^0.$$

The ions are produced in the mass spectrometer according to the relation

$$qA(C^+) = D(C-3H-X) + qI(C^+) + \text{kinetic energy} + \text{excitational energy},$$

where q is the charge on the ion, I is the ionization potential of carbon (11.26 volts),[11] and the kinetic and excitational energies represent the total energy in each of these categories possessed by all or any of the neutral fragments (atoms, radicals) or ion produced in the dissociation. For the initial appearance of an ion

TABLE I.

	$A(C^+)$ volts	ΔHf^0[a] electron volts	$L(C)$ electron volts
CH_4	26.9±0.2	−0.69	≤5.99±0.2
CH_3Cl	26.0±0.3	−0.85	≤5.93±0.3
CH_3Br	25.4±0.4	−0.37	≤6.06±0.4
CH_3I	24.4±0.4	+0.21	≤5.86±0.4

[a] F. Rossini *et al.*, "Selected Values of Chemical and Thermodynamical Properties," Circular 500, Natl. Bur. Standards Wash., D. C. (1952).

we have

$$A(C^+) \geq D(C-3H-X) + I(C^+)$$

or

$$L(C) \leq A(C^+) - I(C^+) + \Delta Hf^0 - \tfrac{3}{2}D(H_2) - \tfrac{1}{2}D(X_2).$$

The values are tabulated in Table I with[12]

$$D(H_2) = 4.48 \text{ ev}, \quad D(Cl_2) = 2.48 \text{ ev}, \quad D(Br_2) = 1.97 \text{ ev},$$

and

$$D(I_2) = 1.54 \text{ ev}.$$

These values with the experimental errors are consistent with 5.885 ev as the heat of sublimation of carbon. The assumption of other dissociation processes (e.g., C−H−H−HX or C−H_2−H−X which we believe to be unwarranted for these data in any event) in the production of C^+ does not provide as good an agreement with the higher value 7.36 ev.

* Assisted by ONR, Contract N8-ONR 538.
[1] A. G. Gaydon, *Dissociation Energies* (Dover Publications, New York, 1950).
[2] G. Glockler, Disc. Faraday Soc. **10**, 26 (1951).
[3] Brewer, Gilles, and Jenkins, J. Chem. Phys. **16**, 797 (1948). See, however, a criticism of this work by L. H. Long, J. Chem. Phys. **16**, 1087 (1948).
[4] Simpson, Thorn, and Winslow, AEC General Chemistry Report. ANL-4264 (Argonne Natl. Lab., 1949).
[5] A. L. Marshall and F. J. Norton, J. Am. Chem. Soc. **72**, 2166 (1950).
[6] H. D. Hagstrum, Revs. Modern Phys. **23**, 185 (1951).
[7] C. A. McDowell and J. W. Warren, Disc. Faraday Soc. **10**, 53 (1951).
[8] D. B. Penick, Rev. Sci. Inst. **6**, 115 (1935).
[9] D. P. Stevenson, J. Chem. Phys. **18**, 1347 (1950).
[10] T. Mariner, and W. Bleakney, Phys. Rev. **72**, 807 (1947).
[11] C. E. Moore, "Atomic Energy Levels," Circular 467, Natl. Bur. Standards, Washington, D. C. (1949).
[12] G. Herzberg, *Spectra of Diatomic Molecules* (D. Van Nostrand Company, Inc., New York, 1950).

The Anomalous Susceptibilities of Three-Membered Ring Compounds*

J. R. LACHER, J. W. POLLOCK, AND J. D. PARK
Department of Chemistry, University of Colorado, Boulder, Colorado
(Received March 31, 1952)

PASCAL[1] was the first to study the effect of the cyclopropane ring on the susceptibility of a compound. He employed the ethyl esters of the carboxylic acids of cyclopropane and concluded there was a paramagnetic correction term of 3.4×10^{-6} associated with the cyclopropane ring. Farquharson and Sastri[2] also found a paramagnetic ring correction term of 4.1×10^{-6}. These investigators compared the susceptibilities of cycloalkane carboxylic acids with those of the normal aliphatic acids containing the same number of carbon atoms. No susceptibility measurements on

TABLE I. Molar susceptibilities.

Compound	$-\chi\times10^{+6}$	Compound	$-\chi\times10^{+6}$	Δ
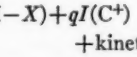	39.9	$CH_3-CH=CH_2$[a]	31.5	8.4
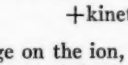	30.7	$CH_3-CH=O$[b]	22.1	8.6
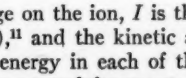	42.5	$CH_3-CH_2-CH=O$[b]	33.7	8.8

[a] Lacher, Pollock, Johnson, and Park, J. Am. Chem. Soc. **73**, 2838 (1951).
[b] *International Critical Tables* (McGraw-Hill Book Company, Inc., New York, 1928), Vol. VI, p. 361.

cyclopropane, ethylene oxide, and propylene oxide have been reported in the literature. Accordingly, we have studied these compounds using the Quincke method previously described.[3] The materials were obtained from commercial sources and purified by a careful distillation in a Hypercal Podbielniak column. The results are given in Table I. For comparison the susceptibilities of the corresponding straight chain isomers as reported in the literature are also included in the table.

The molar diamagnetic susceptibilities for these compounds are unusually large, being about 8.6 units greater than the corresponding straight-chain isomer. The susceptibility for cyclopropane is considerably greater than the value of -31.7×10^{-6} calculated from Pascal's increments;[1] while Farquharson and Sastri's data[2] permit a calculated value of -30.8×10^{-6}. The present data are, however, consistent with the chemical and spectroscopic properties of ethylene oxide and cyclopropane. Walsh[4] has suggested that these compounds contain carbon atoms having trigonal wave functions. If such is the case, the compounds will be magnetically anisotropic. Some of the electrons will be able to precess about the plane of the ring making the susceptibility considerably greater than that of the corresponding straight chain isomer. The effect of p_z electrons on the susceptibilities of aromatic compounds has been discussed by Pauling[5] and Lonsdale.[6] If we assume that cyclopropane has three trigonal carbon atoms with atomic susceptibilities of $-(3/4)6\times10^{-6}$ and that each hydrogen atom contributes -2.9×10^{-6}, then the anisotropy may be calculated to be -27×10^{-6}. In order to account for this, the three p_z electrons must precess in a ring having a radius of 1.46A. In cyclopropane a carbon nucleus is about 0.7A from the center of the triangle; in addition the radius of the orbitals of the valence electrons is approximately 0.7A. Their sum is close to the calculated radius of 1.46A.

In the case of ethylene and propylene oxide one may calculate an anisotropy of -19.8×10^{-6} if one takes the contribution of the bridge oxygen to be $-(3/4)4.6\times10^{-6}$. The effective radius of precession of the p_z electrons becomes 1.25A, which is somewhat less than shown by cyclopropane.

* This work was supported by the ONR, contract N6-onr-231, Task Order VI, project No. NR-056-105.

[1] P. Pascal, Comp. rend. **181**, 656 (1925).
[2] J. Farquharson and M. Sastri, Trans. Faraday Soc. **33**, 1474 (1937).
[3] Lacher, Scruby, and Park, J. Am. Chem. Soc. **71**, 1797 (1949).
[4] A. D. Walsh, Trans. Faraday Soc. **45**, 179 (1948).
[5] L. Pauling, J. Chem. Phys. **4**, 673 (1936).
[6] K. Lonsdale, Proc. Roy. Soc. (London) **159A**, 149 (1937).

Hydrogen Bond Energies in Carboxylic Acids

M. M. Jones,* W. R. Gilkerson,† and G. A. Gallup†
Bailey Chemical Laboratory, University of Kansas, Lawrence, Kansas
(Received April 14, 1952)

THE heat of dissociation of carboxylic acid dimers in the vapor phase may be calculated from a consideration of the van der Waals interaction energy. Account is taken of the orientation, induced dipole, and dispersion interactions between the carbonyl and hydroxyl bonds, as well as cross terms.

A number of approximations were necessary in order that the complexity of the calculation not be greater than its importance merits. These are (a) that the carbonyl and hydroxyl bonds may be considered as classical dipoles with spherically symmetrical polarizability; (b) that the elementary units of bond interaction are additive; (c) the relative orientation and bond distances in the two acid molecules remain constant throughout the association process and are those found experimentally in the formic acid dimer; (d) the principal contributors to such interaction are the carbonyl and hydroxyl bonds. Since we have used London's simplified dispersion relation, all of the assumptions inherent in its derivation are included.

The process considered is the approach of two acid molecules from an infinite separation, to form the dimer configuration given by Pauling[1] for formic acid. The interaction energy relations used were the following:

$$\text{orientation;}\quad U_0=-2\frac{\mu_1\mu_2}{r^3}\cos\vartheta_1\cos\vartheta_2$$

$$\text{induction;}\quad U_I=-\frac{\mu_1^2\alpha_2}{2r^6}(1+3\cos^2\vartheta_1)$$

$$\text{dispersion;}\quad U_D=-\frac{3\alpha_1\alpha_2}{2r^6}\frac{J_1J_2}{J_1+J_2},$$

where μ is the bond moment,[2] α its polarizability,[3] r the distance between bond centers, and J the bond ionization energy.[4]

The calculated heat of dimerization is 15.9 kcal, while the measured values are 14.1 and 16.4 kcal for formic[5] and acetic[6] acids, respectively. It may be concluded that, to a fairly good approximation, the "hydrogen bond" in carboxylic acids may be accounted for on the basis of intermolecular forces operating over a longer range than that usually ascribed to bonding forces. The validity of the type of calculation made here has been critically discussed by London,[7] but he seemed principally concerned with applications to extended conjugated systems, of which ours is not an example.

* du Pont Fellow.
† AEC Predoctoral Fellows.
[1] L. Pauling, *The Nature of the Chemical Bond* (Cornell University Press, Ithaca, New York, 1948), p. 306.
[2] W. A. Waters, *Physical Aspects of Organic Chemistry* (D. Van Nostrand Company, Inc., New York, 1950), p. 94.
[3] S. Glasstone, *Textbook of Physical Chemistry* (D. Van Nostrand Company, Inc., New York, 1946), pp. 530–8.
[4] A. E. Remick, *Electronic Interpretations of Organic Chemistry* (John Wiley & Sons, Inc., New York, 1943), p. 225.
[5] A. S. Coolidge, J. Am. Chem. Soc. **50**, 2166 (1928).
[6] F. H. MacDougall, J. Am. Chem. Soc. **58**, 2585 (1936).
[7] F. London, J. Phys. Chem. **46**, 305 (1942).

Carbon-Oxygen Exchange in Chemisorbed Carbon Monoxide

R. P. Eischens and A. N. Webb
Beacon Laboratories of The Texas Company, Beacon, New York
(Received April 7, 1952)

A QUESTION of interest to the study of the chemisorption of carbon monoxide on iron is whether the carbon is desorbed with the same oxygen to which it was bonded prior to the adsorption. A mixture of $C^{13}O$ and CO^{18} was chemisorbed on iron and then desorbed. The presence of $C^{13}O^{18}$ in the desorbed gas in amounts greater than expected from normal abundance ratios shows that an intermolecular oxygen exchange occurs.

The $C^{13}O$ was prepared by reduction over zinc at 425°C[1] of $C^{13}O_2$ obtained by the addition of perchloric acid to $BaC^{13}O_3$.[2] The CO^{18} was obtained from the Research Institute of Temple University.

The designation $C^{13}O$ as used here refers to carbon monoxide in which the C^{13} abundance has been enriched to 37.9 percent and CO^{18} refers to carbon monoxide in which the O^{18} abundance has been enriched to 14.4 percent. The C^{13} abundance in CO^{18} and the O^{18} abundance in the $C^{13}O$ are normal.

The analysis of the $C^{13}O$ and CO^{18} are shown in Table I.[3]

The O^{18} abundance in the CO_2 is the same as in the CO^{18}; however, the O^{18} abundance in the oxygen is normal.

The iron was prepared by reduction of Fe_2O_3 with purified hydrogen for 6 days at 400°C. The Fe_2O_3 was prepared from the nitrate by conventional precipitation methods.

The volume of nitrogen in the BET monolayer was 89 cc for the 91.1 g sample. The reduction was resumed after the BET determination and continued for an additional 8 days. After the reduction the sample was pumped at 400°C for 2 hours at a pressure of 1×10^{-5} mm to remove the hydrogen.

It was assumed that the iron would chemisorb 91.5 cc of carbon monoxide. A mixture of 39.6 cc of $C^{13}O$ and 57.9 cc of CO^{18} was admitted to the iron at −78°C. Only 75.7 cc were rapidly adsorbed. The remaining 15.8 cc were pumped off with a hand oper-

ated Toepler pump. The chemisorbed carbon monoxide was pumped off with a combination mercury diffusion-Sprengler pump.[4] When the rate of pumping at a specified temperature appeared to be negligible, the temperature was increased. The carbon monoxide collected at each temperature was kept separate and analyzed.

TABLE I.

	$C^{12}O$	CO^{18}
Total carbon monoxide	99.7	90.6
Nitrogen	···	1.6
Oxygen	···	0.4
Carbon dioxide	···	6.0
Hydrogen	0.1	1.4
Methane	0.2	···

The amount of $C^{13}O^{18}$ present at equilibrium was calculated to be 1.4 percent. There is a theoretical blank of 0.1 percent due to the natural abundance of C^{13} and O^{18}. This was confirmed by an experimental blank of 0.1 which was obtained with a sample of the gas mixture which had been exposed to the hot mercury encountered in the gas collecting pump.

The results of the experiment are given in Table II. Here are recorded the temperature at which the carbon monoxide was

TABLE II.

Temp. °C	Volume	Time	$C^{13}O^{18}$
Unadsorbed	15.8	0	···
−78	13.7	28	···
−33	12.5	118	0.3
0	16.1	164	···
25	14.4	236	0.4
60	12.2	284	0.6
120–160	4.9	336	1.3
Loss	1.9	···	···

pumped off, the volume of the batch in cc stp, the accumulated pumping time in hours, and the percentage of the carbon monoxide which is $C^{13}O^{18}$.

The mass spectrometer analyses of the $C^{13}O^{18}$ ratio are accurate to 5 percent of the reported value in the 0.1–0.3 percent range.

The $C^{13}O^{18}$ analyses for the nonadsorbed gas and the batches collected at −78 and 0°C were not successful because the sample bulbs leaked prior to the mass spectrometer determination. This lowered the total carbon monoxide concentration to levels so low that the isotopic composition could not be accurately measured.

The batch collected at 120–160°C is unusual in that about half of the 4.9 cc is carbon dioxide. This carbon dioxide is in isotopic equilibrium with the carbon monoxide.

These data show that significant oxygen exchange occurs at temperatures as low as −33°C, and equilibrium is almost attained within a reasonable time at 120–160°C.

The exchange could be explained by postulating a mechanism which involves an intermediate complex. In the complex a single carbon is attached to two oxygens and can be desorbed with either one. A second mechanism in which the carbon-oxygen bond is ruptured so that atomic species of oxygen and carbon exist on the surface could also be postulated. The data are not sufficient to distinguish between these two mechanisms.

Further work is being done on this problem. The direction of this work is toward the use of purer CO^{18} and study of the exchange at temperatures lower than −33°C.

We are grateful to Dr. L. C. Roess for his interest and cooperation in this work.

[1] R. B. Bernstein and T. I. Taylor, Science **106**, 498 (1948).
[2] The $BaC^{13}O_3$ was obtained from the AEC.
[3] All of analyses reported here were determined with a Consolidated Engineering Type 21–101 mass spectrometer. The analyses were carried out by M. S. Donovan under the supervision of J. H. Shively.
[4] I. E. Puddington, Ind. Eng. Chem. Anal. Ed. **16**, 592 (1944).

Experimental Efforts to Find Radioactivity Induced by the Firing of Shaped Charges

G. J. PLAIN, J. C. MCLAUGHLIN, AND F. K. ODENCRANTZ
U. S. Naval Ordnance Test Station, Inyokern, China Lake, California
(Received March 31, 1952)

EVIDENCES of nuclear transmutations produced by the detonation of shaped charges have been reported.[1] It was reported that when splinters of silver, copper, zinc, and iron from plates of these metals which had been subjected to shaped charges were exposed to a Geiger-Mueller counter an increase in radioactivity was indicated. Especially in the case of silver there was reported a strong indication that owing to the explosion the isotope Ag^{108} had been formed.

In order to form Ag^{108} from ordinary silver either of these two reactions might be feasible, the addition of a neutron to Ag^{107}, or the emission of a neutron from Ag^{109}; the second of these appears highly improbable. From a consideration of the temperature and particle velocities[2] involved in the detonation, the possibility of nuclear transmutations leading to such radioactive isotopes seems extremely unlikely. A proton or neutron, having a velocity of 100,000 ft/sec, which appears to be a conservative upper limit of velocity of the particles in the gas stream, has an energy of only 5 electron volts, and we are aware of no mechanism for neutron production at these low energies. On the other hand, thermonuclear processes seem insufficiently prolific, for the contribution of the thermal velocity at a temperature of 20,000°K would be approximately only 70,000 ft/sec. The stream velocity and temperature could be assumed to be considerably higher without increasing the energy by an order of magnitude.

In an investigation of this effect, nine shaped charges[3] have been fired into targets of brass, aluminum, silver, zinc, and lithium. Three of the charges were 2 inches in diameter of Composition C, with $\frac{1}{8}$-inch brass liners and cone angles of 60 degrees. Two of these were fired into silver targets and one into a brass target from stand-off distances of 6 inches. Three of the charges were 6 inches in diameter, contained 25 pounds of Composition C-3, had $\frac{1}{4}$-inch steel liners and 60-degree cone angles. One of these was fired into an aluminum target from a stand-off distance of 12 inches, one was fired into a zinc target, and the third was fired into a lithium target, the latter two from stand-off distances of 2 feet. The remaining three charges were 4 inches in diameter, of Composition C-3, with 0.004-inch brass liners and 60-degree cone angles. Two of these were fired into silver targets and the third into a zinc target, all from stand-off distances of 12 inches.

A radiation survey meter (Technical Associates, Model F-1 with TA-G4 tube) was taken to the scene of firing and the charge, the target, and the backstop were carefully surveyed for any indications of radioactivity before firing. Immediately after the firings, the targets (or fragments in the case of the 6-inch charges) were checked for radioactivity. The targets and fragments were then brought into the laboratory, and a check for radioactivity was made with a more sensitive radiation detector (Radiation Counter Laboratories Model 100 Mark 1 Geiger tube).

Those targets which were subjected to the 2-inch charges were then sectioned through their craters[4] and a section placed on a photographic plate, being insulated from it by a thin sheet of paper. In those cases where the targets were shattered, fragments were placed on the photographic plate. Those targets subjected to the 4-inch charges showed very little physical damage. Chips from the exposed surface of the silver and zinc were placed on photographic plates. The plates used were C.T.C. Pan and Kodak Spectroscopic Plates.

Contrary to what is reported in reference 1, we found no evidence, either from the radiation counters or from the photographic plates, that any radioactivity was produced by the firing of the shaped charges.

[1] Zygmunt Fonberg, J. Chem. Phys. **19**, 383 (1951).
[2] W. M. Evans and A. R. Ubbelohde, Research (London) **3**, 376 (1950).
[3] Birkhoff, MacDougall, Pugh, and Taylor, J. Appl. Phys. **19**, 563 (1948).
[4] W. M. Evans and A. R. Ubbelohde, Research (London) **3**, 331 (1950).

The *Ortho-Para* Conversion of Deuterium in Molecular Electric Fields

Y. L. SANDLER*
Department of Physical Chemistry, Hebrew University, Jerusalem, Israel
(Received April 7, 1952)

WE have previously shown[1] that an *ortho-para* conversion of deuterium takes place in diamagnetic liquids which only partly can be of magnetic origin. In the latter case it would be expected to be about 10 times slower than the conversion observed with light hydrogen. The ratio of the rate constants actually found for H_2O was only 2.6. This discrepancy was explained as due to an interaction of the inhomogeneous electric fields of the solvent molecules with the electric quadrupole moments of the deuterons in D_2, for the existence of which there had been no previous experimental evidence.

Casimir[4] derived a simple expression for the relative transition probabilities in the deuterium conversion due to a magnetic dipole and due to an electric charge. By replacing the electric field in H_2O by equivalent charges on the nuclei, he obtained an electric conversion rate practically equal to the rate deduced from the experiments,[1] using the quadrupole value for the deuteron meanwhile obtained by the molecular beam method.[2,3]

The deuterium previously used[1] had a rather low *ortho*-concentration. After a method for producing higher concentrations (83 percent) had been worked out[5] the measurements were repeated. It was found that the previously given ratio values were too low. In view of this and doubts expressed more recently,[6] the results of new determinations are reported here, including measurements with the electric dipole liquids D_2O and SO_2, having only small or no nuclear magnetism.

The experimental procedure was the same as previously described; however, the design of the reaction vessels was improved, increasing their ratio of liquid to gas volume. The measured half-lives (true half-life τ/fraction of deuterium in solution) now were about 5 weeks for CS_2 and CCl_4 and roughly 2 weeks for all the other solvents. From 3 to 6 independent runs were made with each solvent. The largest deviations were about 20 percent. The great majority of the results, however, agreed to within 5 percent, always giving higher half-lives than the few deviating results; the latter were not taken into account in computing the results.

The new results are given in Table I, together with the previous results for light hydrogen.[1] The ratios given in the last column now

TABLE I.

	Hydrogen		Deuterium		
Solvent	τ min	$k\times10^5$ lit min^{-1} mole^{-1}	τ min	$k\times10^5$ lit min^{-1} mole^{-1}	k_{H_2}/k_{D_2}
H_2O	183	6.83	830	1.50	4.5
D_2O	420	2.98	1350	0.93	3.2
C_6H_6	360	17.0	2500	2.46	7.0
CS_2	1800	2.32	9300	0.45	5.2
CCl_4	2500	2.67	14,000	0.48	5.6
SO_2	...	...	...	...	2.1

change in the expected way, in accordance with the expected relative contribution of magnetic and electric interactions to the total conversion of deuterium. They range from 7 for C_6H_6, with a large magnetic contribution due to its 6 protons and probably practically no electric contribution, down to 2.1 for SO_2 with a large electric dipole moment but no nuclear magnetism. For CS_2 and CCl_4 a lower ratio was found than for C_6H_6. This probably is connected with the longer reaction time causing a larger error in the measured rate for D_2 and possibly, in part, with the high polarity of the bonds in these molecules.

For evaluating the rate constant of the electric conversion k_{el} in H_2O and D_2O, it seems the best procedure in the present case to choose a factor 7 as an apparent magnetic ratio, as found for C_6H_6. We then obtain $k_{el}=k_{D(2)}-(1/7)k_{H(2)}=5\times10^{-6}$ lit mole^{-1} min^{-1}, both for H_2O and D_2O. Using a magnetic ratio 10, this would lead to $k_{el}=8\times10^{-6}$ for H_2O and 6×10^{-6} for D_2O. Apart from not being equal, these values must be a little too high; for, if 10 is the correct magnetic ratio, the experimental rates for D_2 still seem to be somewhat too high, as seen from the ratios obtained for C_6H_6, CS_2, and CCl_4. The present value $k_{el}=5\times10^{-6}$ is almost 4 times lower than the value deduced from the previous experiments.

Casimir's formula (2)[4] should read[6]

$$k_{magn}/k_{el}=j(j+1)g^2/n_e^2\cdot1.09\times10^4.$$

With $n_e=\frac{1}{3}$ and $k_{magn}=4\times10^{-6}$ for the two protons in H_2O,[4] this leads to $k_{el}=6\times10^{-6}$. The effect of the negative equivalent charge on the oxygen nucleus is not included here; it is not easily estimated accurately. In any case the rates due to the separate charges are not additive and generally no more than a correct order of magnitude can be expected from this type of estimate. Therefore, the agreement with the experimental value may be considered quite satisfactory.

* Present address: Division of Chemistry, National Research Laboratories, Ottawa, Canada.
[1] L. Farkas and Y. L. Sandler, Trans. Faraday Soc. **35**, 337 (1939).
[2] Kellog, Rabi, Ramsey, and Zacharias, Phys. Rev. **55**, 318 (1939).
[3] A. Nordsieck, Phys. Rev. **58**, 310 (1940).
[4] Casimir, Physica **7**, 169 (1940).
[5] L. Farkas and Y. L. Sandler, J. Am. Chem. Soc. **62**, 2877 (1940).
[6] M. Hamermesh, Phys. Rev. **73**, 638 (1948).

Borides of Some Transition Metals*

BENJAMIN POST
Polytechnic Institute of Brooklyn, Brooklyn 2, New York,
AND
FRANK W. GLASER
American Electro Metal Corporation, Yonkers, New York
(Received April 14, 1952)

A NUMBER of hitherto unreported transition metal borides were prepared in the course of a high temperature investigation of several metal-carbon-boron systems.[1] Some structural characteristics of these new phases have been determined by means of an x-ray diffraction investigation of powdered samples.

In the tungsten-boron system, Kiessling[2] has described one monoboride, WB; the unit cell is tetragonal and contains 8 WB, with $a=3.115$A, and $c=16.93$A. In the present investigation it was found that this compound is transformed, reversibly, at approximately 1850 ± 50°C to an orthorhombic modification, with $a=3.19$A, $b=8.40$A, and $c=3.07$A, and with 4 WB per unit cell. This orthorhombic form is isomorphous with CrB.[3] The space group determined for the latter is $D_{2h}^{17}-Cmcm$. A similar transformation in MoB has been reported by Steinitz.

In the titanium-boron system, Ti_2B_5, isomorphous with W_2B_5, has been prepared. The unit cell of Ti_2B_5 is hexagonal and contains 2 Ti_2B_5; $a=2.98$A and $c=13.98$A. Another compound, of probable composition Ti_2B, has also been prepared. The unit cell is tetragonal, with $a=6.11$A, $c=4.56$A, and contains 4 Ti_2B. The lattice is primitive. The space group has not as yet been determined unambiguously.

The existence of a face-centered cubic monoboride of titanium, previously reported by Ehrlich,[5] has been confirmed. Recently, Brewer[6] suggested that Ehrlich's compound was probably TiN. In the present investigation, the preparation of the face-centered cubic compound, corresponding to TiB, was repeated several times with careful exclusion of nitrogen from the reaction chamber. The absence of nitrogen (and carbon) from the reaction product was subsequently confirmed by chemical analysis. The product appeared to be the same as that reported by Ehrlich, except that a_0 was found to be 4.24 ± 0.02A compared with 4.20A reported by Ehrlich.

In the zirconium-boron system, mixtures containing equal atomic proportions of boron and metal were heated to 900°, 1000°, and 1200°C. X-ray diagrams of the product obtained by heating

to 900°C showed the presence of ZrB_2 and zirconium metal. The unit cell of the metal expanded from $a=3.21$A and $c=5.12$A, to $a=3.37$A and $c=5.57$A, indicating considerable solution of boron in the metal. At 1000°C the hexagonal pattern of the metal was replaced by the pattern of a face-centered cubic compound with $a_0=4.65\pm0.03$A.

This appeared, on the basis of boron content and by analogy with TiB, to be ZrB. The possibility that the pattern was that of ZrC, which is also face-centered cubic, with $a_0=4.68$A, was ruled out on the basis of chemical analysis of the product which showed a carbon content of only 0.23 percent. At 1200°C the face-centered cubic compound decomposes. Above this temperature the pattern of a new, unidentified compound appears.

A detailed account of the preparative methods, physical properties, ranges of stability, and crystal structures of these compounds will be published in the near future.

* A portion of this work was carried out under contract with the ONR. The authors wish to thank the agency for permission to publish these data.
[1] F. W. Glaser, J. Metals **4**, 391 (1952); Trans. Am. Mining Met. Engrs. TP 3281E (1952).
[2] R. Kiessling, Acta Chem. Scand. **1**, 893 (1947).
[3] L. H. Anderson and R. Kiessling, Acta Chem. Scand. **4**, 160 (1950).
[4] R. Steinitz, J. Metals **4**, 148 (1952).
[5] P. Ehrlich, Z. angew. Chem. **59**, 163 (1947).
[6] Brewer, Sawyer, Templeton, and Dauben, J. Am. Ceram. Soc. **34**, No. 6 (1951).

On the Vector Map of Crystalline Horsehemoglobin*

DOROTHY WRINCH
Department of Physics, Smith College, Northampton, Massachusetts
(Received April 14, 1952)

PERUTZ has published certain sections of the 3-dimensional vector map of his horse methemoglobin crystal (normal wet) obtained by calculation from observed relative intensities.[1] It is the purpose of this communication to suggest an interpretation of the outstanding feature of this map, called by Perutz "the 5A shell," a region of high vector density completely surrounding the origin.

In the sections, we remark the following features which require interpretation: (a) a vector density decreasing with distance from the origin and remaining above the average value for the crystal (i.e., positive in the sections) up to some distance short of 4A; (b) a below-average density (i.e., negative in the sections) thereafter in all directions up to *ca* 4A; (c) an above-average density in all directions for *ca* 4–6A only; (d) certain regions within the 4/6A shell of specially high density and (e) the existence, in the predominatingly below-density region, 6A to about 9½A, of certain narrow corridors of slightly above-average density.

To interpret the vector map in general, and (a) to (e) in particular, we are limited to the two components of the crystal: (1) the protein component (*MW ca* 66,700) and (2) the enormous water component,[2] which amounts to about 6 HOH molecules per amino acid residue in the protein.

There is no difficulty in accounting for (a) in terms of nearest and next-nearest covalently bonded atoms in (1) and atoms held in a hydrogen bridge in (1) and (2). But the crucial question arises: why is there a below-average number of pairs of atoms somewhat less than 4A apart in *all* orientations, and an above-average number of pairs of atoms at 4/6A apart in *all* orientations? No rod-like or plate-like structure for the protein molecules will yield this essentially 3-dimensional distribution of vectors: on the other hand, an essentially 3-dimensional cage-like structure, scaled to to yield the 4/6A vectors, would be of impossibly small dimensions for the protein molecules.

There remains only the second component of the crystal, in terms of which an interpretation of the 5A shell may be sought. In the vector map of water,[3] we find a possible interpretation of (a), (b), and (e). We suggest that, as for water itself, the local drop in vector density at distances less than 4A from the origin may be interpreted in terms of water complexes, HOH molecules held by hydrogen bridges; nearest neighbors yield vectors shorter than say, 3A, and next-nearest neighbors vectors of length, say, 4.5A, with no intermediate situations. We further suggest that the interpretation of the corridors is the presence of some extended water particles in certain orientations.

To interpret and explain (d) we recall the water complexes in the 29-hydrate of phosphotungstic acid,[4] and the fact that they lie in definite orientations to the anions. Further, this structure analysis demonstrates that the structure of the definite water complexes is determined by the structure of the anions, as would be expected. Hence, the discussion of the one remaining finding, (c), is properly postponed until, in a subsequent publication, the evidence of the vector map regarding the structural type of the hemoglobin molecules has been evaluated. Only then can we discuss whether the almost universal drop in vector density after 6A is predominantly due to the small size of most of the water complexes or to the morphology of the protein molecules themselves.

That a major factor in the "5A peaks" in the vector map of crystalline wet insulin[5] may be the presence of water complexes in the crystal, has already been suggested.[6] A fuller discussion of the part played by the water complements in the vector maps both of hemoglobin and insulin will be given elsewhere.

* This work is supported by the ONR.
[1] M. F. Perutz, Proc. Roy. Soc. (London) **A195**, 474 (1949).
[2] Boyes-Watson, Davidson, and Perutz, Proc. Roy. Soc. (London) **A191**, 83 (1947).
[3] S. Katzoff, J. Chem. Phys. **2**, 841 (1934).
[4] A. J. Bradley, Proc. Roy. Soc. (London) **A157**, 113 (1936).
[5] D. Crowfoot, Russian Chem. J. **G15**, 215 (1946).
[6] D. Wrinch, Internatl. Cong. Crystallography, Abstract P7 (1951).

Nonisotropic Propagation of Combustion Waves*

GEORGE H. MARKSTEIN
Cornell Aeronautical Laboratory, Inc., Buffalo, New York
(Received April 14, 1952)

IN a recent publication Manton, von Elbe, and Lewis[1] propose as primary cause of combustion wave instability the "diffusional change of mixture composition in curved regions of a combustion wave." This aspect of the phenomenon has also been stressed by others.[2-6]

The decisive role of preferential diffusion of reactants is indeed supported by considerable experimental evidence. In the writer's linearized treatment,[7] this effect, and all other transport phenomena, including the always stabilizing influence of heat conduction and diffusion of chain carriers, were lumped into a parameter μ. The analysis yielded results in agreement with experiment only if the net effect of all transport phenomena was stabilizing ($\mu>0$), counteracting the always present hydrodynamic instability.

Manton, von Elbe, and Lewis criticize this treatment on the grounds that "first-order solutions are inherently incapable of predicting the amplitude ultimately attained by the perturbations"; "the stabilizing effect of wave propagation normally so much overshadows the disturbance created by hydrodynamic instability that the wave has practically a smooth noncellular surface," and that according to this treatment "all combustion waves should break into cells of definite size."

The writer agrees fully with the statement regarding the inadequacy of a linearized treatment for predicting the amplitudes ultimately attained. Basically, the limitation to finite amplitudes is provided by the nonlinearity of the differential equations and boundary conditions. Unfortunately, no adequate methods seem to exist as yet for solving the pertinent nonlinear partial differential equations directly. Furthermore, the possible existence of a steady-state solution of finite amplitude, its stability, and the stability of the initial state of zero amplitude are three separate problems that should be sharply distinguished. The writer's treatment was concerned exclusively with the last-named problem.

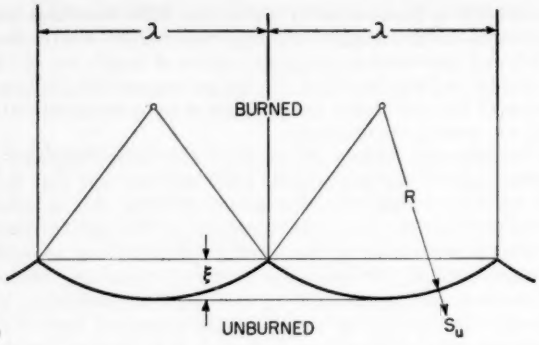

FIG. 1. Stabilizing effect of wave propagation.

One nonlinear effect, connected with the kinematics of combustion wave propagation, was selected for discussion in reference 1. The proposed application of Huyghens' construction would be strictly applicable only if the wave would propagate into a rigid medium. Although this is hardly the case, it is nevertheless instructive to analyze this problem, i.e., the stabilizing effect of wave propagation *per se*.

An initially sinusoidal section of a flame propagating into unburned gas at rest would soon assume a shape (Fig. 1) consisting of circular arcs that preserve their wavelength λ while their amplitude ξ gradually decreases. With $dR/dt=S_u$ (burning velocity, assumed constant) and $\lambda=$const., one obtains

$$d\xi/dt=-2S_u(2\xi/\lambda)^2[1-(2\xi/\lambda)^2]^{-1},$$

and, for $2\xi/\lambda<1$,

$$d\xi/dt=-2S_u(2\xi/\lambda)^2[1+(2\xi/\lambda)^2+\cdots].$$

Hence, the stabilizing effect of wave propagation is quadratic in ξ and therefore could never completely compensate a first-order instability (by definition linear in ξ), thereby creating a smooth noncellular surface.

The remaining argument against the writer's analysis concerns the alleged prediction that *all* flames should break into cells. Actually, the treatment yields a minimum wavelength for instability: $\lambda_{min}=4\pi\mu L\rho_u/(\rho_u-\rho_b)$ (notation of reference 7, gravity neglected[8]). If the significant dimension of the apparatus is smaller than λ_{min}, only damped perturbations are possible, i.e., the theory predicts stability. The writer feels that the currently available experimental data do not exclude the possibility that highly stable flames (μ large) might break into cells in vessels of larger dimensions than those hitherto employed.

Thus, a decision between the opposing views seems to be primarily a matter of further experimentation. Work at elevated pressures (reducing λ_{min}) might overcome limitations of vessel dimensions. Mapping the flow upstream of a cellular flame might enable one to decide whether S_u is a minimum ($\mu>0$) or a maximum at the wave troughs.

Regarding deficiencies of the writer's analysis, various simplifying assumptions were made and explicitly stated.[7] It would seem, however, that these assumptions (e.g., neglect of viscosity) might affect primarily the quantitative results, rather than the validity of the underlying model.

* This research was conducted under the auspices of Project SQUID, jointly sponsored by the ONR and the Office of Air Research under Contract N6-ORI-119, T.O. 1.

[1] Manton, von Elbe, and Lewis, J. Chem. Phys. **20**, 153 (1952).
[2] F. Goldmann, Z. Physik. Chem. **B5**, 307 (1929).
[3] Clusius, Kölsch, and Waldmann, Z. Physik. Chem. **A189**, 131 (1941); and later work by K. Clusius *et al.*
[4] N. P. Drozdov and Ya. B. Zeldovich, J. Phys. Chem. (URSS) **17**, 134 (1943).
[5] H. Behrens, Naturwiss. **32**, 297, 299 (1944); Z. Physik. Chem. **196**, 78 (1950).
[6] W. Jost, Z. Physik. Chem. **193**, 332 (1944); Z. Naturforsch. **6a**, 403 (1951).
[7] G. H. Markstein, J. Aero. Sci. **18**, 199 (1951).
[8] A discussion of gravity effects will be given elsewhere.

Seat of Joshi Effect in A/C Silent Discharges

S. R. KHASTGIR
Wireless Laboratory, Physics Department, Benares Hindu University, Benares 5, India
(Received April 9, 1952)

IN a recent paper published in this journal, Agashe[1] has furnished experimental evidence to show that the positive column has an important role in the production of the Joshi effect in the discharge tube and that possibly the surface layer at the electrodes has little or no effect. The object of this communication is to report the results of some experiments carried out in this laboratory on the positive and negative Joshi effects in "sleeve"-discharge tubes containing iodine vapor and hydrogen to study in a similar manner the effect of illuminating the different parts of each discharge tube successively by a narrow beam of strong light.

With a 500-watt electric light inside a closed box fitted with a slit-system and an adjustable shutter, a narrow beam of 1.5-mm width was made to fall on the different parts of each discharge tube. Employing 110 or 220 volts (50 cycles/sec) a suitable step-up transformer and a "Variac" for obtaining a variable voltage for the primary, suitable high voltages were obtained from the secondary, for the excitation of the tube. The discharge current was measured with a germanium crystal detector unit having a mirror galvanometer in series with the crystal circuit. With each tube requisite voltages were applied to obtain the negative and positive Joshi effects which were measured, respectively, by the observed decrease and increase of the discharge current, when the different parts of the discharge tube were illuminated, part by part, by the narrow beam of light. Each "sleeve" electrode consisted of a one-turn fine copper wire wound round the outer glass surface of the discharge tube.

Typical experimental results with iodine vapor showing negative and positive Joshi effects, at suitable voltages, for different distances of the illuminated part as measured from one of the "sleeve" electrodes are shown in Fig. 1. One typical set of results

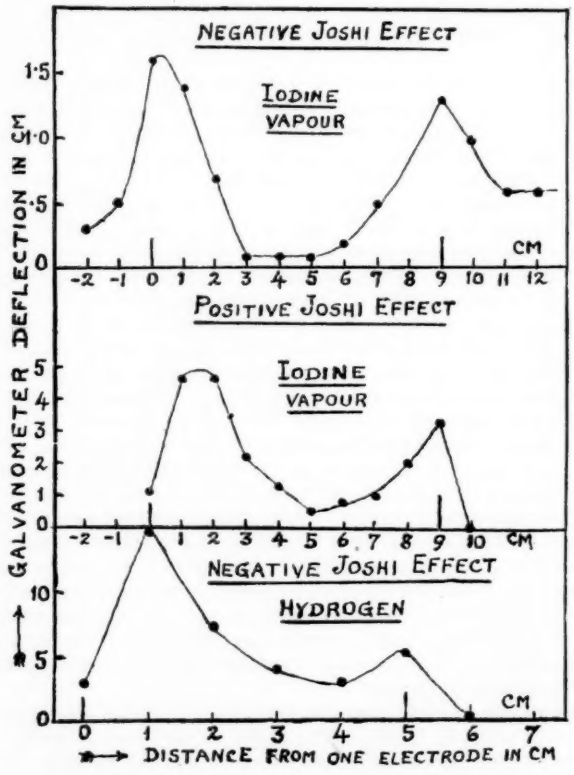

FIG. 1. Galvanometer deflections *versus* distance from one electron in the tube.

with hydrogen "sleeve" tube, showing negative Joshi effect is also shown in the same figure. General features of these results are as follows:

(1) The amount of Joshi effect (negative or positive) was found to have maximum values at (or very near) the two electordes.

(2) The effect showed an abrupt fall as the beam of light was shifted from either electrode towards the middle of the discharge tube.

(3) The effect observed in the middle region was found to be minimum. The minimum value was not inappreciable in many cases.

(4) The observed maximum effects at (or very near) the electrodes appeared to be dependent on the wall charges.

It is abundantly clear from the experimental results that both the positive and negative Joshi effects should be associated predominantly with the electrode regions. It can also be said that the small amount of Joshi effect observed when the middle region of the discharge tube was illuminated could be attributed to the stray light reaching the electrode regions after being scattered from the illuminated glass side of the discharge tube. Whether or not this should be regarded as a contribution of the discharge column is indeed difficult to say with any certainty.

With regard to the experimental results of Agashe, it should be noted that the electrodes in his experiments were plane metal electrodes fitted on to the flat ends of the discharge tube and that when either of the electrodes was illuminated by the beam of light, the latter grazed the surface of either electrode, the angle of incidence being 90°. Under such circumstances, according to the cosine - law of intensity variation, the intensity of light falling on either electrode should be minimum and there should be practically no Joshi effect. We are inclined to think that little or no photoreduction of discharge current observed by Agashe, when the electrode regions were illuminated, is to be attributed to this cause. It should also be noted that the length of the discharge tube in Agashe's experiments was as short as 4.5 cm. With such a short discharge tube, there must be some diffused or scattered light from the illuminated glass side of the discharge tube (which was also fitted with a paper scale) reaching either electrode, and this should certainly contribute to some extent to the net photoreduction of the discharge current. The light scattered from the gas or vapor at low pressure must, however, be too small to produce any appreciable effect. In view of the above considerations regarding the effect of light scattered from the illuminated glass side of the discharge tube to either electrode and in consideration of our experimental results with the "sleeve"-discharge tubes filled with iodine vapor and hydrogen, it can only be said that the experimental evidence substantiating the role of the positive column in the production of Joshi effect should be considered inconclusive.

The experiments, the typical results of which are reported here, have been performed by P. S. V. Setty, Miss K. Kulkarni, and C. M. Srivastava under my supervision. A detailed paper will be published elsewhere.

[1] V. V. Agashe, J. Chem. Phys. **19**, 1002 (1951).

Induced Decomposition of Acetaldehyde by Radicals

ROBERT K. BRINTON AND David H. VOLMAN
Department of Chemistry, University of California, Davis, California
(Received April 9, 1952)

Studies on the thermal[1] and photochemical[2] decomposition of mixtures of azomethane and acetaldehyde and on the thermal decomposition of di-*t*-butyl peroxide-acetaldehyde mixtures[3] have shown that the decomposition of acetaldehyde may be induced at temperatures far below the ordinary thermal decomposition temperature. A radical R capable of hydrogen abstraction can initiate the chain

$$R+CH_3CHO=RH+CH_3CO \quad k_1, \tag{1}$$

$$CH_3CO=CH_3+CO \quad k_2. \tag{2}$$

Methyl radicals in the presence of acetaldehyde may produce methane by reaction (1) or ethane by combination,

$$CH_3+CH_3=C_2H_6 \quad k_3. \tag{3}$$

If reactions (1) and (3) are the only mechanisms for the production of methane and ethane, R in this case being CH_3, then

$$\frac{d(CH_4)/dt}{[d(C_2H_6)/dt]^{\frac{1}{2}}}=\frac{k_1}{k_3^{\frac{1}{2}}}(CH_3CHO). \tag{4}$$

The thermal decomposition of a mixture of acetaldehyde and di-*t*-butyl peroxide has been studied from 124° to 156°C. Under these conditions either the *t*-butoxy radicals produced by the unimolecular nonchain decomposition of the di-*t*-butyl peroxide[4] or methyl radicals from the thermal decomposition of the *t*-butoxy radicals may act as the abstracting radical R in mechanism (1). The experimental procedure was similar to the technique described previously.[5] A gaseous mixture of acetaldehyde and di-*t*-butyl peroxide of known composition was expanded into a one-liter reaction chamber contained in an oil thermostat. The decomposition was followed manometrically to a small percentage decomposition and an analysis made on the reaction products by mass spectrometric methods.

The validity of the above expression relating the rates of formation of methane and ethane is shown in Fig. 1. The close correspondence of the experimental points to a straight line relationship indicates that the hydrogen abstraction by methyl radicals and the second-order homogeneous combination of methyl radicals must be the only important processes leading to the production of methane and ethane. An Arhhenius plot of these data yields an activation energy $E_1-\frac{1}{2}E_3=7.5>0.3$ kcal/mole. If Gomer and Kistiakowsky's[6] value of $k_3=2.1\times10^{12}T^{\frac{1}{2}}$ (moles/cc)$^{-1}$ and $E_3=0$ are taken for methyl radical combination,

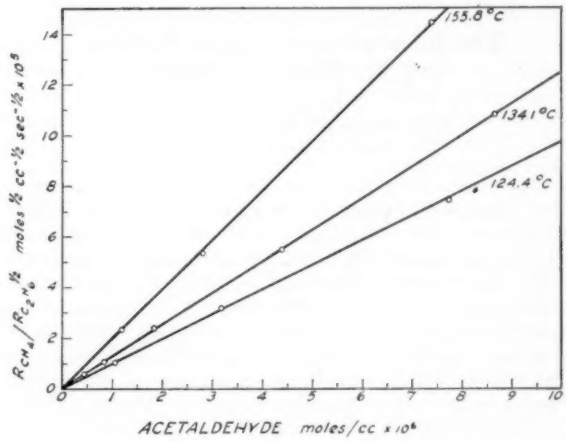

FIG. 1. Plot of experimental results corresponding to Eq. (4).

$$k_1=4.2\times10^{10}T^{\frac{1}{2}}e^{-(7.5/RT)}(\text{moles/cc})^{-1}\ \text{sec}^{-1}.$$

Assignment of a collisional diameter of 3.7A to the reaction of methyl radical and acetaldehyde molecule, a value similar to that used by Gomer and Kistiakowsky for the analogous reaction with acetone, gives a steric factor for reaction (1) of about 3.7×10^{-3}. This is in good agreement with the steric factor of a large number of other hydrogen abstraction reactions reported by Trotman-Dickenson and Steacie.[7] It is interesting to note that these authors predicted a steric factor of about unity for the abstraction reaction in the case of acetaldehyde on the basis of the rate of the reaction and the activation energy of about 10 kcal/mole usually attributed to this reaction.

Recently Danby, Buchanan, and Henderson[8] have shown that a relationship analogous to (4) holds for the rates of formation of methane and ethane in the high temperature photolysis of acetal-

dehyde. That the same general chain, mechanism, and chain ending steps are taking place in both the high temperature photolysis and the induced reaction seems rather conclusive. The over-all activation energy reported for the high temperature photolysis of acetaldehyde by various investigators is in the range 8.3 to 10 kcal/mole.[9] This energy has generally been identified as equivalent to E_1 although Blacet and Loeffler[10] attributed it to E_2. Since the most recent values of E_2 reported are in the range 13–16 kcal/mole,[11,12] it appears likely that the activation energies reported for acetaldehyde photolysis may not be identified specifically with either E_1 or E_2 but rather with some function of both E_1 and E_2.

[1] A. O. Allen and D. V. Sickman, J. Am. Chem. Soc. **56**, 2031 (1934).
[2] F. E. Blacet and A. Taurog, J. Am. Chem. Soc. **61**, 3024 (1939).
[3] Boyer, Niclause, and Letort, Compt. rend. **231**, 475 (1950).
[4] Raley, Rust, and Vaughan, J. Am. Chem. Soc. **70**, 88 (1948).
[5] R. K. Brinton and D. H. Volman, J. Chem. Phys. **20**, 25 (1952).
[6] R. Gomer and G. B. Kistiakowsky, J. Chem. Phys. **19**, 85 (1951).
[7] A. F. Trotman-Dickenson and E. W. R. Steacie, J. Chem. Phys. **19**, 329 (1951)
[8] Danby, Buchanan, and Henderson, J. Chem. Soc. 1426 (1951).
[9] E. W. R. Steacie, *Atomic and Free Radical Reactions* (Reinhold Publishing Corporation, New York), p. 190.
[10] F. E. Blacet and D. E. Loeffler, J. Am. Chem. Soc. **64**, 893 (1942).
[11] D. H. Volman and W. M. Graven, J. Chem. Phys. **20**, 919 (1952).
[12] F. B. Marcotte and W. A. Noyes, Jr., J. Am. Chem. Soc. **74**, 783 (1952).

The Infrared Spectrum of Pyrrole and the Hydrogen Bond

P. TUOMIKOSKI
University of Helsinki, Finland

(Received April 7, 1952)

IN a recent article Fuson, Josien, Powell, and Utterback[1] report that they have discovered the sharp unassociated NH absorption peaks of pyrrole in dilute solutions. In 1950 the author found that the second harmonic NH absorption of pyrrole in carbon disulfide showed a sharp peak at 0.997μ, whereas the corresponding peak in benzene at 1.004μ was of a broader and flatter type and in acetone at 1.012μ similar in form and position to the band of pure pyrrole at 1.013μ. An explanation like that for the solvent influence, and especially for the influence of surroundings containing π-electrons, on the OH absorption has been suggested.[2] The NH_2 absorption of aniline was somewhat influenced by the solvents, most of all by acetone, while essential differences in the NH absorption of diethylamine in those solvents were undetectable.[3] These variations were connected with the differing molecular structures of the compounds containing NH bonds, which further appear in the wide range of basicity of these molecules, an idea used by Gordy,[4] who studied the relations between absorption bands and basicities respecting acidities of the solution components, and by Bernal and Megaw[5] when they studied interatomic distances (OH···O bonds) in metallic hydroxides.

In the same year a paper about solutions of pyrrole in carbon tetrachloride and acetone by Zeshyulinskij[6] appeared, which had results equivalent to those of the author mentioned above. Although Zeshyulinskij's measurements did not seem to be so accurate as those of the author, the results were withheld to be published later in a more comprehensive study. The statements of Fuson *et al.* have, however, made a preliminary announcement necessary, all the more so as a close examination makes it doubtful whether, on the basis of spectroscopy alone, the bond between like NH containing molecules, responsible for the association band, should be called a hydrogen bond[7] as Fuson *et al.* insist.

We may clarify our ideas with the help of Fig. 1, drawn from our measurements made with a glass prism in the overtone region and with a rocksalt prism in the fundamental region (the associated and unassociated bands were well resolved in both regions). Assuming the surroundings to be homogeneous with a dielectric constant D and taking into account the reacting field of the polarized surroundings on the oscillating dipole one finds that the frequency shift should roughly be proportional to the expression $(D-1)/(2D+1)$, as Kirkwood[8] pointed out. This relation has been verified in the cases of hydrogen chloride,[8] ethanol,[2] and methanol.[9] Calling the proportionality constant C, the greatest shift could, according to this relation, be formally as large as $C/2$, or about 3 percent in actual cases. Shifts of approximately this magnitude are caused by acetone, mesithylene, and on the NH frequency of pyrrole itself. These can be interpreted as resulting from orientations of the OH and the NH groups, respectively, towards highly polarizable regions, the dipole polarization included, in neighboring molecules. For these reasons we are not fully justified in speaking of hydrogen bonds, when the relative frequency shifts $\Delta\nu/\nu$gas are of the order of 3 percent or less, because those shifts may be derived from electrostatics. In this connection one should recall the limitations, given by Bernal,[5,10] on the use of terms such as hydrogen and hydroxyl bonds.

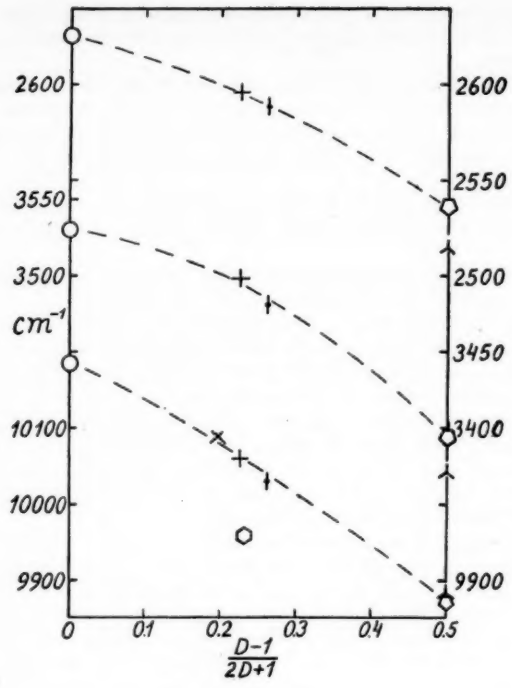

FIG. 1.

Now the mutual potential energy, which depends both on the distance between the molecules and on their relative orientation, serves as a measure of the strength of the intermolecular bond. As verified by the alcohols,[11] an amount of several kilocalories per mole is needed to overcome the thermal energy at ordinary temperatures and cause the unassociated absorption band practically to vanish. On the other hand, the OH frequency difference between unassociated (gaseous) and associated (liquid) alcohol molecules greatly exceeds the amount derived from Kirkwood's expression;[12] consequently, the absence of the unassociated bands in the spectrum of pure pyrrole—the author's experiments on the second harmonic band of pyrrole showed no appreciable changes, when the temperature was raised from 20 to 50°C—would at first sight appear peculiar. The only explanation, and a very plausible one, is that the pyrrole molecule has several highly polarizable regions and no region with a relatively low polarizability in contrast to alcohol molecules, in which, e.g., the intensity of the unassociated bands increases with the chain length,[13] i.e., with the relative amount of the weakly polarizable part of the molecule. A careful determination of heats of solution of pyrrole and other amines would undoubtedly set the comparison with the alcohols on a more solid foundation.

Finally, it is to be noted that acetone shifts the fundamental NH and ND frequencies to somewhat lower frequencies. A solu-

tion of pyrrole in diethylamine again is accompanied by a considerable evolution of heat and a lowering of the frequency amounting to 10 percent.[14] The pyrrole-*N*-*d* exchanges spontaneously the deuterium atom for ordinary hydrogen in solutions in diethylamine. Perhaps one may call the association hydrogen bonding at least, when a marked exchange reaction of the hydrogens takes place.

The author is indebted to E. Pulkkinen, Mag. phil., and P. Hirsjärvi, Mag. phil., for purifying of substances and making some measurements.

[1] Fuson, Josien, Powell, and Utterback, J. Chem. Phys. **20**, 145 (1952); M. L. Josien and N. Fuson, Compt. rend. **232**, 658 (1951).
[2] P. Tuomikoski and Suomen Kemistilehti **B23**, 44 (1950) (see reference 2); W. Lüttke and R. Mecke, Z. Elektrochem. **53**, 241 (1949).
[3] Similar results were reported long ago by R. Freymann, Ann. phys. (10) **20**, 242 (1933); he did not, however, use acetone as a solvent.
[4] W. Gordy, J. Chem. Phys. **7**, 93 (1939); **9**, 215 (1941); W. Gordy and S. C. Stanford, J. Chem. Phys. **8**, 170 (1940); **9**, 204 (1941).
[5] J. D. Bernal and H. D. Megaw, Proc. Roy. Soc. (London) **A151**, 384 (1935).
[6] B. M. Zeshyulinskij, Žurnal Fiz. Chim. **24**, 1442 (1950).
[7] Ethyleneimine, which according to H. W. Thompson and G. P. Harris, J. Chem. Soc. 301 (1944), shows a 3 percent difference between the unassociated and associated NH frequencies is probably no exception.
[8] Compare W. West and R. T. Edwards, J. Chem. Phys. **5**, 14 (1937).
[9] L. H. Jones and R. M. Badger, J. Am. Chem. Soc. **73**, 3132 (1951).
[10] J. D. Bernal, Trans. Faraday Soc. **33**, 210 (1937); **36**, 912 (1940).
[11] K. L. Wolf, Trans. Faraday Soc. **33**, 179 (1937); R. Mecke, Disc. Faraday Soc. **9**, 161 (1950).
[12] J. Errera and P. Mollet, Nature **138**, 882 (1936); Buswell, Deitz, and Rodebush, J. Chem. Phys. **5**, 501 (1937); J. J. Fox and A. E. Martin, Proc. Roy. Soc. (London) **A162**, 419 (1937).
[13] J. Kreuzer, Z. Physik **118**, 325 (1941); compare R. M. Badger and S. H. Bauer, J. Chem. Phys. **5**, 839 (1937).
[14] This is in accordance with the statements of Buswell, Downing, and Rodebush, J. Am. Chem. Soc. **62**, 2759 (1940). In addition, agreeing with the opinions of these authors, one may attribute the gradual frequency shifts of pyrrole with concentration to the polarizability of the liquid in bulk, the dipole polarizability now excluded; compare Tuomikoski, Pulkkinen, Hirsjärvi, and Toivonen, Suomen Kemistilehti **B23**, 53 (1950).

The Use of Ionization Probability Curves for the Analysis of CO and N_2 Mixtures

W. M. Hickam and R. E. Fox
Westinghouse Research Laboratories, East Pittsburgh, Pennsylvania
(Received March 28, 1952)

Workers have realized that appearance potentials provided a means for identifying gases. The large spread tolerated in the electron energy in the past has limited the use of the ionization probability curve in analytical work. A method has recently been reported from this laboratory[1] which yields ionization probability (P_i) curves produced by an essentially monoenergetic electron beam. It has been demonstrated for a number of gases, including CO and N_2, that the P_i curves rise linearly from the ionization potential for a change in electron energy of several volts. For any particular gas, the slope of the P_i curve is a linear function of the pressure. Since CO and N_2 have ionization potentials differing by 1.57 volts, their P_i curves can be sufficiently resolved and used for determining the composition of a mixture of these two gases.

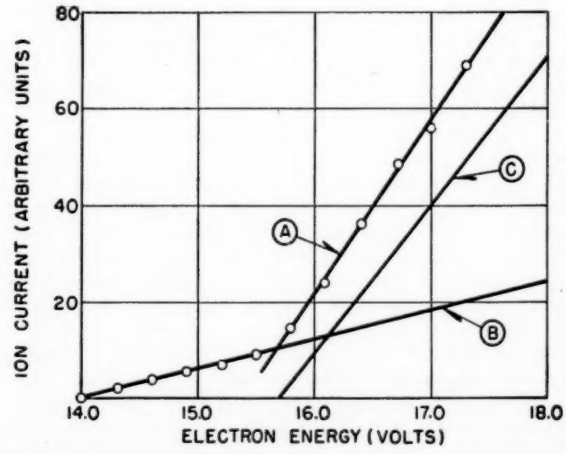

Fig. 1. An ionization probability curve (*A*) for a blend of CO and N_2. Curve *C* is the ionization probability curve for N_2 obtained by subtracting the CO extrapolated curve (*B*) from curve *A*.

Table I.

Run	Blend value % CO	Blend value % N_2	Mass spectrometer value % CO	Mass spectrometer value % N_2
1 *A*	35.0	65.0	34.5	65.5
1 *B*	35.0	65.0	34.8	65.2
2	20.4	79.6	19.8	80.2

The mass spectrometer used in these experiments was of the type with a sectored magnetic field in which the ions were deflected through 90 degrees on a five-inch radius. The ion source was adapted to use the techniques described previously. Since the mass spectrometer yields only relative ionization cross sections, the instrument was calibrated somewhat in the conventional manner. A sample of pure CO was admitted at a known pressure and the P_i curve taken over a range of several volts. Similarly, a P_i curve was taken for pure N_2. The slopes of these calibration curves yield the ionization per volt per unit pressure for each gas. A binary blend of these two gases was next admitted and a P_i curve taken over the same energy range. A typical P_i curve for a mixture of approximately 80 percent N_2 and 20 percent CO is shown in curve *A*, Fig. 1. The ion current for CO appears at 14.0 volts and rises linearly with the electron energy to the ionization potential of N_2^+. From this point the P_i curve is produced by both CO^+ and N_2^+ ions. To obtain the N_2 contribution, the straight line extrapolation of the CO curve *B* is subtracted from curve *A* yielding curve *C*.

The results of analyses made on two separate blends are shown in Table I.

The method of analysis is not limited to binary blends, nor is it essential that a mass spectrometer be used for specialized cases. An ionization chamber which permitted use of the described technique for obtaining a near monoenergetic electron beam should be sufficient as demonstrated by the above analysis for which no mass separation was employed.

[1] Fox, Hickam, Kjeldaas, and Grove, Phys. Rev. **84**, 859 (1951).

Some Observations on the CS "Radical"

P. J. Dyne* and D. A. Ramsay
Division of Physics, National Research Council, Ottawa, Canada
(Received April 2, 1952)

During our studies of free-radical spectra, we have obtained some results on the stability of the CS "radical." The spectrum of CS has been observed by various workers both in emission[1–3] and absorption,[4–6] and lifetimes up to 4 minutes have been recorded.[4–6] Analysis of the rotational structure of the emission bands[3] indicates that the ground state of the molecule is $^1\Sigma^+$. It is therefore more strictly described as a molecule and might be expected to be indefinitely stable in the gas phase.

In the present experiment CS was prepared (1) in a high frequency discharge through CS_2 and (2) by photolysis of CS_2. In the discharge technique[7] a pulse lasting $\frac{1}{10}$ sec from a 5-kw radio-frequency oscillator was passed through CS_2 vapor at a pressure of 5 mm Hg in a large discharge tube 4 ft long and 8 in. in diameter. In the photolysis technique CS was produced both by the flash photolysis[8] of CS_2 at 10-cm pressure and by continuous irradiation of CS_2 in a quartz tube at 10-cm pressure with a Hanovia high pressure quartz mercury lamp. The CS was detected in absorption by means of the strong double-headed (0, 0) band at 2576A, using a Hilger medium quartz spectrograph and a flash tube as a source of the continuous background.[9]

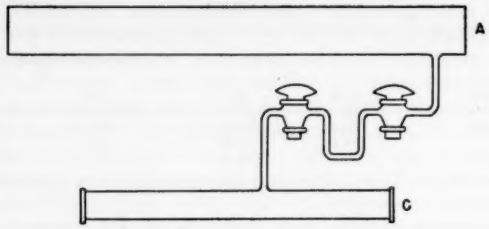

FIG. 1. Apparatus diagram.

The following observations were made:

(1) The lifetime of the CS radical was somewhat variable depending on the conditions in the containing vessel. Lifetimes of 30 min were observed using the photolysis technique, the CS being transferred from the preparation tube *A* to a clean glass observation tube *C* (Fig. 1). Similar lifetimes were observed in the large discharge tube.

(2) By inserting a cold trap at −110°C between *A* and *C*, the CS_2 was completely condensed while some CS passed through into *C*. In this way spectrograms were obtained showing CS absorption but not CS_2 absorption.

(3) By cooling the trap with liquid N_2, the CS was also condensed out. This process, however, was not reversible, the CS polymerizing in the trap to form a dark brown deposit first reported by Dewar and Jones.[9]

(4) CS could be stored in an intermediate vessel, placed between *A* and *C* for periods of ~10 min prior to its observation in *C*. Packing the intermediate vessel with glass wool or short lengths of glass tubing reduced this lifetime to less than 1 min. A brown deposit was formed on the glass wool packing at the point where CS first entered.

(5) Attempts were made to increase the concentration of CS in tube *C* by means of a Toepler pump. It was found, however, that the rate of removal of CS in *C* was of the same order as the rate at which it could be introduced by a Toepler pump of reasonable size.

These experiments show that there is a heterogeneous reaction removing CS from the system and suggest that in the gas phase CS shows the chemical stability of a normal molecule.

The authors are indebted to Dr. G. Herzberg for many helpful discussions.

* National Research Laboratories Postdoctorate Fellow.

[1] L. C. Martin, Proc. Roy. Soc. (London) **A89**, 127 (1913).
[2] W. Jevons, Proc. Roy. Soc. (London) **A117**, 351 (1928).
[3] F. H. Crawford and W. A. Shurcliff, Phys. Rev. **45**, 860 (1934).
[4] V. Kondratiev, Compt. rend. U.S.S.R. **20**, 547 (1938).
[5] G. Porter, Proc. Roy. Soc. (London) **A200**, 284 (1950).
[6] R. F. Barrow, Disc. Faraday Soc. No. 9, 81 (1950).
[7] P. J. Dyne, Can. J. Phys. **30**, 79 (1952).
[8] D. A. Ramsay, J. Chem. Phys. (to be published).
[9] J. Dewar and H. O. Jones, Proc. Roy. Soc. (London) **A85**, 574 (1911), and earlier papers.

Oxidation of Aqueous Ferrous Ammonium Sulfate Solutions by Betatron Radiation

R. W. HUMMEL AND J. W. T. SPINKS
Department of Chemistry, University of Saskatchewan, Saskatoon, Canada
(Received April 14, 1952)

THE ideal dosimeter would give a response proportional to the radiation energy absorbed, and its calibration should preferably be independent of photon energy. A solution of ferrous ammonium sulfate in 0.8*N* H_2SO_4 when properly prepared and handled, appears to satisfy these requirements. On irradiation, ferrous ions are oxidized to ferric ions, while ferric ions are not reduced.[1] The number of ferrous ions oxidized is proportional to the dose and is independent of photon energy from the soft x-ray region to the radium γ-ray region.[2] It is also independent of intensity over a wide range, although Miller cites experiments indicating that the radiation yield decreases at intensities greater than 100 r/sec.[3] The yield is independent of initial ferrous ion concentration from 10^{-2} to less than 10^{-4} M.[4] The temperature coefficient is negligible at ferrous ion concentrations initially greater than about 5×10^{-5} M, while at lower concentrations the coefficient is still small and readily determined.[5]

TABLE I.

Workers	Radiations	*G*
Fricke, *et al.*[a,b]	x-rays	18.0
Shishacow[c]	x-rays	15.9
Miller (polystyrene cells)[d]	Ra γ-rays	20.5
Miller (Pyrex cells)[d]	Ra γ-rays	18.2
Johnson[e]	2 Mev x-rays	17.3 ±0.5
Present work	24.5 Mev peak x-rays	15.8
Present work	Ra γ-rays	16.8

[a] H. Fricke and E. J. Hart, J. Chem. Phys. **3**, 60 (1935).
[b] H. Fricke and S. Morse, Phil. Mag., Series 7, **7**, 129 (1929).
[c] See reference 1.
[d] See reference 3.
[e] E. R. Johnson, J. Chem. Phys. **19**, 1204 (1951).

We have irradiated ferrous ammonium sulfate solutions, made 0.8N in H_2SO_4, with both radium gamma-rays and betatron x-rays, and find that the behavior with betatron x-rays of 24.5- and 18-Mev peak energy is closely similar to that with radium gamma-rays. In the betatron experiments, the solutions were irradiated in stoppered glass test tubes supported in a rotating Lucite block such that the betatron rays passed through about 4 cm of Lucite before entering the solutions. Dose determinations were made with a 25 r Victoreen condenser-type ionization chamber. Measurements made with betatron x-rays were subject to a small correction (1.4 percent) to allow for the difference in flux as measured calorimetrically compared with that measured with a 25 r chamber.[6]

The values for *G*, the number of ferrous ions oxidized per 100 ev of photon energy absorbed, are listed in Table I together with the results of other workers on the same system.

Excluding Miller's value obtained using polystyrene cells, the mean of the tabulated *G* values is 17.0, with a standard deviation of 0.9. It appears that for ferrous ammonium sulfate solutions the value of *G* in 0.8*N* H_2SO_4 is practically the same for x-rays of 24.5-Mev peak energy as for considerably lower energies.

The response of this system to x-rays and γ-rays depends on ionization of the aqueous medium and the subsequent production of free radicals and hydrogen peroxide which oxidize the ferrous ions. There appears to be no reason to believe that the occurrence of pair production as an energy absorption process would alter the oxidation mechanism. The chemical change depends on the presence of free radicals and their local concentrations, not on the way they are produced. The local concentrations of free radicals produced by electron pairs should not be very different from those produced by Compton electrons or photoelectrons. The possibility of nuclear reactions, such as $Fe^{56}(\gamma, n)Fe^{55}$ and $Fe^{56}(\gamma, p)Mn^{55}$, certainly exists at 24.5 Mev, but the loss of ferrous ions by a (γ, p) reaction would not be measurable by chemical methods under our conditions.

It would seem then that aqueous ferrous ammonium sulfate solutions can be used with advantage for x-ray dosimetry up to at least 24 Mev. In addition, integral dose measurements in a phantom would be facilitated. It should, perhaps, also be mentioned that, in principle, a dosimeter should show the same response to radiation as the material being irradiated. In this respect, for tissue irradiation, using a chemical dosimeter would appear to be fundamentally sounder than using the usual ionization thimble.

We are grateful to the Physics Department, University of Saskatchewan, for use of the betatron.

[1] N. A. Shishacow, Phil. Mag. **14**, 198 (1932).
[2] H. Fricke and S. Morse, Am. J. Roentgenol. Radium Therapy **18**, 426 (1927).
[3] N. Miller, J. Chem. Phys. **18**, 79 (1950).
[4] H. Fricke and S. Morse, Phys. Rev. **31**, 1117 (1928).
[5] R. W. Hummel and J. W. T. Spinks (to be published).
[6] J. S. Laughlin and J. W. Beattie, Rev. Sci. Instr. **22**, No. 8, 572 (1951).

THE JOURNAL OF

CHEMICAL PHYSICS

Volume 20 Number 6

1952

Published by the

AMERICAN INSTITUTE OF PHYSICS

[illegible] Chemical Physics

BOARD [illegible]

JOSEPH [illegible]

[illegible]

Term ending December 31, 1955

[illegible] CLEVELAND
[illegible] CRAWFORD, JR.
[illegible] HALFORD
[illegible] KIRKWOOD
[illegible]
[illegible] KISTIAKOWSKY
[illegible] LAIDLER
[illegible] E. KLEIN
[illegible] NIELSEN

H. G. [illegible]
H. E. [illegible]
J. O. [illegible]
DONALD F. HORNIG
JOHN E. PLATT
D. P. STEVENSON
ANTHONY TURKEVICH

Term ending December 31, 1954

THEODORE H. BERLIN
B. P. DAILEY
A. W. LAWSON
HARALD H. NIELSEN
HARRISON SHULL
CHARLES P. SMYTH
FRANK H. WESTHEIMER

THE JOURNAL OF CHEMICAL PHYSICS is published monthly by the American Institute of Physics. Its purpose is to bridge a gap between journals of physics and journals of chemistry. The artificial boundary between physics and chemistry has been in actual fact completely obliterated, and a large and active group is engaged in research which is as much the one as the other. It is to this group that the Journal is rendering its principal service and offers its greatest appeal, both as a prompt and adequate medium for the publication of research and as a convenient and carefully edited assemblage of pertinent information.

Instructions for Contributors

Send manuscripts to Joseph E. Mayer, Department of Chemistry, University of Chicago, Chicago 37, Illinois. Submission of a manuscript is a representation that it has not been published elsewhere, that it is not under consideration for publication elsewhere. Textual matter (abstract, text, bodies of tables, tabular matter, bibliography, figure captions) must be in English, typewritten (including mathematical expressions) double spaced with wide margins on a durable white paper, preferably letter size. The original copy, not the carbon, should be submitted. Consult current issues of this Journal for style, spelling, abbreviations, and form. Authors' contributions are requested to pay a publication charge of $6.00 per page, which, if honored, entitles them to 100 reprints. Additional reprints will be sent with galley proofs.

An abstract must accompany each article. It should be intelligible by itself and is a brief summary.

Mathematical expressions should be typewritten as far as possible. Be sure to distinguish between capital and small letters. Indicate clearly superior and inferior characters: commas, periods, etc. Avoid complicated superscripts and subscripts. Frequently it is possible to avoid complicated expressions by representing parts of them by single symbols. In the simpler Greek letters write out their names in full. Use fractional exponents instead of roots, and the solidus (/) for fractions wherever fractional exponents appear as factors, numbered equations, etc.

Tables may be typewritten on sheets separate from the running text. Each table must have a caption which will make the data in the table intelligible without reference to the text. Avoid complicated column headings.

Wherever possible figures should be planned for the width of a column (3 in.). A convenient reduction ratio is about 2:1 or 3:1. Lettering should be large enough on the original that when reduced it shall not be less than about 1/16 in. (~1.5 mm). Line drawings must be in *india ink* on white paper or tracing cloth. Coordinate paper is not desirable but if used must be blue lined and the coordinate lines which are to show must be inked over. Photographs should have maximum black and white contrast. Identify each original drawing or photograph on the back with the author's name and the figure number. Figures should be numbered consecutively. Captions should be typed on a separate sheet of paper.

A limited number of alterations in proof are unavoidable, but the cost of making extensive alterations after the article has been set in type will be charged to the author.

Proof and all correspondence concerning papers in the process of publication should be addressed to the Publication Manager, American Institute of Physics, 57 East 55 Street, New York 22, New York.

Subscription Price

	U. S. and Canada	Elsewhere
To members of the American Institute of Physics and Affiliated Societies	$12.00	$13.00
To all others	15.00	16.00

Back Number Prices

Yearly rate when complete year is available: $13.00.
Single copies: $1.25 each.

Subscriptions, renewals, and orders for single copies should be addressed to the American Institute of Physics, 57 East 55 Street, New York 22, New York.

Changes of address should be sent to the American Institute of Physics.

[illegible] Prince and Lemon Streets, Lancaster, Pennsylvania.

[illegible] as second-class matter December 30, 1932, at the Post Office at Lancaster, Pa., under the Act of August 24, 1912.
[illegible] of postage provided for in paragraph (d-2), section 34.40, P. L. & R. of 1948, authorized February 3, 1933.